

ulm university universität
uulm

Fakultät für Ingenieurwissenschaften,
Informatik und Psychologie

Institut für theoretische Informatik

Direktor: Prof. Dr. Uwe Schöning

Analysis of Mutation Strength Adaptation within Evolution Strategies on the Ellipsoid Model and Methods for the Treatment of Fitness Noise

Dissertation zur Erlangung des Doktorgrades Dr.rer.nat. der Fakultät für Ingenieurwissenschaften, Informatik und Psychologie der Universität Ulm

von
Michael Lorenz Hellwig
aus Korbach

Ulm, September 2016

Amtierender Dekan:	Prof. Dr. Frank Kargl
Gutachter:	Prof. Dr. Hans-Georg Beyer
Gutachter:	Prof. Dr. Uwe Schöning
Tag der Promotion:	30. Januar 2017

Abstract

This work addresses the theoretical and empirical analysis of Evolution Strategies (ESs) on quadratic functions, in particular on Positive Definite Quadratic Forms (PDQFs). Referring to this subset as the ellipsoid model, the analysis excludes such PDQFs with only a few dominating eigenvalues in the Hessian matrix diagonal. To perform the theoretical analysis, the so-called dynamical systems approach, which is known from the analysis of self-adaptive ES, is transferred to the specific problem formulations. In this context, the limit of large search space dimensions, $N \to \infty$, is considered and the dynamics are based on expected values. The resulting description represents the exact asymptotic (long-term) behavior.

The first part focuses on theoretical investigations concerning two common mutation strength adaptation mechanisms and the corresponding dynamical behavior of the evolutionary systems. In particular, cumulative step-size adaptation as well as a specific hierarchically organized ES are under consideration. Connecting these findings to existing results of σ-self-adaptation, the analysis of the currently most common mutation strength adaptation methods in ES is completed.

Regarding the behavior of the $(\mu/\mu_I, \lambda)$-ES with cumulative step size adaptation (CSA) a non-linear system of difference equations is derived that describes the mean-value evolution of the ES. This system is successively simplified to finally allow for deriving closed-form solutions of the steady state behavior in the asymptotic limit case of large search space dimensionality. It is shown that the system exhibits linear convergence order. The steady state mutation strength is calculated and it is demonstrated that compared to standard settings in σ self-adaptive ESs, the CSA control rule allows for an approximately μ-fold larger mutation strength. This explains the superior performance of the CSA in non-noisy environments. The results are used to derive a formula for the expected running time. Conclusions regarding the choice of the cumulation parameter c and the damping constant D are drawn.

Further, the ability of a hierarchically organized evolution strategy (meta-Evolution Strategy) with isolation periods of length one to optimally control its mutation strength is investigated. By application of the dynamical systems analysis approach, a first step towards the analysis of the meta-Evolution Strategy behavior is conducted. A non-linear system of difference equations is derived to describe the mean-value evolution of the respective hierarchically organized strategy. In the asymptotic limit case of large search space dimensions, this system is suitable to derive closed-form solutions which describe the long-term behavior of the meta-Evolution Strategy. The steady state mutation strength is bracketed within an interval depending on the mutation strength control parameter. Compared to standard settings in cumulative step-length adaptation evolution strategies the meta evolution strategy realizes almost similar normalized mutation strengths. The performance of the meta-Evolution Strategy turns out to be very robust in terms of choosing its control parameters. The results allow for the derivation of the expected running time of the algorithm. Finally, the results

are extended to meta-ES with longer isolation periods. While the respective strategies reveal the ability to reduce fluctuation in the upper level selection process for small control parameter choices, they do not indicate a potential for a long-term progress enhancement.

The second part of this work expands the regarded optimization problem by the concept of fitness noise. To this end, the noisy ellipsoid model is motivated considering two contrasting noise models, i.e. additive noise of constant variance and noise of constant normalized variance. After transferring previous sphere model results to the noisy ellipsoid model two Evolution Strategies are examined that promise to successfully deal with the noise perturbations.

The first attempt investigates the ability of meta-ES to simultaneously control mutation strength and the population size on the noise sphere model. The analysis of the strategy's long-term behavior is presented. An expression describing the asymptotical growth of the normalized mutation strength is calculated that allows for the prediction of the meta-ES dynamics. The theoretical results are empirically evaluated, indicating that the noise influence on the meta-ES selection process results in rather large deviations from the predicted long-term behavior. This suggests that the particular meta-ES variant is not well enough suited to deal with the noisy optimization problem. Adjustments of the selection decision are connected to additional expenses in terms of function evaluations and conclusively increase the optimization effort considerably.

A second approach proposes the design of a noise detection technique which is able to identify noise related stagnation in the fitness dynamics of an ES on the noisy ellipsoid model. The noise detection is integrated into the well-known Covariance Matrix Self-Adaptation Evolution Strategy (CMSA-ES). It recognizes stagnations by use of a linear regression analysis of the observed fitness sequence in the evolutionary process and appropriately controls the population size of the CMSA-ES. The suggested strategy successfully deals with the regarded noise variants on the ellipsoid model. Additionally, the empirical proof-of-concept allows for a remarkable observation. That is, according to a theorem by Astete-Morales, Cauwet, and Teytaud, "Simple Evolution Strategies (ES)" that optimize quadratic functions disturbed by additive Gaussian noise of constant variance can only reach a simple regret log-log convergence slope $\geq -1/2$ (lower bound). The population size controlled CMSA-ES (pcCMSA-ES) presented is able to perform better than the $-1/2$ limit. It is shown experimentally that the pcCMSA-ES is able to reach a slope of -1 being the theoretical lower bound of all comparison-based direct search algorithms.

Acknowledgements

This thesis is the result of my research work at the Vorarlberg University of Applied Sciences (FHV). It has been realized during the research project "Direct search methods under noise II: Analysis and Design" that was supported by the Austrian Science Fund FWF under grant P22649-N23. I also acknowledge the support of the Austrian Research Promotion Agency FFG by the funding program COMET (COMpetence centers for Excellent Technologies) in the K-Project Advanced Engineering Design Automation (AEDA).

First of all, I am most grateful to my advisor Prof. Hans-Georg Beyer for providing me the opportunity to do research in the field of Evolution Strategies. I cannot thank him enough for the revealing discussions, his invaluable comments, and his constant support.

Furthermore, I give thanks to Prof. Uwe Schöning for the time he spent reviewing my manuscript. I appreciate his great interest in my work, his expedient comments as well as the constant help concerning the administrative process.

I would like to acknowledge the support from FHV and the University Ulm. Thanks to my co-workers at the Research Center PPE I will always recall many pleasant memories. In this regard, I most sincerely thank Dr. Steffen Finck for numerous inspiring discussions.

A lot of thanks to the people at the Faculty of Computer Science at the Dalhousie University of Halifax where I was welcome to conduct some of my research. Thanks to Prof. Dr. Dirk V. Arnold I learned a lot in this time.

Last, but not least, I would like to thank my parents and my whole family for the never faltering support. I am particularly grateful for the encouragement and the patience of Adina and Frida. Without them, none of this would have been possible.

Contents

Abstract iii

Acknowledgements v

1. Introduction 1
1.1. Underlying publications 4

2. Fundamental principles of Evolution Strategies 5
2.1. Mutation strength adaptation techniques 8
2.1.1. The 1/5th rule 9
2.1.2. σ self-adaptation 9
2.1.3. Cummulative step size adaptation 11
2.1.4. Hierarchically organized Evolution Strategies 12
2.2. Covariance matrix adaptation 13
2.3. Analysis technique: the dynamical systems approach 14

I. Analysis of mutation strength control on the ellipsoid model 19

3. The ellipsoid model 21
3.1. The fitness environment 22
3.2. Evolution Strategies on the ellipsoid model 24
3.2.1. Measuring the evolutionary progress 25
3.2.2. Performance analysis results of σ-self-adaptation 29
3.3. A comparison of mutation strength control analysis results 31

4. Analysis of cumulative step-size mutation strength adaptation 37
4.1. The $(\mu/\mu_I, \lambda)$-CSA-ES algorithm 37
4.2. Deriving the evolution equations 39
4.3. The steady state dynamics 45
4.3.1. Self-adaptation response approximation for CSA 45
4.3.2. The eigenvalue problem 51
4.3.3. The normalized steady state mutation strength 53
4.4. Closed-form expressions in the steady state 57
4.5. The expected running time 63
4.6. Summary 64

5. Analysis of mutation strength adaptation by meta-Evolution Strategies 67
5.1. The $[1, 2(\mu/\mu_I, \lambda)^\gamma]$-meta-ES algorithm 67
5.2. Single generation isolation time 69
5.2.1. The evolution equations 69
5.2.2. Discussing the deviations for small mutation control parameters . . 74
5.2.3. The normalized mutation strength dynamics 78
5.2.4. Derivation of the steady state dynamics 82
5.2.5. The expected running time 89
5.3. Extension to multiple generation isolation periods 91
5.3.1. One-generation experiments 91
5.3.2. Evolution equations for isolation over multiple generations 93
5.3.3. The normalized mutation strength dynamics 96
5.3.4. Predicting the expected steady state progress 99
5.4. Summary 104

II. Evolution Strategies on the noisy ellipsoid model 107

6. The noisy ellipsoid model 109
6.1. Introduction to noisy optimization 109
6.2. The noisy optimization problem 110
6.3. Performance measures under noise 111
6.3.1. The noisy quadratic progress rate 112
6.3.2. Simple Regret 113
6.4. Noise models 114
6.4.1. Fitness noise of constant variance 114
6.4.2. Fitness noise of constant normalized variance 116

7. Meta-ES analysis on the noisy sphere model 119
7.1. The $[1, 4(\mu/\mu_I, \lambda)^\gamma]$-meta-ES 120
7.2. Theoretical analysis of the inner strategy 121
7.3. The population size dynamics 125
7.3.1. Noise-free fitness environment 125
7.3.2. Addressing fitness noise 127
7.4. The mutation strength dynamics 128
7.4.1. Deriving the mutation strength dynamics 128
7.4.2. The normalized mutation strength dynamics 131
7.5. Simulations 136
7.5.1. A discussion of the fluctuations 139
7.5.2. On enhancing the selection decision 140
7.6. Summary 142

8. The population control CMSA-ES on the noisy ellipsoid model **143**
8.1. Introduction . . . 143
8.2. The CMSA-ES . . . 144
8.3. Stagnation detection by use of linear regression analysis . . . 146
8.4. The population control CMSA-ES algorithm . . . 148
8.5. Experimental investigations . . . 150
8.6. Inspecting the simple regret dynamics . . . 152
8.7. Summary . . . 154

9. Outlook **157**

Appendix **159**

A. Deriving the CSA dynamics **161**
A.1. The expected value of $\|\langle \mathbf{z} \rangle^{(g)}\|^2$ . . . 161
A.2. The expected change of the scalar product . . . 162
A.3. The normalized mutation strength dynamics . . . 166

B. Deriving the meta-ES dynamics **167**
B.1. The normalized mutation strength dynamics . . . 167
B.2. Deriving the oscillation interval . . . 170
B.3. Approximating the progress over an isolation period of multiple generations 171

C. Meta-ES on the noisy sphere model **175**
C.1. Comparing the noise-free population dynamics . . . 175
C.2. Derivation of the mutation strength dynamics . . . 176
C.3. Approximation of the discriminator function . . . 179

Bibliography **181**

List of Algorithms

2.1. A conceptual Evolution Strategy 8

3.1. The standard $(\mu/\mu_I, \lambda)$-ES with constant mutation strength 24

4.1. Pseudo code of the $(\mu/\mu, \lambda)$-CSA-ES 38

5.1. A hierarchical ES: The $[1, 2(\mu/\mu_I, \lambda)^\gamma]$-meta-ES 68
5.2. The $[1, 2(\mu/\mu_I, \lambda)^\gamma]$-meta-ES applying $\tilde{\Delta}$-cumulation 77

7.1. The $[1, 4(\mu/\mu_I, \lambda)^\gamma]$-meta-ES 121

8.1. The $(\mu/\mu_I, \lambda)$-CMSA-ES 144
8.2. The $(\mu/\mu_I, \lambda)$-pcCMSA-ES algorithm using linear regression analysis . . . 149

List of Figures

3.1. Illustration of the ellipsoid model in two dimensions 23
3.2. Comparison of the theoretically gained expected running times 35

4.1. Typical dynamics of the $(3/3_I, 10)$-CSA-ES on the ellipsoid model 38
4.2. The dynamics of iterative scheme I 42
4.3. Comparison of the dynamics resulting from iterative scheme I and II 43
4.4. The dynamics of scheme II 44
4.5. Comparison of iterative systems II and III 48
4.6. Validation of iterative scheme IV 50
4.7. Numerical solution of the eigenvalue problem 52
4.8. Steady state condition of the CSA-ES 55
4.9. Influence of the damping parameter D 56
4.10. The steady state mode eigenvalue 57
4.11. Comparison of CSA strategy parameter settings on the sphere model 60
4.12. Illustration of the σ^* oscillation for small D 61
4.13. The convergence rate of the CSA-ES 62
4.14. Expected running time of the CSA-ES 63

5.1. The meta-ES dynamics on the ellipsoid model $q_i = i$ 71
5.2. The normalized mutation strength dynamics on the ellipsoid model $q_i = i$. 72
5.3. The meta-ES dynamics on the ellipsoid model $q_i = i^2$ 73
5.4. The meta-ES dynamics for small values of α 74
5.5. One-generation experiments on the ellipsoid model with $a_i = i$ 75
5.6. Signal-to-noise ratio of one-generation experiments 76
5.7. The meta-ES dynamics using $\tilde{\Delta}$-cumulation 78
5.8. The normalized mutation strength dynamics 80
5.9. The influence of α on the steady state 81
5.10. The σ^* distribution in the steady state 82
5.11. Steady state dynamics comparison in $N = 40$ 84
5.12. Steady state dynamics comparison in $N = 200$ 85
5.13. Numerical solutions of the eigenvalue problem 86
5.14. Convergence rates 88
5.15. The expected running time 90
5.16. One-generation experiments for $\gamma > 1$ 92
5.17. The influence of γ on the selection decision 93
5.18. The meta-ES dynamics on the ellipsoid model for $\gamma = 3$ 96
5.19. Influence of α on the meta-ES dynamics for $\gamma > 1$ 98

5.20. The distribution of the normalized steady state mutation strength for $\gamma = 3$. 99
5.21. Illustration of admissible γ values 102
5.22. Steady state mode eigenvalue of the meta-ES using $\gamma > 1$ 103
5.23. Expected running time of the meta-ES with $\gamma > 1$ 105

7.1. Illustration of the meta-ES dynamics on the noisy sphere model 124
7.2. The noise-free meta-ES dynamics 126
7.3. Numerically deriving the sign of the discriminator function 130
7.4. Relating the point of discontinuity to the noise strength 131
7.5. Trade-off of the discriminator function approximation 133
7.6. The asymptotical σ^* and σ^*_ϵ dynamics 134
7.7. Asymptotic long-term behavior of the meta-ES on the noisy sphere model . 135
7.8. Experimental verification for $\alpha = 1.05$ 137
7.9. Experimental verification for $\alpha = 1.2$ 138
7.10. On the occurring deviation for small α values 140
7.11. The effect of resampling on the experimental dynamics 141

8.1. The CMSA-ES dynamics subject to additive noise 145
8.2. The CMSA-ES dynamics subject to distance proportional noise 146
8.3. The pcCMSA-ES dynamics on the noisy ellipsoid model $q_i = i$ 151
8.4. The pcCMSA-ES dynamics subject to additive noise 153
8.5. The pcCMSA-ES dynamics subject to distance proportional noise 154

A.1. Approximation quality validation 164

B.1. The Q-term dynamics 170

1. Introduction

In the field of optimization, in recent years a rise of the size and the problem complexity of optimization tasks could be registered. Moreover, the mathematical model of the optimization problem might rely on internal simulations as well as measured data which can impose a certain level of uncertainty. Consequently, classical deterministic strategies disclose weaknesses as the gradient information can be inaccessible, i.e. the derivatives w.r.t. decision parameters might be unavailable, unreliable or impractical to obtain. Due to a concurrent increase of computational power, Direct Search Methods gradually became the focus of attention in fields like Operations Research, Engineering or Noisy Optimization. Direct Search Methods share the property that they update the decision parameters based only on information obtained from evaluations of the objective function of the underlying optimization problem. In this context, different approaches have to be mentioned: response surface models, pattern search approaches, strategies that approximate the derivatives, or nature-inspired strategies. All these techniques try to create a local model of the objective function by interpretation of the evaluated decision parameters. Prominent approaches without limitations include the simplex method [Nelder and Mead, 1965; Torczon, 1997], the Kriging method [Oliver and Webster, 1990], the NEWUOA algorithm [Powell, 2006], and the CMA-ES algorithm [Hansen and Ostermeier, 2001]. For an overview of Direct Search Methods, it is referred to [Kolda et al., 2003; Audet, 2014].

Regarding the area of nature-inspired strategies, it comprises well-known approaches like Particle Swarm Optimization [Khare and Rangnekar, 2013], Ant Colony Optimization [Mohan and Baskaran, 2012] and particularly Evolutionary Algorithms (EAs). Using mechanisms inspired by biological evolution, such as reproduction (i.e. recombination and mutation) and selection, an EA is a generic population-based heuristic optimization algorithm. EA regard candidate solutions as individuals in a population whose quality is determined by a fitness function (commonly the objective function of the optimization problem). The successive application of the reproduction and selection operators evolves the population towards the optimization goal. Evolutionary Algorithms themselves can be separated into three subclasses: Genetic Algorithms [Holland, 1975], Evolutionary Programming [Fogel et al., 1966], and Evolution Strategies [Rechenberg, 1973]. Investigations of the latter type build the subject of this thesis. Evolution Strategies (ES) are most typically concerned with the optimization of real-valued optimization problems. Albeit application to combinatorial problems are of course possible, there are few publications regarding combinatorial optimization. The present work particularly focuses on the theoretical analysis and the assessment of state-of-the-art Evolution Strategies which has developed a long-standing tradition in years past. In the first place, the scope of the theoretical analysis is not so much the application to complex optimization problems but the theoretical description of the evolution dynamics as well as the identification of advantageous strategy parameter settings.

These examinations are typically performed on relatively simple test functions.

Aiming at (near) optimal performance, Evolution Strategies usually employ a mutation strength adaptation mechanism throughout the optimization process. The mutation strength σ determines the average step-length of the search step within the ES algorithm. The thesis addresses the problem of analyzing the mutation strength adaptation on Positive Definite Quadratic Forms (PDQFs), the so-called ellipsoid model. In this respect, it contributes to the current analysis of mutation strength adaptation mechanisms on the ellipsoid model which commenced with the work of [Beyer and Melkozerov, 2014] investigating mutative self-adaptation, i.e., the $(\mu/\mu_I, \lambda)$-σSA-ES. That paper introduced a new progress measure, the quadratic progress rate, allowing for the description of the dynamics of the quadratic distances of the parental state to the optimizer. Yielding an estimate for the optimal learning rate that differs from previous sphere model results, the work completed the analysis of isotropic self-adaptive standard ES. In the present work, this analysis approach is carried forward regarding two other popular mutation strength adaptation approaches, namely cumulative step size adaptation (CSA) and hierarchically organized ES (meta-ES).

Chapter 2 summarizes the most important principles of Evolution Strategies. These are necessary to follow the analyses and understand the next chapters. The first part of the thesis is concerned with the analysis of commonly applied mutation strength adaptation methods for ES on the ellipsoid model. To this end, the quadratic optimization problem under consideration, i.e. the ellipsoid model, is motivated in Chapter 3. The chapter also recaps the most prominent research findings in the context of the ellipsoid model and compares them to anticipated findings from the two following analyses in order to provide an overview of the analysis goals. Taking into account the $(\mu/\mu_I, \lambda)$-CSA-ES which uses cumulative step-length adaptation to control the mutation strength, the detailed analysis is carried out in Chapter 4. Deriving an approximation of the cumulation path allows for the extension of the dynamical systems analysis approach developed in [Beyer and Melkozerov, 2014] to the analysis of the CSA-ES on the ellipsoid model. This way, it is possible to describe the long-term dynamics of the CSA-ES and identify reasonable recommendations for the choice of the strategy parameters. In Chapter 5, the dynamical systems analysis approach is applied to a hierarchically organized ES variant, more precisely, to the $[1, 2(\mu/\mu_I, \lambda)^\gamma]$-meta-ES. The corresponding dynamics are divided into a mean value parts and fluctuation terms. The mean value dynamics of the quadratic distances of the parental state to the optimizer are given by the quadratic progress rate [Beyer and Melkozerov, 2014]. This way, it is possible to model the evolution equation of the mutation strength dynamics for isolation time $\gamma = 1$ in the first step, see Sec. 5.2. The obtained system of evolution equations allows for the analytical description of the steady state dynamics of the meta-ES variant. The approach is then extended to approximate the dynamics of meta-ES employing larger isolation periods, i.e. using isolation times $\gamma > 1$.

Regarding the second part of this thesis, the optimization problem is extended by adding fitness noise to the evaluation result of the objective function. Considering two different types of noise, i.e. additive noise of constant variance and constant normalized variance, respectively, the noisy ellipsoid model is introduced in Chapter 6. Existing theoretical findings from the context of the noisy ellipsoid model are provided. Joined with generalizations of known sphere model results, these findings support the following investigations. In a first

approach, a specific meta-ES variant which simultaneously controls its population size as well as its mutation strength is investigated on the noisy sphere in Chapter 7. Considering the additive noise model, a theoretical analysis of the asymptotical long-term behavior of the strategy is performed that results in the description of the respective dynamics. However, experimental runs of the meta-ES algorithm reveal deviations related to the idealized modeling of the inner selection process. After discussing the cause of the deviations, adjustments to improve the noise biased selection process of the upper level ES are examined.

Drawing conclusions from shortcomings of the meta-ES approach, the population size control is transferred into the state-of-the-art covariance matrix self-adaptation Evolution Strategy (CMSA-ES) in Chapter 8. The hierarchical structure is omitted and the decision to increase or decrease the population is based on a hypothesis test. This way of proceeding allows for saving a great amount of function evaluations during the algorithm run. The test decision relies on an integrated linear regression analysis of the observed fitness sequence during the evolutionary process. Denoting the newly designed algorithm population control CMSA-ES (pcCMSA-ES), its ability to deal with noise of different characteristics is verified in a proof of concept on the noisy ellipsoid model. Being related to a lower runtime bound derived by [Astete-Morales et al., 2015], the observation of the pcCMSA-ES long-term behavior reveals a remarkable performance on the ellipsoid model with additive noise.

The thesis concludes in Chapter 9 with an outlook on possible future research directions related to the investigations presented in both parts of the present work.

1.1. Underlying publications

This thesis is based in part on the following publications

(i) Beyer, H.-G., Hellwig, M., Mutation strength control by meta-ES on the sharp ridge, Soule, T., Moore, J. H. (Ed.): GECCO, pp. 305–312, ACM, 2012, ISBN: 978-1-4503-1177-9. (DOI: 10.1145/2330163.2330208)

(ii) Beyer, H.-G., Hellwig, M., Controlling population size and mutation strength by meta-ES under fitness noise, Neumann, F., De Jong, K. A. (Ed.): FOGA, pp. 11–24, ACM, 2013, ISBN: 978-1-4503-1990-4. (DOI: 10.1145/2460239.2460242)

(iii) Hellwig, M., Arnold, D. V., Comparison of Constraint Handling Mechanisms for the $(1, \lambda)$-ES on a Simple Constrained Problem, *Evolutionary Computation*, pp. 1–23, 2016, ISSN: 1063-6560. (DOI: 10.1162/EVCO_a_00139)

(iv) Beyer, H.-G., Hellwig, M., The Dynamics of Cumulative Step Size Adaptation on the Ellipsoid Model, *Evolutionary Computation*, pp. 24–57, 2016, ISSN: 1063-6560. (DOI: 10.1162/EVCO_a_00142)

(v) Hellwig, M., Beyer, H.-G., Mutation Strength Control via Meta Evolution Strategies on the Ellipsoid Model, *Theoretical Computer Science*, Volume 623, 11 April 2016, Pages 160-179, ISSN 0304-3975. (DOI: 10.1016/j.tcs.2015.12.011)

(vi) Hellwig, M., Beyer, H.-G., Evolution under Strong Noise: A Self-Adaptive Evolution Strategy Can Reach the Lower Performance Bound - the pcCMSA-ES, Parallel Problem Solving From Nature – PPSN XIV, pp. 26–36, LNCS 9921, Springer, 2016, ISBN: 978-3-319-45822-9. (DOI: 10.1007/978-3-319-45823-6_3)

The contribution of the author of this thesis to the above mentioned publications is at least 50%. Chapter 4 is based on a revised version of (iv); Results from (v) are presented in Section 5.1 and 5.2 of Chapter 5. In Section 5.3 these observations are extended to meta-ES that use isolation periods of multiple generations. Regarding the second part of this thesis, Chapter 7 developed on the basis of (ii). Finally, an extended version of publication (vi) establishes the design of the population control algorithm in Chapter 8.

The publications (iii) and (i) emerged during the research work for this thesis. They cover slightly different topics in the context of Evolution Strategies, in the broadest sense constrained optimization problems. Confining to a common theme these publications build no integral part of this thesis.

2. Fundamental principles of Evolution Strategies

This section provides a recapitulation of elementary principles needed to understand the operating principles as well as the potential of Evolution Strategies (ES). Building a subclass of Evolutionary Algorithms, Evolution Strategies represent nature-inspired optimization strategies that can be applied in all fields of optimization including continuous, discrete, combinatorial search spaces Y without and with constraints as well as mixed search spaces. Considering an optimization problem of general form

$$\mathbf{y}^* = \arg \operatorname{opt}_{\mathbf{y} \in Y} F(\mathbf{y}), \tag{2.1}$$

the objective function $F(\mathbf{y})$ is optimized over the search space Y. In the context of Evolution Strategies, $F(\mathbf{y})$ might be accessible in analytical form, via simulations, or in terms of experimental measurements. The only requirement on the objective function is that it can be evaluated for each search space parameter vector $\mathbf{y} \in Y$. Having no information on the internal structure of the optimization problem other than output responses to specific input data, it is also referred to as black-box optimization. Extending $F(\mathbf{y})$ in (2.1) to a set of objective functions, it is also possible to apply ES in the context of multi-objective optimization. Thus Evolution Strategies are independent of problem specific information like assumptions on the analytic form of F, e.g. information on F being linear (or quadratic) or the availability of the objective function's derivatives. They rely on fitness evaluations of the candidate solutions generated during the optimization process. The optimization itself is performed by iterative application of two mathematical operators: *selection* and *variation*.

The basic representations of the ES distinguish the way of selection being performed. They are denoted by

$$(\mu/\rho + \lambda)\text{-ES} \qquad \text{and} \qquad (\mu/\rho, \lambda)\text{-ES}, \tag{2.2}$$

respectively. Here, the number of parents is specified by the parameter μ while ρ refers to the number of parents involved in the procreation process of a single offspring candidate solution. The overall offspring population size is given by the parameter λ. Individuals of a population represent possible candidate solutions to the optimization problem (2.1). Following the notations (2.2), the μ best individuals are selected as parents of the subsequent generation according to the ranking of their fitness values $\tilde{F}(\mathbf{y})$. An ES individual

$$a \coloneqq (\mathbf{y}, \mathbf{s}, \tilde{F}(\mathbf{y})) \tag{2.3}$$

comprises the object parameter vector $\mathbf{y} \in Y$, the individual's observed fitness $\tilde{F}(\mathbf{y})$, and optionally a set of individual strategy parameters $\mathbf{s}$. Notice, that in the simplest case the

observed fitness of an offspring individual $\mathbf{y}$ is equal to the corresponding objective function value $F(\mathbf{y})$. The distinction between $\tilde{F}(\mathbf{y})$ and $F(\mathbf{y})$ becomes necessary if the observed fitness $\tilde{F}(\mathbf{y})$ is the result of an evaluation process $F(\mathbf{y})$ which is disturbed by noise. Furthermore, the observed fitness may be the outcome of other search operators applied to the objective function. Especially in the context of hierarchical Evolution Strategies (meta-ES) the observed fitness $\tilde{F}(\mathbf{y})$ can be the result of another (internal) Evolution Strategy.

In general, the *selection operator* is deterministically based on the observed fitness ranking of the candidate solutions. Since it reduces the offspring population to the original size, it is also referred to as truncation selection. The number of candidate individuals considered for selection is distinguished via the "plus" and "comma" notations, see (2.2). "Plus"-selection or elitist selection does not take into account the age of a candidate solution. That is, the μ best of $\mu + \lambda$ individuals are selected from both the former parental as well as the current offspring individual set. As a result, the selection is elitist, i.e. the parents represent the μ all-time best candidate solutions to the optimization problem. This selection scheme has the benefit, that the Evolution Strategy will not diverge from good solutions. On the other hand, this behavior may lead to stagnation in the neighborhood of local optima. While the best-so-far candidate solution is most probably lost when considering "comma"-selection, it provides a remedy to the stagnation behavior near local optima as it allows for a more unbiased exploitation of the search space. This selection scheme is also referred to as non-elitist selection. The μ parent individuals are deterministically selected from the λ offspring candidate solutions. Thus individuals die out after one iteration step and only the best offspring (the youngest individuals) survive to the next generation. In the context of selection the notation

$$y_{m;\lambda}, \quad 1 \leq m \leq \lambda \tag{2.4}$$

refers to the mth best out of λ offspring by means of their fitness values (i.e., in case of minimization the offspring with the mth smallest fitness value). Notice, the proportion of the parental population size μ relative to the number of offspring λ is referred to as *truncation ratio*

$$\vartheta = \frac{\mu}{\lambda}. \tag{2.5}$$

Regarding the *variation operator*, it can be separated into a recombination and a mutation step. Variation is applied to provide a diverse population. To this end, it combines information from multiple parents to generate new offspring individuals. According to (2.2), for recombination $2 < \rho \leq \mu$ parent individuals are chosen randomly out of the μ parents. One of the most commonly used recombination principles is intermediate recombination. Intermediate recombination is denoted by a subscript I within the ES notation, i.e. $(\mu/\rho_I \overset{+}{,} \lambda)$. It makes use of the average value of all ρ parents, i.e. intermediate recombination calculates their center of mass. The center of mass of the considered parent individuals is also referred to as the (parental) centroid

$$\langle \mathbf{y} \rangle = \frac{1}{\rho} \sum_{k=1}^{\rho} \mathbf{y}_k, \quad 1 < \rho \leq \mu. \tag{2.6}$$

The most commonly used choice is $\rho = \mu$. A generalization of intermediate recombination is provided by weighted multi-recombination, $(\mu/\rho_W \, ^+_, \, \lambda)$. There, a weighted average over the considered parent individuals is calculated. The weights may depend on the parental fitness values for greater heredity of information from better parent individuals. Considering equal weights intermediate recombination is included within the concept of weighted recombination. Another recombination approach is dominant recombination which is denoted by $(\mu/\rho_D \, ^+_, \, \lambda)$. In this case, for each component of the object parameter vector a single parent is drawn uniformly from all ρ parents to hand over the value of its respective component. In contrast to dominant recombination, intermediate ($\rho = \mu$) and weighted multi-recombination result in the same single point for all offspring. That is, they alone do not create variation within the new population and mutation is necessary to provide the desired population diversity. Conclusively, all offspring are then generated by application of the mutation operator on the same single object parameter vector, i.e. the parental centroid. Generally, mutation is performed by adding a vector $\mathbf{z}_l$ drawn from a multivariate distribution with zero mean and covariance matrix $C \in \mathbb{R}^{N \times N}$. Thus a new offspring population of size λ is obtained as

$$\mathbf{y}_l = \langle \mathbf{y} \rangle + \mathbf{z}_l, \qquad l = 1, \ldots, \lambda. \tag{2.7}$$

Mutation therefore is unbiased as it does not point in direction of improved fitness in expectation. Especially in the context of real-valued search spaces, the normal distribution $\mathcal{N}(0, C)$ has some beneficial features for the design of the mutation operator. On the one hand, it provides a stable distribution since sums of independent normally distributed random variables are again normally distributed. On the other hand, the normal distribution is suitable to implement isotropic mutations which result in maximum entropy. The isotropic mutation distribution follows $\sigma\mathcal{N}(0, I)$. It is invariant under rotations around its mean. Both properties simplify the theoretical analysis of Evolution Strategies considerably.

The standard deviation $\sigma > 0$ is referred to as the mutation strength of the mutation operator. The mutation strength may loosely be regarded as step size of the variation step. It regulates the diversity between the offspring of a single generation. Albeit neither intermediate nor weighted multi-recombination alone do support the diversity of the population, their application provides an advantage to Evolution Strategies. This beneficial property of recombination is well-known as the principle of *genetic repair*. As elaborated in [Beyer, 2001], *genetic repair* extracts the similarities from the recombined individuals of the population. For intermediate recombination with $\rho = \mu$ the averaging reduces the step length taken in adverse directions by a factor of about $\sqrt{\mu}$ but rather does not affect the step length in favorable directions.

A conceptual algorithm of the standard $(\mu/\rho \, ^+_, \, \lambda)$-ES is presented in Alg. 2.1. The repeated interaction of variation (lines 3–7) and selection (lines 8–10) drives the parental population in direction of the optimizer. The iterative process stops if a predefined termination condition is satisfied, e.g. after the maximum number of function evaluations or iteration steps (generations) has been reached, or after having approached an acceptable target precision. More comprehensive overviews of evolution strategies are provided in [Beyer and Schwefel, 2002; Hansen et al., 2015].

The behavior of an Evolution Strategy is usually determined by strategy specific parame-

Algorithm 2.1 The $(\mu/\rho \overset{+}{,} \lambda)$ Evolution Strategy.

1: Initialize parent population $P_\mu = \left\{a_1, \ldots, a_\mu\right\}$.
2: **repeat**
3: Generate offspring population P_λ of size λ by application of:
4: Randomly select ρ out of μ parents from P_μ.
5: Recombine the ρ selected individuals to build a single offspring $\langle \mathbf{y} \rangle$.
6: Mutate the objective parameter vector $\langle \mathbf{y} \rangle$ of the individual.
7: Measure the fitness $\tilde{F}(\mathbf{y}_l)$ of the offspring $\mathbf{y}_l = \langle \mathbf{y} \rangle + \mathbf{z}_l$.
8: Select the new parent population from either
9: the offspring population P_λ ("comma"-selection) or
10: the offspring P_λ and former parent population P_μ ("plus"-selection).
11: **until** termination condition

ters. Specifically, for performance improvements the strategy parameters have to be chosen appropriately. A distinction is made between exogenous and endogenous strategy parameters. Those parameters that remain invariable during the optimization process are called exogenous strategy parameters. Exogenous strategy parameters usually include but are not necessarily restricted to learning rates, populations sizes, the mixing number ρ, or, in the context of meta-ES, the isolation time γ. On the contrary, endogenous strategy parameters are dynamically controlled internally during the evolution. However, this distinction is inconclusive and may vary depending on the ES under consideration. The internal adaptation of strategy specific parameters is necessary as ES represent dynamic processes with initial parameter settings which might become inappropriate when approaching the optimizer. A common example for an endogenous parameter is the mutation strength. The adaptation techniques of the endogenous strategy parameters are classified into three groups. Parameter control can be accomplished via statistical rule-based techniques, self-adaptation, or through hierarchically organized ES. The next section provides a brief presentation of the most commonly applied mutation strength adaptation methods in the field of Evolution Strategies.

2.1. Mutation strength adaptation techniques

The performance of Evolution Strategies (ES) depends on the distribution of the offspring population in the search space. Adaptation of the mutation strength σ regulates the extend of variation (or roughly the step-length of the search steps) used to generate offspring from parents. Thus optimal σ control is able to bias the evolution process towards beneficial search space regions. There are basically four established methods to learn/control the mutation strength simultaneously to the evolution of the object parameter: the 1/5-rule [Rechenberg, 1973], σ-self adaptation (σSA) [Rechenberg, 1973; Schwefel, 1977], cumulative step size adaptation (CSA) [Ostermeier et al., 1994], and hierarchically organized ES (meta-ES) [Rechenberg, 1978; Herdy, 1992; Rechenberg, 1994]. Each of this adaptation techniques can successfully be integrated into Alg. 2.1 in between lines 10 and 11.

Understanding and analyzing the working principles of these adaptation techniques by considering the ES in conjunction with the objective functions to be optimized allows for deeper insights into the dynamical behavior of ES as well as for an advantageous choice of strategy (and adaptation) specific parameters. At this point the four mutation strength adaptation techniques are recapped in order to provide an overview as well as a basis for the theoretical investigations in the subsequent sections.

2.1.1. The $1/5$th rule

An early rule-based mutation strength adaptation approach is the $1/5$th rule, [Rechenberg, 1973]. It is based on measurements of the success probability of the offspring individuals of a single generation. The success probability is the ratio of the successful offspring to all offspring individuals. The $1/5$th rule is motivated by the following considerations: On linear functions isotropic mutation operators have the success probability $1/2$. That is, on average 50% of the offspring will be an improvement over the parental centroid. This observation can be locally transferred to general smooth functions, since smooth functions can be locally approximated by the linear part of their Taylor expansions. Thus for small mutation strengths σ, i.e. small variances of the isotropic mutation operator, the success probability becomes $1/2$. On the other hand, it can be observed that the success rate on most non-linear fitness environments is indeed decreasing with increasing mutation strength. This motivates the idea to increase the mutation strength if large success rates are observed and to decrease σ for small success rates, respectively. The $1/5$th threshold value originates from theoretical investigations on the corridor as well as on the sphere function. These functions are thought to represent opposing special cases of nonlinear smooth functions. After having derived the optimal success rates for the $(1+1)$-ES on these functions, Rechenberg [Rechenberg, 1973] suggested to use a compromise value of $1/5$ as the success rate which determines whether to reduce or increase the mutation strength. The $1/5$ rule is usually used in $(1+1)$-ES, since other Evolution Strategies exhibit different success probabilities. Particularly, it is neither applicable to multi-modal optimization problems nor under the influence of fitness noise. Hence, in practical applications it has been gradually substituted by novel approaches while the respective conceptual insight remains useful.

2.1.2. σ self-adaptation

Self-adaptation represents a strategy parameter control mechanism which complies with the evolution principles. Alike the object parameter vector, in self-adaptation also the endogenous strategy parameters are exposed to variation and selection operators. Considering mutation strength control a popular approach is denoted σ self-adaptation (σSA). It was developed by Rechenberg who introduced the concept of inheritance of individual mutabilities to the field of Evolution Strategies, [Rechenberg, 1973]. First analyses of the $(1,\lambda)$-ES on the sphere model were continued by Schwefel and Beyer, [Schwefel, 1975, 1977; Beyer, 1995]. Later in [Beyer, 2001], the complete investigation of the $(\mu/\mu,\lambda)$-ES was carried out. This was followed by the consideration of other fitness environments, like ridge functions [Meyer-Nieberg and Beyer, 2008], or a subset of positive definite quadratic

forms [Finck, 2011]. The analysis of σSA on positive definite quadratic forms, also referred to as the ellipsoid model, was performed in [Beyer and Melkozerov, 2014] and extended to the noisy case in [Melkozerov and Beyer, 2015]. Important results of these analyses are provided in more detail in Chapters 3, and Chapter 6, respectively.

Regarding the working principles of σSA, in each iteration the offspring candidate solutions are generated together with an individual mutation strength σ_l. The mutation strength σ can be interpreted as an intrinsic scaling factor. It is derived from the average mutation strength of the best individuals of the preceding generation $\langle\sigma\rangle$ and is varied by multiplication with a log-normally distributed random number

$$\sigma_l = \langle\sigma\rangle \exp\left(\tau \mathcal{N}(0,1)\right). \tag{2.8}$$

This mutation is performed multiplicatively in order to always guarantee a positive standard deviation σ of the offspring distribution. According to Eq. (2.8), the algorithm controls σ by use of the exogenous learning parameter τ. It determines the rate and accuracy of the self-adaptation process. According to [Beyer, 1995], the standard mutation strength learning parameter setting is $\tau = 1/\sqrt{2N}$. The offspring are generated by adding vectors z_l of normally distributed random numbers with mean zero and individual standard deviation σ_l to the parental centroid of the preceding generation

$$y_l = \langle y\rangle + \sigma_l \mathcal{N}(0, I). \tag{2.9}$$

After identification of the best offspring individuals, these accumulate their individual mutation strengths within the centroid

$$\langle\sigma\rangle = \frac{1}{\mu}\sum_{i=1}^{\mu}\sigma_{m:\lambda}. \tag{2.10}$$

By using intermediate recombination for those σ_l of the best offspring, their information is again passed to the subsequent generation. Following this procedure, the individuals are supposed to adapt a nearly optimal mutation strength during the evolution process.

Regarding small population sizes μ the self-adaptation faces the problem of selection noise. That is, advantageous offspring candidate solutions may be realized by use of rather poor mutation strengths and vice versa. Consequently, the evolution may decelerate if the selected direction z_l and standard deviation σ_l are not positively correlated. This phenomenon can lead to major stochastic fluctuations in σ which may lead to very small mutation strength realizations. Since evolution favors short-term success, the strategy then approaches a local optimum or even ends up exhibiting premature convergence in great distance from the optimizer. Considering intermediate recombination in combination with an appropriate parental population size the magnitude of the σ fluctuations can be implicitly regulated. Recombination then causes a reduction of the magnitude of mutation strength fluctuations and biases $\log\sigma$ to larger values [Hansen, 2006a]. In the context of constant fitness noise disturbances, this bias in fact is considered to be a desirable property. That is, the ES tends to increase small mutation strengths up to a magnitude which is sufficiently large enough to provide beneficial information to the fitness function, cf. [Meyer-Nieberg, 2007].

2.1.3. Cummulative step size adaptation

Another common approach to mutation strength adaptation is non-local derandomized adaptation, or cumulative step size adaptation (CSA), respectively. This mutation strength control mechanism has been introduced in [Ostermeier et al., 1994] and is popular due to its use in the CMA-ES [Hansen and Ostermeier, 2001]. It directly addresses the problem of selection noise as explained above by collecting a record of information over multiple previous generations. The performance analyses of the CSA [Arnold and Beyer, 2004] reveal its potential for near optimal mutation strength adaptation even for rather small population sizes and independent from the search space dimension. This paragraph briefly motivates the principles of CSA. The reader is referred to [Hansen, 2006b] for a more comprehensive introduction into cumulative step size adaptation and the way its standard strategy parameter settings are determined.

Starting from an initial point, e.g. $\mathbf{s}^{(0)} = \mathbf{0}$, the cumulative step size adaptation compiles a so-called search path $\mathbf{s} \in \mathbb{R}^N$. This is done by implementing a fading record of past steps taken by the strategy according to

$$\mathbf{s}^{(g+1)} \leftarrow (1-c)\mathbf{s}^{(g)} + \sqrt{\mu c(2-c)}\frac{\langle \mathbf{z} \rangle^{(g)}}{\sigma^{(g)}}. \tag{2.11}$$

The length of its memory is determined by the choice of the constant strategy parameter $c \in (0, 1)$ which is referred to as the cumulation parameter. CSA updates the mutation strength from generation g to $g + 1$ conforming to the rule

$$\sigma^{(g+1)} \leftarrow \sigma^{(g)} \exp\left(\frac{\|\mathbf{s}^{(g+1)}\|^2 - N}{2DN}\right), \tag{2.12}$$

with damping parameter $D > 0$ that scales the magnitude of the updates. Notice, update rule (2.12) is different from the original mutation strength update [Hansen and Ostermeier, 2001], in the way that it adapts σ based on the squared length of the search path rather than based on search path length [Arnold, 2002]. The variant in Eq. (2.12) is advantageous for theoretical investigations. With appropriately chosen parameters both variants often show a similar behavior. A suggestion of standard settings of c and D for CSA has been proposed in [Hansen, 1998] as

$$c = \frac{1}{\sqrt{N}} \quad \text{and} \quad D = \frac{1}{c}. \tag{2.13}$$

Including observations of weighted recombination operators, these recommendations for intermediate recombination have been updated in [Hansen and Ostermeier, 2001] to

$$c = \frac{2}{2+N} \quad \text{and} \quad D = 1 + \frac{1}{c}. \tag{2.14}$$

During the evolutionary process the decision whether the mutation strength is decreased or increased depends on the sign of the numerator $\|\mathbf{s}^{(g+1)}\|^2 - N$ in (2.12). Hence, the length of the evolution path is compared with its expected length under random selection. The basic

idea is that long search paths indicate that selected mutation vectors predominantly point in one direction and could be replaced with fewer but longer steps. A short search path suggests that the strategy is moving back and forth and thus should benefit from smaller step sizes. If the unconstrained setting with randomly selected offspring candidate solutions is considered the search path has the expected squared length of N. In this case, the mutation strength performs a random walk on log scale. That is, in expectation the logarithm of the mutation strength does not change at all.

The length of the evolution path is an intuitive and empirically well-validated goodness measure for the overall step length. Nevertheless, it fails to adapt nearly optimal step sizes on very noisy objective functions [Beyer and Arnold, 2003]. That is, when using rather large population sizes the CSA-ES is likely to exhibit premature convergence in the presence of severe fitness noise.

2.1.4. Hierarchically organized Evolution Strategies

Another way of mutation strength adaptation can be realized by application of hierarchically organized Evolution Strategies, similarly referred to as meta-ES. Their use can be motivated by interpreting the step size control as an optimization problem. Consequently, an evolutionary strategy can be applied to learn the optimal step size according to the underlying optimization problem itself. Acting this way, a two-level strategy is constructed. On the lower level multiple independent Evolution Strategies (inner ESs) with different step-sizes are operating in the search space of the original optimization problem. The upper level strategy (outer ES) operates in the strategy parameter space of the lower level strategies. That is, after some time of isolation the outer ES compares the performances of the inner ESs and adapts σ accordingly. Variation and selection are used on both levels. The formal meta-ES notation was introduced in [Rechenberg, 1978, 1994] and reads

$$[\mu'/\rho', \lambda'(\mu/\rho, \lambda)^{\gamma}]. \tag{2.15}$$

According to this notation, λ' populations conducting $(\mu/\rho, \lambda)$-ESs run in parallel over a number of γ generations. That is, the parameter γ determines the length of the so called isolation period of the inner ES. Each of these λ' inner ESs is realized with different strategy parameters that remain constant during the isolation period. The outer ES then selects those μ' populations which turn out to have the best strategy parameters w.r.t. a previously defined selection criterion. The way of recombination is specified by the parameter ρ'.

Of course, the adaptation by use of meta-ES is not limited to mutation strength but can be applied to other strategy parameters. In fact, hierarchically organized ESs have proven themselves useful for learning the optimal strategy parameters depending on the underlying optimization problem. For example, [Herdy, 1993] empirically investigated the problem of finding the optimal offspring population size and obtained near optimal values on hyperplane and sphere models. In [Herdy, 1992], Herdy also expanded the approach of hierarchically organized strategies to a third level aiming at optimal control of the isolation time of the inner strategies. In principle, adding hierarchy levels for the optimization of more strategy parameters is possible. But it should be mentioned that adding higher levels to the meta-ES becomes very expensive in terms of function evaluations.

A primary theoretical contribution to the topic of hierarchically organized strategies was presented in [Arnold and MacLeod, 2008] investigating multiple step size adaptation mechanisms including the $[1, 2(\mu/\mu_I, \lambda)^\gamma]$-meta-ES on the class of ridge functions. While the work of Arnold and MacLeod excluded the sharp ridge, that respective analysis of the meta-ES variant was accomplished in [Beyer and Hellwig, 2012]. Hierarchically organized strategies appeared to demonstrate the best potential on ridge functions of all adaptation techniques considered. With increasing isolation time γ, nearly optimal performance was achieved. Also in the presence of noise, meta-ES proved to be more robust than the other approaches [Arnold and MacLeod, 2008]. Considering the sphere model, [Beyer et al., 2009] examined the ability of meta-ES to optimally control the mutation strength, as well as the parental population size μ of the inner ESs. The theoretical analysis allowed for an improved understanding of the influence of the mutation strength control parameter on the performance of the meta-ES.

2.2. Covariance matrix adaptation

The mutation operator within Evolution Strategies generally samples new offspring candidate solutions according to a multivariate normal distribution. While mutation aims at variation by adding a vector of random variables with zero mean and standard deviation σ, it does not necessarily incorporate information about pairwise dependencies between the variables in the distribution. These interdependencies are represented by the covariance matrix of the distribution. That is, besides the ability of an evolution strategy to realize a near optimal mutation strength, the other major component of state-of-the-art Evolution Strategies is the adaptation of the covariance matrix.

Covariance matrix adaptation (CMA) is a method to iteratively learn a beneficial covariance matrix of the offspring distribution appropriate to the underlying fitness landscape. Without CMA the ES samples the mutation distribution independently in each component of the given coordinate system. This turns out to be adverse considering problems with fitness landscapes which exhibit elongated valleys not aligned to the coordinate system. Thus particularly in ill-conditioned fitness environments, the use of CMA provides a very efficient optimization approach by sampling from distributions with correlations.

By application of CMA, a second order model of the underlying objective is learned which is similar to the approximation of the inverse Hessian matrix in the Quasi-Newton method in classical optimization. In contrast to most classical methods, fewer assumptions on the nature of the underlying objective function are made. Only the ranking between candidate solutions is exploited for learning the sample distribution and neither derivatives nor additional function evaluations are required. CMA controls the full covariance matrix of the mutation distribution while it is invariant under coordinate changes. The approach was introduced by [Hansen and Ostermeier, 1996] and, together with cumulative step size adaptation (CSA), it is integral part of the well-known covariance matrix adaptation Evolution Strategy (CMA-ES), [Hansen and Ostermeier, 2001]. In combination with σ self-adaptation CMA is also applied within the covariance matrix self-adaptation Evolution Strategy (CMSA-ES), [Beyer and Sendhoff, 2008]. Particularly, current variants of these two algorithms can

be considered state-of-the-art in continuous domain evolutionary computation.

Alike the way of mutation strength control in CSA, the covariance matrix adaptation maintains a search path in order to accumulate mutation steps. It employs the best mutation vectors of the current or of multiple preceding generations (search path) in order to update the covariance matrix in such a way that the beneficial search directions will be more likely to be sampled in future generations. While covariance matrix adaptation appropriately distributes the mutations according to the underlying fitness environment, it is not able to include the corresponding mutation strength control. On the one hand the optimal overall mutation strength cannot be well approximated by the covariance matrix and on the other hand the appropriate learning rates for the covariance matrix update turn out to be too slow to provide useful alteration rates for the mutation strength [Hansen, 2006b]. By now, there exist distinct update variants that can improve the adaptation process, e.g. the rank-μ update of the covariance matrix. The reader is referred to [Hansen and Ostermeier, 2001; Beyer and Sendhoff, 2008; Hansen et al., 2015] for more comprehensive motivations.

2.3. Analysis technique: the dynamical systems approach

This preliminary chapter concludes with the introduction of the approach used for the theoretical analysis of the specific Evolution Strategies considered in this thesis. Regarding the dynamical behavior of Evolution Strategies, many investigation approaches have been conducted throughout the years. The approaches include the experimental running time comparisons of ES algorithms, experimental parameter tuning as well as theoretical considerations. Depending on the underlying optimization problem and the Evolution Strategy applied the theoretical analyses were performed in multiple ways. In 1995, the first theoretical framework for the analysis of self-adaptive ES was provided in [Beyer, 1995]. Other analyses [Arnold, 2007; Arnold and Beyer, 2010; Finck, 2011] that also considered CSA-ES variants were performed along the line developed in [Arnold, 2002]. The analysis approach, which turned out to be most successful in recent years, considers the ES together with the specific objective function as a dynamical system [Meyer-Nieberg and Beyer, 2012]. That is, the goal of the analysis is to determine the time evolution of the system. Since ES are probabilistic algorithms, this analysis concerns the dynamics of stochastic, most often non-linear, systems. In the remainder of this section the dynamical systems approach is presented with regard to the *sphere model* defined by the objective function $F(\boldsymbol{y}) = \sum_{i=1}^{N} y_i$.

The first theoretical framework of [Beyer, 1995] used approximate equations to describe the dynamics of self-adaptive Evolution Strategies. Before the dynamics of Evolution Strategies can be analyzed, the variables that characterize the system must be determined. Regarding Evolution Strategies, one is interested in studying the dynamical behavior of the fitness values, or the distance of candidate solutions from the optimizer (depending on the fitness model), as well as the dynamics of other endogenous strategy parameters that undergo self-adaptation, e.g. the mutation strength. The approach then aims at modeling and analyzing the evolution of these state variables over time. Let the random variable

$R^{(g)} = \|\mathbf{y}^{(g)} - \mathbf{y}^*\|$ denote the distance of the presently recommended search point $\mathbf{y}^{(g)}$ at generation g from the optimizer $\mathbf{y}^*$ and let σ refer to the mutation strength. The transition between consecutive states of the ES can then be interpreted as a Markov process

$$\begin{pmatrix} R^{(g+1)} \\ \sigma^{(g+1)} \end{pmatrix} \leftarrow \begin{pmatrix} R^{(g)} \\ \sigma^{(g)} \end{pmatrix}. \tag{2.16}$$

The derivation of closed-form equations that describe this transition is usually not possible. Making use of a step-wise approach to extract the key features of the process, one is able to obtain approximate equations that describe the change of the dynamical system, i.e. the progress with respect to the object parameter vector $\mathbf{y}$ as well as the corresponding mutation strength. The change of both random variables can then be divided into two parts: the expected change and related stochastic fluctuations. Conclusively, it is possible to express the system's state in generation $g + 1$ by use of the evolution equations

$$\begin{aligned} R^{(g+1)} &= R^{(g)} - \varphi(R^{(g)}, \sigma^{(g)}) + \epsilon_r(R^{(g)}, \sigma^{(g)}) \\ \sigma^{(g+1)} &= \sigma^{(g)} \left(1 + \psi(R^{(g)}, \sigma^{(g)})\right) + \epsilon_\sigma(R^{(g)}, \sigma^{(g)}). \end{aligned} \tag{2.17}$$

The evolution equations are stochastic difference equations which describe the systems change in one generation. The expected change in terms of the distance from the optimizer is expressed by the progress rate

$$\varphi(R^{(g)}, \sigma^{(g)}) = \mathrm{E}\left[R^{(g)} - R^{(g+1)} \mid R^{(g)}, \sigma^{(g)}\right]. \tag{2.18}$$

As it is depending on the present state of the dynamical system the progress rate provides a so-called local performance measure. The progress rate of an Evolution Strategy relies on the characteristics of the specific strategy. Furthermore, it is determined by the considered fitness environment, for instance, by the search space dimensionality.

Since the evolution of the mutation strength is generally realized by multiplication with a random variable, its relative expected change is of interest. Thus a different progress measure is used for the mutation strength dynamics. The progress measure is called the self-adaptation response (SAR) ψ and reads

$$\psi(R^{(g)}, \sigma^{(g)}) = \mathrm{E}\left[\frac{\sigma^{(g+1)} - \sigma^{(g)}}{\sigma^{(g)}} \,\middle|\, \sigma^{(g)}, R^{(g)}\right]. \tag{2.19}$$

The SAR function returns the expected relative change of the mutation strength between two consecutive generations.

Taking a look at the quantities ϵ_r and ϵ_σ, these represent the respective fluctuation parts of the evolutionary process. The distributions of these fluctuations are unknown and might be approximated by expansion into Gram-Charlier (or Edgeworth) series with respect to a reference density. Evidently, the conditional expectation of both fluctuation terms is zero. The variance remains to be determined which can be done using the evolution equations, themselves. Assuming that the stochastic terms $\epsilon_r, \epsilon_\sigma$ are appropriately approximated by a normal distribution, cutting off the expansion after the first term allows to determine the

standard deviation of the fluctuation term. This calculation of the second moments involves the corresponding second-order progress rate, and the second-order self-adaptation response, respectively. The treatment of the fluctuation terms is demonstrated in detail within [Meyer-Nieberg, 2007]. However, in many theoretical investigations the consideration of only the expected quantities is sufficient, since the effect of the fluctuations may be neglectable in the asymptotic limit case, i.e. considering search space dimensions $N \to \infty$. The ability to abandon the fluctuations allows to formulate more tangible system dynamics. The evolution equations without perturbation parts are generally referred to as deterministic evolution equations. The deterministic system of evolution equations reads

$$\begin{aligned} R^{(g+1)} &= R^{(g)} - \varphi(R^{(g)}, \sigma^{(g)}) \\ \sigma^{(g+1)} &= \sigma^{(g)} \left(1 + \psi(R^{(g)}, \sigma^{(g)})\right). \end{aligned} \tag{2.20}$$

System (2.20) serves well to derive general characteristics of an Evolution Strategy, e.g. the optimal mutation strength or the convergence rate. Such quantities are extracted from stationary (or steady) states of the evolution process. In the context of the sphere model, a steady state in a specific state variable of the deterministic system implies either $R^{(g+1)} = R^{(g)}$, or $\sigma^{(g+1)} = \sigma^{(g)}$, or the equality of a corresponding normalized quantity over subsequent generations. Demanding an equilibrium of the $R^{(g)}$ dynamics causes the stagnation of the ES in most cases.

Regarding the evolution equation of the normalized mutation strength commonly provides a more descriptive representation. It usually allows for the calculation of a stationary state without requiring a standstill of the $R^{(g)}$ dynamics. The assumption of the existence of such a steady state is initiated by evidence that maximal improvements during a single generations are connected to a mutation strength which scales with the distance to the optimizer. In the case of the *sphere model* the evolution equation of the normalized mutation strength is obtained as

$$\sigma^{*(g+1)} = \sigma^{*(g)} \left(\frac{1 + \psi(R^{(g)}, \sigma^{*(g)})}{1 - \frac{\varphi^*(R^{(g)}, \sigma^{*(g)})}{N}} \right), \tag{2.21}$$

with the sphere model specific normalizations

$$\varphi^* = \varphi \frac{N}{R^{(g)}} \quad \text{and} \quad \sigma^{*(g)} = \sigma^{(g)} \frac{N}{R^{(g)}}. \tag{2.22}$$

Note, the accurate normalization is determined by the fitness environment, the search space dimensionality N and the considered distance measure R, respectively.

The most advanced dynamical systems analysis approach on Evolution Strategies has been presented in [Beyer and Melkozerov, 2014] where the $(\mu/\mu_I, \lambda)$-σSA-ES on the ellipsoid model has been investigated. In that paper, a new progress measure was introduced: the quadratic progress rate. It considers the expected change of the squared components of the parameter vector during a single generation. The quadratic progress rate of the ith component is defined as

$$\varphi_i^{II}(\mathbf{y}^{(g)}, \sigma^{(g)}) = \mathrm{E}\left[(y_i^{(g)})^2 - (y_i^{(g+1)})^2 \mid \mathbf{y}^{(g)}, \sigma^{(g)} \right]. \tag{2.23}$$

While [Beyer and Melkozerov, 2014] completes the analysis of isotropic self-adaptive standard ES, a similar analysis of mutation strength control via CSA or by use of hierarchically organized Evolution Strategies is not advanced that much. The extension of the dynamical systems approach to these two kinds of mutation strength adaptation mechanisms is nontrivial and forms the major subject of the first part of this thesis.

Part I.

Analysis of mutation strength control on the ellipsoid model

3. The ellipsoid model

Theoretical investigation of evolution strategies applied to the optimization of the general case of positive definite quadratic forms (PDQFs) have hardly been carried out so far. In [Jägersküpper, 2006] the first theoretical analysis of evolution strategies on a special PDQF was performed. Considering the (1 + 1)-ES with isotropic mutation and the 1/5th-rule for mutation strength adaptation, the work succeeded in proving a running time of $O(\xi \cdot N)$ with ξ being the problem's condition number. The analysis was carried out by deriving the probability of a successful evolution step, i.e. an improvement of the current best fitness value, and then considering the behavior over multiple steps.

Other fitness models theoretically considered so far concerned the cigar function [Arnold, 2007; Arnold and Beyer, 2010] and another special case of PDQFs consisting of a mixture of two sphere models [Beyer and Finck, 2008]. These analyses were performed along the line developed in [Arnold, 2002]. Moreover, the investigations took into account population-based evolution strategies as well as other mutation strength adaptation techniques, i.e. CSA and σ self-adaptation, respectively. These investigations were able to extend earlier results and allowed for the determination of beneficial strategy parameter settings. On the contrary, using approximations they lack the mathematical thoroughness of the results obtained by Jägersküpper. Due to the inherent symmetries of the considered fitness models (cigar and mixture of two spheres, respectively), the dynamics in the $\mathbb{R}^N$ search space could be lumped together, thus reducing the dynamics to a few state variables describing the approach to the optimizer.

A different analysis direction was pursued in the publications of Beyer and Melkozerov [Melkozerov and Beyer, 2010; Beyer and Melkozerov, 2014] which examined the dynamics of the σSA-ES on more general PDQFs using the dynamical systems approach. That work introduced the component-wise quadratic progress rate as a new progress measure which is recapped in Sec. 3.2.1. While the work completed the analysis of isotropic self-adaptive standard ES, a similar analysis of CSA and meta-ES for σ control is not advanced that much.

The research questions in this work address the theoretical analysis the of the $(\mu/\mu_I, \lambda)$-ES in connection with mutation strength adaptation by CSA and meta-ES on the ellipsoid model. The focus is on the description of the evolutionary behavior by a system of difference equations. Based on the dynamical system, the analysis aims at the determination of advantageous (optimal) strategy parameters, convergences rates as well as the expected running times of the strategies.

Additionally, the second part of the thesis considers noisy optimization. Therefore, two contrasting noise models are taken into account on the ellipsoid model. The ability of a specific meta-ES variant is investigated to successfully approach the optimizer on the noisy sphere model. The focus is on the theoretical prediction of the population size as well as the

mutation strength adaptation. Finally, a population control evolution strategy which is able to deal with strong noise influences on the noisy ellipsoid model is developed.

Before the analysis of the mutation strength adaptation methods can be performed, the considered test function class has to be introduced. The motivation of the optimization problem is accompanied with important theoretical results needed within the analysis. At the end of this chapter, the final analysis results of the first thesis part are anticipated and compared to existing findings of σSA. This way, a holistic view of the mutation strength adaptation analysis on the ellipsoid model is provided which is thought to support the comprehensibility of the following chapters.

3.1. The fitness environment

Mutation strength adaptation is integrated into standard Evolution Strategies and analyzed in regard of their ability to solve an unconstrained optimization problem of the form

$$\min_{\mathbf{y}\in\mathbb{R}^N} F(\mathbf{y}). \tag{3.1}$$

As the objective function determines the fitness of a candidate solution, objective functions which provide a high level of generality are of interest. On the contrary, demanding generality usually comes with an increase of the difficulty level for theoretical analyses.

The function class to be considered throughout this thesis is a subset of quadratic functions: the family of positive definite quadratic forms (PDQFs). A positive definite quadratic form in $\mathbb{R}^N$ is a real-valued function of the form

$$Q(\mathbf{y}) = \sum_{i\leq j} q_{ij} y_i y_j. \tag{3.2}$$

Each quadratic form can be represented by a symmetric matrix $\mathbf{Q} \in \mathbb{R}^{N\times N}$

$$Q(\mathbf{y}) = \mathbf{y}^\top \mathbf{Q}\mathbf{y}. \tag{3.3}$$

The positive definiteness is consequently ensured by requiring

$$\mathbf{y}^\top \mathbf{Q}\mathbf{y} > 0 \quad \forall \mathbf{y} \in \mathbb{R}^N \setminus \{0\}. \tag{3.4}$$

Because each positive definite symmetric matrix can be transformed into diagonal form, without loss of generality each PDQF can be represented by an $N \times N$ diagonal matrix of the form

$$\mathbf{Q} = \operatorname{diag}(q_1, \dots q_N) \quad \text{with } q_i \geq 0 \quad \forall i = 1, \dots, N. \tag{3.5}$$

Notice, that in the case of (3.5) the diagonal elements q_i directly represent the eigenvalues of the matrix $\mathbf{Q}$.

Since the level set of a PDQF defines an ellipsoid in the N-dimensional search space, the fitness environment considered is also referred to as *the ellipsoid model*. The objective function which defines the fitness environment reads

$$F(\mathbf{y}) = \sum_{i=1}^{N} q_i y_i^2, \quad q_i > 0. \tag{3.6}$$

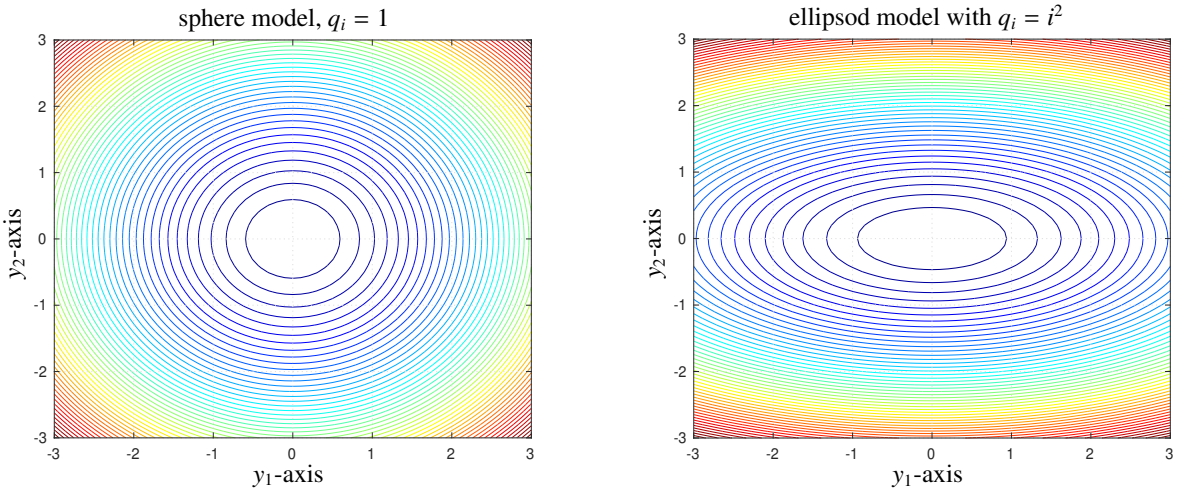

Figure 3.1.: Illustration of the contour lines of the ellipsoid models $q_i = 1, \forall i$, and $q_i = i^2$ in the two dimensional search space ($N = 2$).

Here, the parameter N represents the corresponding search space dimensionality and q_i are referred to as the coefficients of the ellipsoid model. The ellipsoid model represents the general case of PDQFs for the $(\mu/\mu_I, \lambda)$-ES with isotropic mutations. Due to the isotropy of the mutation vectors, the ES is invariant to arbitrary rotations of the coordinate system. Regarding the ellipsoid model (3.6) the optimizer of the corresponding optimization problem (3.1) resides at the origin of the coordinate system, $\mathbf{y}^* = 0$.

In consistency with the well-known sphere model, the name ellipsoid model refers to the shape of the contour lines of the objective function F which define ellipses in the two-dimensional search space. An illustration of the contour lines of the two-dimensional sphere model, and the ellipsoid model $q_i = i^2$ is provided in Fig. 3.1. Special cases of the ellipsoid model include the sphere model ($q_i = 1\ \forall i$), the cigar function ($q_1 = 1,\ q_i = \xi\ \forall i \neq 1$) and the discuss function ($q_1 = \xi,\ q_i = 1\ \forall i \neq 1$) with condition number $\xi \in \mathcal{R}_+$.

Throughout the analyses, three ellipsoid model test cases are frequently considered for the verification of the theoretical results. The first test case represents the sphere model

$$q_i = 1, \quad \forall i = 1, \ldots, N, \tag{3.7}$$

which is used to validate the compliance of the conclusions obtained in this thesis with existing sphere model results. The other test environments are exemplarily chosen as the ellipsoid models with coefficients

$$q_i = i, \quad \forall i = 1, \ldots, N, \tag{3.8}$$

and

$$q_i = i^2, \quad \forall i = 1, \ldots, N. \tag{3.9}$$

The latter ellipsoid models are taken into account to consider different magnitudes of the problem conditioning. Considering a solution to the optimization problem, the condition number is a measure of the achievable maximal numerical precision. A problem conditioning close to one is denoted *well-conditioned* while large condition numbers correspond to

Algorithm 3.1 The standard $(\mu/\mu_I, \lambda)$-ES with constant mutation strength

```
1: Initialize (σ, ⟨y⟩, μ, λ, γ);
2: g ← 1;
3: repeat
4:     for l ← 1 to λ do
5:         y_l ← ⟨y⟩ + σ N_l(0, I);
6:         F_l ← F(y_l);
7:     end for
8:     ⟨y⟩ ← (1/μ) Σ_{m=1}^{μ} y_{m;λ};
9:     g ← g + 1;
10: until termination condition
11: return [⟨y⟩, F(⟨y⟩)];
```

ill-conditioned problems. Regarding ill-conditioned functions, small changes in the components of the object parameter vector that are associated to huge eigenvalues result in large changes of the output quantity. The condition number of the respective problems can be expressed in terms of the ratio between the largest and the smallest eigenvalue of the system's Hessian matrix. That is, taking into account (3.3) the condition number is defined as

$$\xi(Q) = \frac{\kappa_{\max}(Q)}{\kappa_{\min}(Q)}, \tag{3.10}$$

where $\kappa_{\max}(Q)$ and $\kappa_{\min}(Q)$ are the maximal and minimal eigenvalues of Q, respectively. For the special cases mentioned above, this implies that the condition number is identical to the largest eigenvalue of the corresponding diagonal matrix Q, i.e. the largest diagonal element q_i of Q. Accordingly, the condition numbers of the ellipsoid models (3.8) and (3.9) are N and N^2, respectively.

3.2. Evolution Strategies on the ellipsoid model

The basic Evolution Strategy under consideration within this thesis is the $(\mu/\mu_I, \lambda)$-ES with isotropic mutations. Excluding a mutation strength control mechanism, the corresponding pseudo code is presented in Alg. 3.1. During the following Chapters, variants of this Evolution Strategy differing in the kind of mutation strength adaptation or equipped with population (and distribution) update mechanisms will be investigated. The algorithm illustrates a standard $(\mu/\mu_I, \lambda)$-Evolution Strategy which operates with constant strategy parameters. It generates a population of λ offspring. This is done by adding the product of the mutation strength σ and a vector of independent, standard normally distributed components to the centroid $\langle \mathbf{y} \rangle$ of the previous generation. The μ best candidates (w.r.t. their function values F_l) are used to build the new parental centroid $\langle \mathbf{y} \rangle$. This procedure is iterated until a predefined termination criterion is met, e.g. the optimizer has been approached up to a predefined precision, or a maximal number of iterations has been performed, respectively. A mutation strength control mechanism (alike σSA or CSA) can be easily integrated into the algorithm.

Therefore, the according mutation strength update is inserted after the calculation of the parental centroid.

In the following Chapters, two approaches for mutation strength adaptation will be applied to Alg 3.1: cumulative step-size adaptation and meta-ES. For each approach the resulting dynamical behavior is theoretically analyzed on the fitness environment defined by the ellipsoid model. This description allows for conclusions regarding beneficial strategy parameter settings. Hence, predictions of the respective convergence rates and expected running times can be provided. In the first place, the basic theoretical results of Alg. 3.1 needed for the analyses are presented in the next paragraphs. Furthermore, the findings obtained in the context of σ self-adaptation ES on the ellipsoid model are summarized.

3.2.1. Measuring the evolutionary progress

Let's consider important developments relevant for the investigations on the ellipsoid model. These have been obtained within the analyses of the σSA-ES [Melkozerov and Beyer, 2010; Beyer and Melkozerov, 2014]. The results keep their validity in the context of mutation strength adaptation by CSA-ES as well as by meta-ES.

The progress measure of interest in the conducted analyses addresses the expected change in the search space that can be realized by the evolution strategy in direction of the optimizer. Notice, that unless otherwise stated the parental centroid $\langle \mathbf{y} \rangle^{(g)}$ recommended by Alg. 3.1 as the currently best candidate solution will be identified with the parental parameter vector $\mathbf{y}^{(g)}$ during this thesis. Accordingly, the expected progress of an ES is measured between two consecutive parental centroids $\mathbf{y}^{(g)}$ and $\mathbf{y}^{(g+1)}$.[1]

The progress rate of the $(\mu/\mu_I, \lambda)$-ES along the ith axis of the ellipsoid model (3.6) is defined as the expected change of the parental parameter vector component y_i from generation g to generation $g+1$

$$\varphi_i := \mathrm{E}\left[y_i^{(g)} - y_i^{(g+1)} \,\middle|\, \mathbf{y}^{(g)}, \sigma^{(g)} \right]. \tag{3.11}$$

This so-called first-order progress rate is depending on the parameter vector and mutation strength states in generation g. For reasons of clarity and comprehensibility the abbreviation

$$\Sigma q := \sum_{i=1}^{N} q_i, \tag{3.12}$$

is used for the sum of the ellipsoid model coefficients, or the trace of the matrix Q corresponding to the PDQF (3.5), respectively.

According to [Melkozerov and Beyer, 2010], the first order progress rate is derived as

$$\varphi_i(\sigma^{(g)}) = \frac{\sigma^{(g)} c_{\mu/\mu,\lambda} q_i y_i^{(g)^2}}{\sqrt{\sum_{j=1}^{N} q_j^2 y_j^{(g)^2}}}. \tag{3.13}$$

Representation (3.13) is asymptotically exact in the limit of large search space dimensions $N \to \infty$. In order to reduce the dependence of the progress rate on the location of the

[1] Refraining to conserve the notation $\langle \mathbf{y} \rangle^{(g)}$ throughout the analyses allows for more neatly arranged equations.

search space parameter vector, two normalizations are introduced. The normalized mutation strength is constituted by multiplication of the mutation strength with the quotient of Σq and the square root in the denominator of (3.13)

$$\sigma^{*(g)} := \frac{\sigma^{(g)}\Sigma q}{\sqrt{\sum_{j=1}^{N} q_j^2 y_j^{(g)^2}}}. \tag{3.14}$$

This mutation strength normalization corresponds to the fitness environment determined by the ellipsoid model (3.6). Notice, that by assuming $q_i = 1 \forall i$ Eq. (3.14) includes the established mutation strength normalization on the sphere model. Further, a progress rate normalization is obtained by

$$\varphi_i^* := \varphi_i \Sigma q. \tag{3.15}$$

These normalizations allow to obtain convenient and condensed equations as representation of the evolution dynamics. By inserting the normalized quantities into (3.13), the normalized progress rate was calculated in [Melkozerov and Beyer, 2010]. It reads

$$\varphi_i^*(\sigma^*) = \sigma^* c_{\mu/\mu,\lambda} q_i y_i. \tag{3.16}$$

Notice, the term $c_{\mu/\mu,\lambda} := e_{\mu,\lambda}^{1,0}$ denotes the progress coefficient of the $(\mu/\mu_I, \lambda)$-ES. It is a special case of the *generalized progress coefficients* introduced in [Beyer, 2001]

$$e_{\mu,\lambda}^{a,b} = \frac{\lambda - \mu}{\sqrt{2\pi}^{a+1}} \binom{\lambda}{\mu} \int_{-\infty}^{\infty} (-t)^b \mathrm{e}^{-\frac{a+1}{2}t^2} \left(1 - \Phi(t)\right)^{\lambda-\mu-1} \Phi(t)^{\mu-a} \mathrm{d}t, \tag{3.17}$$

where $\Phi(t)$ represents the cumulative distribution function of the standard normal variate. They take into account the impact of order statistics when selecting the μ best of of λ offspring on the progress rate derivation and rely on the truncation ratio of the ES.

The first-order progress rate yields good component-wise predictions of the expected approach of the parental centroid towards the optimizer as long as the distance to the optimizer is sufficiently large compared to the respective progress rate values. Otherwise the perturbations of the evolutionary process superimpose the mean value dynamics (3.11). That is, the predictive quality of the first-order progress rate decreases when approaching the optimizer [Melkozerov and Beyer, 2010]. Consequently, the more stable quadratic progress measure was conceived. The quadratic progress rate of the $(\mu/\mu_I, \lambda)$ evolution strategy along the ith axis of the ellipsoid model (3.6) is the expected change of squared component y_i^2 of the parental centroid between two consecutive generations g and $g+1$

$$\varphi_i^{II} := \mathrm{E}\left[y_i^{(g)^2} - y_i^{(g+1)^2} \,\middle|\, \mathbf{y}^{(g)}, \sigma^{(g)} \right]. \tag{3.18}$$

It has first been introduced in [Beyer and Melkozerov, 2014]. There, the derivation yields

the asymptotically exact formulation

$$\begin{aligned}\varphi_i^{II}(\sigma^{(g)}) =& \frac{2\sigma^{(g)} c_{\mu/\mu,\lambda} q_i y_i^{(g)^2}}{\sqrt{\sum_{j=1}^N q_j^2 y_j^{(g)^2}}\sqrt{1+\frac{\sigma^{(g)}\sum_{j=1}^N q_j^2}{2\sum_{j=1}^N q_j^2 y_j^{(g)^2}}}} \\ & - \frac{\sigma^{(g)^2}}{\mu}\left(1+\frac{\left((\mu-1)e_{\mu,\lambda}^{2,0}+e_{\mu,\lambda}^{1,1}\right)q_i^2 y_i^{(g)^2}}{\sum_{j=1}^N q_j^2 y_j^{(g)^2}\left(1+\frac{(\sigma^{(g)})^2\sum_{j=1}^N q_j^2}{2\sum_{j=1}^N q_j^2 y_j^{(g)^2}}\right)}\right).\end{aligned} \tag{3.19}$$

This first, rather cumbersome, formulation implicitly relies on the search space dimension. Following the sphere model terminology, Eq. (3.19) is sometimes referred to as the "N-dependent" quadratic progress rate representation. Normalization according to (3.11), and (3.15), as well as abandoning the $\sigma^2/2$ terms in the denominators, yields

$$\varphi_i^{II*}(\sigma^*) = 2y_i\varphi_i^*(\sigma^*) - \frac{\sigma^{*2}}{\mu\Sigma q}\left[\sum_{j=1}^N q_j^2 y_j^2 + \left((\mu-1)e_{\mu,\lambda}^{2,0} - e_{\mu,\lambda}^{1,1}\right)q_i^2 y_i^2\right]. \tag{3.20}$$

As demonstrated in [Beyer and Melkozerov, 2014], neglecting the $\sigma^2/2$ terms is admissible if the condition

$$\sigma^{*2}\sum_{j=1}^N q_j^2 \Big/ \left(2(\Sigma q)^2\right) \ll 1 \tag{3.21}$$

holds. In the form of Eq. (3.20), the quadratic progress rate formula depends on the first-order progress rate φ_i^*, cf. Eq. (3.16), as well as on a negative term which corresponds to the progress rate loss.

Because expression (3.20) is rather complex, for the theoretical analysis a simplified φ_i^{II*} formula was derived in [Beyer and Melkozerov, 2014]. Under the assumption that the search space dimensionality is considerably greater than the parental population size and if there exists no dominating coefficient q_i, i.e. if the conditions

$$N \gg \mu \quad \text{and} \quad \forall i \,:\, \sum_{j\neq i} q_j^2 \gg q_i^2 \tag{3.22}$$

are fulfilled, the normalized quadratic progress rate is asymptotically equal to

$$\varphi_i^{II*}(\sigma^*) \simeq 2\sigma^* c_{\mu/\mu,\lambda} q_i y_i^2 - \frac{\sigma^{*2}}{\mu\Sigma q}\sum_{j=1}^N q_j^2 y_j^2. \tag{3.23}$$

Renormalization can be obtained by applying (3.14) and (3.15) and yields

$$\varphi_i^{II}(\sigma^{(g)}) = \frac{2\sigma^{(g)} c_{\mu/\mu,\lambda} q_i y_i^{(g)^2}}{\sqrt{\sum_{j=1}^N q_j^2 y_j^{(g)^2}}} - \frac{\sigma^{(g)^2}}{\mu}. \tag{3.24}$$

The quadratic progress rate can be used to describe the expected approach to the optimizer for each squared component of the parental centroid [Beyer and Melkozerov, 2014]. It exhibits the typical features of a well-defined progress measure, namely a gain and a loss term which depend on the mutation strength. This ensures the existence of an optimal mutation strength. Additionally, the loss term is inversely proportional to the parental population size μ. That is, the genetic repair effect of recombination can be observed on the ellipsoid model. Nevertheless, it has to be mentioned that the derivation of the asymptotic quadratic progress rate φ_i^{II} is accompanied with a loss of generality as ellipsoid models with dominating coefficients have to be excluded from the analysis. For example, the predictions obtained will not be compatible to the discuss function ($q_1 = \xi,\ q_i = 1\ \forall i \neq 1$ with condition number $\xi \gg 1$). Making use of the "N-dependent" representation in Eq. (3.19) would allow for the incorporation of the general ellipsoid model case. Unfortunately, the derivation of an analytical formula describing the mutation strength transition becomes impractical. However, the quadratic progress rate sufficiently approximates the expected one-generation change of the evolutionary system on multiple ellipsoid models. Its renormalized version (3.24) will be the basis for the derivation of the evolution equations considering CSA-ES and meta-ES in the next chapters.

Eventually, at this point another abbreviation has to be introduced in order to reduce the length of the the upcoming equations. Defining

$$R_q(\mathbf{y}^{(g)}) \coloneqq \sqrt{\sum_{j=1}^{N} q_j^2 y_j^{(g)^2}}, \tag{3.25}$$

this quantity, for instance, can be retrieved in the denominator of the quadratic progress rate (3.24). In the context of the ellipsoid model, the term $R_q(\mathbf{y}^{(g)})$ is denoted as weighted residual distance to the optimizer. It can be interpreted as the weighted norm of an objective parameter vector $\mathbf{y} \in \mathbb{R}^N$ with weights $q_j^2,\ j = 1, \ldots, N$, according to the ellipsoid coefficients. Notice, considering the sphere model ($q_j = 1,\ \forall j = 1, \ldots, N$) this residual distance resembles the Euclidean norm of the $\mathbb{R}^N$ which is commonly used to measure the distance from the optimizer.

Having a look at the Evolutions Strategy in Alg. 3.1, the ES evolves the populations without use of mutation strength control, i.e. $\sigma^{(g)} = \sigma = const.$. In this case, the ES approaches a residual steady state distance in the vicinity of the optimizer of the ellipsoid model in the long-run. Within this steady state the strategy is not longer able to generate any progress in expectation. That is, under consideration of (3.25) the residual steady state distance can be derived by stetting the progress rate formula (3.24) to zero

$$\frac{2\sigma c_{\mu/\mu,\lambda} q_i y_i^{(g)^2}}{\sqrt{\sum_{j=1}^{N} q_j^2 y_j^{(g)^2}}} - \frac{\sigma^2}{\mu} = 0. \tag{3.26}$$

Multiplying both sides of (3.26) with the ellipsoid coefficient q_i, and taking the sum over all

components $i = 1, \ldots, N$ yields

$$\frac{2\sigma c_{\mu/\mu,\lambda} R_q^2(\mathbf{y}^{(g)})}{\sqrt{\sum_{j=1}^{N} q_j^2 y_j^{(g)^2}}} - \frac{\sigma^2 \Sigma q}{\mu} = 0. \tag{3.27}$$

Solving this equation for the weighted residual distance $R_q(\mathbf{y}^{(g)})$ results in a formula that predicts the residual steady state distance

$$\hat{R}_{ss} = \frac{\sigma \Sigma q}{2\mu c_{\mu/\mu,\lambda}}. \tag{3.28}$$

Notice, that (3.28) generalizes the steady state distance on the sphere model presented in [Beyer et al., 2009]. The steady state depends on the mutation strength σ, the population sizes μ and λ, as well as the considered ellipsoid model and its dimensionality. After evolving over a sufficiently long period of time the ES presented in Alg. 3.1 approaches this steady state.

3.2.2. Performance analysis results of σ-self-adaptation

The conclusive analysis of the $(\mu/\mu_I, \lambda)$-σ-SA Evolution Strategy on the ellipsoid model was carried out in [Beyer and Melkozerov, 2014]. On the basis of the quadratic progress rate (3.24) the authors study the dynamical behavior of the evolutionary system. Making use of the dynamical systems approach the system can be modeled by a set of nonlinear difference equations. In the system's steady state it is possible to find closed-form solutions which were verified via experimental runs of the real $(\mu/\mu_I, \lambda)$-σSA-ES. The approach allowed for an analytical calculation of an approximate learning parameter formula for the σSA. Here, the main results are recapped to allow performance comparisons to the mutation strength adaptation analyzes performed in this thesis.

While the quadratic progress rate φ_i^{II}, (3.24), characterizes the component-wise expected change in the search space, the expected relative change of the mutation strength is monitored by the problem-specific self-adaptation response function

$$\psi = \mathrm{E}\left[\frac{\sigma^{(g+1)} - \sigma^{(g)}}{\sigma^{(g)}} \,\middle|\, \sigma^{(g)}\right]. \tag{3.29}$$

The self-adaptation response (SAR) function of the $(\mu/\mu_I, \lambda)$-ES using σ self-adaptation on the ellipsoid model is also derived in [Melkozerov and Beyer, 2010] as a function of the mutation strength $\sigma^{(g)}$. Its asymptotically exact representation was derived in the limit of $N \to \infty$ and $\sigma \to 0$ and reads

$$\psi(\sigma^{(g)}) = \tau^2 \left(\frac{1}{2} + e_{\mu,\lambda}^{1,1} - \sigma^{(g)} \frac{c_{\mu/\mu,\lambda} \Sigma q}{R_q(\mathbf{y}^{(g)})} \right), \tag{3.30}$$

with exogenous learning parameter τ. Making use of (3.24) and (3.30) allowed to set up a system of $N + 1$ deterministic evolution equations which could be used to derive a condition

that ensures positive progress on the ellipsoid model. The resulting evolution criterion states that convergence to the optimizer in expectations requires to adapt a normalized mutation strength (3.14) that satisfies

$$\sigma^* \leq 2\mu c_{\mu/\mu,\lambda}. \tag{3.31}$$

However, closed-form solutions to the system of evolution equations turned out to be hard to determine. This problem was tackled by an *Ansatz* in terms of exponential functions which emerged from observations of the system's dynamical behavior. A more detailed explanation of the respective *Ansatz* is given within the analysis conducted in Chapter 4.

The *Ansatz* successfully solves the system in its steady state and permits to calculate the ensuing steady state convergence rate of the ES. Regarding the sphere model, a convergence rate formula depending on the normalized progress rate was found

$$\nu(\sigma^*_{ss}) = \frac{2}{N}\left(c_{\mu/\mu,\lambda}\sigma^*_{ss} - \frac{(\sigma^*_{ss})^2}{2\mu}\right). \tag{3.32}$$

Its maximum is obtained for a normalized steady state mutation strength of $\sigma^*_{opt} = \mu c_{\mu/\mu,\lambda}$. Accordingly, the SAR function allows for the derivation of the optimal learning parameter on the sphere model

$$\tau_{opt} = \sqrt{\frac{\mu c^2_{\mu/\mu,\lambda}}{2N\left(\mu c^2_{\mu/\mu,\lambda} - e^{1,1}_{\mu,\lambda} - \frac{1}{2}\right)}}. \tag{3.33}$$

This representation is similar to the known τ_{opt} formula derived in [Meyer-Nieberg, 2007]. Besides replicating sphere model results the investigations allowed for generalizations to the ellipsoid model. Defining the smallest ellipsoid coefficient by $\breve{q} = \min_{i=1,\ldots,N} q_i$, an approximation of the steady state convergence rate of the $(\mu/\mu_I, \lambda)$-σSA-ES on the ellipsoid model is calculated as

$$\nu(\sigma^*_{ss}) = \frac{2}{\Sigma q}\left(\breve{q}c_{\mu/\mu,\lambda}\sigma^*_{ss} - \frac{(\sigma^*_{ss})^2\breve{q}^2}{2\mu\Sigma q}\right). \tag{3.34}$$

Considering the standard learning parameter choice $\tau = 1/\sqrt{N}$ the actual normalized steady state mutation strength σ^*_{ss} realized by the σSA-ES could also be determined

$$\sigma^*_{ss} = \frac{1/2 + e^{1,1}_{\mu,\lambda}}{c_{\mu/\mu,\lambda}} \cdot \frac{1}{1 - \breve{q}/(\tau^2\Sigma q)}. \tag{3.35}$$

However, as explained in [Beyer and Melkozerov, 2014], Eq. (3.34) does not allow for the calculation of an analytical expression of either the optimal normalized steady state mutation strength σ^*_{opt} or the optimal learning parameter τ_{opt}. That is, an approximation of the (near) optimal steady state mutation strength had to be derived with help of a linearization of Eq. (3.34). Conclusively, a formula for the upper bound of the steady state mutation strength $\hat{\sigma}^*$ on non-spherical ellipsoid models could be determined

$$\hat{\sigma}^* = 2\upsilon_0 c_{\mu/\mu,\lambda}\mu\left(1 - \frac{N\breve{q}}{\Sigma q}\right), \tag{3.36}$$

where $0 < \upsilon_0 < 1$ represents a value close to 1 which accounts for the deviation of the upper bound to the actually optimal mutation strength. The corresponding steady state convergence rate to this mutation strength realization was found to be

$$\nu(\hat{\sigma}^*) = \frac{4\upsilon_0 c^2_{\mu/\mu,\lambda}\mu\check{q}}{\Sigma q}\left(1 - \frac{N\check{q}}{\Sigma q}\right). \tag{3.37}$$

Finally, these results permitted to obtain an recommendation of the (near) optimal learning parameter on the ellipsoid model

$$\tau_{opt} = \sqrt{\frac{\check{q}}{\Sigma q} \cdot \frac{1}{1 - \dfrac{1 + 2e^{1,1}_{\mu,\lambda}}{4\upsilon_0 c^2_{\mu/\mu,\lambda}\mu(1 - N\check{q}/\Sigma q)}}}. \tag{3.38}$$

This formula provides a generalization of the τ_{opt} expression derived in the context of the special PDQF [Finck and Beyer, 2012]. Even so, the work of Beyer and Melkozerov showed that the (μ/μ_I)-σSA-ES progress is very sensitive to the choice of the learning parameter τ. The optimal choice of τ is acutely problem dependent. Hence, particularly in practical applications, i.e. in disregard of knowledge about the fitness environment, the recommended standard parameter settings are likely to result in suboptimal performance of the strategy.

3.3. A comparison of mutation strength control analysis results

This section anticipates the analysis results of cumulative step-size adaptation (CSA) and meta-ES presented in the following two chapters. Providing the comparison of the three most common mutation strength adaptation approaches in the field of ES aims at an intelligible overview of the results of the first thesis part. This is supposed to support the comprehensibility of the analytic way of proceeding. The detailed derivations regarding CSA-ES are presented in Chapter 4, and for the case of adaptation by meta-ES[2] in Chapter 5, respectively.

A similarity of the three different adaptation techniques is that their normalized mutation strength dynamics (3.14) approach a stationary state in the long run. This normalized steady state mutation strength σ^*_{ss} depends on the population sizes (μ, and λ) as well as on the exogenous strategy specific parameters. It governs the steady state performance of the corresponding evolution strategies. Observations of the long-term behavior of the ES dynamics prompt to expressing the component-wise squared object parameter dynamics by means of exponential functions, i.e. via

$$y_i^{(g)^2} = b_i \mathrm{e}^{-\nu g}, \quad b_i > 0,\ \nu > 0, \quad i = 1, \ldots, N. \tag{3.39}$$

[2] At this point, only the results for the $[1, 2(\mu/\mu_I, \lambda)^1]$-meta-ES are considered. Making use of longer isolation periods $\gamma > 1$, the respective dynamical steady state behavior is presented in the second part of Chapter 5.

	strategy parameters	norm. mutation strength σ^*_{ss}	convergence rate ν_{ss}
σSA	$\tau = \frac{1}{\sqrt{N}}$	$\frac{1/2 + e^{1,1}_{\mu,\lambda}}{c_{\mu/\mu,\lambda}} \cdot \frac{1}{1 - \frac{\breve{q}}{\tau^2 \Sigma q}}$	$\frac{2(1/2 + e^{1,1}_{\mu,\lambda})}{1 - \frac{\breve{q}}{\tau^2 \Sigma q}} \cdot \frac{\breve{q}}{\Sigma q}$
CSA	$c = \frac{1}{\sqrt{N}},\ D = \frac{1}{c}$	$\frac{\mu c_{\mu/\mu,\lambda}}{\left(1 - \frac{cDN}{(1-c)} \frac{\breve{q}}{\Sigma q}\right)}$	$\frac{2\mu c^2_{\mu/\mu,\lambda}}{\left(1 - \frac{cDN}{(1-c)} \cdot \frac{\breve{q}}{\Sigma q}\right)} \frac{\breve{q}}{\Sigma q}$
meta-ES	$\alpha = 1.2$	$2\mu c_{\mu/\mu,\lambda} \frac{\alpha}{(1+\alpha^2)}$	$4\mu c^2_{\mu/\mu,\lambda} \frac{\alpha}{(1+\alpha^2)} \cdot \frac{\breve{q}}{\Sigma q}$

Table 3.1.: Comparison of the analysis results regarding the most commonly used mutation strength adaptation methods in the context of evolution strategies. The predictions are valid in the range of recommended standard parameter settings.

In this representation the quantity ν is referred to as the convergence rate of the y_i^2 dynamics. It depends on the realized normalized steady state mutation strength σ^*_{ss} and determines the strategy's long-term decline while approaching the optimizer. The exponential modeling (3.39) is valid for all three adaptation methods. Only the respective convergence rates differ depending on the mutation strength adaptation approach applied.

Following (3.39), in the steady state of the evolution strategies all object parameter vector components exhibit the same exponential descend. That is, after a transient phase the strategies approach the optimizer in each component with the same progress per generation. Conclusively, in the steady state the strategies permanently move into the direction of the optimizer. This is an remarkable observation since it can be interpreted as the ability of the ES variants to adapt the Newton direction towards the optimizer. That is, in their steady state the ES variants in expectation gradually step in Newton direction towards the optimizer on the ellipsoid model. The corresponding step length and thus the long-term behavior of the ESs is determined by the steady state convergence rates $\nu_{ss} := \nu(\sigma^*_{ss})$. Accordingly, it relies on the ability of the mutation strength adaptation methods to establish a beneficial steady state σ^*_{ss}. It turns out, that the convergence rates are governed by the ratio of the smallest eigenvalue and the sum Σq of all eigenvalues, or ellipsoid coefficients q_i, respectively.

Table 3.1 illustrates the steady state mutation strengths as well as the corresponding steady state convergence rates that are realized by application of the three adaptation techniques. The quantities depend on the characteristics of the ellipsoid model, the population sizes used within the ES, and the strategy specific parameters. Provided that the search space dimension is sufficiently large, it is observed that σSA realizes a normalized steady state mutation strength value around $\sigma^*_{ss} \approx 1$ on the ellipsoid models $q_i = i, i^2$. This value falls below the realization of the other two approaches by a factor of μ. Cumulative step-size adaptation as well as meta-ES establish a normalized steady state mutation strength near $\mu c_{\mu/\mu,\lambda}$ which was derived as the optimal σ^*_{ss} value in the context of the sphere model. As

	norm. mutation strength $\sigma^*_{ss}\vert_{q_i=i}$	convergence rate $\nu_{ss}\vert_{q_i=i}$
σSA	$\frac{1/2+e^{1,1}_{\mu,\lambda}}{c_{\mu/\mu,\lambda}} \cdot \frac{N+1}{N-1}$	$\frac{4(1/2+e^{1,1}_{\mu,\lambda})}{(N-1)N}$
CSA	$\frac{\mu c_{\mu/\mu,\lambda}}{\left(1-\frac{2\sqrt{N}}{(\sqrt{N}-1)(N+1)}\right)}$	$\frac{4\mu c^2_{\mu/\mu,\lambda}}{\left(1-\frac{2\sqrt{N}}{(\sqrt{N}-1)(N+1)}\right)} \cdot \frac{1}{N(N+1)}$
meta-ES	$\mu c_{\mu/\mu,\lambda}\frac{2.4}{2.44}$	$4\mu c^2_{\mu/\mu,\lambda}\frac{2.4}{2.44} \cdot \frac{1}{N(N+1)}$

Table 3.2.: The specific steady state results obtained on the ellipsoid model with $q_i = i$.

will be explained in Chapters 4 and 5 neither realization is really optimal on non-spherical ellipsoid models. Instead the realized steady state mutation strength of CSA-ES and meta-ES depends on the condition number of the optimization problem and is found inside the interval

$$\sigma^*_{opt} \in (\mu c_{\mu/\mu,\lambda}, 2\mu c_{\mu/\mu,\lambda}). \tag{3.40}$$

At least for the CSA case, σ^*_{ss} can be channeled in direction of the optimal normalized steady state mutation strength σ^*_{opt} by tuning the parameters c, and D, respectively. Interestingly, the meta-ES adapts its normalized steady state mutation strength in the vicinity of $\mu c_{\mu/\mu,\lambda}$ independently of the underlying fitness environment.

Conclusively, the corresponding steady state convergence rates of the CSA and meta-ES reach larger values. In contrast to the σSA-ES, these strategies exhibit a considerably better performance on the ellipsoid model. Alike the σ^*_{ss} realization, the established convergence rates of both ES variants are proportional to the parental population size μ. The convergence rate of the σSA-ES is by this factor μ smaller. The tables illustrate that the convergence rates of the considered ellipsoid models $q_i = i, i^2$ decrease with increasing search space dimensionality N. This performance reduction is anti-proportional to N^2 for $q_i = i$ and to N^3 for $q_i = i^2$, respectively. On both ellipsoid models the σSA-ES reaches a $\sigma^*_{ss} \approx 1$ while CSA-ES and meta-ES approach values near $\sigma^*_{ss} \approx \mu c_{\mu/\mu,\lambda}$.

Considering the ellipsoid model test cases $q_i = i, i^2$ mentioned in Sec. 3.1 the explicit results are displayed in Tab. 3.2, and Tab. 3.3. The calculations make use of the sum identities

$$\sum_{i=1}^{N} i = \frac{N(N+1)}{2} \qquad \text{as well as} \qquad \sum_{i=1}^{N} i^2 = \frac{N(N+1)(2N+1)}{6}. \tag{3.41}$$

Having derived the steady state convergence rates allows for the calculation of the expected running time of the algorithm variants. To this end, the steady state fitness dynamics are determined by use of the exponential *Ansatz* (3.39). Starting at generation g_0 for an evolution interval of g subsequent generations yields the description

$$F(\mathbf{y}^{(g_0+g)}) = \sum_{j=1}^{N} q_j^2 {y_j^{(g_0+g)}}^2 = \sum_{j=1}^{N} q_j^2 b_j \mathrm{e}^{-\nu(g_0+g)} = F(\mathbf{y}^{(g_0)})\mathrm{e}^{-\nu g}. \tag{3.42}$$

That is, in the strategy's steady state the objective function drops exponentially fast with time constant $\tau = 1/\nu$. The representation of the fitness dynamics provides an estimate for the expected running time G of the algorithm needed to improve the objective function value by a factor $2^{-\beta}$. From (3.42) one obtains

$$2^{-\beta} = \frac{F(\mathbf{y}^{(g_0+G)})}{F(\mathbf{y}^{(g_0)})} = \mathrm{e}^{-\nu G}, \tag{3.43}$$

and by taking the logarithm and inserting the steady state convergence rates ν_{ss}, the expected running time G of the different ES variants becomes

$$G \simeq \frac{\beta \ln(2)}{\nu_{ss}}, \tag{3.44}$$

with ν_{ss} according to Tab. 3.1. The approximated expected running time G is asymptotically proportional to the quotient of the sum of the ellipsoid coefficients Σq and the smallest coefficient $\breve{q}$. In particular, regarding the fitness model (3.6) the result can be extended to the general fitness model (3.3)

$$Q(\mathbf{y}) = \mathbf{y}^\top \mathbf{Q}\mathbf{y} \tag{3.45}$$

with positive definite matrix $\mathbf{Q} \in \mathbb{R}^{N\times N}$. In this situation, $\breve{q} = \min(q_i)$ is identified with the smallest eigenvalue $\breve{\kappa}$ of the corresponding eigenvalue problem

$$\mathbf{Q}\mathbf{u} = \kappa\mathbf{u}. \tag{3.46}$$

As the trace of $\mathbf{Q}$ consists of the sum of its eigenvalues one obtains $\Sigma q = \mathrm{Tr}[\mathbf{Q}]$. Hence, considering the three ES variants on the general fitness model yields:

$$G \propto \frac{\mathrm{Tr}[\mathbf{Q}]}{\breve{\kappa}}. \tag{3.47}$$

Meaning that the expected running time of the two mentioned ellipsoid models increases with order N^2 for $q_i = i$, and with N^3 for $q_i = i^2$, respectively.

	norm. mutation strength $\sigma^*_{ss}\vert_{q_i=i^2}$	convergence rate $\nu_{ss}\vert_{q_i=i^2}$
σSA	$\frac{1/2 + e^{1,1}_{\mu,\lambda}}{c_{\mu/\mu,\lambda}} \cdot \frac{1}{1 - \frac{6}{(2N+1)(N+1)}}$	$\frac{12(1/2 + e^{1,1}_{\mu,\lambda})}{(2N+1)(N+1)N - 6N}$
CSA	$\frac{\mu c_{\mu/\mu,\lambda}}{\left(1 - \frac{6\sqrt{N}}{(\sqrt{N}-1)(N+1)(2N+1)}\right)}$	$\frac{12\mu c^2_{\mu/\mu,\lambda}}{\left(1 - \frac{6\sqrt{N}}{(\sqrt{N}-1)(N+1)(2N+1)}\right)} \cdot \frac{1}{N(N+1)(2N+1)}$
meta-ES	$\mu c_{\mu/\mu,\lambda}\frac{2.4}{2.44}$	$12\mu c^2_{\mu/\mu,\lambda}\frac{2.4}{2.44} \cdot \frac{1}{N(N+1)(2N+1)}$

Table 3.3.: The specific steady state results obtained on the ellipsoid model with $q_i = i^2$.

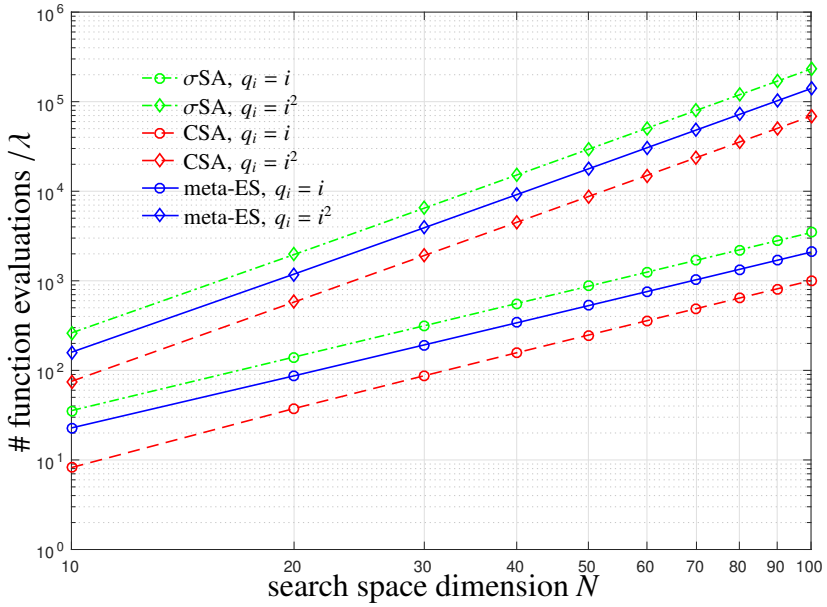

Figure 3.2.: The expected number of function evaluations per offspring individual is plotted against the search space dimension from $N = 10$ to $N = 100$. An improvement of $2^{-\beta}$ with $\beta = 2$ is required and the standard strategy parameter settings from Tab. 3.1 are used.

Notice, that in the context of meta-ES the expected running time G refers to the iteration number of the outer strategy. In order to make the meta-ES result comparable to σSA and CSA the actual number of function evaluations needed for the improvement is regarded. While $(\mu/\mu_I, \lambda)$-σSA-ES and $(\mu/\mu_I, \lambda)$-CSA-ES evaluate the fitness of λ offspring per generation, the $[1, 2(\mu/\mu_I, \lambda)^1]$-meta-ES uses twice as much function evaluations as it employs two separate inner $(\mu/\mu_I, \lambda)$-ESs. Concentrating on specific population sizes $\mu = 3$ and $\lambda = 10$ the ES variants' performances are compared in Fig. 3.2. Therefore, the expected number of function evaluations per offspring are plotted against the search space dimension N on the ellipsoid models $q_i = i, i^2$. The standard strategy parameters as well as the steady state convergence rates from Tab. 3.1 are used. Considering the expected number of function evaluations needed for an improvement of $2^{-\beta}$, e.g. $\beta = 2$, it can be observed that the $(3/3_I, 10)$-CSA-ES (red) performs best regardless of the ellipsoid model case. On both models, the $[1, 2(3/3_I, 10)^1]$-meta-ES (blue) needs approximately twice the number of function evaluations to gain the same improvement. As it approaches a steady state mutation strength outside the interval (3.40), the expected running time of the $(3/3_I, 10)$-σSA-ES (green) and with that its expected number of function evaluation exceeds those of the other two strategies.

In [Beyer and Melkozerov, 2014], the experimental verification of the displayed σSA-ES running times is demonstrated. The comparison of experimental measurements with the theoretical results from CSA-ES analysis as well as those of the meta-ES analysis can be found in Chapter 4, and Chapter 5, respectively. In all cases the experimental results show a very good agreement with the presented theoretical predictions.

4. Analysis of cumulative step-size mutation strength adaptation

Within this chapter the behavior of the $(\mu/\mu_I, \lambda)$-Evolution Strategy (ES) with cumulative step size adaptation (CSA) is analyzed on the ellipsoid model (3.6). The analysis is performed making use of the dynamical systems approach motivated in Sec. 2.3. In the first place, the considered Evolution Strategy is introduced in detail. The analysis starts with the derivation of a nonlinear system of difference equations that describes the mean value evolution of the ES. This system is successively simplified to finally allow for deriving closed-form solutions of the steady state behavior in the asymptotic limit case of large search space dimensions. The steady state mutation strength is calculated and it is shown that the system exhibits linear convergence order. Additionally, conclusions regarding the choice of the cumulation parameter c and the damping constant D are drawn. The convergence rate results are used to derive a formula for the expected running time.

4.1. The $(\mu/\mu_I, \lambda)$-CSA-ES algorithm

This section presents the Evolution Strategy variant under consideration: the $(\mu/\mu_I, \lambda)$-CSA-ES. Its pseudo-code is presented in Alg. 4.1. First the initial parental parameter vector, also referred to as the parental centroid $\mathbf{y}^{(0)}$, the initial mutation strength $\sigma^{(0)}$, and the initial search path $\mathbf{s}^{(0)} = \mathbf{0} \in \mathbb{R}^N$ are specified. Then from line 3 to 5 λ offspring $\mathbf{y}_l$ are generated by adding the product of the mutation strength σ and an N-dimensional random mutation vector $\mathbf{z}_l$ to the parental centroid. The components of each $\mathbf{z}_l$ are independent and identically distributed standard normal variates. The corresponding fitness function value F_l of each offspring is calculated in line 6. In line 8 the mutation vectors of the μ best offspring w.r.t. their fitness are recombined to generate their centroid $\langle \mathbf{z} \rangle^{(g)}$. In this context the subscript $m;\lambda$ denotes the mth best of the λ offspring, cf. (2.4).

On the one hand, the centroid of the μ best mutation vectors is used in line 9 to compose a new parental centroid $\mathbf{y}^{(g+1)}$, and on the other hand, to update the search path $\mathbf{s}^{(g+1)}$ in line 10. This search path contains a fading record of the strategy's previous steps. The length of its memory is determined by the choice of the constant parameter $c \in (0, 1)$, referred to as the cumulation parameter. The mutation strength $\sigma^{(g+1)}$ is then updated in line 11 by multiplication with an exponential value depending on the length of the search path $\mathbf{s}$ as well as the damping parameter D. The sign of $\|\mathbf{s}^{(g+1)}\|^2 - N$ determines whether the mutation strength is increased or decreased. Long search paths indicate that the steps made by the ES collectively point in one direction and could be replaced with fewer but longer steps. Short search paths suggest that the strategy steps back and forth and thus that smaller step sizes

Algorithm 4.1 Pseudo code of the $(\mu/\mu, \lambda)$-CSA-ES.

Initialize $\left(\mathbf{y}^{(0)}, \mathbf{s}^{(0)}, \sigma^{(0)}\right)$;
$g \leftarrow 0$;
repeat
  for $l = 1$ to λ **do**
    $\mathbf{z}_l \leftarrow \mathcal{N}(0, \mathbf{1})$;
    $\mathbf{y}_l \leftarrow \mathbf{y}^{(g)} + \sigma^{(g)}\mathbf{z}_l$;
    $F_l \leftarrow F(\mathbf{y}_l)$;
  end for
  $\langle \mathbf{z} \rangle^{(g)} \leftarrow \frac{1}{\mu} \sum_{m=1}^{\mu} \mathbf{z}_{m;\lambda}$;
  $\mathbf{y}^{(g+1)} \leftarrow \mathbf{y}^{(g)} + \sigma^{(g)} \langle \mathbf{z} \rangle^{(g)}$;
  $\mathbf{s}^{(g+1)} \leftarrow (1-c)\mathbf{s}^{(g)} + \sqrt{\mu c(2-c)} \langle \mathbf{z} \rangle^{(g)}$;
  $\sigma^{(g+1)} \leftarrow \sigma^{(g)} \exp\left(\frac{\|\mathbf{s}^{(g+1)}\|^2 - N}{2DN}\right)$;
  $g \leftarrow g + 1$;
until termination condition

should be beneficial. After termination the strategy returns the current parental centroid which is considered as an approximation of the optimizer of the objective function $F(\mathbf{y})$.

The dynamic behavior of the $(\mu/\mu_I, \lambda)$-CSA-ES on the ellipsoid model (3.6) is illustrated in Fig. 4.1. It presents the results of typical runs of the ES focusing on the squared components of the parental centroid $\mathbf{y}^{(g)}$, as well as the mutation strength dynamics. The CSA specific parameters are set according to the recommendations $c = 1/\sqrt{N}$ and $D = 1/c$, see also 2.1. All curves are averaged over 10^4 independent runs. After a transient phase, the y_i^2 dynamics are approaching the optimizer at the same rates. Also the mutation strength is continuously reduced with the passing number of generations.

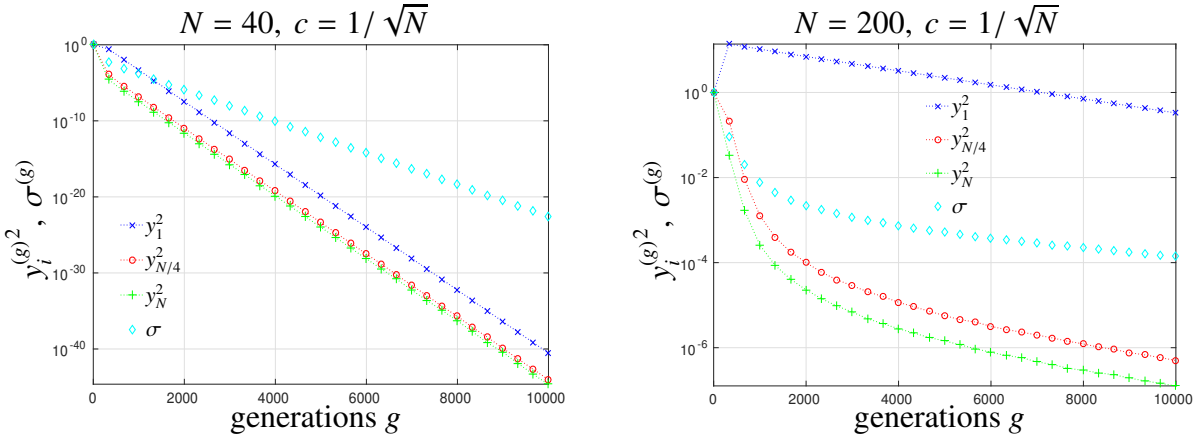

Figure 4.1.: The dynamics of the $(3/3_I, 10)$-CSA-ES on the ellipsoid model with $a_i = i$. The component-wise quadratic deviation y_i^2 from the optimizer is displayed for $i = 1, 10, 40$. The light blue data points $\diamond$ represent the mutation strength σ. Algorithm 4.1 is initialized at $\sigma^{(0)} = 1$, and $\boldsymbol{y}^{(0)} = \mathbf{1} \in \mathbb{R}^N$.

4.2. Deriving the evolution equations

Having motivated the $(\mu/\mu_I, \lambda)$-CSA-ES, this section aims at the theoretical analysis of its dynamical behavior on the ellipsoid model (3.6). In this context, the quadratic progress rate quantifies the expected change of the object parameter vector between two consecutive generations. In order to build the evolution equations of the CSA-ES on the ellipsoid model the description of the mutation strength transition from generation g to generation $g + 1$ is necessary. In the case of the σSA-ES on the general quadratic fitness model the framework of the dynamical systems approach [Beyer, 2001] could be applied rather naturally. It states that the stochastic process of the ES from generation g to generation $g + 1$ can be divided into mean value parts and fluctuation terms (ϵ_i and ϵ_σ) as mentioned in Sec. 2.3.

$$y_i^{(g+1)^2} = y_i^{(g)^2} - \varphi_i^{II}(\sigma^{(g)}, \mathbf{y}^{(g)}) + \epsilon_i\left(\sigma^{(g)}, \mathbf{y}^{(g)}\right), \tag{4.1}$$

$$\sigma^{(g+1)} = \sigma^{(g)}\left(1 + \psi(\sigma^{(g)}, \mathbf{y}^{(g)})\right) + \epsilon_\sigma\left(\sigma^{(g)}, \mathbf{y}^{(g)}\right). \tag{4.2}$$

The mean value parts in Eq. (4.1) are directly given by the quadratic progress rate φ_i^{II}, i.e. by Eq. (3.20) and (3.24), respectively. The self-adaptation response (SAR) function $\psi(\sigma^{(g)}, \mathbf{y}^{(g)})$ governs the mean value dynamics of Eq. (4.2).

As it turns out, unlike the σ-SA-ES the CSA-ES lacks a simple formula for the expected change of the mutation strength σ. Due to the influence of the search path update on the mutation strength evolution, the description of the mutation strength dynamics is more complex. In the first place, this problem is tackled by describing the expected change of σ by use of a system of recurrence equations. The first difference equation is directly inferred from the CSA-ES algorithm as it concerns the mutation strength control rule. According to Alg. 4.1, line 12, the expected mutation strength in generation $g + 1$ is

$$\mathrm{E}\left[\sigma^{(g+1)}\right] = \mathrm{E}\left[\sigma^{(g)} \exp\left(\frac{\|\mathbf{s}^{(g+1)}\|^2 - N}{2DN}\right)\right]. \tag{4.3}$$

According to line 11 of Alg. 4.1, the variation within the search path $\mathbf{s}$, and consequently that of its squared length $\|\mathbf{s}^{(g+1)}\|^2$, is decreasing when considering small cumulation parameters $c \to 0$. That is, in the asymptotic limit ($N \to \infty$) the random variate $\|\mathbf{s}^{(g+1)}\|^2$ can be replaced by the respective expected value $\mathrm{E}\left[\|\mathbf{s}^{(g+1)}\|^2\right]$ and Eq. (4.3) becomes

$$\mathrm{E}\left[\sigma^{(g+1)}\right] \simeq \mathrm{E}\left[\sigma^{(g)}\right] \exp\left(\frac{\mathrm{E}\left[\|\mathbf{s}^{(g+1)}\|^2\right] - N}{2DN}\right). \tag{4.4}$$

Obtaining a recurrence equation requires the knowledge of the squared length of the search path in generation $g + 1$. Due to line 11 of Alg. 4.1, it follows

$$\|\mathbf{s}^{(g+1)}\|^2 = (1-c)^2\|\mathbf{s}^{(g)}\|^2 + 2(1-c)\sqrt{\mu}\,\sqrt{c(2-c)}\,\mathbf{s}^{(g)^\top}\langle\mathbf{z}\rangle^{(g)} + \mu c(2-c)\,\|\langle\mathbf{z}\rangle^{(g)}\|^2. \tag{4.5}$$

Conclusively, the calculation of the expected change of the search path's squared norm $\mathrm{E}\left[\|\mathbf{s}^{(g+1)}\|^2 - \|\mathbf{s}^{(g)}\|^2\right]$ requires the determination of the expected values of the scalar product

$\mathbf{s}^{(g)\top}\langle\mathbf{z}\rangle^{(g)}$ and that of the squared norm of the parental centroid's mutation vector $\|\langle\mathbf{z}\rangle^{(g)}\|^2$ in generation g. The latter expectation is calculated in Appendix A.1 as

$$\mathrm{E}\left[\|\langle\mathbf{z}\rangle^{(g)}\|^2\right] = \frac{1}{\mu}\left(N + \frac{(\mu-1)e^{2,0}_{\mu,\lambda} + e^{1,1}_{\mu,\lambda}}{1 + \frac{\sum_{j=1}^{N} a_j^2}{R_q^2(\mathbf{y}^{(g)})}\frac{\sigma^{(g)2}}{2}}\right). \tag{4.6}$$

As demonstrated within the appendix A, a considerably simpler expression can be obtained if the conditions in (3.22) are fulfilled. In that situation, Eq. (4.6) asymptotically becomes

$$\mathrm{E}\left[\|\langle\mathbf{z}\rangle^{(g)}\|^2\right] \simeq \frac{N}{\mu}. \tag{4.7}$$

This facilitation is asymptotically correct for $N \to \infty$ and will additionally be justified by comparisons of the two different iteratively generated dynamics (using Eq. (4.6) or Eq. (4.7), respectively) with the dynamics of real $(\mu/\mu_I, \lambda)$-CSA-ES runs in Fig. 4.2 and Fig.4.4.

Regarding the expected value of the scalar product $\mathbf{s}^{(g)\top}\langle\mathbf{z}\rangle^{(g)}$ of the search path $\mathbf{s}$ and the mutation vector centroid $\langle\mathbf{z}\rangle$ a closed-form solution is unapparent. This problem can be circumvented expressing the expected scalar product value by use of another difference equation which is then added to the evolution equations of the dynamical system. The respective difference equation is calculated in Appendix A.2 as

$$\begin{aligned}\mathrm{E}\left[s_i^{(g+1)}\langle z\rangle_i^{(g+1)}\right] \simeq{}& (1-c)\left(1 - \frac{c_{\mu/\mu,\lambda} q_i \sigma^{(g)}}{R_q(\mathbf{y}^{(g)})}\right)\mathrm{E}\left[s_i^{(g)}\langle z\rangle_i^{(g)}\right] \\ &+ \sqrt{\mu c(2-c)}\left(\frac{c^2_{\mu/\mu,\lambda} q_i^2 y_i^{(g)2}}{R_q^2(\mathbf{y}^{(g)})} - \frac{c_{\mu/\mu,\lambda} q_i \sigma^{(g)}}{R_q(\mathbf{y}^{(g)})}\mathrm{E}\left[\left(\langle z\rangle_i^{(g)}\right)^2\right]\right).\end{aligned} \tag{4.8}$$

Equation (4.8) employs the expectation $\mathrm{E}\left[(\langle z\rangle_i^{(g)})^2\right]$. That is, its complexity can also be reduced in the asymptotic limit case by consideration of Eq. (4.7), or (A.8), respectively. Consequently, the recurrence equation of the expected scalar product values becomes

$$\begin{aligned}\mathrm{E}\left[s_i^{(g+1)}\langle z\rangle_i^{(g+1)}\right] \simeq{}& (1-c)\left(1 - \frac{c_{\mu/\mu,\lambda} q_i \sigma^{(g)}}{R_q(\mathbf{y}^{(g)})}\right)\mathrm{E}\left[s_i^{(g)}\langle z\rangle_i^{(g)}\right] \\ &+ \sqrt{\mu c(2-c)}\left(\frac{c^2_{\mu/\mu,\lambda} q_i^2 y_i^{(g)2}}{R_q^2(\mathbf{y}^{(g)})} - \frac{c_{\mu/\mu,\lambda} q_i \sigma^{(g)}}{R_q(\mathbf{y}^{(g)})}\frac{1}{\mu}\right).\end{aligned} \tag{4.9}$$

The combination of the results in Eq. (4.6) and Eq. (4.8) together with Eq. (4.3) allows for the compilation of a difference equation which describes the expected change of the squared length of the search path

$$\begin{aligned}\mathrm{E}\left[\|\mathbf{s}^{(g+1)}\|^2\right] = (1-c)^2\,\mathrm{E}\left[\|\mathbf{s}^{(g)}\|^2\right] \\ + 2(1-c)\sqrt{\mu c(2-c)}\,\mathrm{E}\left[\mathbf{s}^{(g)\top}\langle\mathbf{z}\rangle^{(g)}\right] \\ + \mu c(2-c)\,\mathrm{E}\left[\|\langle\mathbf{z}\rangle^{(g)}\|^2\right].\end{aligned} \tag{4.10}$$

Iterative Scheme of Evolution Equations I

$$y_i^{(g+1)^2} \leftarrow y_i^{(g)^2} - \frac{2\sigma^{(g)} c_{\mu/\mu,\lambda} q_i y_i^{(g)^2}}{R_q(\mathbf{y}^{(g)}) \sqrt{1 + \frac{\sigma^{(g)} \sum_{j=1}^{N} a_j^2}{2R_q^2(\mathbf{y}^{(g)})}}} + \frac{\sigma^{(g)^2}}{\mu} \left(1 + \frac{\left((\mu-1) e_{\mu,\lambda}^{2,0} + e_{\mu,\lambda}^{1,1} \right) q_i^2 y_i^{(g)^2}}{R_q^2(\mathbf{y}^{(g)}) \left(1 + \frac{\sigma^{(g)} \sum_{j=1}^{N} a_j^2}{2R_q^2(\mathbf{y}^{(g)})} \right)} \right) \tag{I.1}$$

$$\mathrm{E}\left[s_i^{(g+1)} \langle z \rangle_i^{(g+1)} \right] \leftarrow \mathrm{E}\left[s_i^{(g)} \langle z \rangle_i^{(g)} \right] (1-c) \left(1 - \frac{c_{\mu/\mu,\lambda} q_i \sigma^{(g)}}{R_q(\mathbf{y}^{(g)})} \right) + \frac{\sqrt{\mu c(2-c)}\, c_{\mu/\mu,\lambda}^2 q_i^2 y_i^{(g)^2}}{R_q^2(\mathbf{y}^{(g)})} - \frac{\sqrt{\mu c(2-c)}}{\mu} \frac{c_{\mu/\mu,\lambda} q_i \sigma^{(g)}}{R_q(\mathbf{y}^{(g)})} \left(1 + \frac{\left((\mu-1) e_{\mu,\lambda}^{2,0} + e_{\mu,\lambda}^{1,1} \right) q_i^2 y_i^{(g)^2}}{R_q^2(\mathbf{y}^{(g)}) + \frac{\sigma^{(g)^2}}{2} \sum_{j=1}^{N} a_j^2} \right) \tag{I.2}$$

$$\mathrm{E}\left[\|\mathbf{s}^{(g+1)}\|^2 \right] \leftarrow \mathrm{E}\left[\|\mathbf{s}^{(g)}\|^2 \right] (1-c)^2 + 2(1-c) \sqrt{\mu c(2-c)} \sum_{i=1}^{N} \mathrm{E}\left[s_i^{(g)} \langle z \rangle_i^{(g)} \right] + c(2-c) \left(N + \left((\mu-1) e_{\mu,\lambda}^{2,0} + e_{\mu,\lambda}^{1,1} \right) \Big/ \left(1 + \frac{\sum_{j=1}^{N} a_j^2}{R_q^2(\mathbf{y}^{(g)})} \frac{\sigma^{(g)^2}}{2} \right) \right) \tag{I.3}$$

$$\sigma^{(g+1)} \leftarrow \sigma^{(g)} \exp\left(\frac{\mathrm{E}\left[\|\mathbf{s}^{(g+1)}\|^2 \right] - N}{2DN} \right) \tag{I.4}$$

Table 4.1.: Iterative scheme **I** summarizes the evolution equations of the $(\mu/\mu_I, \lambda)$-CSA-ES.

In the context of CSA-ES the derivation of a closed SAR formula appears to be a hard task even in the steady state case. That is, in the first step it has to be substituted by the obtained difference equations, before in Sec. 4.3.1 an asymptotical approximation of the SAR function will be derived. In order to keep the analysis tractable the fluctuation terms of the dynamical system (ϵ_i and ϵ_σ) are disregarded. Furthermore, asymptotically correct simplifications have to be derived for the deterministic evolution equations. These approximations are compared with experimental $(\mu/\mu_I, \lambda)$-CSA-ES runs. The system of evolution equations describing the dynamical behavior of the $(\mu/\mu_I, \lambda)$-CSA-ES is summarized in Tab. 4.1. The SAR function is substituted by use of $N + 2$ difference equations (4.4), (4.8), and (4.10) which monitor the mutation strength transition between two consecutive generations. Notice, that Eq. (I.2) is obtained by insertion of (A.6) into (4.8), and that the componentwise difference equations (4.8) have been used instead of Eq. (A.25) for usability reasons. Whether the modeling approach yields meaningful results can be checked by comparison of the iteratively generated dynamics of the system of evolution equations **I**, Tab. 4.1, with

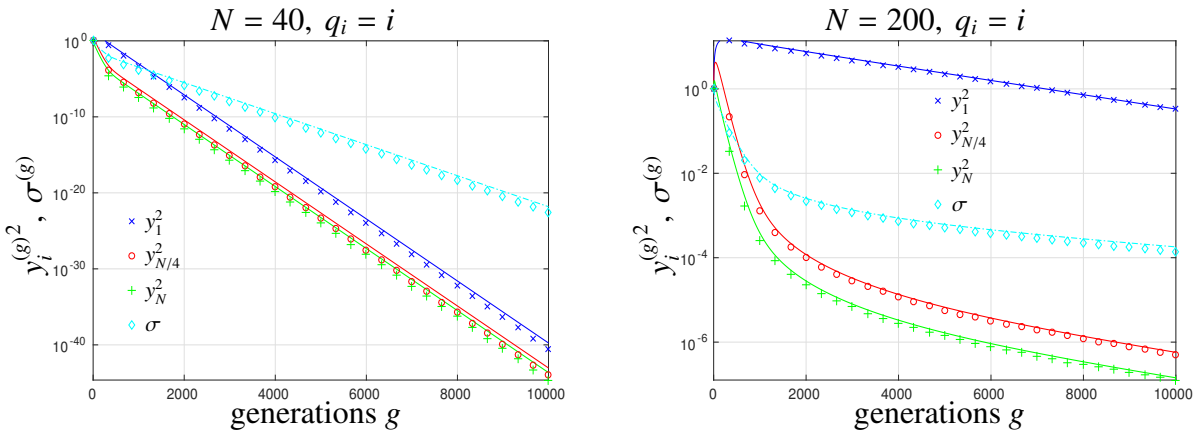

Figure 4.2.: Iteratively generated dynamics of scheme **I** compared to real runs of the $(3/3_I, 10)$-CSA-ES using $q_i = i$, $N = 40$ and $N = 200$. The results of the evolution equations in **I** for the y_i^2 dynamics, as well as the σ dynamics, are illustrated by the solid lines. The discrete data points display the corresponding experimental results which are averaged over 10^4 independent runs of the ES. Experiments and iteration are initialized at $\sigma^{(0)} = 1$, and $\boldsymbol{y}^{(0)} = \mathbf{1} \in \mathbb{R}^N$ using the recommended CSA specific strategy parameters $c = 1/\sqrt{N}$ and $D = 1/c$.

experimental results of real $(\mu/\mu, \lambda)$-CSA-ES runs in Fig. 4.2. The typical long-term behavior of the ES on the ellipsoid model $q_i = i$ is observed. Starting from $\sigma^{(0)} = 1$, $\mathbf{y}^{(0)} = \mathbf{1}$, the respective dynamics are obtained by iteration of scheme **I**. Cumulation and damping parameter have been set to $c = 1/\sqrt{N}$ and $D = 1/c$. Considering a small dimensionality N, the experimental data of the ES slightly deviate from the theoretical predictions. These deviations diminish with increasing search space dimensionality. In fact, on both sides a good agreement of iterative and experimental dynamics can be observed.

However, for further analytical investigations one is interested in a more convenient system of evolution equations. To this end, the progress rate (3.19) used in (I.1) is substituted by its asymptotical representation from Eq. (3.24), yielding (II.1). (II.2) is composed by use of the recurrence equation (4.9) instead of (4.8), The evolution equation of $\|\mathbf{s}\|^2$ in (II.3) is obtained by inserting the simplification (4.7) into (4.10). Finally, the mutation strength transition (I.4) is simplified by considering the first two terms of the Taylor expansion

$$\exp\left(\frac{\mathrm{E}\left[\|\mathbf{s}^{(g+1)}\|^2\right] - N}{2DN}\right) = 1 + \frac{\mathrm{E}\left[\|\mathbf{s}^{(g+1)}\|^2\right] - N}{2DN}\left(1 + \frac{1}{2D}\left(\frac{\mathrm{E}\left[\|\mathbf{s}^{(g+1)}\|^2\right]}{N} - 1\right) + \ldots\right), \quad (4.11)$$

Notice, higher order terms in (4.11) can be neglected assuming $D \to \infty$. This is true in the asymptotic limit case, since D usually increases with the search space dimensionality N and $\|\mathbf{s}^{(g+1)}\|^2 \simeq N$. Conclusively, inserting (4.11) into (I.4) yields (II.4) and one obtains a second iterative scheme **II**, Tab. 4.2. The simplifications within the modified iterative scheme **II** are justified by comparing its dynamics to the dynamics of the scheme **I**, Tab. 4.1. This comparison is provided in Fig. 4.3. The iteratively generated dynamics are displayed for $q_i = i^2$, $c = 1/\sqrt{N}$, and $D = 1/c$. Both iterative systems are initialized at $\sigma^{(0)} = 1$, and $\boldsymbol{y}^{(0)} = \mathbf{1} \in \mathbb{R}^N$.

Iterative Scheme of Evolution Equations II

$$y_i^{(g+1)^2} \leftarrow y_i^{(g)^2}\left(1 - \frac{2\sigma^{(g)}c_{\mu/\mu,\lambda}q_i}{R_q(\mathbf{y}^{(g)})}\right) + \frac{\sigma^{(g)^2}}{\mu} \tag{II.1}$$

$$\begin{aligned}\mathrm{E}\left[s_i^{(g+1)}\langle z\rangle_i^{(g+1)}\right] \leftarrow\ & \mathrm{E}\left[s_i^{(g)}\langle z\rangle_i^{(g)}\right](1-c)\left(1 - \frac{c_{\mu/\mu,\lambda}q_i\sigma^{(g)}}{R_q(\mathbf{y}^{(g)})}\right) \\ & + \frac{c_{\mu/\mu,\lambda}^2\sqrt{\mu c(2-c)}}{R_q(\mathbf{y}^{(g)})}\left(\frac{q_i^2 y_i^{(g)^2}}{R_q(\mathbf{y}^{(g)})} - \frac{q_i\sigma^{(g)}}{\mu c_{\mu/\mu,\lambda}}\right)\end{aligned} \tag{II.2}$$

$$\begin{aligned}\mathrm{E}\left[\|\mathbf{s}^{(g+1)}\|^2\right] \leftarrow\ & \mathrm{E}\left[\|\mathbf{s}^{(g)}\|^2\right](1-c)^2 + 2(1-c)\sqrt{\mu c(2-c)}\sum_{i=1}^{N}\mathrm{E}\left[s_i^{(g)}\langle z\rangle_i^{(g)}\right] \\ & + c(2-c)N\end{aligned} \tag{II.3}$$

$$\sigma^{(g+1)} \leftarrow \sigma^{(g)}\left(1 + \frac{\mathrm{E}\left[\|\mathbf{s}^{(g+1)}\|^2\right] - N}{2DN}\right) \tag{II.4}$$

Table 4.2.: Iterative scheme **II** is obtained by simplification of the iterative scheme **I**.

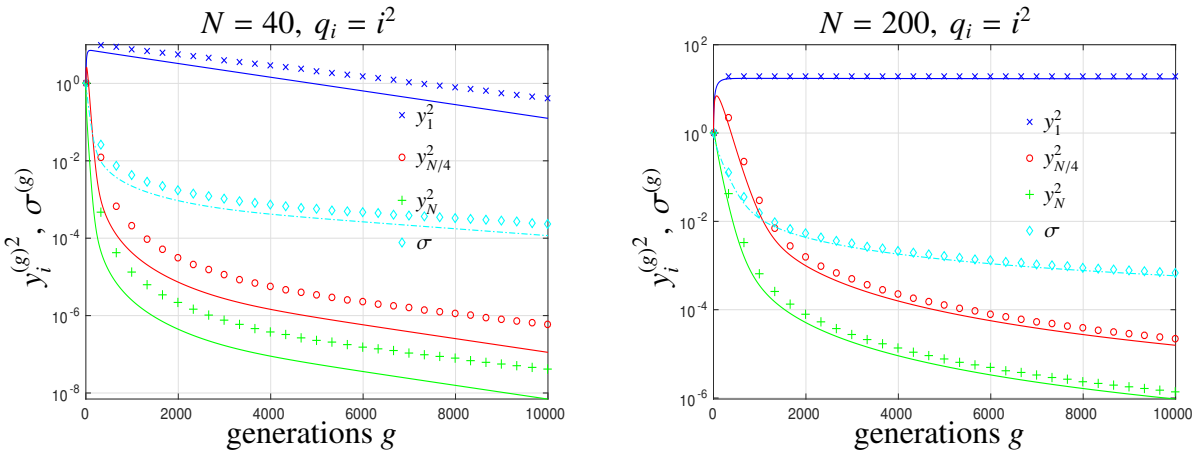

Figure 4.3.: Comparison of the dynamics of the iterative schemes **I** and **II** simulating a $(3/3_I, 10)$-CSA-ES with $q_i = i^2$, $N = 40$, and $N = 200$ respectively. The iteratively generated y_i^2 dynamics (for $i = 1, N/4, N$), as well as the iterative σ dynamics are displayed. While the data points illustrate the results of the evolution equations from **I**, the results of **II** are represented by the curves. Both iterative schemes are initialized at $\sigma^{(0)} = 1$, and $\boldsymbol{y}^{(0)} = \mathbf{1} \in \mathbb{R}^N$, and use the recommended CSA specific strategy parameters $c = 1/\sqrt{N}$ and $D = 1/c$.

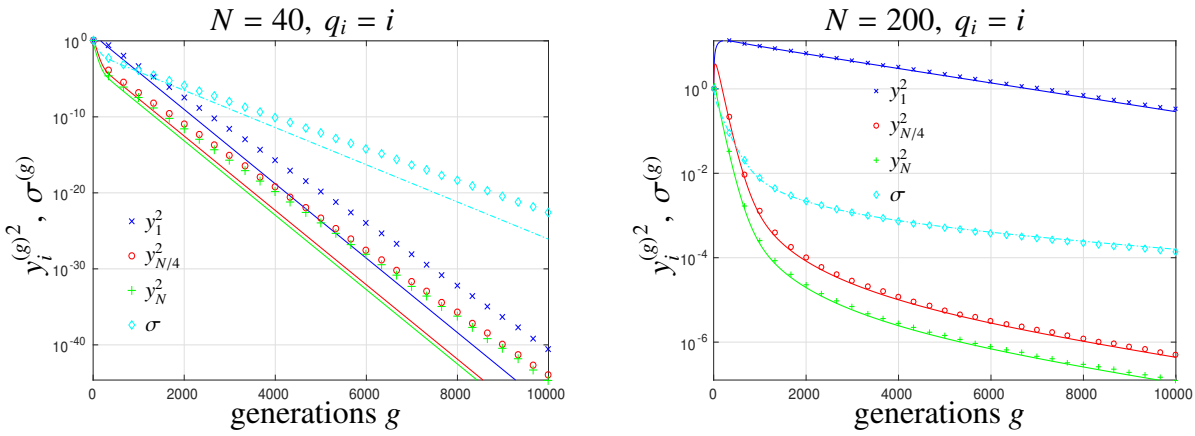

Figure 4.4.: Iteratively generated dynamics of scheme **II** compared to real runs of the $(3/3_I, 10)$-CSA-ES using $q_i = i$, $N = 40$ and $N = 200$. The results of the evolution equations in **II** for the y_i^2 dynamics, as well as the σ dynamics, are illustrated by the solid lines. The discrete data points display the corresponding experimental results which are averaged over 10^4 independent runs of the ES. All experiments and the iterative system **II** are initialized at $\sigma^{(0)} = 1$, and $\boldsymbol{y}^{(0)} = \mathbf{1} \in \mathbb{R}^N$ making use of the recommended CSA specific strategy parameters $c = 1/\sqrt{N}$ and $D = 1/c$.

The dynamics of the systems **I** and **II** show deviations considering search space dimension $N = 40$. Using a higher dimensionality $N = 200$, the agreement of both iterative dynamics increases significantly. Both systems of evolution equations show the same long-term behavior and agree for sufficiently high dimensions N. Making use of the evolution equations **II** in Tab. 4.2 is reasonable because it allows for a tractable investigation of the CSA-ES. Thus it will be the basis for the derivations in the following sections. The compliance of the predictions from the iterative scheme **II** with experimental runs of the ES is illustrated in Fig. 4.4. The good approximation quality justifies the modeling approach by the use of the iterative scheme **I** or **II**, respectively. That is, for small dimensional problems the use of iterative scheme **I** will provide more precise predictions of the ES dynamics. Considering higher dimensional spaces both systems provide a reliable modeling of the ES behavior. Two phases in the dynamics of the $(\mu/\mu, \lambda)$-CSA-ES can be observed in the illustrations. After the start of the optimization the ES dynamics enter a transient phase. This is followed by approaching a steady state behavior. The transient period is characterized by a decrease of the y_i^2 curves and the σ values. The rate of this decline increases with i. That is, y_1 decreases significantly slower than y_N. The steady state behavior is featured by a slower decrease with the same rate for all single components y_i^2, $i = 1, \ldots, N$. In particular, the y_i^2 dynamics fall with a log-linear law. The steady state of the σ values exhibits a log-linear behavior as well, but with a different rate of decline.

Remember the three ES variants compared in Sec. 3.3, i.e. $(\mu/\mu_I, \lambda)$-σSA-ES, $(\mu/\mu_I, \lambda)$-CSA-ES and $[1, 2(\mu/\mu_I, \lambda)^\gamma]$-meta-ES. The dynamical behavior observed in Fig. 4.4 represents a similarity of the ESs regardless of the mutation adaptation approach. The remarkable steady state observation that the optimizer is approached at the same rate in each parameter

vector component, can be identified with the ability of the ES variants to adapt the Newton direction of the optimization problem. Hence, on the ellipsoid model the CSA-ES is expected to gradually step in Newton direction towards the optimizer.

4.3. The steady state dynamics

The observed behavior of the Evolution Strategy suggests that the strategy exhibits a stationary behavior after leaving the transient phase. The rate of the constant log-linear decline in the steady state phase is calculated in the following. For this purpose, system **II** in Tab 4.2 of $2N + 2$ evolution equations is reduced once more by derivation of an approximate SAR function that characterizes the mutation strength dynamics. Applying a specific *Ansatz* the resulting system is transformed in an eigenvalue problem which can be solved numerically. Finally, the approach allows for the derivation of the normalized mutation strength dynamics as well as for an intuition of parameter influences on the strategy's progress. The results are used in the next section to calculate closed solutions for the strategy's normalized steady state mutation strength σ^*_{ss} on the ellipsoid model. Thereby, conclusions about advantageous strategy parameter settings can be drawn. Further, in its steady state the evolutionary system allows to determine convergence rate results on the ellipsoid model. On this basis, the expected running time of the CSA-ES can be derived.

4.3.1. Self-adaptation response approximation for CSA

After having validated the modeling of the system of evolution equations **II** (Table 4.2), finding a closed form solution to the system of $2N + 2$ nonlinear difference equations still appears to be a difficult task. The goal of the subsequent section is to substitute the $N + 2$ equations which model the σ dynamics, i.e. (II.2) to (II.4) in Table 4.2, by one single evolution equation. As it turns out, considering the steady state dynamics allows for the derivation of a suitable SAR approximation. That is, the search path $\mathbf{s}$ dynamics in the strategy's steady state can be used to provide an asymptotically exact approximation of a function analogous to the self-adaptation response function of σ self-adaptation ES [Beyer and Melkozerov, 2014]. To this end, the steady state dynamics of the difference equations (II.2) and (II.3) are investigated. In the first step the steady state dynamics of the scalar product components $\mathrm{E}\left[s_i^{(g)}\langle z\rangle_i^{(g)}\right]$ are examined. Afterwards the focus is on the resulting steady state dynamics of the complete search path. Using the steady state condition for the scalar product components

$$\mathrm{E}\left[s_i^{(g+1)}\langle z\rangle_i^{(g+1)}\right] = \mathrm{E}\left[s_i^{(g)}\langle z\rangle_i^{(g)}\right] =: \left(s_i\langle z\rangle_i\right)_{ss}, \tag{4.12}$$

and solving (II.2) for $\left(s_i\langle z\rangle_i\right)_{ss}$ yields

$$\left(s_i\langle z\rangle_i\right)_{ss} = c^2_{\mu/\mu,\lambda}\sqrt{\frac{\mu(2-c)}{c}}\,\frac{\dfrac{q_i^2 y_i^2}{R_q^2(\mathbf{y})} - \dfrac{q_i\sigma_{ss}}{\mu c_{\mu/\mu,\lambda} R_q(\mathbf{y})}}{1 + \dfrac{(1-c)}{c}\dfrac{c_{\mu/\mu,\lambda} q_i \sigma_{ss}}{R_q(\mathbf{y})}}. \tag{4.13}$$

Applying the mutation strength normalization (3.14) one obtains

$$\left(s_i\langle z\rangle_i\right)_{ss} = c^2_{\mu/\mu,\lambda}\sqrt{\frac{\mu(2-c)}{c}}\,\frac{\dfrac{q_i^2 y_i^2}{R_q^2(\mathbf{y})} - \dfrac{q_i\sigma^*_{ss}}{\mu c_{\mu/\mu,\lambda}\Sigma q}}{1+\dfrac{(1-c)}{c}\dfrac{c_{\mu/\mu,\lambda}q_i\sigma^*_{ss}}{\Sigma q}}. \tag{4.14}$$

A simplification of Eq. (4.14) is obtained by requiring that the second addend in the denominator is sufficiently small, i.e., by demanding that the condition

$$\frac{(1-c)}{c}\frac{c_{\mu/\mu,\lambda}q_i\sigma^*_{ss}}{\Sigma q} \ll 1 \tag{4.15}$$

is fulfilled. Eq. (4.15) has to be satisfied for all $i = 1\ldots,N$, i.e. particularly for the largest coefficient $\max_{i=1,\ldots,N} q_i =: \hat{q}$, leading to

$$\frac{(1-c)}{c}\frac{c_{\mu/\mu,\lambda}\hat{q}\sigma^*_{ss}}{\Sigma q} \ll 1. \tag{4.16}$$

Rearranging the terms and taking into account $\sigma^*_{ss} \leq 2\mu c_{\mu/\mu,\lambda}$, see (4.31), condition (4.15) becomes

$$\frac{\hat{q}}{\Sigma q} \ll \frac{c}{(1-c)}\frac{1}{2\mu c^2_{\mu/\mu,\lambda}}. \tag{4.17}$$

By resolving (4.17) for c, the condition can also be formulated as

$$c \gg \frac{1}{1+\frac{\Sigma q}{2\mu c^2_{\mu/\mu,\lambda}\hat{q}}}. \tag{4.18}$$

Notice, that in the three considered cases of the ellipsoid model with coefficients $q_i = 1, i, i^2$ the requirement (4.18) is not always fulfilled when choosing the cumulation parameter proportional to the reciprocal of the search space dimension $c \propto 1/N$. However, choices $c \propto 1/\sqrt{N}$ will yield asymptotically exact results. If (4.17) is satisfied, the respective term on the left-hand side of (4.15) can be neglected in (4.14) yielding

$$\left(s_i\langle z\rangle_i\right)_{ss} = c^2_{\mu/\mu,\lambda}\sqrt{\frac{\mu(2-c)}{c}}\left(\frac{q_i^2 y_i^2}{R_q^2(\mathbf{y})} - \frac{q_i\sigma^*_{ss}}{\mu c_{\mu/\mu,\lambda}\Sigma q}\right). \tag{4.19}$$

After addition of all components the steady state of the scalar product reads

$$\left(\mathbf{s}^\top\langle\mathbf{z}\rangle\right)_{ss} = c^2_{\mu/\mu,\lambda}\sqrt{\frac{\mu(2-c)}{c}}\left(1 - \frac{\sigma^*_{ss}}{\mu c_{\mu/\mu,\lambda}}\right). \tag{4.20}$$

Now that a description of the steady state of the scalar product is found, the next step is concerned with the derivation of the steady state of the squared length of the search path vector $\|\mathbf{s}\|^2$. Again the use of the steady state condition

$$\mathrm{E}\left[\|\mathbf{s}^{(g+1)}\|^2\right] = \mathrm{E}\left[\|\mathbf{s}^{(g)}\|^2\right] =: \|\mathbf{s}\|^2_{ss} \tag{4.21}$$

combined with Eq. (II.3) yields an asymptotically exact expression for the $\|\mathbf{s}\|^2$ dynamics in the proximity of the steady state

$$\|\mathbf{s}\|^2_{ss} = (1 - c(2-c))\,\|\mathbf{s}\|^2_{ss} + 2(1-c)\sqrt{\mu c(2-c)}\,(\mathbf{s}^\top \langle \mathbf{z} \rangle)_{ss} + Nc(2-c). \tag{4.22}$$

Solving this for $\|\mathbf{s}\|^2_{ss}$ and plugging in (4.14), Eq. (4.22) becomes

$$\|\mathbf{s}\|^2_{ss} = N + 2\frac{1-c}{c}\mu c^2_{\mu/\mu,\lambda} \sum_{i=1}^{N} \frac{\dfrac{q_i^2 y_i^2}{R_q^2(\mathbf{y})} - \dfrac{q_i \sigma^*_{ss}}{\mu c_{\mu/\mu,\lambda} \Sigma q}}{1 + \dfrac{(1-c)}{c}\dfrac{c_{\mu/\mu,\lambda} q_i \sigma^*_{ss}}{\Sigma q}}, \tag{4.23}$$

or

$$\|\mathbf{s}\|^2_{ss} = N + 2\frac{1-c}{c}\mu c^2_{\mu/\mu,\lambda}\left(1 - \frac{\sigma^*_{ss}}{\mu c_{\mu/\mu,\lambda}}\right) \tag{4.24}$$

respectively, by using simplification (4.20). Equation (4.24) has a simple interpretation: The steady state length square of the evolution path $\|\mathbf{s}\|^2_{ss}$ assumes the length square of the random path if the normalized steady state mutation strength σ^*_{ss} is exactly $\mu c_{\mu/\mu,\lambda}$. Since the latter is the optimal value for the sphere model, in a scale invariant picture, it can be used to control the mutation strength. The renormalized version of Eq. (4.23)

$$\|\mathbf{s}\|^2_{ss} = N + 2\frac{1-c}{c}\mu c^2_{\mu/\mu,\lambda} \sum_{i=1}^{N} \frac{\dfrac{q_i^2 y_i^2}{R_q^2(\mathbf{y})} - \dfrac{q_i \sigma_{ss}}{\mu c_{\mu/\mu,\lambda} R_q(\mathbf{y})}}{1 + \dfrac{(1-c)}{c}\dfrac{c_{\mu/\mu,\lambda} q_i \sigma_{ss}}{R_q(\mathbf{y})}} \tag{4.25}$$

serves as an approximation for the short-term behavior of the search path which describes the progress of the search path between two consecutive generations sufficiently well. Applying Eq. (4.25) to (II.4) the mutation strength dynamics can be modeled by the single evolution equation

$$\sigma^{(g+1)} = \sigma^{(g)}\left(1 + \frac{\mu c^2_{\mu/\mu,\lambda}}{DN}\frac{(1-c)}{c} \sum_{i=1}^{N} \frac{\dfrac{q_i^2 y_i^{(g)2}}{R_q^2(\mathbf{y}^{(g)})} - \dfrac{q_i \sigma^{(g)}}{\mu c_{\mu/\mu,\lambda} R_q(\mathbf{y}^{(g)})}}{1 + \dfrac{(1-c)}{c}\dfrac{c_{\mu/\mu,\lambda} q_i \sigma^{(g)}}{R_q(\mathbf{y}^{(g)})}}\right). \tag{4.26}$$

The second addend within the braces can be interpreted as the self-adaptation response (SAR) function $\tilde{\psi}$ of the $(\mu/\mu, \lambda)$-CSA-ES in the steady state. Using (3.14) the normalized version of $\tilde{\psi}$ reads

$$\tilde{\psi}\left(\sigma^{*(g)}, \mathbf{y}^{(g)}\right) = \frac{\mu c^2_{\mu/\mu,\lambda}}{DN}\frac{(1-c)}{c} \sum_{i=1}^{N} \frac{\dfrac{q_i^2 y_i^{(g)2}}{R_q^2(\mathbf{y}^{(g)})} - \dfrac{q_i \sigma^{*(g)}}{\mu c_{\mu/\mu,\lambda} \Sigma q}}{1 + \dfrac{(1-c)}{c}\dfrac{c_{\mu/\mu,\lambda} q_i \sigma^{*(g)}}{\Sigma q}}. \tag{4.27}$$

Iterative Scheme of Evolution Equations III

$$y_i^{(g+1)^2} \leftarrow y_i^{(g)^2} - \varphi_i^{II}\left(\sigma^{(g)}, \mathbf{y}^{(g)}\right), \qquad \text{(III.1)}$$

$$\sigma^{(g+1)} \leftarrow \sigma^{(g)}\left(1 + \tilde{\psi}\left(\sigma^{(g)}, \mathbf{y}^{(g)}\right)\right). \qquad \text{(III.2)}$$

Table 4.3.: Iterative scheme **III** is composed of the difference equations describing the y_i^2 dynamics, see (II.1), as well as the σ dynamics which is now modeled with help of the strategy's SAR function (4.27).

Considering (4.26) and (4.10), (4.7), the strategy's mean value dynamics in the steady state can be described by the iterative scheme **III** in Table 4.3, where $\tilde{\psi}\left(\sigma^{(g)}, \mathbf{y}^{(g)}\right)$ is obtained from (4.27) by substitution of σ^* using (3.14). Since the mean value dynamics are considered the fluctuation terms $\epsilon_i\left(\sigma^{(g)}, \mathbf{y}^{(g)}\right)$, and $\epsilon_\sigma\left(\sigma^{(g)}, \mathbf{y}^{(g)}\right)$ are neglected in Tab. 4.3. A comparison of the iteratively generated dynamics from scheme **III** to those of scheme **II** is displayed in Fig. 4.5. The good agreement of both dynamics for small dimension $N = 40$, as well as for high dimensionality $N = 200$, validates the use of the SAR function $\tilde{\psi}$ (4.27) to model the ES dynamics.

Provided that (4.17) is fulfilled, the terms of the SAR function in (4.26) can be further simplified, leading to

$$\tilde{\psi}\left(\sigma^{(g)}, \mathbf{y}^{(g)}\right) = \frac{\mu c_{\mu/\mu,\lambda}^2}{DN}\frac{(1-c)}{c}\left(1 - \frac{\sigma^{(g)}\Sigma q}{\mu c_{\mu/\mu,\lambda} R_q(\mathbf{y}^{(g)})}\right). \qquad (4.28)$$

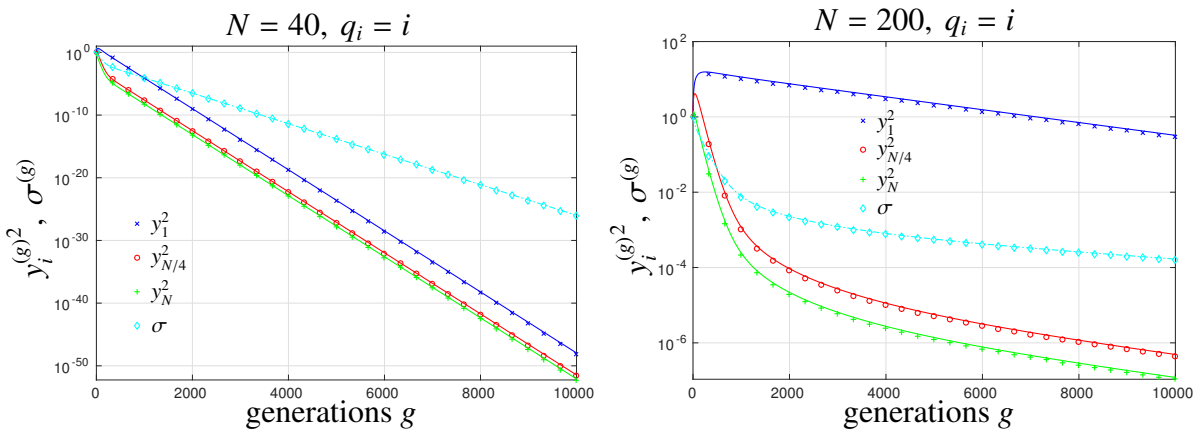

Figure 4.5.: Comparison of the iterative systems **II** and **III** simulating a $(3/3, 10)$-CSA-ES. The dynamics of the component-wise squared distances to the optimizer y_i resulting from system **II** are illustrated by the solid lines. The blue dashed line represents the corresponding σ dynamics. The results of scheme **III** are displayed by the discrete data points. Both iterative schemes are initialized at $\sigma^{(0)} = 1$, $\boldsymbol{y}^{(0)} = \mathbf{1} \in \mathbb{R}^N$, and with $c = 1/\sqrt{N}$ and $D = 1/c$.

Iterative Scheme of Evolution Equations IV

$$y_i^{(g+1)^2} \leftarrow y_i^{(g)^2} - \varphi_i^{II}\left(\sigma^{(g)}, \mathbf{y}^{(g)}\right), \tag{IV.1}$$

$$\sigma^{(g+1)} \leftarrow \sigma^{(g)}\left(1 + \frac{\mu c_{\mu/\mu,\lambda}^2}{DN}\frac{(1-c)}{c}\left(1 - \frac{\sigma^{(g)}\Sigma q}{\mu c_{\mu/\mu,\lambda} R_q(\mathbf{y}^{(g)})}\right)\right). \tag{IV.2}$$

Table 4.4.: Iterative scheme **IV** is composed of the y_i^2 difference equations, see (III.1), and the σ dynamics which is modeled using the simplified SAR function in (4.28).

Hence, making use of (4.28), the iterative scheme **III** transforms into the simplified iterative scheme **IV** in Tab. 4.4.

The approximation quality of system **IV** is validated in Fig. 4.6 for different choices of the cumulation parameter c and the search space dimensionality N. On the right-hand side of Fig. 4.6 the cumulation parameter c is set to $c = 1/N$ in such a way that condition (4.17) is not satisfied (provided that the ellipsoid coefficients are $q_i = i$). As a consequence one observes larger deviations between the two iterative schemes **III** and **IV**. However, these deviations are generally more pronounced in the transient phase of the evolutionary process that is emphasized in the plots due to the use of a logarithmic scale for the horizontal axes. The left-hand side displays a scenario where condition (4.17) is fulfilled ($c = 1/\sqrt{N}$). Especially with growing dimensionality a visually good agreement of both systems of evolution equation can be noticed. Having qualitatively validated the modeling approach, the deduction of closed-form solutions to the system **III** can be performed according to the approach introduced in [Beyer and Melkozerov, 2014].

Taking a look at Fig. 4.5 one observes that after transition periods of different length all y_i^2 curves approach a log-linear behavior with the same slopes. The same log-linear trend holds true for the σ dynamics, but it exhibits a different slope. This observation suggests that the system **III** asymptotically reaches a log-linear systems behavior. Therefore, modeling closed-form solutions by exponential functions is reasonable. Thus, in the proximity of the steady state the following *Ansatz* can be used to solve the equations

$$\begin{aligned} y_i^{(g)^2} &= b_i \mathrm{e}^{-\nu g}, \quad b_i > 0,\ \nu > 0, \\ \sigma^{(g)} &= \sigma_0 \mathrm{e}^{-\frac{\nu}{2} g}, \quad \sigma_0 > 0. \end{aligned} \tag{4.29}$$

This *Ansatz* has already been introduced in [Beyer and Melkozerov, 2014] in order to solve the evolution equations of the σSA-ES in the asymptotic limit ($g \to \infty$). It already takes the observed different slopes of y_i^2 and σ correctly into account. As a consequence, by inserting (4.29) into the normalization formula (3.14) one obtains the constant normalized steady state mutation strength

$$\sigma^* = \sigma_0 \frac{\Sigma q}{\sqrt{\sum_{j=1}^N q_j^2 b_j}} =: \sigma_{\mathrm{ss}}^*. \tag{4.30}$$

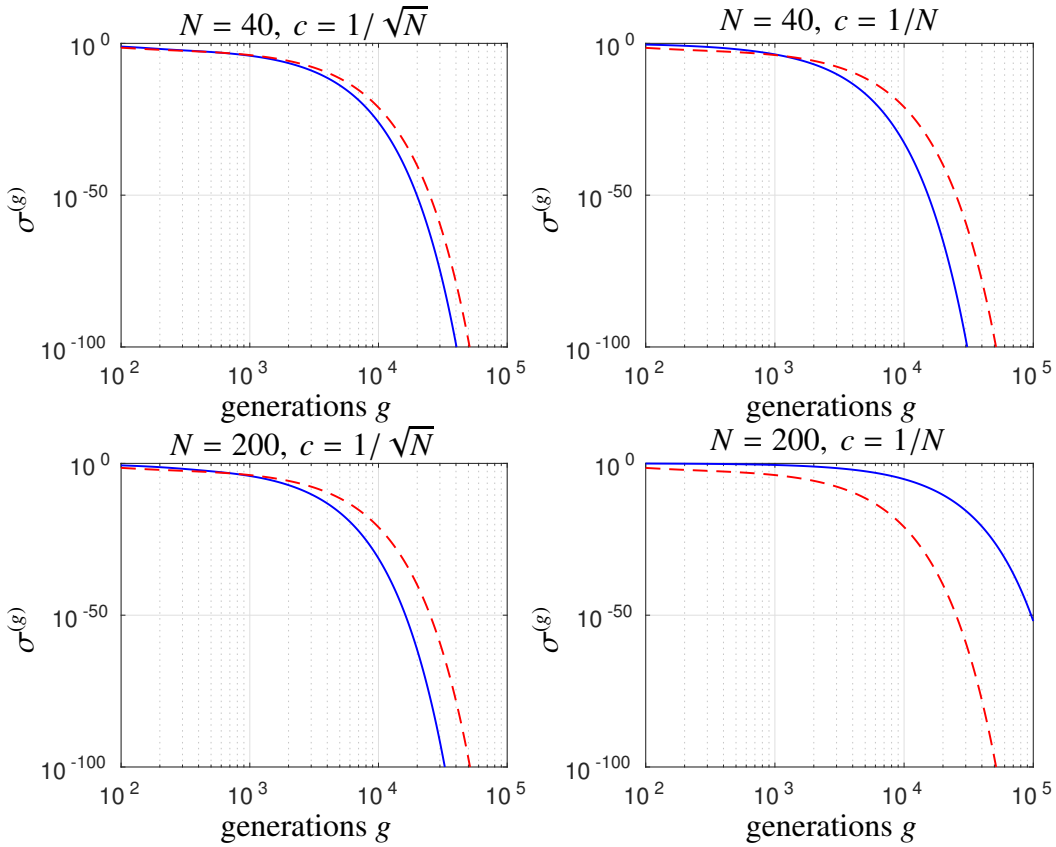

Figure 4.6.: Comparison of the σ dynamics simulating a $(3/3, 10)$-CSA-ES by use of the iterative schemes **III** and **IV** for the ellipsoid model $q_i = i$. The solid blue lines represent the σ dynamics resulting from iterative scheme **III**. The dashed red lines display the respective dynamics of scheme **IV**. While the cumulation parameter is set to $c = 1/\sqrt{N}$ on the left-hand side, it is $c = 1/N$ on the right-hand side of the illustration. The iterative schemes are initialized at $\sigma^{(0)} = 1$, and $\boldsymbol{y}^{(0)} = \mathbf{1} \in \mathbb{R}^N$. Both upper figures display the results for search space dimension $N = 40$. In the figures below $N = 200$ is chosen.

However, convergence to the optimizer requires that in expectation $y_i^{(g+1)^2} \leq y_i^{(g)^2}$. That is, according to Beyer and Melkozerov [2014], from (III.1) one can directly derive the convergence criterion

$$\sigma^* \leq 2\mu c_{\mu/\mu,\lambda}. \tag{4.31}$$

To this end, (III.1) is renormalized using (3.14). Eq. (4.31) is then created by multiplication with q_i and by taking the sum over all N components.

In the next step, the system **III** will be solved with the help of *Ansatz* (4.29). To that point, an eigenvalue problem will be established in the next section. In order to keep this thesis self-contained, the eigenvalue problem arising from (4.29) is considered in detail. This is done analogously to the modus operandi presented in [Beyer and Melkozerov, 2014].

4.3.2. The eigenvalue problem

Making use of the *Ansatz* (4.29) the squared distance to the optimizer y_i^2 and the mutation strength σ in generation $g+1$ can be expressed by means of their states in generation g

$$\begin{aligned} y_i^{(g+1)^2} &= b_i \mathrm{e}^{-\nu(g+1)} = b_i \mathrm{e}^{-\nu g}\mathrm{e}^{-\nu} = y_i^{(g)^2}\mathrm{e}^{-\nu} \\ \sigma^{(g+1)} &= \sigma_0 \mathrm{e}^{-\frac{\nu}{2}(g+1)} = \sigma_0 \mathrm{e}^{-\frac{\nu}{2}g}\mathrm{e}^{-\frac{\nu}{2}} = \sigma^{(g)}\mathrm{e}^{-\frac{\nu}{2}} \end{aligned} \tag{4.32}$$

From Fig. 4.5 it can be deduced that ν must be rather small. That is, $\mathrm{e}^{-\nu}$ can be simplified using Taylor expansion $\mathrm{e}^{-\nu} = 1-\nu+\mathrm{O}(\nu^2)$. Neglecting higher orders terms (4.29) transforms to

$$\begin{aligned} y_i^{(g+1)^2} &= (1-\nu)\, b_i \mathrm{e}^{-\nu g}, \\ \sigma^{(g+1)} &= \left(1-\frac{\nu}{2}\right)\sigma_0 \mathrm{e}^{-\frac{\nu}{2}g}. \end{aligned} \tag{4.33}$$

Inserting the equations of (4.33) into (III.1) and (III.2) of iterative scheme **III** in Tab. 4.3 yields after modification

$$\begin{aligned} \nu b_i &= \frac{2\sigma_0 c_{\mu/\mu,\lambda} q_i b_i}{\sqrt{\sum_{j=1}^N q_j^2 b_j}} - \frac{\sigma_0^2}{\mu}, \\ \nu &= -2\frac{(1-c)}{DNc}\mu c_{\mu/\mu,\lambda}^2 \sum_{i=1}^N \frac{\dfrac{q_i^2 b_i}{\sum_{j=1}^N q_j^2 b_j} - \dfrac{q_i \sigma_0}{\mu c_{\mu/\mu,\lambda}\sqrt{\sum_{j=1}^N q_j^2 b_j}}}{1+\dfrac{(1-c)}{c}\dfrac{c_{\mu/\mu,\lambda} q_i \sigma_0}{\sqrt{\sum_{j=1}^N q_j^2 b_j}}}. \end{aligned} \tag{4.34}$$

Taking Eq. (4.30) into account, one obtains a nonlinear system of $N+1$ equations

$$\nu b_i = \frac{2\sigma_{\mathrm{ss}}^* c_{\mu/\mu,\lambda} q_i b_i}{\Sigma q} - \frac{{\sigma_{\mathrm{ss}}^*}^2 \sum_{j=1}^N q_j^2 b_j}{\mu\,(\Sigma q)^2}, \tag{4.35}$$

$$\nu = -2\frac{(1-c)}{DNc}\mu c_{\mu/\mu,\lambda}^2 \sum_{i=1}^N \frac{\dfrac{q_i^2 b_i}{\sum_{j=1}^N q_j^2 b_j} - \dfrac{q_i \sigma_{\mathrm{ss}}^*}{\mu c_{\mu/\mu,\lambda}\Sigma q}}{1+\dfrac{(1-c)}{c}\dfrac{c_{\mu/\mu,\lambda} q_i \sigma_{\mathrm{ss}}^*}{\Sigma q}}, \tag{4.36}$$

where ν, b_i, and σ_{ss}^* are unknown. Notice, Eq. (4.36) contains the SAR function (4.27) revealing the relation

$$\frac{\nu}{2} = -\tilde{\psi}\left(\sigma_{ss}^*\right). \tag{4.37}$$

Comparing this equation with Eq. (4.29), one sees that the rate by which σ evolves in the steady state is given by the (negative) value of the SAR function $\tilde{\psi}$.

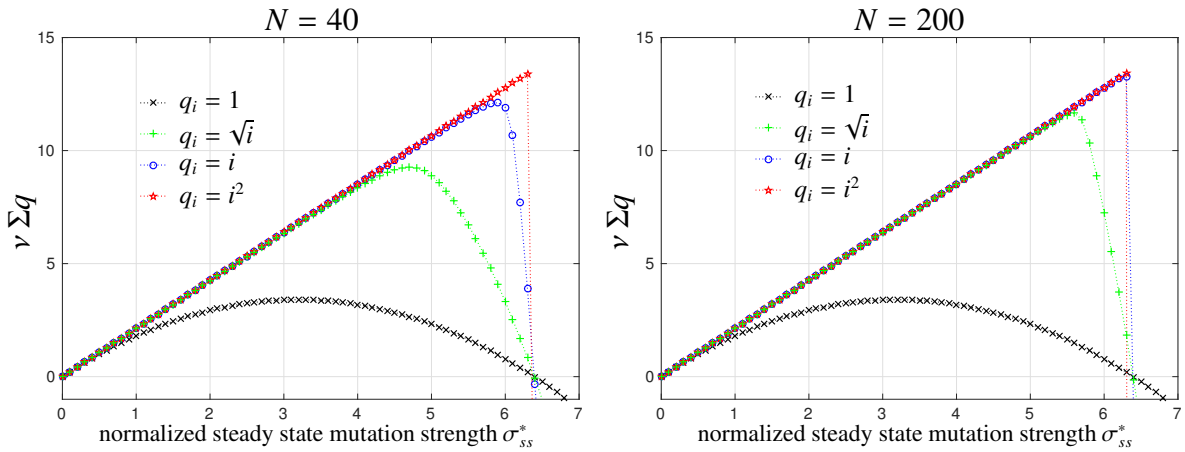

Figure 4.7.: On the dependence of the numerically calculated smallest eigenvalues (multiplied by Σq) on the steady state mutation strength σ^*. The results of the $(3/3, 10)$-CSA-ES are presented for the ellipsoid model with coefficients $q_i = 1, \sqrt{i}, i, i^2$. The search space dimension is $N = 40$ (left figure) and $N = 200$.

Equation (4.35) can be rewritten in matrix form resulting in an eigenvalue problem

$$\mathbf{A} \cdot \mathbf{b} = \nu \mathbf{b}, \tag{4.38}$$

with eigenvector $\mathbf{b} = (b_1, b_2, \ldots, b_N)^\top$, steady state mutation strength $\sigma^*_{ss} = const.$, and an $N \times N$ matrix A component-wise given as

$$(\mathbf{A})_{ii} = 2\sigma^*_{ss} c_{\mu/\mu,\lambda} \frac{q_i}{\Sigma q} - \frac{{\sigma^*_{ss}}^2 q_i^2}{\mu(\Sigma q)^2}, \tag{4.39}$$

$$(\mathbf{A})_{ij} = \frac{-{\sigma^*_{ss}}^2 q_j^2}{\mu(\Sigma q)^2}, \quad i \neq j. \tag{4.40}$$

The matrix $\mathbf{A}$ has N eigenvalues ν and N eigenvectors $\mathbf{b}$. Due to the conditions of the *Ansatz* only those solutions of the eigenvalue problem with $\forall i: \; b_i > 0$ and $\nu > 0$ are acceptable. The *Ansatz* indicates that larger eigenvalues ν result in a much faster decay of the y_i^2 and σ dynamics. That is, in comparison to the smallest eigenvalue the impact of the larger ν values will decrease with $g \to \infty$. Accordingly, one is interested in the smallest eigenvalue ν such that the corresponding eigenvector $\mathbf{b}$ satisfies the condition $\forall i: \; b_i > 0$. Considering the models $q_i = 1, i, i^2$, and additionally $q_i = \sqrt{i}$, the corresponding smallest eigenvalues resulting from (4.38) are shown in Fig. 4.7. The ellipsoid model $q_i = \sqrt{i}$ is included to better assess the transition from the sphere model to the ellipsoid model. For $q_i = i$, as well as $q_i = i^2$, the numerically obtained points exhibit a linear growth over a wide range of σ^* values. While its coefficients are closer to those of the sphere model, even the $q_i = \sqrt{i}$ case exhibits this behavior to a certain extend. The general tendency of the eigenvalue dependence is characterized by a linear ascent and a sudden sharp drop in the vicinity of the maximal value of the normalized mutation strength at $\sigma^* = 2\mu c_{\mu/\mu,\lambda}$. The numerical results presented in Fig. 4.7 are identical to the results presented in [Beyer and Melkozerov, 2014] in the context of the self-adaptation ES.

Due to the linear behavior of the numerically obtained data points for sufficiently small values of σ^* it is possible to derive an analytical expression which describes the early growth. Therefore the quadratic σ^* terms within the eigenvalue problem (4.38) are neglected. This transforms Eqs. (4.39) and (4.40) into a diagonalized problem

$$\forall\, i \neq j:\ (\mathbf{A})_{ij} = 0 \qquad \text{and} \qquad (\mathbf{A})_{ii} = 2\sigma^*_{ss} c_{\mu/\mu,\lambda} \frac{q_i}{\Sigma q}. \tag{4.41}$$

Consequently, the N eigenvalues are identified with the N diagonal elements

$$\nu_i = 2\sigma^*_{ss} c_{\mu/\mu,\lambda} \frac{q_i}{\Sigma q}. \tag{4.42}$$

Since the steady state dynamics of the ES are governed by the smallest positive eigenvalue, the linear part for that ν corresponds to the smallest ellipsoid coefficient q_i. Writing

$$\check{q} \coloneqq \min_{j=1,\ldots,N} q_j \tag{4.43}$$

for the smallest coefficient, the linear parts of the curves in Fig. 4.7 can be expressed by

$$\nu_{lin}(\sigma^*_{ss}) = 2\sigma^*_{ss} c_{\mu/\mu,\lambda} \frac{\check{q}}{\Sigma q}. \tag{4.44}$$

This linear approximation of the steady state mode eigenvalue was already calculated for the σSA analysis in [Beyer and Melkozerov, 2014] and revealed good agreement with numerically obtained results for sufficiently small values of the normalized steady state mutation strength σ^*_{ss}.

4.3.3. The normalized steady state mutation strength

Having found a linear approximation of the steady state mode eigenvalue $\nu_{lin}(\sigma^*_{ss})$ in (4.44), this section addresses the computation of the effective normalized steady state mutation strength σ^*_{ss} realized by the CSA-ES. To this end, a difference equation that describes the change of the normalized mutation strength between two consecutive generations of the ES is derived in Appendix A.3. The evolution equation of the normalized mutation strength σ^* is asymptotically obtained in Eq. (A.34) as

$$\sigma^{*(g+1)} = \sigma^{*(g)} \left(1 + \frac{\sigma^{*(g)} c_{\mu/\mu,\lambda}}{\Sigma q} \frac{\sum_{i=1}^N q_i^3 y_i^{(g)2}}{R_q^2(\mathbf{y}^{(g)})} - \frac{\sigma^{*(g)2}}{2\mu} \frac{\sum_{i=1}^N q_i^2}{(\Sigma q)^2} \right) \left(1 + \tilde{\psi}\left(\sigma^{*(g)}, \mathbf{y}^{(g)}\right) \right), \tag{4.45}$$

with $\tilde{\psi}\left(\sigma^{*(g)}, \mathbf{y}^{(g)}\right)$ from Eq. (4.27). Applying the Ansatz (4.29) to Eq. (4.45), the σ^* evolution equation after resolving the parentheses reads

$$\sigma^{*(g+1)} = \sigma^{*(g)} \left(1 + \frac{\sigma^{*(g)} c_{\mu/\mu,\lambda}}{\Sigma q} \frac{\sum_{i=1}^N q_i^3 b_i}{\sum_{j=1}^N q_j^2 b_j} - \frac{\sigma^{*(g)2}}{2\mu} \frac{\sum_{i=1}^N q_i^2}{(\Sigma q)^2} + \tilde{\psi}\left(\sigma^{*(g)}\right) \right). \tag{4.46}$$

Notice, due to the complex form of $\tilde{\psi}(\sigma^{*(g)})$, Eq.(4.27), all mixed product terms of higher orders are aggregated in the error term $\Delta(\sigma^{*(g)})$. Provided that $cD = O(1)$, this error term vanishes at least by a factor of $1/N$ faster than the other terms in the parentheses of (4.46). This error term is neglected in the next steps to keep the further analysis manageable.

By demanding the steady state condition $\sigma^{*(g+1)} = \sigma^{*(g)} = \sigma^*_{ss}$, Eq. (4.46) can now be used to determine the steady state of the normalized mutation strength. Assuming $\Delta(\sigma^{*(g)}) \to \infty$ and considering the identity in Eq. (4.37) yields

$$\nu \stackrel{!}{=} 2\frac{\sigma^*_{ss} c_{\mu/\mu,\lambda}}{\Sigma q}\frac{\sum_{i=1}^N q_i^3 b_i}{\sum_{j=1}^N q_j^2 b_j} - \frac{{\sigma^*_{ss}}^2}{\mu}\frac{\sum_{i=1}^N q_i^2}{(\Sigma q)^2}. \tag{4.47}$$

By factorization of the quotient $\sum_{i=1}^N q_i^2 \Big/ (\Sigma q)^2$ this transforms into

$$\frac{\nu}{2} = \frac{\sum_{i=1}^N q_i^2}{(\Sigma q)^2}\left(\sigma^*_{ss} c_{\mu/\mu,\lambda}\frac{\Sigma q}{\sum_{i=1}^N q_i^2}\frac{\sum_{i=1}^N q_i^3 b_i}{\sum_{j=1}^N q_j^2 b_j} - \frac{{\sigma^*_{ss}}^2}{2\mu}\right). \tag{4.48}$$

The bracketed term on the right-hand side of (4.48),

$$\tilde{\varphi}^*(\sigma^*_{ss}) := \sigma^*_{ss} c_{\mu/\mu,\lambda}\frac{\Sigma q}{\sum_{i=1}^N q_i^2}\frac{\sum_{i=1}^N q_i^3 b_i}{\sum_{j=1}^N q_j^2 b_j} - \frac{{\sigma^*_{ss}}^2}{2\mu}, \tag{4.49}$$

shares some similarities with the progress rate φ^*_{sp} that was obtained on the sphere model in [Beyer, 2001, p. 217] as

$$\varphi^*_{sp}(\sigma^*) = c_{\mu/\mu,\lambda}\sigma^* - \frac{\sigma^{*2}}{2\mu}. \tag{4.50}$$

Actually, Eq. (4.50) is recovered in (4.49) for the sphere model, i.e. $\forall i : q_i = 1$. Recalling the identity $\nu = -2\tilde{\psi}(\sigma^*_{ss})$, see (4.37), finally yields the steady state condition

$$-\tilde{\psi}(\sigma^*_{ss}) = \frac{\sum_{i=1}^N q_i^2}{(\Sigma q)^2}\tilde{\varphi}^*(\sigma^*_{ss}). \tag{4.51}$$

Inserting $q_i = 1$, $\forall i = 1, \ldots, N$ into (4.51) and considering the corresponding SAR function ψ^*_{sp} yields the well-known steady state condition in the context of the sphere model derived in [Meyer-Nieberg and Beyer, 2005]

$$-\psi^*_{sp}(\sigma^*_{ss}) = \varphi^*_{sp}(\sigma^*_{ss})/N. \tag{4.52}$$

This is remarkable, the novel analysis approach presented describes the steady state by an equation (4.51) that is formally similar to the sphere model theory of the σSA-ES.

Equation (4.51) allows for the calculation of the normalized steady state mutation strength σ^*_{ss}. Regarding both sides of Eq. (4.51) as functions of σ^* the curves intersect at the normalized steady state mutation strength σ^*_{ss} realized by the CSA-ES.

Considering the $(3/3_I, 10)$-ES on the sphere model ($q_i = 1$) as well as on the ellipsoid model $q_i = i^2$, the resulting graphs are shown in Fig. 4.8 using search space dimension

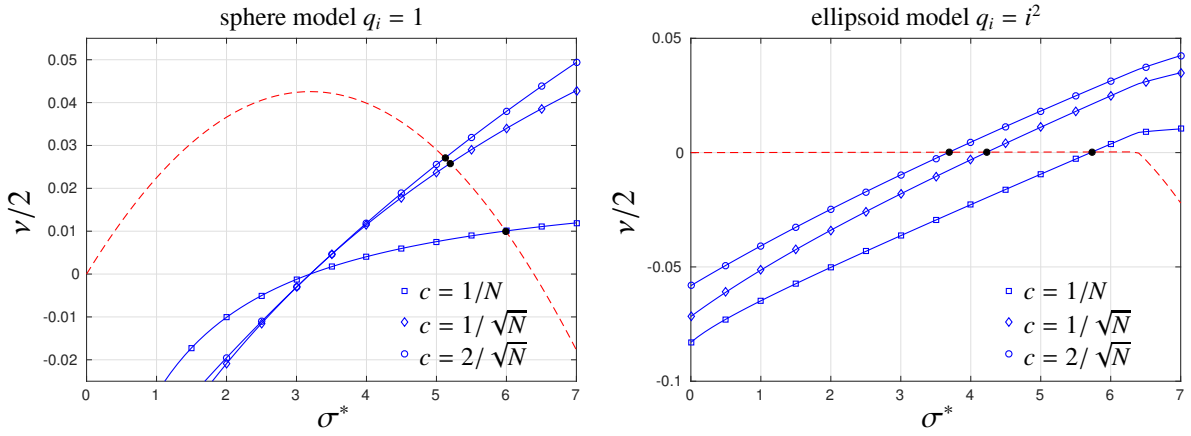

Figure 4.8.: Illustration of steady state condition (4.51) for a $(3/3_I, 10)$-CSA-ES with $D = 1/c$ in search space dimension $N = 40$. Both sides of (4.51) are plotted against the normalized mutation strength σ^*. For three different cumulation parameter choices, the solid blue lines present the progression of the negative SAR approximation $-\tilde{\psi}(\sigma^*)$ (4.27). The right-hand side of Eq. (4.51) is displayed by the dashed red line. The steady state σ^*_{ss} of the normalized mutation strength is located at the intersection points of the respective curves (black dots).

$N = 40$. In each case three different choices of the cumulation parameter are considered: $c = 2/\sqrt{N}$, $c = 1/\sqrt{N}$, and $c = 1/N$. The damping parameter is $D = 1/c$. According to Eq. (4.49), the right-hand side of (4.51) is independent of the choice of the parameters c and D. In Fig. 4.8 this quantity is displayed by the dashed red lines. On the other hand $\tilde{\psi}(\sigma^*_{ss})$ in the representation of (4.27) depends on c and D. Forming the left-hand side of condition (4.51), it is illustrated in Fig. 4.8 by use of solid blue lines. The markers indicate three different choices of the cumulation parameter c. The numerically computed solutions of Eq. (4.51) is represented by the black dots. Variations in c lead to relocations of the intersection point. From this behavior the existence of an optimal c value can be conjectured which tunes the ES to operate at maximal progress rate $\tilde{\varphi}^*$.

According to Eq (4.27) also the damping parameter D of the CSA-ES has an influence on the SAR approximation $\tilde{\psi}(\sigma^*)$. The dependence on D is addressed in Fig. 4.9 for the $N = 40$ case considering the sphere and the $q_i = i$ ellipsoid. The D values are varied holding the cumulation parameter $c = 1/\sqrt{N}$ and $c = 1/N$, respectively, constant. The dashed red line in both figures corresponds to the right-hand side in Eq. (4.51) together with (4.49). The $-\tilde{\psi}(\sigma^*)$ curves, which depend on the parameter D, are represented by the marked blue lines. As on can see, D influences the slope of $-\tilde{\psi}(\sigma^*_{ss})$. That is, increasing D, while keeping c constant, leads to a decrease of the $-\tilde{\psi}$ slope. As a consequence the intersection point of both curves moves to the right, i.e., the normalized steady state mutation strength is increased. Independent of the choice of the damping parameter D, all $-\tilde{\psi}(\sigma^*)$ graphs intersect in the same point σ^*_0 on the x-axis being the zero of $\tilde{\psi}$. Considering the sphere model this intersection point is independent of c. Since $\forall i : q_i = 1$, one obtains $\sigma^*_0 = \mu c_{\mu/\mu,\lambda}$ for the root of (4.27). In the case of the ellipsoid model with $q_i = i$ this zero varies with the cumulation parameter c. It shifts to the right for smaller c values. Hence, the corresponding

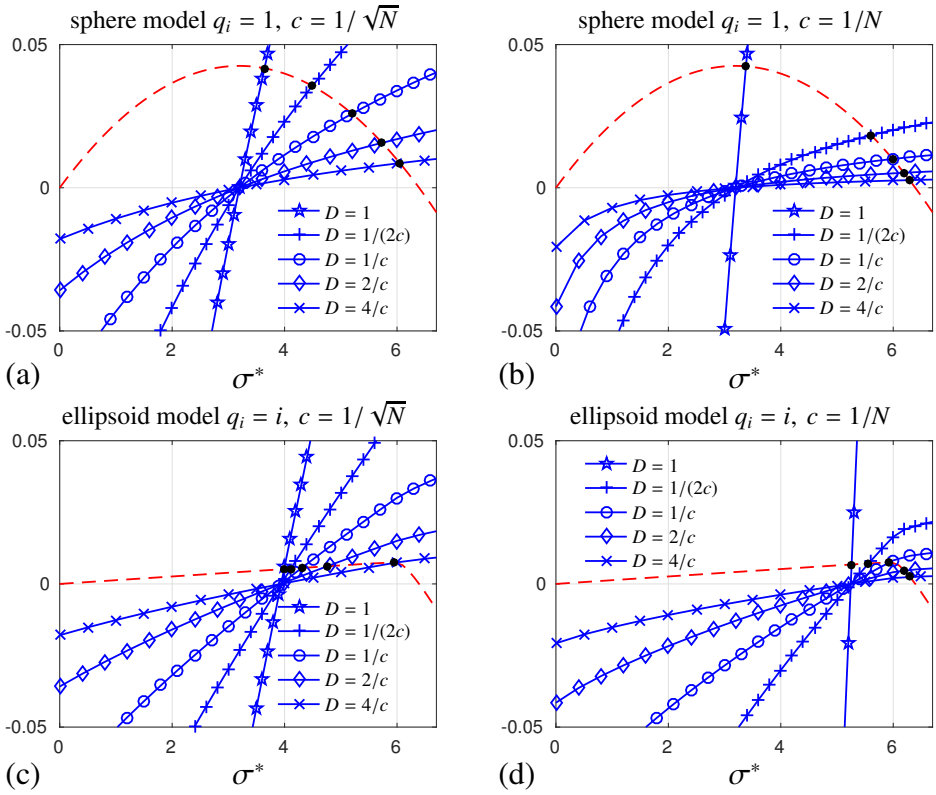

Figure 4.9.: The influence of the damping parameter D on the numerical solution of Eq. (4.51). The dashed red line depicts the right-hand side of (4.51), while the left-hand side is displayed by the solid blue lines for different choices of D. The $(3/3_I, 10)$-CSA-ES operates on the sphere, $q_i = 1$, and the ellipsoid model with $q_i = i$, using cumulation parameter $c = 1/\sqrt{N}$ (figures (a) and (c)) and $c = 1/N$ (figures (b) and (d)) for $N = 40$.

steady state σ^*_{ss} can only be obtained from Eq. (4.27) by numerical root finding.

The dashed red line in Fig. 4.9 represents the right-hand side of (4.51), which is by virtue of (4.49) and (4.48) equal to half the steady state mode eigenvalue ν_{ss}. Via the second equation of (4.29) the latter determines the rate by which the ES approaches the optimizer in the steady state. Since $\nu_{ss}/2$ is determined by σ^*_{ss}, it depends in turn on the choice of D and c. Fig. 4.10 displays these dependencies. To this end, ν_{ss} is multiplied with the term $\Sigma q/2\mu c_{\mu/\mu,\lambda}\check{q}$ in order to reduce the impact of the considered ellipsoid model as well as the impact of the population sizes on the realized progress. The resulting values are then plotted versus $\tau = 1/c$ being the cumulation time constant that influences the fading of the search path memory within the CSA-ES. The sphere model and the ellipsoid $q_i = i^2$ case are considered. As one can see in Fig. 4.10((c) and (d)) for the ellipsoid with $q_i = i^2$, there is almost no influence of the damping constant D formula on the progress rate towards the optimizer in the steady state. This is different to the case of the sphere model. The ellipsoid case $q_i = i$, not displayed in this paper, lies in between these two models.

As for the sphere model, Fig. 4.10 (a) and (b), $D = 1$ seems to be the better choice of the

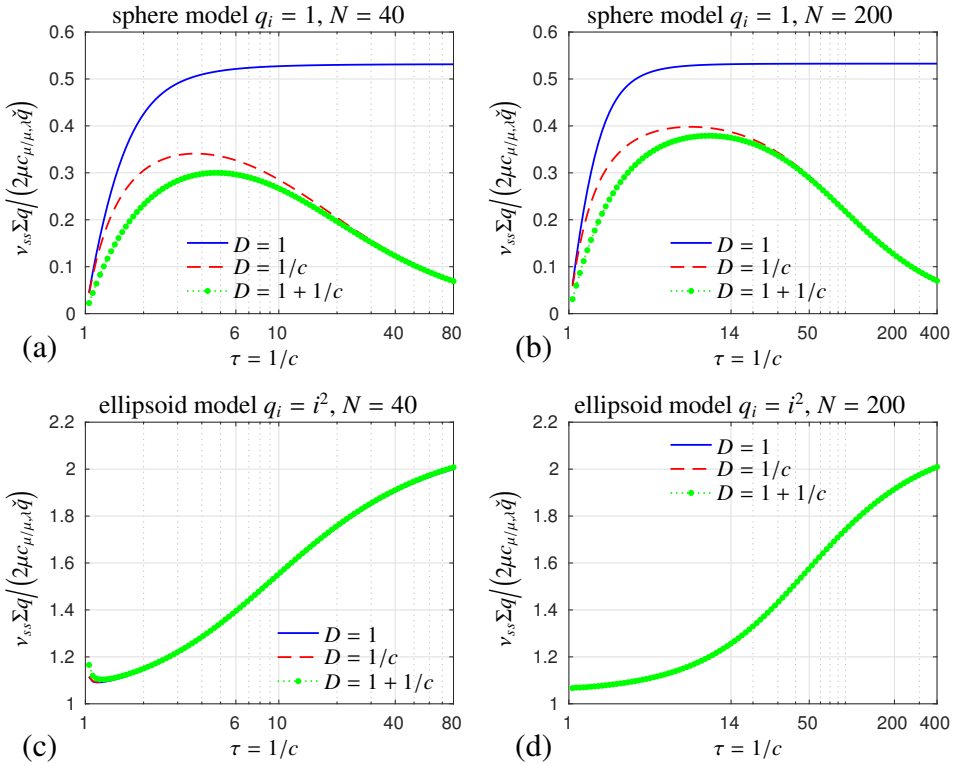

Figure 4.10.: The numerically calculated steady state mode eigenvalue ν_{ss} (4.48) multiplied by the term $\Sigma q/(2\mu c_{\mu/\mu,\lambda}\check{q})$ is plotted against the parameter $\tau = 1/c$. The curves for three different choices of D in search space dimension $N = 40$ and $N = 200$ are illustrated using a $(3/3_I, 10)$-CSA-ES on the sphere (figures (a) and (b)) and the ellipsoid with $q_i = i^2$ (figures (c) and (d)). Note, the curves regarding the ellipsoid overlap almost completely.

damping parameter compared to the standard recommendation in [Hansen and Ostermeier, 2001]. However, this ignores the effect of possible oscillations that have been neglected by considering the asymptotic solution of the iterative schemes using the *Ansatz* (4.29). Using small D values in line 11, Alg. 4.1, such as $D = 1$, results in large generational σ changes being the driving force of σ^* oscillations already empirically observed by Hansen [1998]. These oscillations can lead to considerable regression of the strategy's progress. That is why, larger D values such as $D = \sqrt{N}$ are to be recommended.

4.4. Closed-form expressions in the steady state

Within this section the normalized steady state mutation strength will be derived which in turn yields the convergence rate ν_{ss} and the exprected runtime of the CSA-ES. In order to find an analytical solution it is necessary to start with assumption (4.17)

$$\frac{(1-c)}{c}\frac{c_{\mu/\mu,\lambda}\hat{q}\sigma^*_{ss}}{\Sigma q} \ll 1. \tag{4.53}$$

This allows for the use of the simplified SAR function (4.28) from iterative scheme **IV** (Table 4.4) which after normalization (3.14) reads

$$\tilde{\psi}\left(\sigma^*_{ss}\right) = \frac{\mu c^2_{\mu/\mu,\lambda}}{DN}\frac{(1-c)}{c}\left(1 - \frac{\sigma^*_{ss}}{\mu c_{\mu/\mu,\lambda}}\right) \tag{4.54}$$

in the strategy's steady state. In the first step, considering only the sphere model ($\forall i = 1,\ldots,N : q_i = 1$) allows to replicate previous findings from Arnold and Beyer [2004]. Afterwards, using the linear approximation of the steady state mode eigenvalue the results are extended to more general ellipsoid models.

Derivations for the Sphere Model

On the basis of Eq. (4.51), using (4.54) and (4.49), and inserting the coefficients of the sphere model, i.e. $q_i = 1$, the equality

$$-\frac{\mu c^2_{\mu/\mu,\lambda}}{ND}\frac{(1-c)}{c}\left(1 - \frac{\sigma^*_{ss}}{\mu c_{\mu/\mu,\lambda}}\right) = \frac{1}{N}\left(c_{\mu/\mu,\lambda}\sigma^*_{ss} - \frac{{\sigma^*_{ss}}^2}{2\mu}\right). \tag{4.55}$$

is obtained. In order to solve Eq. (4.55) for σ^*_{ss} it is rearranged to

$${\sigma^*_{ss}}^2 - 2\mu c_{\mu/\mu,\lambda}\left(1 - \frac{(1-c)}{cD}\right)\sigma^*_{ss} - 2\mu^2 c^2_{\mu/\mu,\lambda}\frac{(1-c)}{cD} = 0, \tag{4.56}$$

consequently yielding the normalized steady state mutation strength

$$\sigma^*_{ss} = \mu c_{\mu/\mu,\lambda}\left[1 - \frac{(1-c)}{cD} + \sqrt{1 + \left(\frac{(1-c)}{cD}\right)^2}\right]. \tag{4.57}$$

There are different recommendations regarding the choice of D and c given in [Hansen, 1998]

$$D = \frac{1}{c} \quad \text{with} \quad c = \frac{1}{\sqrt{N}} \tag{4.58}$$

and [Hansen and Ostermeier, 2001]

$$D = 1 + \frac{1}{c} \quad \text{with} \quad c = \frac{4}{N+4} \tag{4.59}$$

which do not influence the outcome of (4.57) as $N \to \infty$. In both of these cases one obtains $cD \to 1$ and $(1-c) \to 1$, thus, yielding

$$\sigma^*_{ss} = \sqrt{2}\mu c_{\mu/\mu,\lambda}. \tag{4.60}$$

This estimate for the normalized steady state mutation strength of the $(\mu/\mu_I, \lambda)$-CSA-ES on the sphere model was already obtained in [Arnold and Beyer, 2004] using another approach. The result indicates that the steady state σ^* is by a factor of $\sqrt{2}$ too large compared to the optimal value $\sigma^*_{opt} = \mu c_{\mu/\mu,\lambda}$ that guarantees maximal convergence rate ν towards the optimizer

for the sphere model. As has been observed in Sec. 4.3.3, Fig. 4.10(a) and (b), choosing smaller D values can improve the situation as far as σ^*_{ss} is concerned. Equation (4.57) can be used to tune D to a certain extend to a target mutation strength $\sigma^*_{target} = \mu c_{\mu/\mu,\lambda}(1+\epsilon)$ $(0 < \epsilon < 1)$. Resolving (4.57) with $\sigma^*_{ss} = \sigma^*_{target}$ for D yields

$$D = 2\frac{\epsilon}{1-\epsilon^2}\frac{(1-c)}{c}. \tag{4.61}$$

Due to its use in the CSA-ES, see Alg. 4.1, the damping parameter D has to satisfy $D \geq 1$. Given a specific choice of the cumulation parameter c, this requirement directly constrains the choice of ϵ in (4.61) and thus the approximation of σ^*_{opt} by the target value σ^*_{target}. Example given, making use of $c = 1\sqrt{N}$ and D according to Eq. (4.61) in search space dimension $N = 40$ determines a target normalized mutation strength $\sigma^*_{target} = \mu c_{\mu/\mu,\lambda}(1+\epsilon)$ with $\epsilon \approx 0.093$ at best (ensuring $D \geq 1$).

Figure 4.11 compares performance of the $(3/3_I, 10)$-CSA-ES according to its strategy parameter settings on the sphere model $q_i = 1, \forall i = 1; \ldots, N$. Therefore, the dynamics of the fitness value $F(\boldsymbol{y}^{(g)})$ ((a) and (c)) as well as the normalized mutation strength $\sigma^{*(g)}$ dynamics ((b) and (d)) are displayed. Being initialized at $\boldsymbol{y}^{(0)} = \mathbf{1} \in \mathbb{R}^N$ and with $\sigma^{(0)} = 1$, all curves display the average of 100 independent CSA-ES runs. The results of different strategy parameter settings are presented considering search space dimensionality $N = 40$, and $N = 200$, respectively. The dynamics obtained by use of the strategy parameter in Eq. (4.58) are illustrated by use of the solid magenta lines. Those realized with setting (4.59) are displayed by the solid green lines. Taking into account different target values $\sigma^*_{target} = \mu c_{\mu/\mu,\lambda}(1+\epsilon)$, the dynamics according to Eq. (4.61) and the use of $c = 1/\sqrt{N}$ are represented by the solid blue ($\epsilon = 0.1$) and red ($\epsilon = 0.25$) lines. The theoretically optimal σ^*_{opt} is displayed by the dashed black line in (b) and (d).

The CSA dynamics relying on the settings according to (4.58) and (4.59) do not significantly differ in their steady state σ^* realization. Considering $N = 40$, the σ^* dynamics of setting (4.58) are located a little closer to the optimal value. Hence, the corresponding fitness dynamics exhibit a slightly faster decline. Regarding $N = 200$, the agreement increases. Making use of the cumulation parameter $c = 1/\sqrt{N}$ together with the damping parameter recommendation (4.61), in both cases allows for an improvement. Targeting a steady state σ^* closer to σ^*_{opt}, and choosing D (4.61) accordingly, accelerates the reduction of fitness dynamics.

However, the applicability of the resulting D (4.61) in real CSA-ES algorithm must be taken with care. It has been already discussed in Sec. 4.3.3 that D-values too small can result in oscillatory σ^* behavior. In particular, even after averaging over 100 independent runs this oscillation behavior can be observed taking into account the blue curve in Fig. 4.11(b) and (d). Considering search space dimension $N = 40$, the choice of $\epsilon = 0.1$ results in a damping parameter realization of $D \approx 1.08$ very close to 1. Despite the fact that the normalized mutation strength dynamics osculates around a σ^* value close to σ^*_{opt}, the oscillations are causing a substantial degradation of the strategy's progress. Avoiding huge oscillations, the CSA-ES that approaches $\sigma*_{target} = 1.25\sigma^*_{opt}$ with parameter setting $c = 1/\sqrt{N}$, $D \approx 2.8$ turns out to perform best. In search space dimension $N = 200$, the use of the same $\epsilon = 0.1$

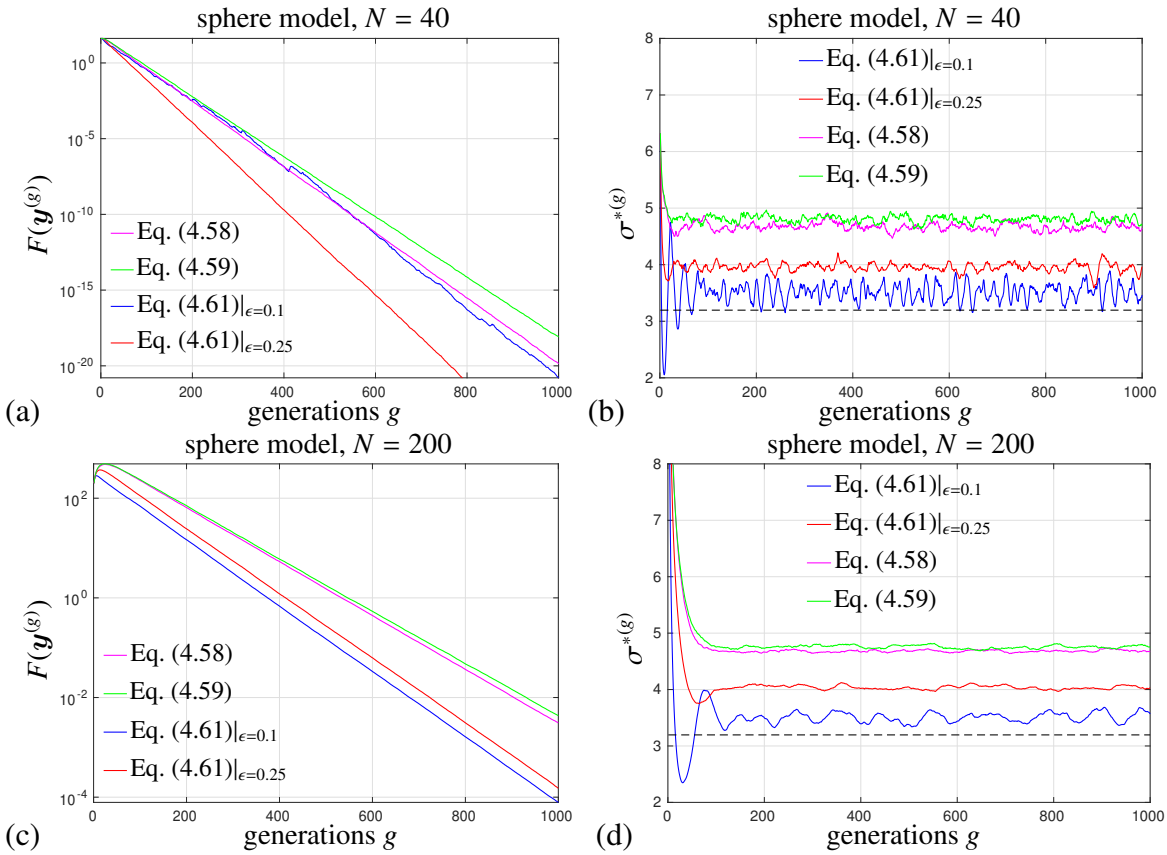

Figure 4.11.: Comparison of the $(3/3_I, 10)$-CSA-ES dynamics realized by application of four different strategy parameter settings for c and D. The fitness dynamics $F(\boldsymbol{y}^{(g)})$ as well as the dynamics of the normalized mutation strength $\sigma^{*(g)}$ are plotted against the number of generations g in search space dimensions $N = 40$, and $N = 200$, respectively. The solid lines of different colors indicate the specific CSA strategy parameters used in Alg. 4.1. The results according to Eq. (4.61) in both cases involve the cumulation parameter choice $c = 1/\sqrt{N}$. All curves are averaged over 100 independent algorithm runs. The dashed black line in (b) and (d) displays the optimal normalized mutation strength on the sphere model, i.e. $\sigma^*_{opt} = \mu c_{\mu/\mu,\lambda}$.

value determines a D close to 2.7. Accordingly, the amplitude of the oscillations in σ^* reduces and the CSA-ES is able to yield outperform the other strategies.

The amplitude of the σ^* oscillations observable in Fig. 4.11(b) and (d) is reflected by the error bar plots in Fig. 4.12. There, the mean value and the standard deviation of the normalized mutation strengths is plotted against the damping parameters D corresponding to the CSA-ES runs in Fig. 4.11. The data points are gathered by measuring mean values and standard deviations of $\sigma^{*(g)}$ over the last 500 generations in every single run and averaging over the number of runs. Optimal and target normalized mutation strength are illustrated by the dashed colored horizontal lines. It can be observed that the CSA-ES with $c = 1/\sqrt{N}$ and D according to (4.61) on average approaches a steady state σ^* close to the intended target.

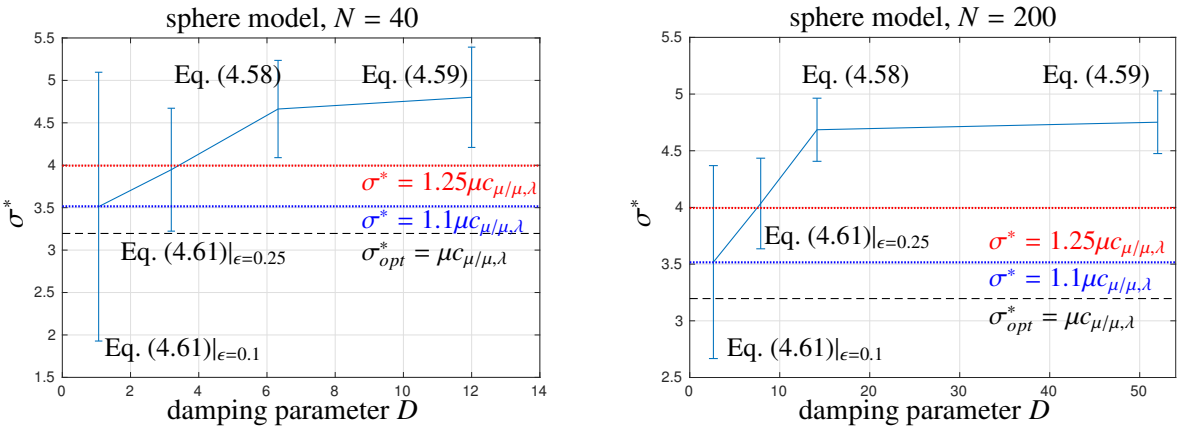

Figure 4.12.: Illustration of the oscillations in the σ^* dynamics corresponding to the damping parameter D choices used in the CSA-ES runs displayed in Fig. 4.11.

Derivation for the Ellipsoid Model

Considering other ellipsoid models than the special case of the sphere model the analytical derivation of the normalized steady state mutation strength from Eq. (4.51) is not possible. For that reason the linear approximation of the smallest eigenvalue ν_{lin} in Eq. (4.44) will be used. Remembering Eq. (4.37) and replacing ν by ν_{lin} one obtains $-\tilde{\psi}\left(\sigma^*_{ss}\right) = \nu_{lin}(\sigma^*_{ss})/2$. Inserting the respective expressions (4.54) and (4.44) results in

$$-\frac{\mu c^2_{\mu/\mu,\lambda}}{DN}\frac{(1-c)}{c}\left(1-\frac{\sigma^*_{ss}}{\mu c_{\mu/\mu,\lambda}}\right) = c_{\mu/\mu,\lambda}\sigma^*_{ss}\frac{\breve{q}}{\Sigma q}. \tag{4.62}$$

Equation (4.62) can then be solved for the normalized steady state mutation strength σ^*_{ss}:

$$-\frac{\mu c_{\mu/\mu,\lambda}}{DN}\frac{(1-c)}{c} + \frac{\sigma^*_{ss}}{DN}\frac{(1-c)}{c} = \sigma^*_{ss}\frac{\breve{q}}{\Sigma q}, \tag{4.63}$$

yielding finally the normalized steady state mutation strength

$$\sigma^*_{ss} = \frac{\mu c_{\mu/\mu,\lambda}}{\left(1-\frac{cDN}{(1-c)}\frac{\breve{q}}{\Sigma q}\right)}. \tag{4.64}$$

It only depends on the ellipsoid model coefficients as well as the choice of strategy parameters of the considered ES. Inserting (4.64) into (4.44) yields the linear approximation of the steady state mode eigenvalue

$$\nu_{ss} = \frac{\breve{q}}{\Sigma q}\frac{2\mu c^2_{\mu/\mu,\lambda}}{\left(1-\frac{cDN}{(1-c)}\frac{\breve{q}}{\Sigma q}\right)}. \tag{4.65}$$

That is, provided that the linear eigenvalue approximation holds, the CSA-ES approaches by virtue of Eq. (4.29) the optimizer with the convergence rate (4.65). With the help of (4.64), a condition on the choice of D can be derived. Requiring the convergence criterion (4.31), i.e. $\sigma^*_{ss} < 2\mu c_{\mu/\mu,\lambda}$, one obtains

$$D < \left(\frac{1}{c}-1\right)\frac{\Sigma q}{2N\breve{q}}. \tag{4.66}$$

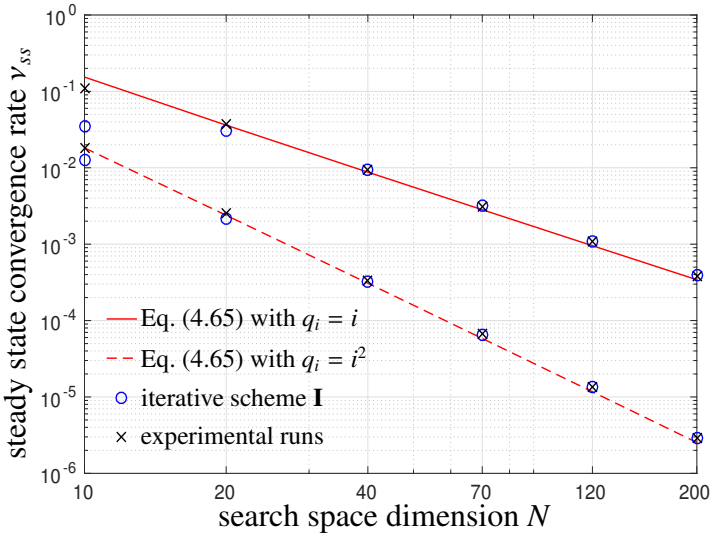

Figure 4.13.: The convergence rates (steady state eigenvalues) realized by the $(3/3_I, 10)$-CSA-ES are plotted against the search space dimension N for the ellipsoid models $q_i = i$ and $q_i = i^2$. Parameters are $c = 1/\sqrt{N}$ and $D = 1/c$. The experimental data are averaged over 100 independent runs.

According to Fig. 4.6 the linear ν approximation (4.44) is valid up to a certain $\check{\sigma}^* < 2\mu c_{\mu/\mu,\lambda}$ only. Therefore, the validity of the Eqs. (4.64, 4.65, 4.66) is restricted, too. Additionally, the derivation of the equations by use of (4.54) is only admissible assuming that condition (4.18) holds which constrains the range of the cumulation parameter

$$\frac{2\mu c_{\mu/\mu,\lambda}^2 \hat{q}}{2\mu c_{\mu/\mu,\lambda}^2 \hat{q} + \Sigma q} < c < 1. \tag{4.67}$$

This must be kept in mind when applying these formulae.

Figure 4.13 compares the theoretical predictions of the steady state convergence rate ν_{ss} with measurements from real $(3/3_I, 10)$-CSA-ES runs, as well as with iteratively generated results by making use of scheme **I**. The ellipsoid models $q_i = i$ and $q_i = i^2$ have been considered. The experimental convergence rates have been obtained by running the $(3/3_I, 10)$-CSA-ES over a sufficient long time until it reached its steady state. Then the y_1^2 values of the last 25% of generations have been averaged over 100 independent runs. After that, a linear polynomial $\ln y_1^2 = -\nu g + \ln b_1$ has been fitted to the experimental y_1^2 data yielding ν in Fig. 4.13. This curve fitting technique has also been applied to the iterative y_1^2 values resulting from scheme **I** of Tab. 4.1. As one can see, there is a good agreement of the linearized theory with the real ES runs. That is why, the equations obtained can be used to estimate the expected runtime of the CSA-ES.

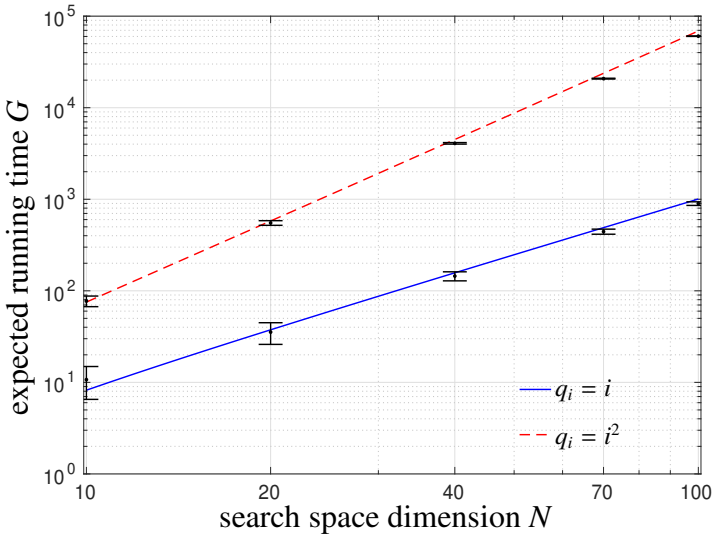

Figure 4.14.: Expected runtime for reducing the objective function value by a factor of 1/4 by the $(3/3_I, 10)$-CSA-ES on the ellipsoids $q_i = i$ and $q_i = i^2$ using $D = 1/c$ and $c = 1/\sqrt{N}$. The predictions of (4.70) are displayed by the solid and the dashed line, respectively. Mean and standard deviation of 100 experimental runs are represented by the error bars.

4.5. The expected running time

The strategy's steady state dynamics are governed by an exponential decrease of the y_i components given by Eq. (4.29) where the inverse time constant ν is determined by (4.44). Inserting (4.29) into the ellipsoid fitness model (3.6) the steady state fitness dynamics can be determined. Starting at generation g_0 sufficiently large such that transient effects have vanished, the fitness value after g generations is

$$F\left(\mathbf{y}^{(g_0+g)}\right) = \sum_{i=1}^{N} q_i b_i \mathrm{e}^{-\nu(g_0+g)} = F\left(\mathbf{y}^{(g_0)}\right)\mathrm{e}^{-\nu g}. \tag{4.68}$$

Consequently, the objective function value decreases exponentially fast with time constant $1/\nu$. Equation (4.68) allows for the estimation of the expected running time G in which the fitness value is improved by a factor of $2^{-\beta}$. Considering $F\left(\mathbf{y}^{(g_0+G)}\right)/F\left(\mathbf{y}^{(g_0)}\right)$, from (4.68) one obtains $\mathrm{e}^{-\nu G} = 2^{-\beta}$ and resolving this for G results in $G = \beta\ln(2)/\nu$. Inserting (4.44) finally yields

$$G = \frac{\beta\ln(2)}{2\sigma^*_{ss}c_{\mu/\mu,\lambda}}\frac{\Sigma q}{\check{q}}. \tag{4.69}$$

That is, the expected runtime G is asymptotically proportional to the quotient of the sum of the ellipsoid coefficients Σq and the smallest coefficient $\check{q} = \min_i(q_i)$. For the two considered ellipsoid models this means that the expected running time increases with order N^2 for $q_i = i$, and with N^3 for $q_i = i^2$, respectively. The same result had been obtained for the $(\mu/\mu_I, \lambda)$-σSA-ES on the ellipsoid model in [Beyer and Melkozerov, 2014]. However, the σSA-ES realizes a different normalized steady state mutation strength σ^*_{ss}. Taking into

account the estimation of the normalized steady state mutation strength for non-spherical ellipsoid models in (4.64) the minimal expected running time becomes

$$\breve{G} = \frac{\beta \ln(2)}{2\mu c^2_{\mu/\mu,\lambda}} \left(\frac{\Sigma q}{\breve{q}} - \frac{cDN}{(1-c)} \right). \tag{4.70}$$

Notice, in order to guarantee validity, the cumulation parameter c and the damping parameter D in Eq. (4.70) have to be chosen according to (4.67) and (4.66), respectively. Smaller choices of c, e.g., would contradict the use of the iterative scheme **IV**. Additionally, it has to be kept in mind that (4.70) is not applicable to the sphere model since the derivation relies on the use of the linear approximation of the steady state mode eigenvalue (4.44) which is not appropriate for the sphere (see also Fig. 4.10).

In Fig. 4.14 the expected runtime of the $(3/3_I, 10)$-CSA-ES on the ellipsoid models $q_i = i, i^2$ is plotted against the search space dimension N. Using cumulation parameter $c = 1/\sqrt{N}$ and damping parameter $D = 1/c$, the theoretical predictions for $\beta = 2$ are validated by comparison with real ES runs. The experimental measurements are averaged over 100 independent ES runs. The standard deviation of the runs is depicted by the error bars. A good agreement between theoretical and experimental results is observed. Furthermore, with growing search space dimension N the standard deviation decreases relative to the mean value realizations.

4.6. Summary

This chapter extended the dynamical systems analysis approach developed for the $(\mu/\mu_I, \lambda)$-σSA-ES [Beyer and Melkozerov, 2014] to the analysis of the CSA-ES on the ellipsoid model. To this end, an analysis approach for the dynamics of the search path cumulation of the CSA-ES was developed and was used as the basis for the analysis of the σ evolution in the CSA-ES.

The dynamics of the $(\mu/\mu_I, \lambda)$-CSA-ES on the ellipsoid model are characterized by a transient and a steady state phase. This behavior is very similar to the dynamics of the self-adaptive $(\mu/\mu_I, \lambda)$-σSA-ES. The main difference being the steady state normalized mutation strength σ^*_{ss} when using standard strategy parameter settings. For typical strategy parameter choices and learning parameter $\tau \propto 1/\sqrt{N}$, the mutation strength σ^*_{ss} is in the vicinity of 1 for the σSA-ES [Beyer and Melkozerov, 2014], the CSA-ES yields $\sigma^*_{\text{ss}} \propto \mu c_{\mu/\mu,\lambda}$. That is, in contrast to the σSA-ES, the normalized mutation strength in CSA-ES is proportional to the number of parents μ. As a result, using standard choices for the strategy parameters, the CSA performs up to a factor of μ better than the σSA-ES. This explains the superior performance of the CSA in non-noisy environments.

As shown in [Beyer and Melkozerov, 2014] one can tune the σSA-ES for optimal performance. However, to this end, the learning parameter must be chosen proportionally to the square root of the quotient of the smallest eigenvalue of the Hessian and its trace - quantities that are usually not known in a black-box optimization scenario. While there is this sensitive dependency of the performance of the σSA-ES on the learning parameter τ that depends on

the Hessian, there are also strategy parameter dependencies in the CSA-ES. There are two parameters D and c that influence the performance of the CSA-ES. Given a fixed c, one can infer from Fig. 4.9 and Eq. (4.27) that D values greater than 1 result in flatter ψ-curves. These in turn shift the steady state σ^* to the right. Depending on the fitness model, this can increase the steady state ν, thus improving the performance of the ES, but it can also result in smaller ν values. This is especially striking for the sphere model, where by virtue of Eq. (4.57) the standard recommendation $D = 1 + 1/c$ [Hansen and Ostermeier, 2001] results in a $\sigma^*_{\text{ss}} = \sqrt{2}\mu c_{\mu/\mu,\lambda}$ that is by a factor of $\sqrt{2}$ larger than the optimal σ^*. Therefore, from the viewpoint of the sphere model, choosing $D = 1$ should be preferred over the choice of $D = 2 + N/4$ being recommended in [Hansen and Ostermeier, 2001]. This choice would also work well for the ellipsoid model and would even simplify the σ update in the pseudo code of the CSA-ES in Alg. 4.1, line 11. However, using $D = 1$ is bought at the expense of oscillatory behavior of σ^* when approaching fitness landscape conditions similar to a sphere model.

The results obtained for the CSA-ES may have implications for the CMA-ES. Since CMA-ES is designed to evolve a covariance matrix that transforms the initial optimization problem into a locally spherical one, such oscillations may likely occur at the end of the learning phase. As a consequence performance may degrade. That is why using $D = 1$ generally cannot be recommended. Alternatively one may use the D formula (4.61) for experimental algorithm tuning. Considering problems for very high search space dimensionalities, using a constant D instead of an N dependent value might be an option to slightly increase the performance of the CMA-ES after having reached the steady state.

Besides the choice of D, there is still a certain freedom of choice concerning c. The reciprocal of which controls the time horizon of path length cumulation. The investigations have shown that the recommended setting of c within $c \propto [1/\sqrt{N}, 1/N]$ has a rather limited influence on the performance of the ES. Smaller c-values result in a somewhat longer transient time, but a slightly better steady state performance.

5. Analysis of mutation strength adaptation by meta-Evolution Strategies

This section regards the third contemporary mutation strength adaptation technique, namely hierarchically organized evolution strategies (meta-ES). It is concerned with analyzing the ability of a meta-ES to optimally control its mutation strength on the ellipsoid model. Particularly, the dynamical behavior of the specific $[1, 2(\mu/\mu_I, \lambda)^\gamma]$-meta-ES is investigated. That is, one upper level strategy is employed to control the mutation strength according to the outcome of two competing inner evolution strategies. By applying the dynamical systems analysis approach to this specific meta-ES variant, a first step towards the analysis of meta-Evolution Strategy behavior on the ellipsoid model is conducted. In the first place, the analysis only regards isolation periods γ of length one. In that situation, the derivation of a non-linear system of difference equations is possible which describes the mean value evolution of the hierarchically organized strategy. In the asymptotic limit case of large search space dimensions the system is suitable to derive closed-form solutions which describe the longterm behavior of the meta-ES. The steady state mutation strength is bracketed within an interval depending on the mutation strength control parameter. Compared to standard settings in cumulative step-length adaptation evolution strategies the meta-ES realizes almost similar normalized mutation strengths. The performance of the meta-Evolution Strategy turns out to be more robust to the choice of its control parameters. The results allow for the derivation of the expected running time of the algorithm which is comparable to the CSA-ES findings of the preceding section. Finally, the meta-ES approach is extended to longer isolation periods ($\gamma > 1$). While the derivation of closed-form solutions is very complex, it is still possible to approximately characterize the dynamical behavior. A bound on the isolation time up to which the approximations guarantee a sufficient quality is provided. Considering the long-term behavior, the convergence rates as well as the expected running time of the algorithm can be approximated.

5.1. The $[1, 2(\mu/\mu_I, \lambda)^\gamma]$-meta-ES algorithm

Establishing the basis of the following investigations, in this section the $[1, 2(\mu/\mu_I, \lambda)^\gamma]$-meta-ES is introduced. As a rather simple variant of a hierarchically organized Evolution Strategy it employs two inner $(\mu/\mu_I, \lambda)$-ESs which evolve from the same initial search space parameter vector $\mathbf{y_p}$ but with different mutation strengths σ. The individual mutation strengths are kept constant within the inner strategies over the isolation period of γ gener-

Algorithm 5.1 The pseudo code of the $[1, 2(\mu/\mu_I, \lambda)^\gamma]$-meta-ES. The Code of the inner ES is displayed in Alg. 3.1.

```
 1: Initialize (σ_p, y_p, μ, λ, γ);
 2: t ← 0;
 3: repeat
 4:     σ_1 ← σ_p α;
 5:     σ_2 ← σ_p / α;
 6:     [y_1, F(y_1)] ← ES(μ, λ, γ, σ_1, y_p);
 7:     [y_2, F(y_2)] ← ES(μ, λ, γ, σ_2, y_p);
 8:     σ_p ← σ_{1;2};
 9:     y_p ← y_{1;2};
10:     t ← t + 1;
11: until termination condition
```

ations. The outer ES controls the mutation strength on a higher level. Its peseudo code is described in Alg. 5.1. In line 4 and 5 the two different mutation strength values σ_1, σ_2 are generated by increasing respectively decreasing the parental mutation strength by the factor $\alpha > 1$. Consequently, one inner $(\mu/\mu_I, \lambda)$-ES runs with mutation strength $\sigma_1 = \alpha\sigma_p$ and one with $\sigma_2 = \sigma_p/\alpha$. Selection is performed in lines 8 and 9 using the standard notation "$m; \lambda'$" indicating the m-th best population out of all λ' populations. The populations are ordered by the function values returned by the respective inner standard ES after having evolved independently over γ generations. The mutation strength of the inner strategy which provides the better fitness function value serves as the new parental mutation strength σ_p. This procedure is repeated until the termination criterion is met (maximal number of function evaluations, fixed number of isolation periods, etc.).

The inner ES applied in lines 6 and 7 is a standard $(\mu/\mu_I, \lambda)$ evolution strategy which operates with constant strategy parameters during the isolation period, cf. Alg. 3.1. It generates a population of λ offspring by adding the product of the mutation strength σ and a vector of independent, standard normally distributed components to the centroid $\mathbf{y} := \langle \mathbf{y} \rangle$ of the previous generation. The μ best candidates (w.r.t. their function values F_l) are used to build the new parental centroid $\langle \mathbf{y} \rangle$. Proceeding this way over γ generations, the inner ES returns the tuple $[\langle \mathbf{y} \rangle, F(\langle \mathbf{y} \rangle)]$.

The description of the inner evolution strategy dynamics provides the basis of the meta-ES analysis. Since the inner ES operates with fixed mutation strength over multiple ($\gamma \geq 1$) generations, the mean value dynamics on the ellipsoid model are expressed by the quadratic progress rate in its N-dependent (3.19) or its asymptotical (3.24) form, respectively. After evolving over a sufficiently long period of time the inner ESs approach their steady states (3.28).

The dynamical behavior of the meta-ES is examined in the next section. The mutation strength dynamics are analyzes comparing the fitness values of the finally generated parental centroids returned by the inner ESs. In order to keep the analysis traceable, in Sec. 5.2 isolation periods of length one ($\gamma = 1$) are investigated as a first step. After that, the potential of using longer isolation periods $\gamma > 1$ will be of interest. As the two inner ESs can be regarded

as running in parallel, the number of isolation periods can be identified with the number of generations during the $\gamma = 1$ case in Sec. 5.2. Both terms may be used synonymously until longer isolation times $\gamma > 1$ are considered in Sec. 5.3.

5.2. Single generation isolation time

During this section the evolution equations of the meta-ES on the ellipsoid model will be derived considering only an isolation time of $\gamma = 1$. Conclusively, the fitness values of the parental centroids returned from both inner strategies are compared after every single generation and the mutation strength is adapted accordingly. First, the corresponding system of evolution equations for the $[1, 2(\mu/\mu_I, \lambda)^1]$-meta-ES is derived. Afterwards, the dynamics of the normalized mutation strength are analyzed. Since the normalized mutation strength dynamics exhibit a strong oscillatory behavior, the observed oscillations are bracketed in lower and upper bounds. Finally, the longterm behavior of the meta-ES[1] can be described allowing for the prediction of the expected running time of the algorithm.

5.2.1. The evolution equations

Following the dynamical systems approach the stochastic process of the ES from generation g to generation $g + 1$ can be divided into mean value parts and fluctuation terms. The mean value parts are directly given by Eq. (3.19) and its asymptotical representation (3.24), respectively. That is, the starting point of the theoretical investigations is again the component-wise difference equation

$$y_i^{(g+1)^2} = y_i^{(g)^2} - \varphi_i^{II}(\sigma^{(g)}) + \epsilon_i, \tag{5.1}$$

where ϵ_i denotes the component-wise fluctuations of the stochastic process. The calculation of the corresponding evolution equation of the meta-ES mutation strength dynamics is performed in the next step. Therefore, the corresponding expected objective function values realized by the two inner Evolution Strategies, operating with different mutation strengths, are compared. The first strategy is equipped with a mutation strength which is increased by the multiplicative factor $\alpha > 1$, while the mutation strength within the other inner strategy is decreased by division with the same parameter α. The mutation strength values are denoted

$$\begin{aligned} \sigma_1^{(g)} &:= \sigma^{(g)}\alpha, \\ \sigma_2^{(g)} &:= \sigma^{(g)}/\alpha. \end{aligned} \tag{5.2}$$

Considering the objective function (3.6) and making use of Eq. (5.1) in conjunction with the asymptotical progress rate representation (3.24) (together with (3.25)), the expected objective function values resulting from the two inner ESs can be computed. The fitness of the parental centroid returned by the first inner strategy employing σ_1 after a single iteration

[1] Unless indicated otherwise, throughout the rest of the section the term "the meta-ES" will refer to the $[1, 2(\mu/\mu_I, \lambda)^1]$-meta-ES variant with isolation time one.

is obtained as

$$\begin{aligned} F_1^{(g+1)} \coloneqq F\left(\sigma_1^{(g)}, \mathbf{y}^{(g+1)}\right) &= \sum_{i=1}^{N} q_i \left(y_i^{(g)2} - \frac{2\alpha\sigma^{(g)} c_{\mu/\mu,\lambda} q_i \left(y_i^{(g)}\right)^2}{R_q(\mathbf{y}^{(g)})} + \frac{\alpha^2 \sigma^{(g)2}}{\mu} \right) + \epsilon_{F_1} \\ &= \sum_{i=1}^{N} q_i y_i^{(g)2} - \frac{2\alpha\sigma^{(g)} c_{\mu/\mu,\lambda}}{R_q(\mathbf{y}^{(g)})} R_q^2(\mathbf{y}^{(g)}) + \frac{\alpha^2 \sigma^{(g)2}}{\mu} \Sigma q + \epsilon_{F_1} \\ &= F\left(\mathbf{y}^{(g)}\right) - 2\alpha\sigma^{(g)} c_{\mu/\mu,\lambda} R_q(\mathbf{y}^{(g)}) + \frac{\alpha^2 \sigma^{(g)2}}{\mu} \Sigma q + \epsilon_{F_1}. \end{aligned} \tag{5.3}$$

Analogously, the fitness value realized by the second inner ES is calculated as

$$\begin{aligned} F_2^{(g+1)} \coloneqq F\left(\sigma_2^{(g)}, \mathbf{y}^{(g+1)}\right) &= \sum_{i=1}^{N} q_i \left(y_i^{(g)2} - \frac{2\sigma^{(g)} c_{\mu/\mu,\lambda} q_i \left(y_i^{(g)}\right)^2}{\alpha R_q(\mathbf{y}^{(g)})} + \frac{\sigma^{(g)2}}{\alpha^2 \mu} \right) + \epsilon_{F_2} \\ &= \sum_{i=1}^{N} q_i y_i^{(g)2} - \frac{2\sigma^{(g)} c_{\mu/\mu,\lambda}}{\alpha R_q(\mathbf{y}^{(g)})} R_q^2(\mathbf{y}^{(g)}) + \frac{\sigma^{(g)2}}{\alpha^2 \mu} \Sigma q + \epsilon_{F_2} \\ &= F\left(\mathbf{y}^{(g)}\right) - \frac{2\sigma^{(g)} c_{\mu/\mu,\lambda}}{\alpha} R_q(\mathbf{y}^{(g)}) + \frac{\sigma^{(g)2}}{\alpha^2 \mu} \Sigma q + \epsilon_{F_2}. \end{aligned} \tag{5.4}$$

In this context, the sum of the corresponding component-wise fluctuations is abbreviated by the terms $\epsilon_{F_1} \coloneqq \sum_{i=1}^{N} q_i \epsilon_i$, and $\epsilon_{F_2} \coloneqq \sum_{i=1}^{N} q_i \epsilon_i$, respectively. According to line 8 of the meta-ES algorithm, see Alg. 5.1, the difference of the fitness values governs the mutation strength adaptation in generation $g + 1$ in the following way

$$\begin{aligned} F_1^{(g+1)} - F_2^{(g+1)} > 0 \Rightarrow \quad \sigma^{(g+1)} = \sigma_2^{(g)}, \\ F_1^{(g+1)} - F_2^{(g+1)} < 0 \Rightarrow \quad \sigma^{(g+1)} = \sigma_1^{(g)}. \end{aligned} \tag{5.5}$$

Defining the difference of the fluctuation sums as $\epsilon_{\Delta F} \coloneqq \epsilon_{F_1} - \epsilon_{F_2}$ and making use of (5.3) and (5.4) the calculation of $F_1^{(g+1)} - F_2^{(g+1)}$ yields

$$\begin{aligned} F_1^{(g+1)} - F_2^{(g+1)} &= -2\sigma^{(g)} c_{\mu/\mu,\lambda} R_q(\mathbf{y}^{(g)}) \left(\alpha - \frac{1}{\alpha}\right) + \frac{\sigma^{(g)2}}{\mu} \Sigma q \left(\alpha^2 - \frac{1}{\alpha^2}\right) + \epsilon_{\Delta F} \\ &= 2c_{\mu/\mu,\lambda} \sigma^{(g)} R_q(\mathbf{y}^{(g)}) \left(\alpha - \frac{1}{\alpha}\right) \left(-1 + \left(\alpha + \frac{1}{\alpha}\right) \frac{\sigma^{(g)}}{2\mu c_{\mu/\mu,\lambda}} \frac{\Sigma q}{R_q(\mathbf{y}^{(g)})}\right) + \epsilon_{\Delta F}. \end{aligned} \tag{5.6}$$

After mutation strength normalization according to (3.14) Eq. (5.6) becomes

$$F_1^{(g+1)} - F_2^{(g+1)} = 2c_{\mu/\mu,\lambda} \sigma^{(g)} R_q(\mathbf{y}^{(g)}) \left(\alpha - \frac{1}{\alpha}\right) \left[\left(\alpha + \frac{1}{\alpha}\right) \frac{\sigma^{*(g)}}{2\mu c_{\mu/\mu,\lambda}} - 1 \right] + \epsilon_{\Delta F}. \tag{5.7}$$

Regarding this representation, the term inside the squared brackets defines a discriminator function that controls the mutation strength evolution. The term ϵ_Δ is introduced to take into account the fluctuation term $\epsilon_{\Delta F}$ within the discriminator function. It reads

$$\Delta(\sigma^{*(g)}) \coloneqq \left(\alpha + \frac{1}{\alpha}\right) \frac{\sigma^{*(g)}}{2\mu c_{\mu/\mu,\lambda}} - 1 + \epsilon_\Delta \tag{5.8}$$

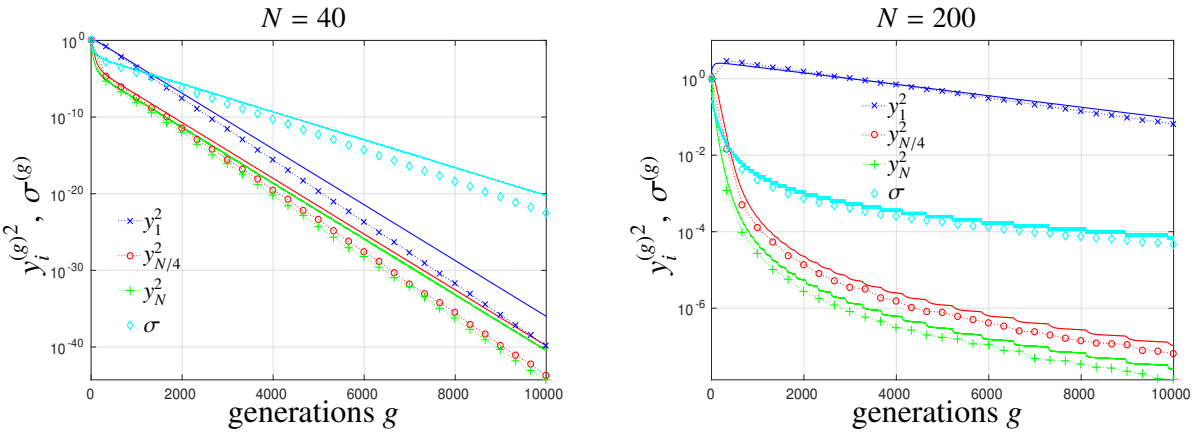

Figure 5.1.: The dynamics of the $[1, 2(3/3_I, 10)^1]$-meta-ES using $\alpha = 1.2$ are displayed for $N = 40$ and $N = 200$ on the ellipsoid model $q_i = i$. The iterative system (5.12) is compared to real runs of Alg. 5.1. The experimental results are displayed as data points while the iteratively generated dynamics are depicted by the colored curves. The experimental dynamics are averaged over 10^4 independent runs. The runs are initialized with $\sigma_0 = 1$ and $y_i^{(0)} = 1\ \forall i$.

Since all other terms on the right-hand side of Eq. (5.7) are positive ($\alpha > 1$), the sign of the difference of the fitness values $F_1^{(g+1)}$ and $F_2^{(g+1)}$ in generation $g + 1$ is equivalent to the sign of $\Delta(\sigma^{*(g)})$

$$\begin{aligned} F_1^{(g+1)} - F_2^{(g+1)} > 0 \Leftrightarrow \quad \Delta(\sigma^{*(g)}) > 0, \\ F_1^{(g+1)} - F_2^{(g+1)} < 0 \Leftrightarrow \quad \Delta(\sigma^{*(g)}) < 0. \end{aligned} \tag{5.9}$$

Because of the relation (5.5), this allows to formulate the evolution equation of the mutation strength σ

$$\sigma^{(g+1)} = \sigma^{(g)} \alpha^{-\text{sign}(\Delta(\sigma^{*(g)}))} + \epsilon_\sigma. \tag{5.10}$$

Here, the term ϵ_σ refers to the fluctuations within the mutation strength evolution.

Having modeled the mutation strength evolution (5.10), the $[1, 2(\mu/\mu_i, \lambda)^1]$-meta-ES is described by the system of $N + 1$ evolution equation

$$\begin{aligned} y_i^{(g+1)2} &= y_i^{(g)2} - \varphi_i^{II}(\sigma^{(g)} \alpha^{-\text{sign}(\Delta(\sigma^{*(g)}))}) + \epsilon_i, \\ \sigma^{(g+1)} &= \sigma^{(g)} \alpha^{-\text{sign}(\Delta(\sigma^{*(g)}))} + \epsilon_\sigma. \end{aligned} \tag{5.11}$$

In order to keep the analysis tractable the fluctuation terms ϵ_i and ϵ_σ are ignored and system (5.11) turns into a system of deterministic evolution equations

$$\begin{aligned} y_i^{(g+1)2} &= y_i^{(g)2} - \varphi_i^{II}(\sigma^{(g)} \alpha^{-\text{sign}(\Delta(\sigma^{*(g)}))}), \\ \sigma^{(g+1)} &= \sigma^{(g)} \alpha^{-\text{sign}(\Delta(\sigma^{*(g)}))}. \end{aligned} \tag{5.12}$$

The quality of the modeling approach can be checked by comparison of the iteratively generated $\mathbf{y}$ and σ dynamics resulting from system (5.12) with experimental runs of the

meta-ES. In Fig. 5.1, 5.2, and 5.3, the dynamics of the $[1, 2(3/3_I, 10)^1]$-meta-ES are illustrated for different search space dimensionalities ($N = 40, 200$) on the ellipsoid models $q_i = i$, and $q_i = i^2$, respectively.

Regarding Fig. 5.1 and Fig. 5.2 the ellipsoid model $q_i = i$ is considered. The graphs in Fig. 5.1 display the the dynamics of the component-wise squared distance to the optimizer (displayed for the components $i = 1, N/4, N$) and the mutation strength. Considering the search space dimensions $N = 40$ and $N = 200$ the iteratively generated dynamics of the evolution equations (5.12) are compared to experimental runs of the $[1, 2(3/3_I, 10)^1]$-meta-ES. In this context, the experimental meta-ES runs are illustrated by the data points while the solid lines represent the iteratively generated dynamics obtained by use of the asymptotic quadratic progress rate (3.24). Further, Fig. 5.2 focuses on the corresponding normalized mutation strength dynamics.

Considering the experiments, the meta-ES runs are generated using the initial parental centroid $y_i^{(0)} = 1 \; \forall i$. The initial mutation strength is $\sigma_0 = 1$. It is adapted using the control parameter $\alpha = 1.2$. The CSA-ES is terminated after 10^4 isolation periods of length $\gamma = 1$. The corresponding experimental dynamics represent the average of 10^4 independent algorithms runs. Figure 5.1 displays the typical behavior of the $[1, 2(\mu/\mu_I, \lambda)^1]$-meta-ES on the ellipsoid model. It can be observed that the agreement of the experimentally and iteratively obtained dynamics increases with growing search space dimensionality. At the beginning of the optimization the dynamics exhibit a transient phase that is characterized by a rapid decline of the $y^2_{N/4}$, y^2_N, and σ curves. This is particularly visible for $N = 200$. The y^2_1 curve decreases as well, but at a much smaller rate. Considering the longterm behavior of the meta-ES all y_i^2 dynamics decrease slower and at the same rate. In the long run the meta-ES continuously decreases the component-wise squared distance to the optimizer as well as the mutation strength. The mutation strength decline is characterized by step-wise oscillation phases. These oscillations are resulting from changes of the sign of the discriminator function $\Delta(\sigma^*)$ governed by the dynamics of the normalized mutation strength σ^*.

Regarding the normalized mutation strength in Fig. 5.2 both phases can be rediscovered.

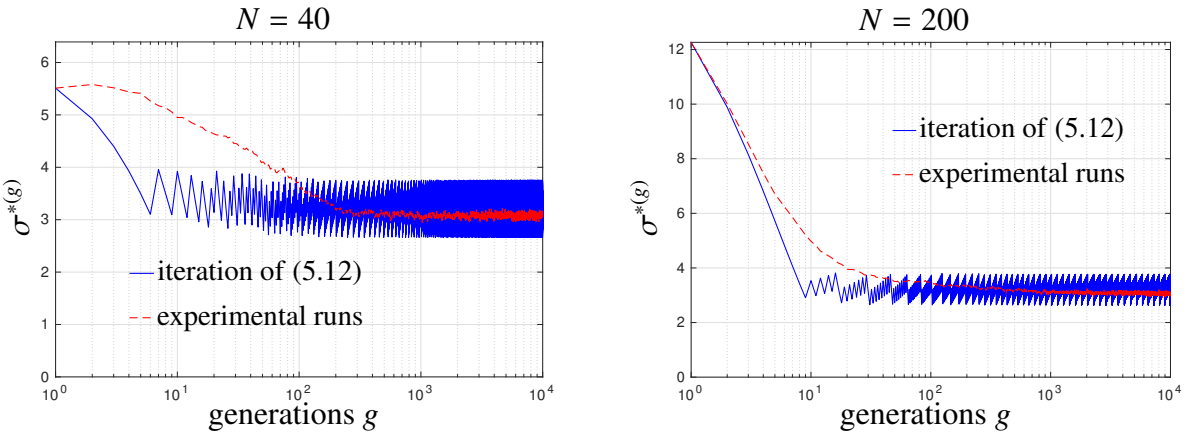

Figure 5.2.: The normalized mutation strength dynamics related to the $[1, 2(3/3_I, 10)^1]$-meta-ES runs displayed in Fig. 5.1. The meta-ES uses the control parameter $\alpha = 1.2$ on the ellipsoid model $q_i = i$.

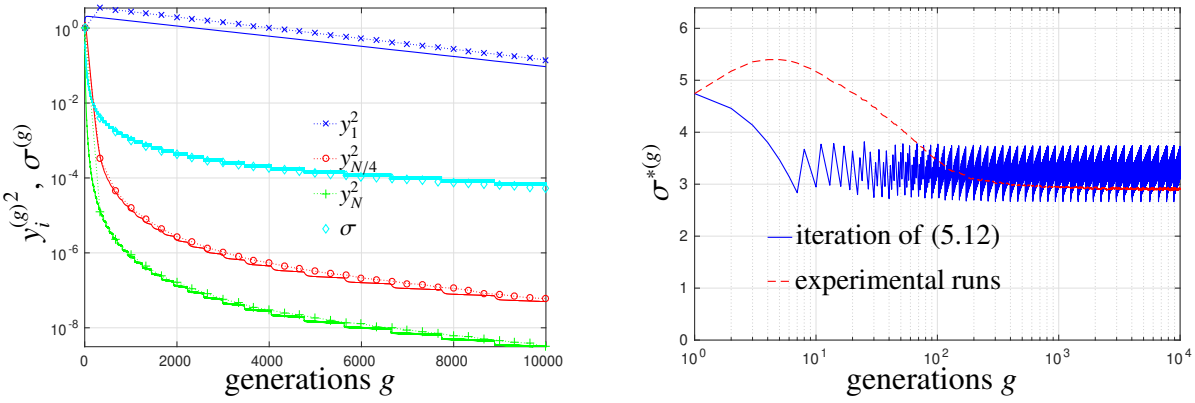

Figure 5.3.: Illustration of the dynamics of the $[1, 2(3/3_I, 10)^1]$-meta-ES on the ellipsoid model $q_i = i^2$ in search space dimension $N = 40$ and $\alpha = 1.2$. The illustration uses the same initialization values used for Fig. 5.1.

With increasing time the σ^* dynamics approach an unstable fixed point. That is, the normalized mutation strength exhibits a "steady state" like behavior oscillating in a limit cycle of large periodicity. Here, stability refers to the classical definition in the context of dynamical systems. The respective dynamics are discussed more closely in Sec. 5.2.2 and Sec. 5.2.3. Since the mutations within the inner ES influence the σ^* evolution the respective limit cycle is subject to mutative noise. In the following, this noisy limit cycle will be referred to as the steady state of the meta-ES. Although being subject to the mentioned oscillations, after approaching its σ^* limit cycle, the σ and y_i^2 dynamics exhibit a log-linear longterm descend. This stable longterm behavior motivates the use of the term "steady state".

Taking into account $q_i = i^2$, the respective dynamics are depicted in Fig. 5.3 for $N = 40$ only. An improved agreement would be observable for the ellipsoid model with coefficients $q_i = i^2$ in search space dimension $N = 200$, the illustration is omitted here.

The overall dynamical behavior very much resembles the observations made in the context of the CSA-ES in Chapter 4. This is due to the fact, that both approaches basically only differ in the way of mutation strength adaptation. However, the rates at which the optimizer is approached in the respective steady states is different. The computation of the convergence rate of the meta-ES is one goal of the following sections.

For $\alpha = 1.2$, the iterative and the experimental dynamics show a good agreement. But the agreement of the experimental results and theoretical predictions in Fig. 5.1 and Fig. 5.2 is not guaranteed when considering smaller values of the control parameter $1 < \alpha < 1.1$. The use of small α values may cause substantial deviations between predictions and real meta-ES runs. Especially in low search space dimensions the deviations can be immense, see to Fig. 5.4 for the impact of small α values on the prediction quality. These deviations are a result of the fluctuations that have been ignored in the iterative system (5.12). Their origin is investigated in more detail within Sec. 5.2.2. Even averaging over multiple meta-ES runs is not sufficient to mitigate their influence on the experimental runs.

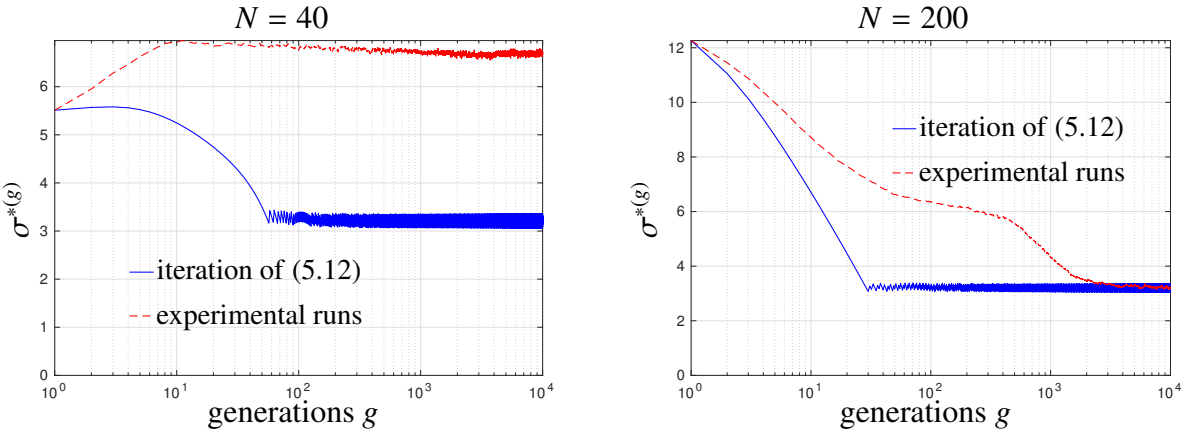

Figure 5.4.: The dynamics of the $[1, 2(3/3_I, 10)^1]$-meta-ES are displayed for $N = 40$ and $N = 200$ on the ellipsoid model ($q_i = i$). The initial mutation strength $\sigma_0 = 1$ is adapted using control parameter $\alpha = 1.05$. The initial parental centroid is $y_i^{(0)} = 1 \; \forall i$.

5.2.2. Discussing the deviations for small mutation control parameters

Particularly, the use of small mutation control parameters α results in huge deviations. Regarding Fig. 5.4 the deviations of experimental and theoretical results for small values of α have to be examined more closely.

Examination the cause of the fluctuations

This section examines the nature of the deviations of the theoretical predictions from the real meta-ES runs. Therefore, one-generation meta-ES experiments are considered in order to check the validity of the iterative dynamics. The one-generation experiments are performed in the following way:

a) A single iteration step of the $[1, 2(\mu/\mu_I, \lambda)^1]$-meta-ES's upper level strategy is executed for a given σ^* value and initial parameter vector $\mathbf{y}^{(0)}$. Therefore, the initial σ^* is renormalized to σ using to Eq. (3.14). Then both inner strategies are iterated over $\gamma = 1$ generations with mutation strength $\sigma\alpha$, and σ/α respectively.

b) According to line 6 and 7 of Alg. 5.1 the function values returned by the inner strategies are used to compute the quantity

$$\tilde{\Delta}(\sigma^*) := \frac{(F_1 - F_2)}{\sigma \sqrt{\sum_{j=1}^{N} a_j^2 y_j^{(0)2}}}. \tag{5.13}$$

c) The steps a) and b) are repeated G times. Finally, the resulting samples are averaged.

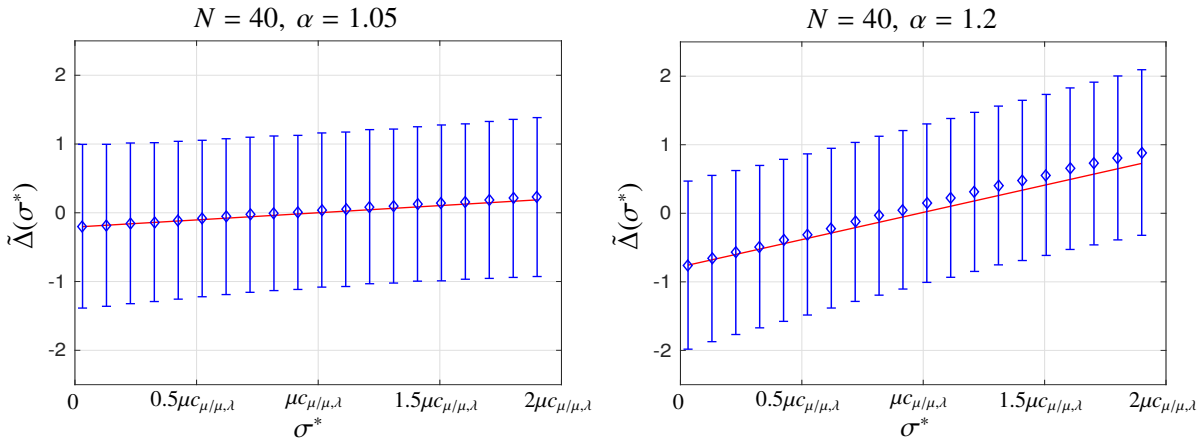

Figure 5.5.: One-generation experiments of the $[1, 2(3/3_I, 10)^1]$-meta-ES on the ellipsoid model ($a_i = i$). The initial parameter vector is $\mathbf{y} = \mathbf{1}$. The comparison of (5.13) and (5.14) is illustrated for $N = 40$ using $\alpha = 1.05$ and $\alpha = 1.2$.

The one-generation experiments for several values of $\sigma^* \in (0, 2\mu c_{\mu/\mu,\lambda}]$ are compared to theoretical predictions of $\tilde{\Delta}(\sigma^*)$ derived from Eq. (5.7) by straight forward rearrangements as

$$\tilde{\Delta}(\sigma^*) = 2c_{\mu/\mu,\lambda}\left(\alpha - \frac{1}{\alpha}\right)\left[\left(\alpha + \frac{1}{\alpha}\right)\frac{\sigma^{*(g)}}{2\mu c_{\mu/\mu,\lambda}} - 1\right]. \tag{5.14}$$

Notice, that $\tilde{\Delta}$ in (5.14) differs from Δ in (5.8) (after omitting the fluctuation terms) only by multiplication with $2c_{\mu/\mu,\lambda}\left(\alpha - \frac{1}{\alpha}\right)$. Provided that $\alpha > 1$ this factor is always positive and does not change the sign of the discriminant function Δ. Thus the predictions of (5.14) can also be used to characterize the mutation strength adaptation of the meta-ES. Correspondingly, Eq. (5.13) is suitable for the experimental validation of this predictions. The one-generation experiments of the $[1, 2(3/3_I, 10)^1]$-meta-ES on the ellipsoid model ($a_i = i$) are illustrated in Fig. 5.5 considering two different values of α. There, the mean values of the real meta-ES runs are obtained by averaging over 2×10^5 one-generation experiments and displayed together with their standard deviations by the error-bars. The solid red line represents the theoretical prediction obtained from Eq. (5.14). The figures show a good agreement of the theoretical predictions with the experimentally obtained data. One observes that the slope of $\tilde{\Delta}(\sigma^*)$-curve increases with growing α. This indicates larger differences of the $\tilde{\Delta}(\sigma^*)$-values realized by two inner strategies operating with different normalized mutation strength. As one would expect, greater values of the mutation strength control parameter α increase the ability of the meta-ES to distinguish the inner strategies. Independently of the choice of α or the search space dimension the magnitudes of the standard deviations exhibit only minor changes. That is, the much lower slope of the $\tilde{\Delta}(\sigma^*)$-curve for small α indicates an increasing influence of the occurring fluctuations on the meta-ES dynamics. As can be observed on the left-hand side of Fig. 5.5 the standard deviations for small α are considerably larger than the mean values. This is also reflected in the corresponding signal-to-noise ratio displayed in Fig. 5.6. The signal-to-noise ratio is by a factor of about 4 to 6 smaller when considering small α values. Particularly, the normalized mutation strength which is

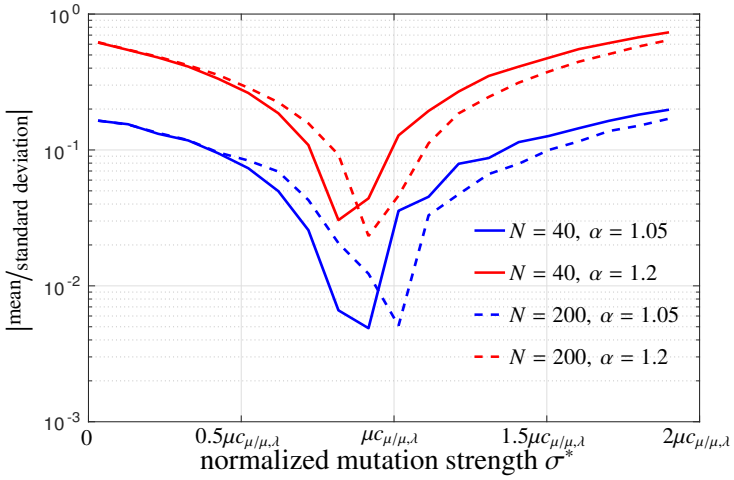

Figure 5.6.: The absolute values of the signal-to-noise ratio (mean divided by standard deviation) of the measurements in Fig. 5.5. The results of the one-generation experiments from $[1, 2(3/3_I, 10)^1]$-meta-ES runs on the Ellipsoid model ($a_i = i$) are illustrated for $N = 40$ and $N = 200$.

approached during the algorithm runs exhibits the highest magnitude of uncertainty. This reflects the oscillation behavior in the selection decision that can also be observed in the steady state of the iteratively generated meta-ES dynamics.

On the one hand the measurements indicate that neglecting the fluctuation terms causes the huge deviations of the experimental and theoretical dynamics appearing in Fig. 5.1 for small values of α. Due to the high fluctuations that occur in the experimental runs almost every second decision to increase or decrease the mutation strength is wrong. Using larger α values improves the agreement of the real meta-ES algorithm runs with the dynamics of the iterative model (5.12). On the other hand, small α values slow down the mutation strength adaptation process. That is, small choices of α might not be suitable to approach the predicted behavior after the huge deviations have been established during the transient phase.

Reduction of the fluctuation influence on the selection

Another approach to examine whether the deviations of the experimental and theoretical dynamics originate from neglecting the fluctuations within the iterative dynamics (5.12) is to incorporate a smoothing technique into the meta-ES algorithm. To this end, the selection decision of the upper level strategy is supported involving the accumulated record of fitness differences $\tilde{\Delta}$ from prior isolation periods. The approach is integrated into the meta-ES algorithm and is referred to as $\tilde{\Delta}$-cumulation.

The $\tilde{\Delta}$-cumulation within the $[1, 2(3/3_I, 10)^1]$-meta-ES algorithm aims at smoothing the occurring ϵ_Δ fluctuations in the experimental dynamics. This approach should increase the experiments' agreement with the theoretical predictions. The $\tilde{\Delta}$-cumulation is integrated into Alg. 5.1 and presented in lines 8 and 9 of Alg. 5.2. The decision whether the muta-

Algorithm 5.2 Pseudo code of the $[1, 2(\mu/\mu_I, \lambda)^\gamma]$-meta-ES with Δ-cumulation. The Code of the inner ES is unchanged, cf. Alg. 3.1.

1: Initialize: $\sigma_p, \mathbf{y_p}, \mu, \lambda, \gamma$;
2: $t \leftarrow 0$; $\hat{\Delta} \leftarrow 0$;
3: **repeat**
4: $\quad \sigma_1 \leftarrow \sigma_p \alpha$;
5: $\quad \sigma_2 \leftarrow \sigma_p / \alpha$;
6: $\quad [\mathbf{y_1}, F(\mathbf{y}_1)] \leftarrow \mathrm{ES}(\mu, \lambda, \gamma, \sigma_1, \mathbf{y_p})$;
7: $\quad [\mathbf{y_2}, F(\mathbf{y}_2)] \leftarrow \mathrm{ES}(\mu, \lambda, \gamma, \sigma_2, \mathbf{y_p})$;
8: $\quad \tilde{\Delta} \leftarrow \dfrac{(F(\mathbf{y}_1) - F(\mathbf{y}_2))}{\sigma_p \sum_{j=1}^{N} a_j^2 (\mathbf{y_p})_j^2}$;
9: $\quad \hat{\Delta} \leftarrow (1-\beta)\hat{\Delta} + \beta\tilde{\Delta}$;
10: $\quad$ **if** $\hat{\Delta} < 0$ **then**
11: $\quad\quad \sigma_p \leftarrow \sigma_1$;
12: $\quad\quad \mathbf{y_p} \leftarrow \mathbf{y_1}$;
13: $\quad$ **else**
14: $\quad\quad \sigma_p \leftarrow \sigma_2$;
15: $\quad\quad \mathbf{y_p} \leftarrow \mathbf{y_2}$;
16: $\quad$ **end if**
17: $\quad t \leftarrow t + 1$;
18: **until** termination condition

tion strength is increased or decreased is no longer based directly on the current sign of the difference of the function values returned by the inner strategies. Instead, the measured $\tilde{\Delta}$-values are accumulated within $\hat{\Delta}$, see line 9. Containing the fading record of the past $\tilde{\Delta}$-values, $\hat{\Delta}$ governs the mutation strength adaptation. In this process the parameter β controls the memory of the $\tilde{\Delta}$-cumulation. The resulting mutation strength dynamics are illustrated in Fig. 5.7 using initial $\tilde{\Delta} = 0$, $\alpha = 1.05$ and cumulation parameters $\beta = 1/\sqrt{3N}$. The normalized mutation strength dynamics are presented in dimensions $N = 40, 200$ and make use the same initial values as the runs in Fig. 5.4. The experimental dynamics are averaged over 10^4 independent runs and compared to the iteratively generated dynamics resulting from Eq. (5.12). The illustrations reveal that the mitigation of the fluctuations moves the dynamics of Alg. 5.2 towards their theoretically predicted behavior. However, the cumulation parameter β needs to be chosen appropriately to ensure a good agreement. The demonstrated choice of $\beta = 1/\sqrt{3N}$ is the result of multiple trial runs. In the short run, using a relatively large cumulation parameter, like $\beta = 1/\sqrt{N}$, results in a much better agreement. On the contrary, smaller β values would cause a significantly longer transient phase. That is, in the beginning it takes more time to learn the appropriate $\hat{\Delta}$ for an algorithm operating with small β. Additionally, a strategy using smaller values of β needs considerably more time to compensate wrong decisions caused by very large fluctuations. Having generated a negative $\hat{\Delta}$ value, inducing an increase of the mutation strength, small parameters β increase the time the meta-ES needs to counteract this trend. That is, the meta-ES mutation strength

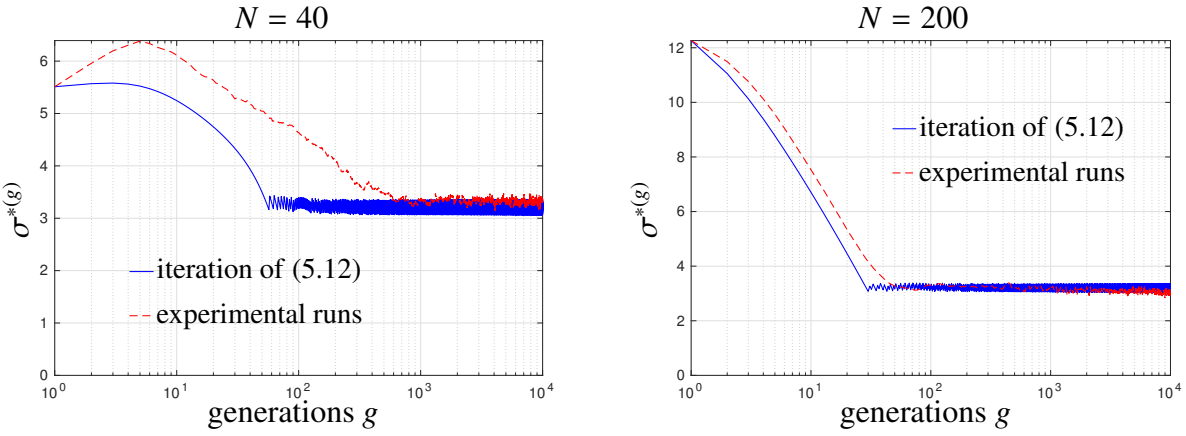

Figure 5.7.: The dynamics of the $[1, 2(3/3_I, 10)^1]$-meta-ES are displayed for $N = 40$ and $N = 200$ on the ellipsoid model ($q_i = i$). The initial mutation strength $\sigma_0 = 1$ is adapted using control parameter $\alpha = 1.05$. The initial parental centroid is $y_i^{(0)} = 1 \; \forall i$.

decline is slowed down. On the other hand, using large values of β close to one of course would decrease the dampening effect of the $\tilde{\Delta}$-cumulation.

Eventually, the results of the application of $\tilde{\Delta}$-cumulation to the meta-ES substantiate the conjecture that the deviations for small values of α (observed in Fig. 5.1) in fact originate from neglecting the fluctuations ϵ_Δ within the theoretical model of the evolution equations (5.12).

5.2.3. The normalized mutation strength dynamics

As observed in Sec. 5.2.1, the iteratively generated mutation strength dynamics decrease over time. The decline exhibits a step-wise oscillatory behavior. These oscillations are a result of changes in the sign of $\Delta(\sigma^{*(g)})$, cf. Eq. (5.8). Since the σ dynamics of the real meta-ES runs are subject to fluctuations, the theoretical oscillations are not exactly reflected by the experimental dynamics in Fig. 5.1. This deviations are also reinforced by averaging over 10^4 independent experimental runs. But regarding the overall behavior, at least for $\alpha > 1.1$ the dynamics show a good agreement. Due to the direct influence on the mutation strength dynamics, it is important to understand the σ^* dynamics. Hence, the goal of this section is taking a closer look at the normalized mutation strength dynamics.

The evolution equation of the normalized mutation strength are derived in App. B.1 as

$$\sigma^{*(g+1)} = \frac{\sigma^{*(g)} \alpha^{-\operatorname{sign}(\Delta(\sigma^{*(g)}))}}{\sqrt{1 - \dfrac{\sum_{j=1}^{N} q_j^2 \varphi_j^{II}(\sigma^{(g)} \alpha^{-\operatorname{sign}(\Delta(\sigma^{*(g)}))})}{R_q^2(\mathbf{y}^{(g)})}}}. \tag{5.15}$$

This is an iterative mapping of the form $\sigma^{*(g+1)} = f_\sigma\left(\sigma^{*(g)}; \alpha\right)$. Such recurrence equations can exhibit qualitatively different dynamics like stable fixed points, limit cycles, and chaotic

behaviors. The influence of the ellipsoid model q_i, as well as that of parameters like α and N, on Eq. (5.15) is not evident. Hence, one is interested in further simplifications that allow for further insights.

According to Appendix B.1, the assumption that the meta-ES is operating in its steady state allows for approximation of evolution equation (5.15), see Eq. (B.17), by

$$\sigma^{*(g+1)} \simeq \frac{\sigma^{*(g)} \alpha^{-\mathrm{sign}(\Delta(\sigma^{*(g)}))}}{\sqrt{1 - \dfrac{2c_{\mu/\mu,\lambda}\sigma^{*(g)}\alpha^{-\mathrm{sign}(\Delta(\sigma^{*(g)}))}\breve{q}}{\Sigma q}}}. \tag{5.16}$$

This recurrence equation of the normalized mutation strength is independent of the distance to the optimizer $\mathbf{y}$ and thus provides a convenient basis for the further analysis. Equation (5.16) can be used to depict the normalized mutation strength.

In Fig. 5.8, the corresponding normalized mutation strength dynamics is displayed using $\alpha = 1.2$. On the left-hand side the σ^* values are plotted against the number of generations. The normalized mutation strength dynamics approach a limit cycle, i.e., the σ^*-values exhibit an oscillatory behavior.

Illustrating the iterative mapping (5.16) as a function of σ^*, the left-hand side of Fig. 5.8 visualizes the unstable fixed point $\sigma^* = \sigma^*_f$ that corresponds to the limit cycle in (a). As observable in Fig. 5.8(b), the normalized mutation strength dynamics do not intersect the line $\sigma^{*(g+1)} = \sigma^{*(g)}$. Instead one observes a discontinuity in (5.16) at $\sigma^* = \sigma^*_0$. This corresponds to the change of increasing σ to decreasing σ from generation g to generation $g + 1$. The transition point is the root of the discriminant function $\Delta(\sigma^*)$. Considering (5.8), the point of discontinuity σ^*_0 is obtained by solving $\Delta(\sigma^*) \stackrel{!}{=} 0$ for σ^*

$$\sigma^*_0 = \frac{2\mu c_{\mu/\mu,\lambda}\,\alpha}{\alpha^2 + 1}. \tag{5.17}$$

Taking into account Eqs. (5.5) and (5.9), the point of discontinuity characterizes the mutation strength dynamics in the following way

$$\begin{aligned} \sigma^* > \sigma^*_0 \quad &\Leftrightarrow \quad \Delta(\sigma^{*(g)}) > 0 \quad \Rightarrow \quad \sigma^{(g+1)} = \sigma^{(g)}/\alpha, \\ \sigma^* < \sigma^*_0 \quad &\Leftrightarrow \quad \Delta(\sigma^{*(g)}) < 0 \quad \Rightarrow \quad \sigma^{(g+1)} = \sigma^{(g)}\alpha. \end{aligned} \tag{5.18}$$

Notice that, for the sphere model $q_i = 1,\ \forall i$ the point of discontinuity has already been derived in [Beyer et al., 2009] and the result is equal to the one in Eq. (5.17) which is obtained by use of the asymptotic quadratic progress rate. The upper limit of the oscillations is denoted $\hat{\sigma}^*$ and the lower limit is referred to as $\breve{\sigma}^*$. Hence, after reaching the limit cycle attractor σ_0, the normalized mutation strength dynamics are confined in an oscillation interval $[\breve{\sigma}^*, \hat{\sigma}^*]$.

In contrast to the sphere model analysis [Beyer et al., 2009] where stable fixed points of the normalized mutation strength have been observed for small choices of α, theoretical results on the ellipsoid model indicate that there exit no a stable fixed points of the iterative mapping (5.16). This is true regardless of the choice of the mutation strength control parameter α. Hence, the next step is concerned with the calculation of the oscillation interval.

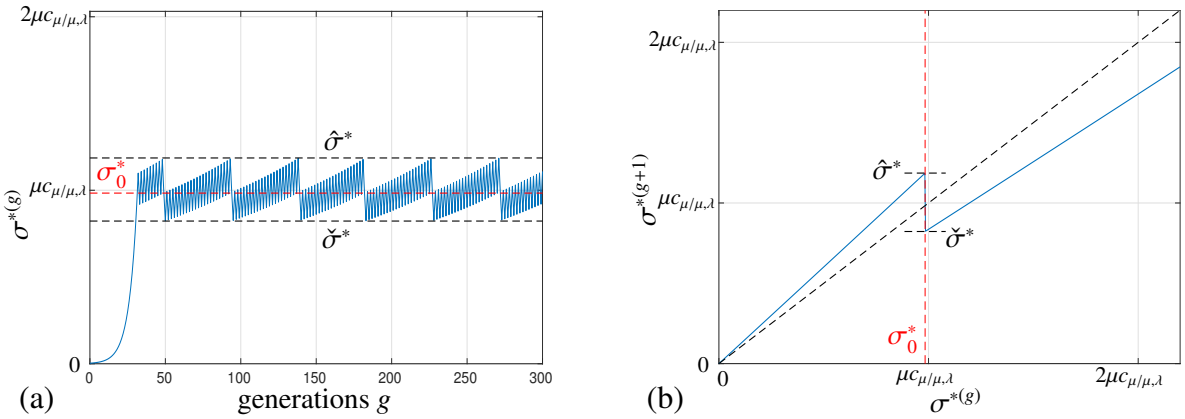

Figure 5.8.: The σ^* dynamics of an $[1, 2(3/3_I, 10)^1]$-meta-ES with $N = 40$ on the ellipsoid model $q_i = i$. Making use of $\alpha = 1.2$ the dynamics are based on the iterative mapping (5.16). The limit cycle in (a) corresponds to the unstable fixed point observed in (b), i.e., the σ^* values oscillate between $\hat{\sigma}^*$ and $\check{\sigma}^*$.

The limits of the oscillation interval are computed in App. B.2. The right-sided limit of the normalized mutation strength oscillation interval is obtained as

$$\hat{\sigma}^* := \lim_{\sigma^* \to \sigma_0^* - 0} \tilde{f}_\sigma(\sigma^*) = \frac{\sigma_0^* \alpha}{\sqrt{1 - \frac{\sum_{j=1}^N q_j^2}{(\Sigma q)^2} \tilde{\varphi}_+^{II*}}} \simeq \frac{2\mu c_{\mu/\mu,\lambda}}{\alpha^2 + 1} \frac{\alpha^2}{\sqrt{1 - 4\mu c_{\mu/\mu,\lambda}^2 \frac{\alpha^2}{1+\alpha^2} \frac{\check{q}}{\Sigma q}}}, \tag{5.19}$$

and the left-sided limit reads

$$\check{\sigma}^* := \lim_{\sigma^* \to \sigma_0^* + 0} \tilde{f}_\sigma(\sigma^*) = \frac{\sigma_0^*}{\alpha \sqrt{1 - \frac{\sum_{j=1}^N q_j^2}{(\Sigma q)^2} \tilde{\varphi}_-^{II*}}} \simeq \frac{2\mu c_{\mu/\mu,\lambda}}{\alpha^2 + 1} \frac{1}{\sqrt{1 - 4\mu c_{\mu/\mu,\lambda}^2 \frac{1}{1+\alpha^2} \frac{\hat{q}}{\Sigma q}}}. \tag{5.20}$$

After evolving over a sufficiently long time the normalized mutation strength dynamics of the meta-ES are bounded in the steady state oscillation interval $[\check{\sigma}^*, \hat{\sigma}^*]$ depicted in Fig. 5.8.

The limits of the steady state oscillation interval are plotted against the mutation strength control parameter α in Fig. 5.9. There, the ellipsoid model $q_i = i$ is considered using search space dimension $N = 40$ in (a), and $N = 200$ in (b), respectively.

The values of $\hat{\sigma}^*$ and $\check{\sigma}^*$ are displayed by the solid green lines. The point of discontinuity σ_0^* resides within these limits and is indicated by the dashed red line. In order to validate the predicted limits they are compared to measurements of the normalized mutation strength for different choices of α. On the one hand, the normalized mutation strength realized by iterative system (5.12) is empirically determined, and on the other hand that of experimental runs of the $[1, 2(3/3_I, 10)^1]$-meta-ES algorithm is measured. The measurements are displayed by the error bars and connected by dotted lines. A single data point represents the mean value of the normalized mutation strength realized by the meta-ES after having approached its limit

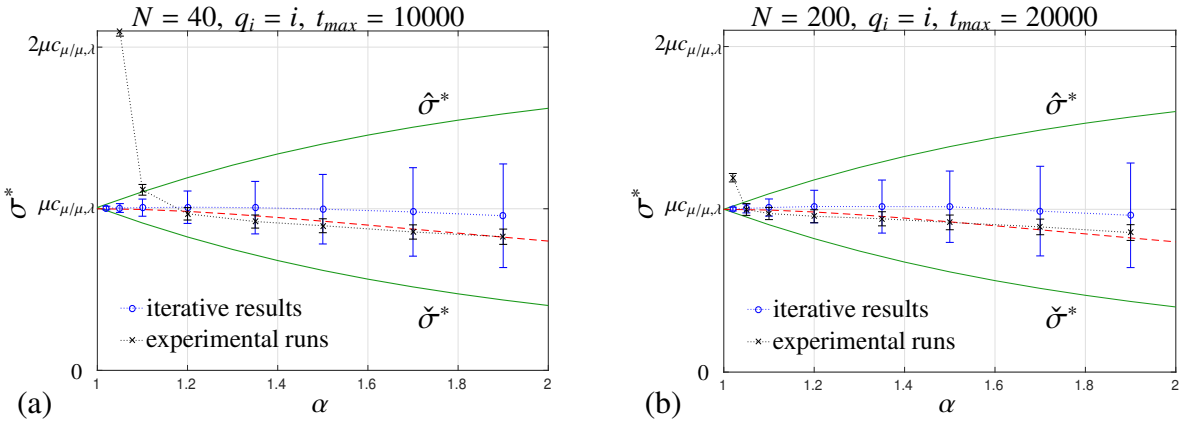

Figure 5.9.: On the influence of α on the steady state normalized mutation strength σ^*. Represented by the solid green lines, the limits (5.19) and (5.20) of the iterative mapping (5.16) are plotted against the mutation strength control parameter α. The point of discontinuity σ_0^* is displayed by the dashed red line. The blue error bar plot illustrates the realizations by iteration of the system of evolution equations. The black error bar plot display the corresponding measurements form experimental runs of the $[1, 2(3/3_I, 10)^1]$-meta-ES averaged over 100 runs. Mean and standard deviation are measured over the last 25% of t_{max} isolation periods ($\gamma = 1$).

cycle attractor. It is obtained by running the meta-ES algorithm for t_{max} isolation periods of $\gamma = 1$ generations using the respective α value to control the mutation strength. Choosing t_{max} sufficiently large to ensure that the strategy is operating in its steady state limit cycle the mean and standard deviation of the σ^* values are measured over the last 25% of the isolation periods. The standard deviation of the iterative results grows with the magnitude of α. By averaging over 100 independent runs of the meta-ES algorithm this effect is diluted considering the experimental results. There, the error bars indicate the position of the mean values after averaging over multiple meta-ES runs instead of displaying the actual standard deviation of σ^* dynamics resulting from a single meta-ES run.

As a matter of course, the iteratively generated results always reside in the oscillation interval. Due to the huge influence of the ϵ_Δ fluctuations that are not incorporated into the iterative model (5.12) the measurements from the experimental runs deviate significantly from the predicted oscillation interval for $\alpha = 1.02$. Regarding smaller search space dimensions N the influence of the fluctuations can be observed up to values about $\alpha = 1.2$. The impact of the ϵ_Δ fluctuations has been discussed in Sec. 5.2.2.

Interestingly, with exception of the experimental results corresponding to very small α values the measured mean values are remarkably close to the point of discontinuity σ_0^*. Hence, it can be deduced that the magnitude of the control parameter α has only minor influence on the expected normalized steady state mutation strength and thus on the overall performance of the meta-ES. That is, operating with larger α parameters improves the ability to discriminate the two inner strategies without degrading the algorithm's performance considerably.

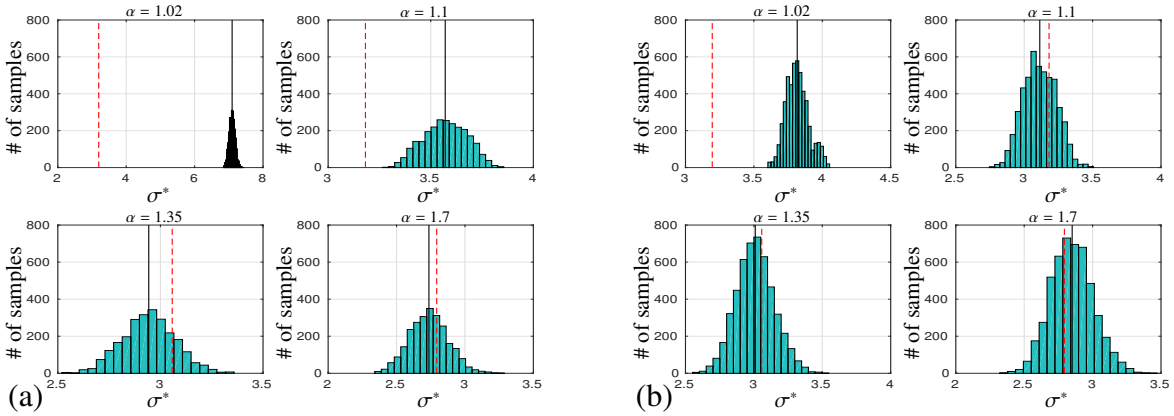

Figure 5.10.: Illustration of the distribution of the normalized mutation strength σ^* after the strategy has approached its steady state behavior. Part (a) displays the distribution considering a search space dimension of $N = 40$. In (b) the dimension $N = 200$ is used. The vertical axis displays the number (#) of samples in a specific bin. The black vertical line corresponds to the measured mean value and the dashed red line displays the point of discontinuity σ_0^* according to Eq. (5.17).

The distribution of the experimentally obtained normalized steady state mutation strength is illustrated using histogram plots in Fig. 5.10. It displays four choices of the control parameter α on the ellipsoid model $q_i = i$ in dimensions $N = 40$, and $N = 200$, respectively. The same configurations as considered in Fig. 5.9 are used. The distributions of the σ^* values are measured considering the final 25% generations obtained from the experimental meta-ES runs. Regarding the distribution corresponding to $\alpha = 1.02$ the influence of the ϵ_Δ fluctuations is observable again. The mean value deviates significantly from the point of discontinuity and the measurements are not evenly distributed around their mean value. In contrast to the $\alpha = 1.02$ case, for $\alpha \geq 1.1$ the deviations between the mean value of the measurements and σ_0^* get reduced. That is, the theoretical model fits the experiments more accurately.

5.2.4. Derivation of the steady state dynamics

The point of discontinuity σ_0^* always resides within the limits of the normalized mutation strength $[\check{\sigma}^*, \hat{\sigma}^*]$, cf. Sec. 5.2.3. For instance, in Fig. 5.9 it is represented by the dashed red line. According to Eq. (5.17) σ_0^* depends on the population size of the meta-ES, as well as on the control parameter α. With growing α, the point of discontinuity slowly decreases. It governs the mutation strength adaptation of the meta-ES in the sense that the strategy will increase the mutation strength as long as $\sigma^* < \sigma_0^*$. On the other hand the meta-ES will instantly reduce the mutation strength if the condition $\sigma_0^* < \sigma^*$ is fulfilled. This behavior results in the limit cycles around σ_0^* that are observed in Fig. 5.8.

As displayed in Fig. 5.9, having approached its steady state the normalized mutation strength of the meta-ES fluctuates in limit cycles around the point of discontinuity. Oper-

ating in its steady state limit cycle around σ_0^* the strategy's normalized mutation strength will not exceed values of $\sigma_0^*\alpha$, neither will it fall below values of σ_0^*/α. Notice, considering small α parameters the described behavior is disturbed by the huge impact of the ϵ_Δ fluctuations mentioned in Sec. 5.2.2. However, in the range of control parameters $\alpha \geq 1.2$ these ϵ_Δ fluctuations are rather small. Further, the histogram plots in Fig. 5.10 suggest that in the steady state the σ^* values are sort of symmetrically distributed around their mean value. For $\alpha \geq 1.2$ this mean value is located near σ_0^*. Thus the meta-ES on average operates with a normalized mutation strength in close proximity to the point of discontinuity. This gives the motivation to model the steady state dynamics of the normalized mutation strength in terms of a mean value $\overline{\sigma}^*_{ss}$ and corresponding fluctuation parts $\epsilon_{\sigma^*_{ss}}$

$$\sigma^*_{ss} = \overline{\sigma}^*_{ss} + \epsilon_{\sigma^*_{ss}}. \tag{5.21}$$

Assuming that the mean value dynamics in Eq. (5.21) are characterized sufficiently well by the point of discontinuity σ_0^* allows for the approximation of the steady state behavior. By omission of the noise term $\epsilon_{\sigma^*_{ss}}$ one obtains

$$\sigma^*_{ss} \simeq \sigma_0^* = 2\mu c_{\mu/\mu,\lambda}\frac{\alpha}{(1+\alpha^2)}. \tag{5.22}$$

Hence, the steady state y_i^2 dynamics of the $[1, 2(\mu/\mu_I, \lambda)^1]$-meta-ES can be derived using $\varphi_i^{II*}(\sigma^*_{ss})$, cf. Eq. (3.23). Accordingly, ignoring of the fluctuations the one-generation change in the component-wise distance to the optimizer in the strategy's steady state is approximated by

$$y_i^{(g+1)^2} \simeq y_i^{(g)^2} - \varphi_i^{II*}(\sigma^*_{ss}), \tag{5.23}$$

i.e., taking into account the normalized quadratic progress rate (3.23), one obtains the difference equation

$$y_i^{(g+1)^2} \simeq y_i^{(g)^2} - 2\sigma^*_{ss}c_{\mu/\mu,\lambda}\frac{q_i}{\Sigma q}y_i^{(g)^2} + \frac{{\sigma^*_{ss}}^2}{\mu}\frac{R_q^2(\mathbf{y}^{(g)})}{(\Sigma q)^2}. \tag{5.24}$$

Making use of the assumption (5.22) transforms (5.24) into

$$y_i^{(g+1)^2} \simeq y_i^{(g)^2} - 4\mu c^2_{\mu/\mu,\lambda}\frac{\alpha}{(1+\alpha^2)}\frac{q_i}{\Sigma q}y_i^{(g)^2} + 4\mu c^2_{\mu/\mu,\lambda}\frac{\alpha^2}{(1+\alpha^2)^2}\frac{R_q^2(\mathbf{y}^{(g)})}{(\Sigma q)^2}. \tag{5.25}$$

Inserting assumption (5.22) into the mutation strength normalization (3.14) the mutation strength dynamics can be calculated as

$$\sigma^{(g)} = \sigma^*_{ss}\frac{R_q(\mathbf{y}^{(g)})}{\Sigma q} = 2\mu c_{\mu/\mu,\lambda}\frac{\alpha}{(1+\alpha^2)}\frac{R_q(\mathbf{y}^{(g)})}{\Sigma q}. \tag{5.26}$$

Consequently, the equations (5.25) and (5.26) build an iterative scheme describing the

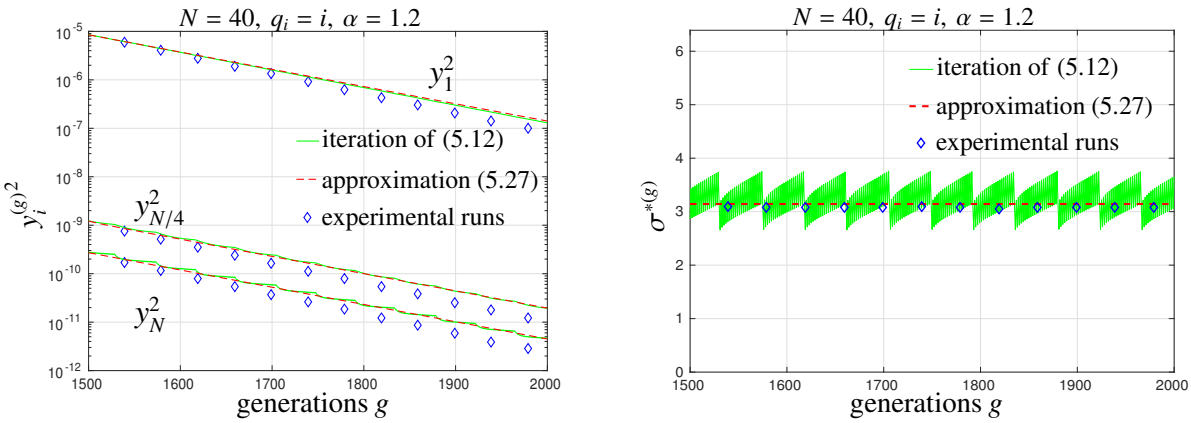

Figure 5.11.: Comparison of the iterative system (5.12) and experimental meta-ES runs with the steady state approximation according to Eq. (5.23) assuming $\sigma^*_{ss} \simeq \sigma^*_0$. The dynamics of the $[1, 2(3/3_I, 10)^1]$-meta-ES with $N = 40$ on the ellipsoid model $q_i = i$ and control parameter $\alpha = 1.2$ are illustrated. The experimental curves are averaged over 100 independent meta-ES runs.

system's steady state evolution behavior

$$\begin{aligned} y_i^{(g+1)2} &\simeq y_i^{(g)2} - 4\mu c^2_{\mu/\mu,\lambda} \frac{\alpha}{(1+\alpha^2)} \frac{q_i}{\Sigma q} y_i^{(g)2} + 4\mu c^2_{\mu/\mu,\lambda} \frac{\alpha^2}{(1+\alpha^2)^2} \frac{R_q^2(\mathbf{y}^{(g)})}{(\Sigma q)^2}, \\ \sigma^{(g+1)} &\simeq 2\mu c_{\mu/\mu,\lambda} \frac{\alpha}{(1+\alpha^2)} \frac{R_q(\mathbf{y}^{(g)})}{\Sigma q}. \end{aligned} \tag{5.27}$$

Moreover, from Eq. (5.25) the steady state objective function dynamics can be derived by use of

$$F^{(g+1)} = F(\mathbf{y}^{(g+1)}) = \sum_{i=1}^{N} q_i y_i^{(g+1)2}, \tag{5.28}$$

resulting in

$$F^{(g+1)} \simeq \sum_{i=1}^{N} q_i y_i^{(g)2} - 4\mu c^2_{\mu/\mu,\lambda} \frac{\alpha}{(1+\alpha^2)} \frac{R_q^2(\mathbf{y}^{(g)})}{\Sigma q} + 4\mu c^2_{\mu/\mu,\lambda} \frac{\alpha^2}{(1+\alpha^2)^2} \frac{R_q^2(\mathbf{y}^{(g)})}{\Sigma q}. \tag{5.29}$$

After minor rearrangements and by considering (5.28) one obtains the steady state F dynamics as

$$F^{(g+1)} \simeq F^{(g)} - 4\mu c^2_{\mu/\mu,\lambda} \frac{\alpha}{(1+\alpha^2)} \frac{R_q^2(\mathbf{y}^{(g)})}{\Sigma q} \left(1 - \frac{\alpha}{(1+\alpha^2)}\right). \tag{5.30}$$

The steady state dynamics resulting from system (5.27) are validated in Fig. 5.11 and 5.12. Therefore, they are compared to the iterative dynamics resulting from system (5.12), as well as to experimental runs of the meta-ES algorithm. In order to ensure that the meta-ES has reached its steady state the iterative system (5.12) is iterated over a sufficiently large number of generations. Within the steady state the iterative dynamics are compared to

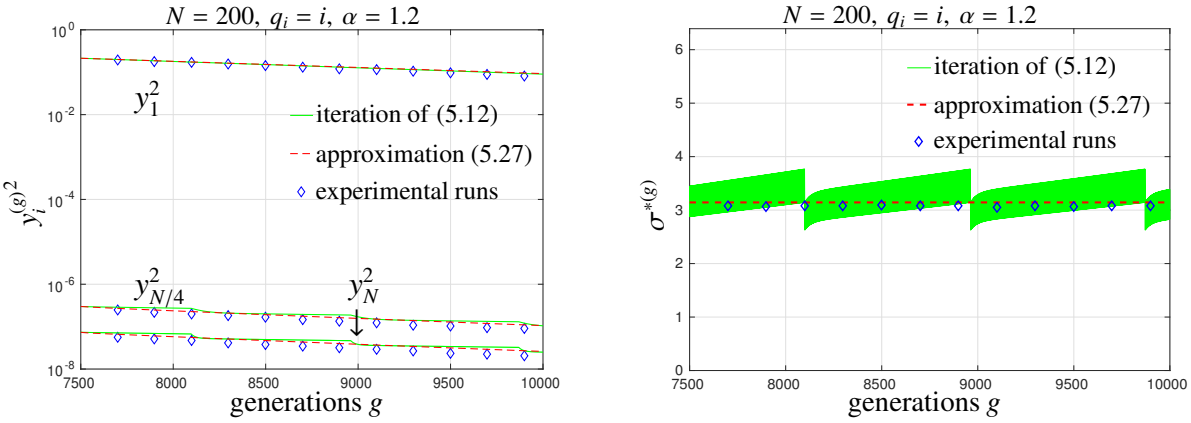

Figure 5.12.: The $[1, 2(3/3_I, 10)^1]$-meta-ES dynamics on the ellipsoid model $q_i = i$ and control parameter $\alpha = 1.2$ are illustrated analogously to Fig. 5.11, but in search space dimension $N = 200$.

the analytically obtained steady state predictions assuming $\sigma^*_{ss} \simeq \sigma^*_0$. The illustration in Fig. 5.11 displays the component-wise squared distance to the optimizer considering the $[1, 2(3/3_I, 10)^1]$-meta-ES with $N = 40$ on the ellipsoid model $q_i = i$ and control parameter $\alpha = 1.2$ on the left-hand side. The right-hand side displays the corresponding normalized mutation strength dynamics. The iterations are starting at $\sigma^0 = 1$ and $\mathbf{y}^{(0)} = \mathbf{1}$. All real meta-ES runs are initialized in the iteratively generated state after 3000 generations in order to shorten the transient phase. The predicted steady state dynamics, see (5.27), show a good agreement with the dynamics resulting from the iterative scheme (5.12). The respective dynamics for $N = 200$ are displayed in Fig. 5.12. Compared to the approximation of the steady state dynamics (5.27) the agreement of the predictions and the experimentally obtained dynamics improves with growing dimensionality. Even in lower dimensions the steady state dynamics resulting from (5.27) exhibit almost the same approximation quality as the iterative dynamics of system (5.12). That is, the assumptions leading to the modeling of the steady state dynamics do not substantially impair the initial iterative model. Having validated the approximation quality, the system (5.27) can be used to analyze the steady state dynamics.

The illustrations suggest that the y_i^2 dynamics in their steady state exhibit a log-linear decline. Thus the system (5.27) can be solved using the exponential *Ansatz*:

$$y_i^{(g)2} = b_i \mathrm{e}^{-\nu g}, \quad b_i > 0, \nu > 0, \tag{5.31}$$

Notice, being introduced in [Beyer and Melkozerov, 2014], this *Ansatz* was already utilized in Chapter 4 in the context of the CSA analysis. As the mutation strength evolution (5.27) depends on the y_i^2 dynamics, it can be expressed in terms of (5.31)

$$\sigma^{(g)} = \frac{2\mu c_{\mu/\mu,\lambda}\alpha}{1+\alpha^2} \frac{\sqrt{\sum_{j=1}^N q_j^2 y_j^{(g)2}}}{\Sigma q} = \frac{2\mu c_{\mu/\mu,\lambda}\alpha}{1+\alpha^2} \frac{\sqrt{\sum_{j=1}^N q_j^2 b_j}}{\Sigma q} \mathrm{e}^{-\frac{\nu}{2}g}. \tag{5.32}$$

Making use of Eq. (5.31) the system's state at generation $g+1$ is directly connected to the

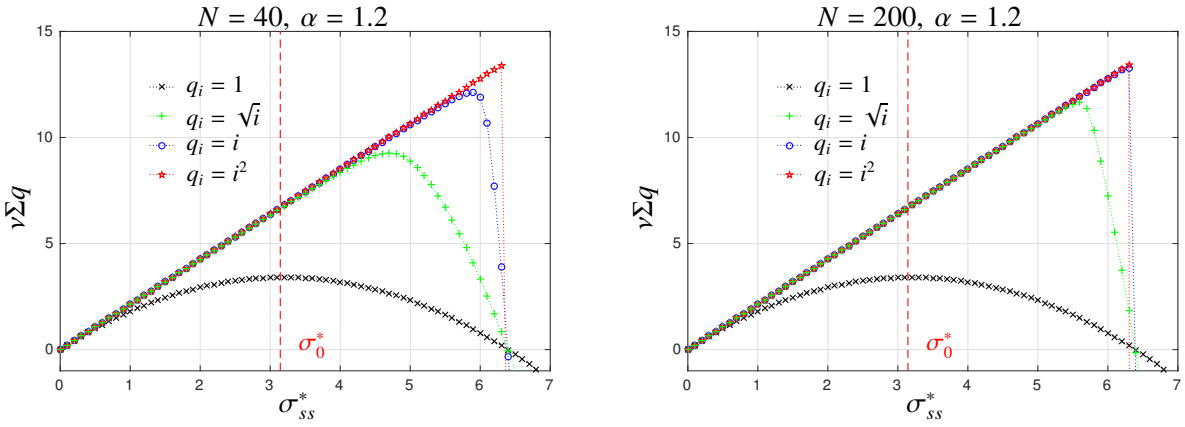

Figure 5.13.: Numerical solutions of the eigenvalue problem (5.34) plotted against the normalized steady state mutation strength σ^*_{ss}. The results of four different ellipsoid models, $q_i = 1$, $q_i = \sqrt{i}$, $q_i = i$, and $q_i = i^2$, are displayed in search space dimension $N = 40$ and $N = 200$ using $\alpha = 1.2$. The point of discontinuity (5.17) is illustrated by the vertical dashed red line.

state at generation g, e.g., $y_i^{(g+1)^2} = b_i \mathrm{e}^{-\nu g}\mathrm{e}^{-\nu} = y_i^{(g)^2}\mathrm{e}^{-\nu}$. Since the slopes of the y_i^2 dynamics are rather small, the term $\mathrm{e}^{-\nu}$ can be simplified to $\mathrm{e}^{-\nu} = 1-\nu+O(\nu^2)$ using Taylor expansion around zero. Applying this to the first equation of system (5.27) using the representation from Eq. (5.24) yields the eigenvalue problem

$$\nu b_i \simeq 2\sigma^*_{ss} c_{\mu/\mu,\lambda}\frac{q_i}{\Sigma q} b_i - \frac{{\sigma^*_{ss}}^2}{\mu}\frac{\sum_{j=1}^N q_j^2 b_j}{(\Sigma q)^2}, \tag{5.33}$$

where ν is the eigenvalue and the b_i are the components of the corresponding eigenvector.

Rewriting (5.33) in matrix form reveals an eigenvalue problem that is equal to the one established in Chapter 4

$$\mathbf{A}\cdot\mathbf{b} \simeq \nu\mathbf{b}, \tag{5.34}$$

where $\mathbf{b} = (b_1, b_2, \ldots, b_N)^\top$,

$$\begin{aligned}(\mathbf{A})_{ii} &= 2\sigma^*_{ss} c_{\mu/\mu,\lambda}\frac{q_i}{\Sigma q} - \frac{{\sigma^*_{ss}}^2}{\mu}\frac{q_i^2}{(\Sigma q)^2},\\ (\mathbf{A})_{ij} &= -\frac{{\sigma^*_{ss}}^2}{\mu}\frac{q_j^2}{(\Sigma q)^2}, \quad i \neq j,\end{aligned} \tag{5.35}$$

and with steady state mutation strength $\sigma^*_{ss} \simeq \sigma^*_0$.

Although the approximation of the meta-ES steady state is only applicable assuming that the meta-ES is operating with a normalized mutation strength in close proximity to the point of discontinuity, i.e., $\sigma^*_{ss} \simeq \sigma^*_0$, the eigenvalue problem can be solved numerically for general values of the normalized steady state mutation strength σ^*_{ss}. Taking into account the ellipsoid models $q_i = 1$, $q_i = \sqrt{i}$, $q_i = i$ and $q_i = i^2$, after multiplication with Σq the resulting eigenvalues are presented in Fig. 5.13. Except for the sphere model ($q_i = 1$) the curves of

the other ellipsoid models show a similar behavior. For $q_i > 1$ the illustration reveals that the eigenvalues exhibit a linear slope for a wide range of rather small σ^*_{ss} values including the vicinity of $\sigma^* = \sigma^*_0 = \sigma^*_{ss}$. With σ^*_{ss} getting larger, one observes a sharp drop of the ν values until for $\sigma^*_{ss} > 2\mu c_{\mu/\mu,\lambda}$ the eigenvalues change their sign.

Regarding σ^*_{ss} values in the close neighborhood of σ^*_0, it can be observed that the eigenvalue can be approximated considering only the linear parts of Eq. (5.33) within the eigenvalue problem (5.34). Thus, the quadratic term in (5.33) can be neglected and the eigenvalue problem simplifies to

$$\nu b_i \simeq 2\sigma^*_{ss} c_{\mu/\mu,\lambda} \frac{q_i}{\Sigma q} b_i. \tag{5.36}$$

Using this representation and inserting the $\sigma^*_{ss} \simeq \sigma^*_0$ the eigenvalues are directly obtained as

$$\nu \simeq 4\mu c^2_{\mu/\mu,\lambda} \frac{\alpha}{(1+\alpha^2)} \frac{q_i}{\Sigma q}. \tag{5.37}$$

The *Ansatz* (5.31) indicates that larger values of ν result in a faster decline of the $y_i^{(g)^2}$ and $\sigma^{(g)}$ dynamics. Regarding the steady state dynamics, for $g \to \infty$, the impact of the larger ν values is neglectable compared to the smallest eigenvalue ν. The smallest positive eigenvalue corresponds to the slowest mode of the meta-ES dynamics and consequently governs the meta-ES steady state. Denoting the smallest ellipsoid coefficient $\check{q} := \min(q_i)$, the steady state mode eigenvalue is derived as

$$\nu \simeq 4\mu c^2_{\mu/\mu,\lambda} \frac{\alpha}{(1+\alpha^2)} \frac{\check{q}}{\Sigma q}. \tag{5.38}$$

The quality of formula (5.38) is verified by comparison with experimental $[1, 2(3/3, 10)^1]$-meta-ES runs considering different choices of the parameter α. To this end, 100 independent meta-ES runs are performed with fixed normalized steady state mutation strength $\sigma^*_{ss} = \sigma^*_0 = 2\mu c_{\mu/\mu,\lambda}\alpha/(1+\alpha^2)$. The mutation strength $\sigma^{(g)}$ is obtained by renormalization in each generation. Then, a linear polynomial $\ln y_i^2 = -\nu g + \ln b_i$ is fitted to the averaged y_i^2 data points yielding N experimental ν values, i.e., one for each y_i^2 curve. The deviations between these N values are very small. For instance, the maximal deviation on the ellipsoid model $q_i = i$ with $N = 40$ is about 2%. Accordingly, the ν values corresponding to the y_1^2 dynamics are plotted in Fig. 5.14 (scaled up by multiplication with Σq) and compared with the analytical predictions in (5.38). Due to the normalization with Σq the theoretical prediction does neither depend on the coefficients of the ellipsoid model nor on the search space dimensionality.

Taking into account the interval of ν values on the vertical axis, the predictions show a good agreement with the experimental data (the maximal relative error is less than 6%). For both ellipsoid models ($q_i = i$ and $q_i = i^2$) the relative error decreases with growing search space dimensionality. The impact of the mutation strength control parameter α on the steady state mode eigenvalue is rather small. On the considered interval of α parameters the resulting eigenvalues differ in a maximal factor of about 1.4. In consequence of the huge fluctuations for small α that are observable in the experimental runs of the meta-ES

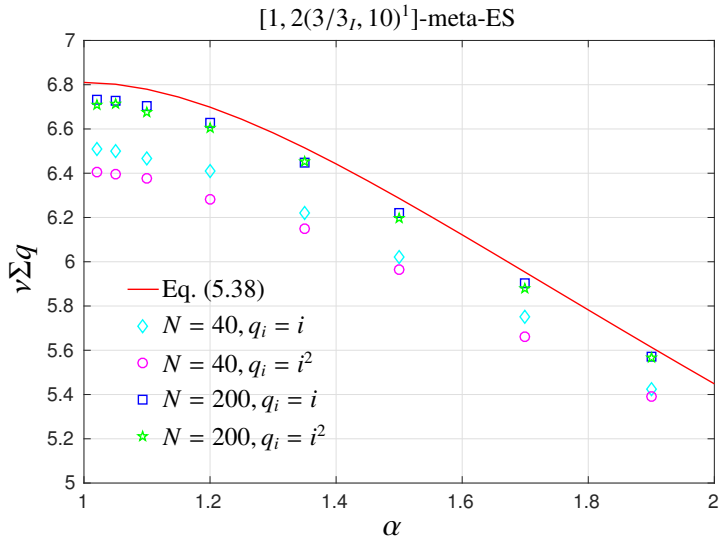

Figure 5.14.: Product of the ν and the sum of the ellipsoid coefficients Σq plotted against the mutation strength control parameters α. The solid red line illustrates the ν value prediction of (5.38) corresponding to eigenvalue problem (5.34). The experimentally obtained ν values on the ellipsoid model $q_i = i$, and $q_i = i^2$, are displayed as data points in search space dimension $N = 40$ and $N = 200$.

algorithm selecting $\alpha = 1.2$ seems to be an appropriate choice to efficiently control the mutation strength.

From Fig. 5.13 it is evident that the linear approximation of the eigenvalue problem (5.36) is not applicable to the sphere model ($q_i = 1$). Therefore, Eq. (5.38) is unsuited for the prediction of the steady state progress on the sphere. Nevertheless, a prediction of the steady state mode eigenvalue on the sphere model can be obtained directly from Eq. (5.33). Requiring $\forall i : \; q_i = 1$ in (5.33) and taking the sum over all $i = 1, \ldots, N$ yields after minor rearrangements

$$\nu \simeq \frac{2c_{\mu/\mu,\lambda}\sigma^*_{ss}}{N} - \frac{{\sigma^*_{ss}}^2}{\mu N}. \tag{5.39}$$

Considering the normalized steady state mutation strength approximation $\sigma^*_{ss} \simeq \sigma^*_0$, and considering (5.17), one obtains the steady state mode eigenvalue

$$\nu \simeq \frac{4\mu c^2_{\mu/\mu,\lambda}}{N} \frac{\alpha}{1+\alpha^2}\left(1 - \frac{\alpha}{1+\alpha^2}\right). \tag{5.40}$$

This formula represents an estimate for the steady state progress of the $[1, 2(\mu/\mu_I, \lambda)^\gamma]$-meta-ES on the sphere model ($q_i = 1$). Notice, Eq. (5.40) is only accessible provided that the meta-ES operates with a normalized steady state mutation strength close to σ^*_0.

On the sphere model, this holds true if the mutation strength control parameter satisfies $\alpha > \alpha_0$. The critical value α_0 has already been derived in Beyer et al. [2009] as

$$\alpha_0 = 1 + \frac{\mu c^2_{\mu/\mu,\lambda}}{2N - \mu c^2_{\mu/\mu,\lambda}}. \tag{5.41}$$

In this situation, the meta-ES approaches a limit cycle around σ_0^*. Considering the σ_0^* representation (5.17) as well as the inequality

$$\frac{\alpha}{1+\alpha^2} \lessapprox \frac{1}{2} \qquad \text{for} \quad \alpha \gtrapprox \alpha_0, \tag{5.42}$$

the point of discontinuity σ_0^* is located in close vicinity to the optimal normalized mutation strength $\sigma_{opt}^* = \mu c_{\mu/\mu,\lambda}$ on the sphere model. Thus, in expectation the meta-ES operates close to its optimal performance. The corresponding steady state convergence rate is provided by Eq. (5.40).

Given the $\alpha < \alpha_0$ case, the normalized mutation strength of the $[1, 2(\mu/\mu_I, \lambda)^1]$-meta-ES on the sphere model approaches a stable fixed point. This stable fixed point resides in the vicinity of $\sigma^* \lessapprox 2\mu c_{\mu/\mu,\lambda}$. According to Beyer et al. [2009], it is not possible to tune α adequately to shift this stable fixed point to the optimal normalized mutation strength $\sigma_{opt}^* = \mu c_{\mu/\mu,\lambda}$ on the sphere model.

5.2.5. The expected running time

Having derived the steady state mode eigenvalue, the steady state fitness dynamics can be determined by use of the Eqs. (3.6) and Eq. (5.31). Hence, starting at generation g_0 for an evolution interval of g generations yields

$$F(\mathbf{y}^{(g_0+g)}) = \sum_{j=1}^{N} q_j^2 y_j^{(g_0+g)^2} = \sum_{j=1}^{N} q_j^2 b_j \mathrm{e}^{-\nu(g_0+g)} = F(\mathbf{y}^{(g_0)})\mathrm{e}^{-\nu g}. \tag{5.43}$$

That is, in the strategy's steady state the objective function drops exponentially fast with time constant $\tau = 1/\nu$. The representation of the fitness dynamics provides an estimate for the expected running time G of the algorithm needed to improve the objective function value by a factor $2^{-\beta}$. Notice, that G in the context of meta-ES refers to the iteration number of the outer strategy. From (5.43) one obtains

$$2^{-\beta} = \frac{F(\mathbf{y}^{(g_0+G)})}{F(\mathbf{y}^{(g_0)})} = \mathrm{e}^{-\nu G}, \tag{5.44}$$

and by taking the logarithm and applying (5.38), G becomes

$$G \simeq \frac{\beta \ln(2)}{4\mu c_{\mu/\mu,\lambda}^2} \frac{(1+\alpha^2)\Sigma q}{\alpha} \frac{}{\breve{q}}. \tag{5.45}$$

The expected running times of the $[1, 2(3/3_I, 10)^1]$-meta-ES on the ellipsoid models $q_i = i, i^2$ are displayed in Fig. 5.15 considering different search space dimensions N. Using control parameter $\alpha = 1.2$ the theoretical predictions for $\beta = 2$ are compared with real ES runs. All experimental results are averaged over 100 independent ES runs and illustrated by error bars with their corresponding standard deviations. One observes a good agreement between experimental results and theoretical predictions. Additionally, the standard deviation decreases with growing search space dimensionality N.

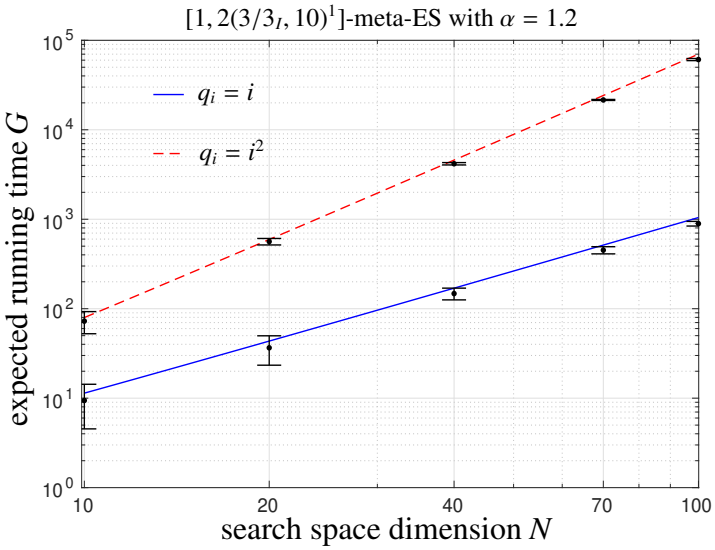

Figure 5.15.: The expected running time (5.45) is plotted against the search space dimension from $N = 10$ to $N = 100$. The experimental data points are averaged over 100 independent meta-ES runs. Mean values and standard deviations of the experimentally obtained data on the ellipsoid models $q_i = i$, and $q_i = i^2$, are displayed by the error bar plots.

The approximated expected running time G is asymptotically proportional to the quotient of the sum of the ellipsoid coefficients Σq and the smallest coefficient $\check{q}$. In particular, regarding the fitness model (3.6) the result also holds for the general PDQF case[2] $F(\boldsymbol{y}) = \boldsymbol{y}^\top \boldsymbol{Q}\boldsymbol{y}$ with positive definite matrix $\boldsymbol{Q} \in \mathbb{R}^{N\times N}$. In this situation, $\check{q} = \min(q_i)$ is identified with the smallest eigenvalue κ of the corresponding eigenvalue problem $\boldsymbol{Q}\boldsymbol{u} = \kappa\boldsymbol{u}$. That is, considering the $[1, 2(\mu/\mu_I, \lambda)^1]$-meta-ES on the general fitness model yields an expected running time G proportional to the quotient of the trace $\Sigma q = \mathrm{Tr}[\boldsymbol{Q}]$ and κ, $G \propto \mathrm{Tr}[\mathbf{Q}]/\check{\kappa}$. Accordingly, as anticipated at the end of Chapter 3, the expected running time of the two mentioned ellipsoid models increases with order N^2 for $q_i = i$, and with N^3 for $q_i = i^2$, respectively.

[2] Notice, that this is a generalization with respect to arbitrary rotations of the ellipsoid model. Again, the case of positive definite matrices $\boldsymbol{Q}$ with dominant eigenvalues has to be excluded, cf. condition (3.22).

5.3. Extension to multiple generation isolation periods

Having analyzed the $[1, 2(\mu/\mu_I, \lambda)^\gamma]$-meta-ES dynamics on the ellipsoid model for isolation time $\gamma = 1$ in Sec. 5.2, this section considers the case of isolation times $\gamma > 1$. Therefore, theoretical analysis from Sec. 5.2 is extended to approximate the meta-ES algorithm's dynamical behavior considering values of $\gamma > 1$. The approximations allow for the derivation of the specific evolution equations for y_i^2, σ, and σ^*. Supplementary, it provides evidence that the use of larger γ values enables the meta-ES to decrease the occurring fluctuations and thus improve the selection decision with regard to the best inner ES.

5.3.1. One-generation experiments

The one-generation meta-ES experiments conducted in Sec. 5.2.2 revealed that the two inner strategies can be discriminated more reliably by the upper level ES if the control parameter α is chosen sufficiently large ($\alpha \geq 1.2$).

As already mentioned in Sec. 3.2.1, operating with fixed strategy parameters the inner ES approaches its steady state over time. Accordingly, it comes into mind that longer isolation periods may result in increasingly distinct inner strategies. Thus the discriminability of the two fitness realizations should be enhanced.

In a first step, this assumption is validated by running one-generation experiments considering isolation times $\gamma > 1$. The one-generation experiments (cf. Sec. 5.2.2 for $\gamma = 1$) are performed in the following way:

a) A single iteration step of the $[1, 2(\mu/\mu_I, \lambda)^\gamma]$-meta-ES upper level strategy is executed for a given σ^* value and initial parameter vector $\mathbf{y}^{(0)}$. Therefore, the initial σ^* is renormalized to σ according to Eq. (3.14). Then both inner strategies are iterated with mutation strength $\sigma\alpha$ and σ/α, respectively, over γ generations.

b) According to line 6 and 7 of Alg. 5.1 the function values returned by the inner strategies are used to compute the quantity

$$\tilde{\Delta}(\sigma^*) := \frac{(F_1 - F_2)}{\sigma \sqrt{\sum_{j=1}^{N} q_j^2 y_j^{(0)^2}}}. \tag{5.46}$$

c) The steps a) and b) are repeated G times. Finally, the resulting samples are averaged.

The sign of the $\tilde{\Delta}$ function governing the mutation strength adaptation depends on the sign of the difference $(F_1 - F_2)$, where F_1 and F_2 are the objective function values returned by the two inner ES operating with $\sigma_1 = \sigma\alpha$ and $\sigma_2 = \sigma/\alpha$, respectively, after evolving over γ generations. Since division by positive values does not change the sign of the quantity, (5.46) is suitable to obtain the experimental $\tilde{\Delta}$ value.

The experimental measurements on the basis of Eq. (5.7) are compared to theoretical predictions of the respective quantity. The theoretical $\tilde{\Delta}(\sigma^*)$ is obtained on the basis of the fitness value difference that is provided in Eq. (5.7). Having neglected the fluctuation term

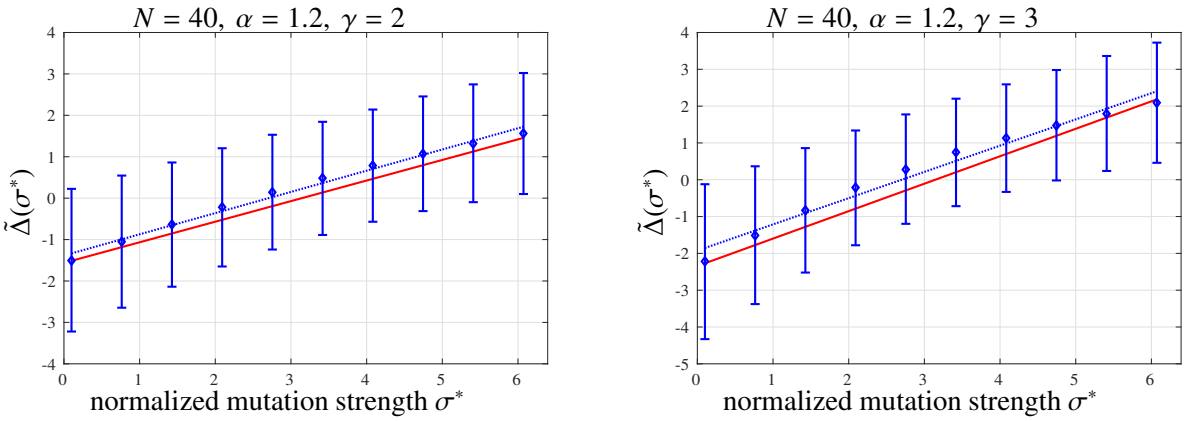

Figure 5.16.: One-generation experiments of the $[1, 2(3/3_I, 10)^\gamma]$-meta-ES on the ellipsoid model $q_i = i$. The initial parameter vector is $\mathbf{y} = \mathbf{1}$. Two different isolation times $\gamma = 2, 3$ are displayed considering $N = 40$ and $\alpha = 1.2$. Each data point represents the mean value of 10^5 one-generation experiments and the corresponding standard deviation is illustrated using error bars. The dashed blue line is the straight line fitted to the experimental mean values. The theoretical predictions of (5.47) are represented by the solid red line.

$\epsilon_{\Delta F}$, it can be transformed into the right-hand side expression in Eq. (5.46) by multiplication with γ and by some straight forwards operations. Accordingly, the corresponding $\tilde{\Delta}$ value is roughly calculated as

$$\tilde{\Delta}(\sigma^*) \simeq 2c_{\mu/\mu,\lambda}\left(\alpha - \frac{1}{\alpha}\right)\left[\left(\alpha + \frac{1}{\alpha}\right)\frac{\sigma^{*(g)}}{2\mu c_{\mu/\mu,\lambda}} - 1\right]\gamma. \tag{5.47}$$

As explained below, Eq. (5.47) is only a good approximation for rather small values of the isolation time γ. Nonetheless, it suffices to illustrate the emerging tendency. The one-generation experiments for several values of $\sigma^* \in (0, 2\mu c_{\mu/\mu,\lambda}]$ are compared to theoretical predictions of $\tilde{\Delta}(\sigma^*)$ derived from Eq. (5.47) in Fig. 5.16. There, the results for the $[1, 2(3/3_I, 10)^\gamma]$-meta-ES on the ellipsoid model $q_i = i$ are illustrated considering $\gamma = 1, 2, 3, 5$, mutation strength control parameter $\alpha = 1.2$ and search space dimension $N = 40$. The experimental results are averaged over 10^5 one-generation experiments and displayed by the error bar plot. Fitting a line to the experimental mean values one is able to approximate the slope of the experimental $\tilde{\Delta}(\sigma^*)$ curve. The solid red line displays the theoretical results of Eq. (5.47).

As anticipated, the increasing slope of the curves points towards an improvement of the meta-ES' ability to distinguish the inner strategies. Unfortunately, the approximation of the discriminator function in (5.47) deteriorates with growing isolation time γ and reduces the agreement of the experimental and theoretical results. Considering a larger search space dimension N would improve the approximation quality. This can be observed in Fig. 5.17. There, the slope of the line fitted to the experimental mean values of the one-generation experiments is compared to the slope of the theoretical $\tilde{\Delta}(\sigma^*)$ curve which can be calculated

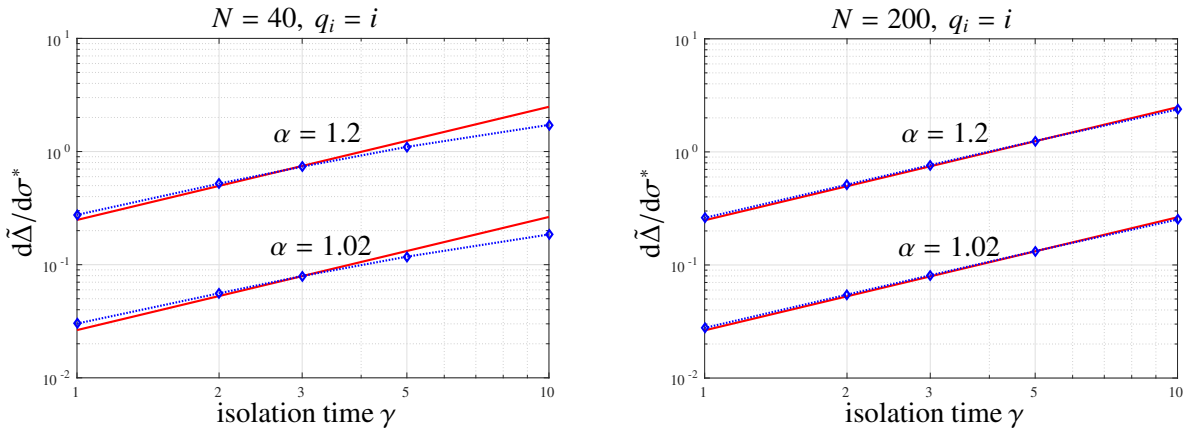

Figure 5.17.: Illustration of the slope (5.48) plotted against the isolation time γ. The predictions and experimental runs are compared using a $[1, 2(3/3_I, 10)^\gamma]$-meta-ES. On the ellipsoid model $q_i = i$ the dimensionalities $N = 40, 200$ are considered. Each figure compares the results of the control parameters $\alpha = 1.02$ and $\alpha = 1.2$. The data point represent the mean value of 10^5 one-generation experiments according to those displayed in Fig. 5.16. The theoretical predictions of (5.48) are represented by the solid red line.

from (5.47) as

$$\frac{\mathrm{d}\tilde{\Delta}}{\mathrm{d}\sigma^*} = \left(\alpha^2 - \frac{1}{\alpha^2}\right)\frac{\gamma}{\mu}. \tag{5.48}$$

The data points are gathered in one-generation experiments considering different parameter settings. In the manner of Fig. 5.16 the mean f values are averaged over 10^5 one-generation experiments. After that a straight line is fitted to the set of mean values, its slope is measured, displayed by the blue data points and connected by the dotted lines. The deviations between experimental results and predictions increase relatively fast in low search space dimensions. But still the experimental measurements show that the meta-ES benefits from the use of longer isolation periods. As mentioned in Sec. 5.1 the slope of the $\tilde{\Delta}$ curves also increases with the magnitude of the control parameter α. That is, both increasing α as well as increasing γ improves the algorithm's decision to adapt the mutation strength properly. Regarding the one-generation experiments of the previous section it can be inferred from Eq. (5.47) that in the range of small γ the isolation time has a linear influence on the fitness dynamics of the $[1, 2(\mu/\mu_I, \lambda)^\gamma]$-meta-ES. This leads to the assertion of modeling the multi generation dynamics of the component-wise squared distance to the optimizer in a similar (i.e. linear) manner.

5.3.2. Evolution equations for isolation over multiple generations

Having substantiated the assumption that longer isolation periods are able to improve the selection decision of the upper level ES, this section addresses the derivation of the respective evolution equations. The evolution equations intend to approximate the $[1, 2(\mu/\mu_I, \lambda)^\gamma]$-

meta-ES evolution between two consecutive isolation periods of length $\gamma > 1$. This is achieved by appropriately incorporating the dynamics of the inner strategies into the theoretical model.

The inner ES operates with fixed mutation strength σ over a isolation period of γ generations. Assuming that the components of the parental centroid y_i^2 are subject to rather small changes within the isolation interval, it is possible to obtain a theoretical model describing the meta-ES dynamics in the range of small isolation times $\gamma > 1$. The approach allows for the derivation of a condition on the maximal choice of γ that ensures a good approximation quality. The evolution equation of the component-wise squared distance to the optimizer is approximated in Appendix B.3 considering $\gamma = 2$. Extending the result obtained in Appendix B.3 to slightly longer isolation times, the component-wise quadratic progress over multiple generations can be roughly generalized for small values of $\gamma > 2$. Assuming that it scales linearly with the isolation time γ, the ${y_i}^2$ transition is obtained as

$$y_i^{(g+\gamma)^2} \simeq y_i^{(g)^2} - \gamma\, \varphi_i^{II}(\sigma^{(g)}, \mathbf{y}^{(g)}). \tag{5.49}$$

Making use of (5.49) allows for the characterization of the y_i^2 evolution in terms of the isolation periods of length γ within the meta-ES algorithm, see Alg. 5.1. In the following, $y_i^{(g+\gamma)^2}$ is identified with the component-wise squared distance to the optimizer after isolation period $t+1$, and $y_i^{(g)^2}$ with that at the end of the previous isolation period t, respectively. The y_i^2 evolution between the two consecutive isolation periods can then be expressed in terms of the quadratic progress rate (3.24)

$$y_i^{(t+1)^2} \simeq y_i^{(t)^2} - \gamma\, \varphi_i^{II}(\sigma^{(t)}, \mathbf{y}^{(t)}). \tag{5.50}$$

An upper bound on the isolation time γ up to which formula (5.50) is admissible can be derived from App. B.3. By applying the normalization (3.14) the bracketed term in Eq. (B.28) becomes

$$\left(1 - \frac{2c_{\mu/\mu,\lambda}\sigma^* q_i}{\Sigma q}\right). \tag{5.51}$$

The fraction can be interpreted as the component-wise modeling error that occurs in each generation within one isolation period. Requiring that the aggregated modeling error is sufficiently small, leads to the condition

$$\gamma \frac{2c_{\mu/\mu,\lambda}\sigma^* q_i}{\Sigma q} \ll 1, \tag{5.52}$$

being equivalent to

$$\gamma \ll \frac{\Sigma q}{2c_{\mu/\mu,\lambda}\sigma^* q_i}. \tag{5.53}$$

Taking into account that the largest ellipsoid coefficient $\hat{q} := \max\{q_i | i = 1, \ldots, N\}$ corresponds to the largest modeling error the isolation time has to suffice

$$\gamma \ll \frac{\Sigma q}{2c_{\mu/\mu,\lambda}\sigma^* \hat{q}}. \tag{5.54}$$

That is, formula (5.50) is applicable provided that the isolation time is considerably smaller than a term proportional to the search space dimension.

The next step is concerned with the description of the mutation strength dynamics. Keeping in mind that the inner ESs operate with fixed strategy parameters, the meta-ES algorithm adapts the mutation strength at the end of each isolation period. The mutation strength control is based on the best objective function value of the parental centroids $\mathbf{y}^{(g+\gamma)}$ returned by the inner strategies. Since γ is just a multiplicative factor within Eq. (5.49), the mutation strength evolution equation for $\gamma > 1$ can derived in the same way as (5.10). Accordingly, the σ evolution from isolation period t to $t+1$ is determined by

$$\sigma^{(t+1)} \simeq \sigma^{(t)} \alpha^{-\mathrm{sign}(\Delta(\sigma^{*(t)}))}, \tag{5.55}$$

with

$$\Delta(\sigma^{*(t)}) := \left(\alpha + \frac{1}{\alpha}\right) \frac{\sigma^{*(t)}}{2\mu c_{\mu/\mu,\lambda}} - 1. \tag{5.56}$$

Notice, that except for not taking into account the fluctuation term, the mutation strength dynamics for $\gamma > 1$ are governed by exactly the same discriminator function Δ as derived the $\gamma = 1$ case, see (5.8). As a consequence the point of discontinuity σ_0^* is not changed considering slightly longer isolation periods $\gamma > 1$. Remembering (5.17), the corresponding point of discontinuity σ_0^* was derived as the root of $\Delta(\sigma^{*(t)})$, and reads

$$\sigma_0^* = 2\mu c_{\mu/\mu,\lambda} \frac{\alpha}{1+\alpha^2}. \tag{5.57}$$

That is, for $\gamma > 1$ the meta-ES is supposed to also approach normalized mutation strength values in the proximity of σ_0^* and then exhibit an oscillating behavior around σ_0^*. This behavior will be investigated in the following section.

Inserting the progress rate formula (3.24) into Eq. (5.50), the system of evolution equations describing the outer meta-ES dynamics for small isolation periods of length $\gamma > 1$ is obtained as

$$\begin{aligned} y_i^{(t+1)^2} &\simeq y_i^{(t)^2} + \gamma \left(\frac{\sigma^{(t)^2}}{\mu} - \frac{2\sigma^{(t)} c_{\mu/\mu,\lambda} q_i y_i^{(t)^2}}{\sqrt{\sum_{j=1}^{N} q_j^2 y_j^{(g)^2}}} \right), \\ \sigma^{(t+1)} &\simeq \sigma^{(t)} \alpha^{-\mathrm{sign}(\Delta(\sigma^{*(t)}))}. \end{aligned} \tag{5.58}$$

The modeling approach resulting in system (5.58) is verified by comparison to experimental meta-ES runs. The results are illustrated in Fig. 5.18 applying the $[1, 2(3/3, 10)^{\gamma}]$-meta-ES with $\gamma = 3$ and $\alpha = 1.2$ to the ellipsoid models $q_i = i, i^2$. Considering search space dimension $N = 40$, the experimental data are averaged over 10^4 independent runs. They are displayed by the data points, while the dashed red line illustrates the normalized mutation strength σ^*. The solid lines display the iteratively generated results of the evolutionary system (5.58).

The illustrations show a quite good agreement between the experimental runs and the theoretical predictions. Unfortunately, the prediction quality of system (5.58) deteriorates rather quickly when using $\gamma > 3$. Conditional on the initialization parameters, the iteration

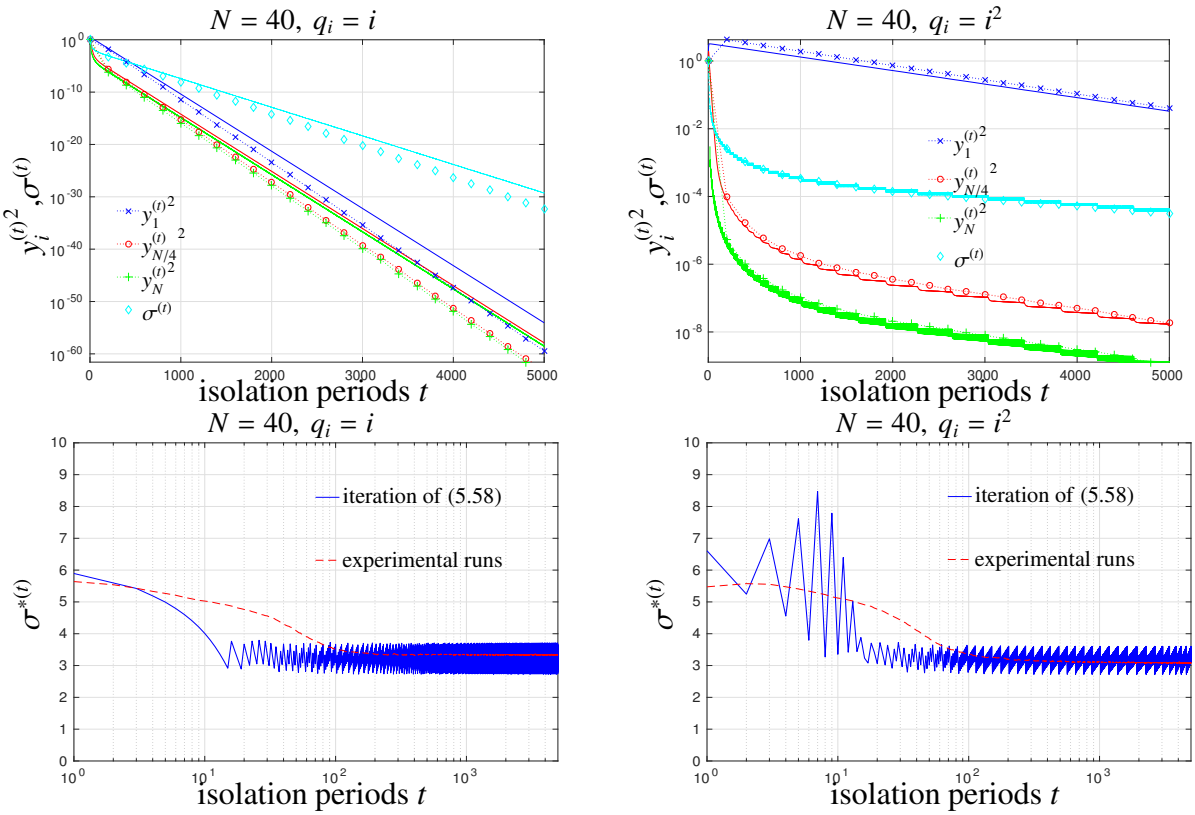

Figure 5.18.: The σ, σ^*, and y_i^2 dynamics of an $[1, 2(3/3_I, 10)^3]$-meta-ES for $\gamma = 3$ displayed considering the ellipsoid models $q_i = i$, and $q_i = i^2$ in dimension $N = 40$. The mutation strength control parameter used is $\alpha = 1.2$.

of (5.58) might result in negative values of the y_i^2 dynamics at worst. This is a consequence of the rather rough generalization from $\gamma = 2$ to larger γ values. However, to some extend the system (5.58) allows for the derivation of more general performance results. These are valid concerning γ values that satisfy the condition mentioned in Eq. (5.54).

In the way of the analysis performed in Sec. 5.2, the next step is concerned with the description of the normalized mutation strength σ^*. Hence, considering $1 \leq \gamma < 20$ an estimate of the $[1, 2(\mu/\mu_I, \lambda)^\gamma]$meta-ES steady state performance is derived that allows for the approximation of the corresponding expected running times.

5.3.3. The normalized mutation strength dynamics

Taking into account the evolution equation of the mutation strength in system (5.58), the corresponding evolution equation of the normalized mutation strength σ^* is computed analogously to the derivation in Sec. 5.2. By considering the mutation strength normalization (3.14) one gets

$$\sigma^{*(t+1)} = \sigma^{(t+1)} \frac{\Sigma q}{\sqrt{\sum_{j=1}^{N} q_j^2 \left(y_j^{(t+1)}\right)^2}} = \sigma^{(t)} \alpha^{-\text{sign}(\Delta(\sigma^{*(t)}))} \frac{\Sigma q}{\sqrt{\sum_{j=1}^{N} q_j^2 \left(y_j^{(t+1)}\right)^2}} \tag{5.59}$$

Expressing the $y_j^{(t+1)^2}$ terms by use of the quadratic progress rate (5.50) the normalized mutation strength becomes

$$\sigma^{*(t+1)} \simeq \sigma^{(t)} \alpha^{-\operatorname{sign}(\Delta(\sigma^{*(t)}))} \Sigma q \frac{1}{\sqrt{\sum_{j=1}^{N} q_j^2 y_j^{(t)^2} - \gamma \sum_{j=1}^{N} q_j^2 \varphi_j^{II}(\sigma^{(t)} \alpha^{-\operatorname{sign}(\Delta(\sigma^{*(t)}))})}}. \tag{5.60}$$

Placing the quotient $\Sigma q / \sum_{j=1}^{N} q_j^2 y_j^{(t)^2}$ outside the brackets yields

$$\sigma^{*(t+1)} \simeq \sigma^{(t)} \alpha^{-\operatorname{sign}(\Delta(\sigma^{*(t)}))} \frac{\Sigma q}{\sqrt{\sum_{j=1}^{N} q_j^2 y_j^{(t)^2}}} \frac{1}{\sqrt{1 - \gamma \frac{\sum_{j=1}^{N} q_j^2 \varphi_j^{II}(\sigma^{(t)} \alpha^{-\operatorname{sign}(\Delta(\sigma^{*(t)}))})}{\sum_{j=1}^{N} q_j^2 y_j^{(t)^2}}}}. \tag{5.61}$$

This expression can be further simplified by normalization (3.14) as well as the result from App. B.1. That is, taking into account Eq. (B.13) and applying the Q approximation (B.16), the σ^* evolution from isolation period t to $t+1$ is governed by

$$\sigma^{*(t+1)} \simeq \frac{\sigma^{*(t)} \alpha^{-\operatorname{sign}(\Delta(\sigma^{*(t)}))}}{\sqrt{1 - \gamma \frac{2 c_{\mu/\mu,\lambda} \sigma^{*(t)} \alpha^{-\operatorname{sign}(\Delta(\sigma^{*(t)}))} \breve{q}}{\Sigma q}}}, \tag{5.62}$$

with $\breve{q} = \min(q_i)$ denoting the smallest ellipsoid coefficient. Equation (5.62) again represents an iterative mapping of the form $\sigma^{*(g+1)} = \bar{f}_\sigma\left(\sigma^{*(g)}; \alpha; \gamma\right)$. Notice, that (5.62) is a straightforward generalization of the recurrence equation (5.16). It characterizes the normalized mutation strength dynamics of the meta-ES for $\gamma \geq 1$. However, it is important to bear in mind that (5.62) is an asymptotic approximation only valid for rather small values of the isolation time γ.

Alike the $\gamma = 1$ case in Sec. 5.2, the normalized mutation strength dynamics resulting from (5.62) can be bracketed within an oscillation interval. The limits of this specific oscillation interval are calculated in the same manner as (5.19) and (5.20) in Sec. 5.2.3. The derivation follows the calculations demonstrated in App. B.2 for the $\gamma = 1$ case. One obtains the right-sided limit of the normalized mutation strength oscillation interval as

$$\hat{\sigma}_\gamma^* := \lim_{\sigma^* \to \sigma_0^* - 0} \tilde{f}_\sigma(\sigma^*) \simeq \frac{2\mu c_{\mu/\mu,\lambda}}{1+\alpha^2} \frac{\alpha^2}{\sqrt{1 - 4\gamma\mu c_{\mu/\mu,\lambda}^2 \frac{\alpha^2}{1+\alpha^2} \frac{\breve{q}}{\Sigma q}}}. \tag{5.63}$$

Analogously, the left-sided limit as

$$\breve{\sigma}_\gamma^* := \lim_{\sigma^* \to \sigma_0^* + 0} \tilde{f}_\sigma(\sigma^*) \simeq \frac{2\mu c_{\mu/\mu,\lambda}}{1+\alpha^2} \frac{1}{\sqrt{1 - 4\gamma\mu c_{\mu/\mu,\lambda}^2 \frac{1}{1+\alpha^2} \frac{\breve{q}}{\Sigma q}}}. \tag{5.64}$$

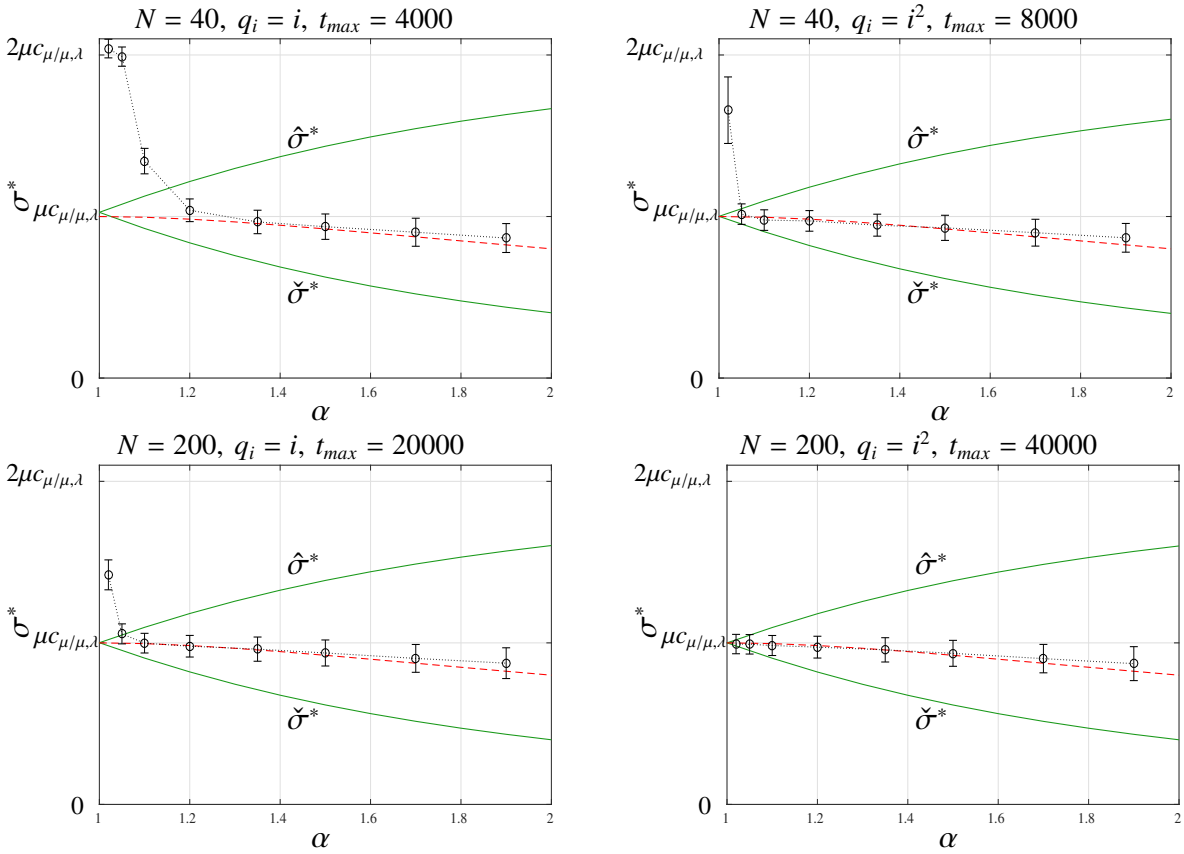

Figure 5.19.: On the influence of α on the steady state normalized mutation strength σ^* of the $[1, 2(3/3_I, 10)^3]$-meta-ES. Taking the ellipsoid models $q_i = i$ and $q_i = i^2$ into consideration the limits (5.63) and (5.64) are displayed by the solid green lines. The point of discontinuity σ^*_0, Eq.(5.17), is illustrated using the dashed red line.The error bar plots represents mean and standard deviation of the experimental results measured over the last 25% of the t_{max} isolation periods.

The validation of the analytical findings is presented in Fig. 5.19. Considering an isolation period of $\gamma = 3$ generations, the ellipsoid models $q_i = i, i^2$ in search space dimensions $N = 40, 200$ are compared with experimental runs of the meta-ES algorithm, Alg. 5.1. The limits (5.63) and (5.64) of the iterative mapping (5.62) are plotted against the mutation strength control parameter α (solid green lines). Within these limits the point of discontinuity σ^*_0 is displayed by the dashed red line. The black error bar plot correspond to experimental data resulting from measurements being averaged over 20 independent $[1, 2(3/3_I, 10)^3]$-meta-ES runs of t_{max} isolation periods. Mean and standard deviation are measured over the last 25% of the t_{max} isolation periods, i.e., after the strategy has approached its limit cycle. Depending on the search space dimension one observes the considerable influence of the ϵ_Δ fluctuations for small $\alpha < 1.2$, already discussed in Sec. 5.2.2. According to that, omitting the fluctuation terms within the analysis causes the deviations from the experimental measurements. Due to the small choices of α the meta-ES realizes relatively small distinctions

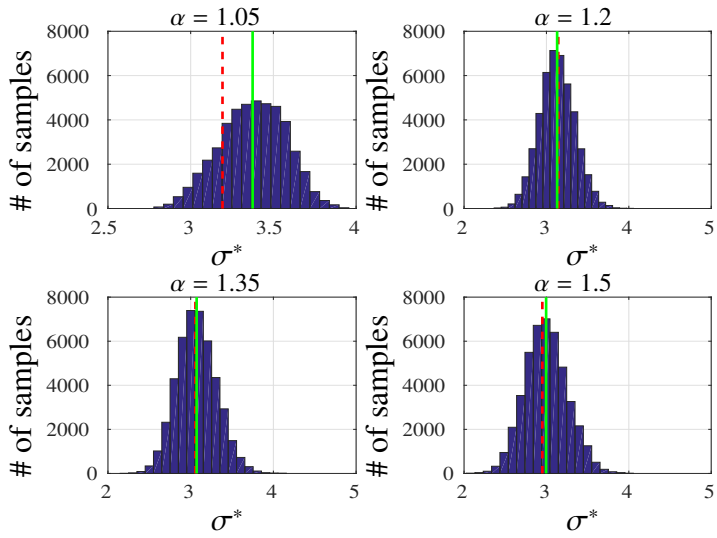

Figure 5.20.: Illustration of the distribution of the normalized mutation strength σ^* after the $[1, 2(3/3_I, 10)^3]$-meta-ES has approached its steady state behavior. The experimental data are averaged over 20 independent runs performed on the ellipsoid model q_i with search space dimension $N = 200$. The green line corresponds to the measured mean value. The dashed red line displays the point of discontinuity σ^*_0 according to Eq. (5.17).

in the inner ES's fitness values. Hence, being affected by the ϵ_Δ fluctuations, the selections decision of the upper level strategy turns out to be wrong in many cases. Additionally, making use of small α values, Alg. 5.1 appears to be unable to readjust the fluctuation caused deviations. Provided that α is sufficiently large, the experimental σ^* dynamics approach steady state values in the vicinity of the point of discontinuity σ^*_0. Conclusively, the algorithm exhibits a similar behavior to that observed in the $\gamma = 1$ case.

Regarding the ellipsoid models $q_i = i$, Fig. 5.20 illustrates the distribution of the experimentally obtained normalized steady state mutation strength for $N = 200$ in histogram plots. Four choices of the control parameter α are displayed. The distributions of the σ^* values are measured considering the final 25% isolation periods obtained from the experimental meta-ES runs with the same configuration as those displayed in Fig. 5.19. For sufficiently large α the experimentally measured mean values reside remarkably close to the point of discontinuity σ^*_0. With decreasing influence of the ϵ_Δ fluctuations for $\alpha > 1.1$ the σ^*_{ss} values appear to be symmetrically distributed around their mean value. This observation supports the modeling of the normalized mutation strength σ^*_{ss} as the sum of the mean value and fluctuation terms in order to investigate the strategy's steady state behavior within the next section.

5.3.4. Predicting the expected steady state progress

According to Fig. 5.19, and Fig. 5.20, the normalized steady state mutation strength realized by the $[1, 2(3/3_I, 10)^\gamma]$-meta-ES ($\gamma > 1$) resides in close proximity to σ^*_0. This observations

prompts towards modeling the expected normalized steady state mutation strength σ^*_{ss} by use of the point of discontinuity σ^*_0. That is, the approximation $\sigma^*_{ss} \simeq \sigma^*_0$, cf. Eq. (5.22), seems again to be reasonable for the investigation the strategy's steady state dynamics. Accordingly, the progress in terms of the component-wise squared distance to the optimizer between two consecutive isolation periods $t+1$ and t of length $\gamma > 1$ is estimated by use of the first equation in the system (5.58). Using the normalizations (3.14), and (3.11), the y_i^2 evolution equation in (5.58) is asymptotically equal to

$$y_i^{(t+1)^2} \simeq y_i^{(t)^2} + \gamma \left(\frac{\sigma^{*(t)^2}}{\mu} \frac{\sum_{j=1}^N q_j^2 y_j^{(t)^2}}{\Sigma q} - \frac{2\sigma^{*(t)} c_{\mu/\mu,\lambda} q_i y_i^{(t)^2}}{\Sigma q} \right). \tag{5.65}$$

The log-linear longterm behavior of the meta-ES dynamics observable in Fig. 5.18 suggests that the dynamics of the upper level ES in their steady state follow the same exponential *Ansatz* motivated in Sec. 5.2. That is, assuming that the meta-ES operates in its steady state, the evolution equation (5.65) can be solved by use of the *Ansatz*

$$y_i^{(t)^2} = b_i \mathrm{e}^{-\tilde{\nu} t}, \quad b_i > 0,\ \tilde{\nu} > 0. \tag{5.66}$$

Like demonstrated in the $\gamma = 1$ case, the *Ansatz* allows for the identification of the parental centroid's component-wise squared distance to the optimizer at the end of isolation period $t+1$ with that after isolation period t

$$y_i^{(t+1)^2} = b_i \mathrm{e}^{-\tilde{\nu}(t+1)} = b_i \mathrm{e}^{-\tilde{\nu} 1} \mathrm{e}^{-\tilde{\nu}} = y_i^{(t)^2} \mathrm{e}^{-\tilde{\nu}}. \tag{5.67}$$

Taking into account sufficiently small values of $\tilde{\nu}$ allows for the Taylor expansion of the exponential function $\mathrm{e}^{-\tilde{\nu}} \simeq (1 - \tilde{\nu})$. This way Eq. (5.67) becomes

$$y_i^{(t+1)^2} \simeq y_i^{(t)^2} (1 - \tilde{\nu}). \tag{5.68}$$

Inserting (5.68) into (5.65) and applying the *Ansatz* (5.66) yields the corresponding eigenvalue problem

$$\tilde{\nu} b_i = 2\gamma c_{\mu/\mu,\lambda} \sigma^*_{ss} \frac{q_i}{\Sigma q} b_i - \gamma \frac{{\sigma^*_{ss}}^2}{\mu} \frac{\sum_{j=1}^N q_j^2 b_j}{(\Sigma q)^2}. \tag{5.69}$$

with components b_i of the eigenvector $\mathbf{b} = (b_1, b_2, \ldots, b_N)^\top$ and eigenvalue $\tilde{\nu}$.

Notice, corresponding to the meta-ES using isolation periods of length $\gamma > 1$ the eigenvalue problem (5.69) differs from the $\gamma = 1$ situation (Sec. 5.2) only by the multiplicative factor γ. This is due to the linear approximation of the progress rate (5.50) that describes the progress over a period of γ consecutive generations. The numerical solutions to this eigenvalue problem have a structure similar to those presented in Fig. 5.13. Though, the solutions will be scaled by the factor γ. That is, for $q_i > 1$ the eigenvalues show a linear rise for a wide range of σ^*_{ss} values until they exhibit a sharp drop as σ^*_{ss} approaches its limit of positive progress at $2\mu c_{\mu/\mu,\lambda}$, cf. (3.31).

The observations in Fig. 5.19 and Fig. 5.20 substantiate the modeling of the normalized steady state mutation strength by means of its mean value dynamics denoted as $\overline{\sigma}^*_{ss}$ and the corresponding fluctuation parts $\epsilon_{\sigma^*_{ss}}$ yielding

$$\sigma^*_{ss} = \overline{\sigma}^*_{ss} + \epsilon_{\sigma^*_{ss}}. \tag{5.70}$$

Assuming that the mean value dynamics in Eq. (5.70) are characterized sufficiently well by the point of discontinuity σ_0^* allows for the approximation of the steady state behavior. Neglecting the fluctuation term $\epsilon_{\sigma_{ss}^*}$, and applying $\overline{\sigma}_{ss}^* \simeq \sigma_0^*$ to (5.70), the normalized steady state mutation strength can be approximated by

$$\sigma_{ss}^* \simeq \sigma_0^* = 2\mu c_{\mu/\mu,\lambda} \frac{\alpha}{(1+\alpha^2)}. \tag{5.71}$$

This approximation has a direct implication on the isolation time condition (5.54). Hence, by insertion of (5.71) one obtains

$$\gamma \ll \frac{(1+\alpha^2)}{4\mu c_{\mu/\mu,\lambda}^2 \alpha^2} \frac{\Sigma q}{\hat{q}}. \tag{5.72}$$

Conclusively, the system of evolution equations (5.58) approximates the dynamical behavior of the $[1, 2(3/3_I, 10)^\gamma]$-meta-ES on the ellipsoid model sufficiently well as long as requirement (5.72) is effectively satisfied. That is, given fixed population sizes and a parameter α, the isolation time has to be considerably smaller than a term proportional to the quotient of the trace of the problems Hessian matrix and the corresponding smallest eigenvalue $\mathrm{Tr}[\boldsymbol{Q}]/\check{\kappa}$, see also Sec. 5.2.5.

In Fig. 5.21 the condition (5.72) is plotted against the search space dimension considering the ellipsoid models $q_i = i$ and $q_i = i^2$. The illustration makes use of the mutation strength control parameter $\alpha = 1.2$ and population sizes $\mu = 3$ and $\lambda = 10$. Variations in α have only a minor impact on the illustrated boundaries. On the other hand, the use of larger parental populations causes a rapid decrease of the boundary values. Taking into account the truncation ratio of the populations $\vartheta = \mu/\lambda$, the condition can be expressed as

$$2\gamma\lambda \ll \frac{(1+\alpha^2)}{2\vartheta c_{\mu/\mu,\lambda}^2 \alpha^2} \frac{\Sigma q}{\hat{q}}. \tag{5.73}$$

Conclusively, the approximation quality of system (5.58) is correlated to the number of function evaluations $2\gamma\lambda$ employed during a single isolation period.

In the line of Sec. 5.2.4, when regarding non-spherical ellipsoid models the numerical solution of the eigenvalue problem (Fig. 5.13) suggests that the solutions around σ_0^* can be determined by use of the linear parts of Eq. (5.69). Hence, considering normalized steady state mutation strength values in the close neighborhood of the point of discontinuity, i.e. $\sigma_{ss}^* \approx \sigma_0^*$, the quadratic term in (5.69) can be neglected and the eigenvalues that govern the meta-ES long-term decline are directly obtained by

$$\tilde{\nu} \simeq 2\gamma c_{\mu/\mu,\lambda} \sigma_{ss}^* \frac{q_i}{\Sigma q}. \tag{5.74}$$

Inserting (5.71) results in the approximation of the eigenvalues corresponding to the eigenvalue problem (5.69)

$$\tilde{\nu} \simeq 4\gamma\mu c_{\mu/\mu,\lambda}^2 \frac{\alpha}{(1+\alpha^2)} \frac{q_i}{\Sigma q}. \tag{5.75}$$

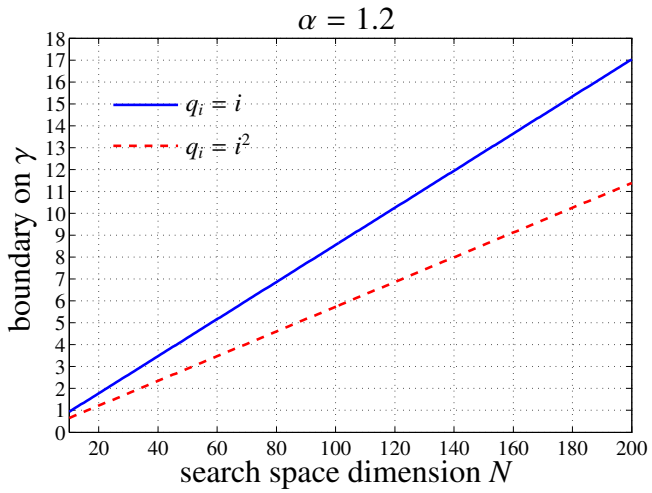

Figure 5.21.: Illustration of the boundary (5.72) on γ up to which the approximation are still admissible. The parental population is set to $\mu = 3$ and the mutation strength control parameter is $\alpha = 1.2$.

Since the smallest positive eigenvalue of (5.69) corresponds to the slowest mode of the meta-ES dynamics, this eigenvalue determines steady state dynamics of the meta-ES. Remembering that the smallest ellipsoid coefficient is denoted by $\breve{q} := \min(q_i)$, the steady state mode eigenvalue is derived as

$$\tilde{\nu} \simeq 4\gamma\mu c^2_{\mu/\mu,\lambda} \frac{\alpha}{(1+\alpha^2)} \frac{\breve{q}}{\Sigma q}. \tag{5.76}$$

According to *Ansatz* (5.66), Equation (5.76) represents an estimate of the expected steady state progress of the $[1, 2(\mu/\mu_I, \lambda)^\gamma]$-meta-ES for isolation periods of (short) length $\gamma > 1$. In that respect, it generalizes the analysis conducted in Sec. 5.2 to longer isolation times.

Formula (5.76) is validated by comparison to measurements from experimental meta-ES runs in Fig. 5.22. The illustrated solid red line shows the steady state convergence rate (5.76) being normalized by multiplication with $\Sigma q/\gamma$ and plotted against different realizations of the mutation strength control parameter α. Due to the normalization the theoretical prediction does neither depend on the coefficients of the ellipsoid model nor on the isolation time γ. The experimental results are averaged over 50 independent $[1, 2(3/3, 10)^\gamma]$-meta-ES runs operating with fixed normalized steady state mutation strength $\sigma^*_{ss} = \sigma^*_0 = 2\mu c_{\mu/\mu,\lambda}\alpha/(1+\alpha^2)$. The mutation strength $\sigma^{(g)}$ is obtained by renormalization in each generation. The gathered data points are used to obtain N experimental ν values, i.e., one for each y_i^2 component. According to the $\gamma = 1$ case in Fig. 5.14, those ν values corresponding to the dynamics of the first component, i.e. the y_1^2 dynamics, are considered. In comparison to the theoretical predictions of Eq. (5.76) the experimental ν values are displayed by use of the data points in Fig. 5.22. This procedure is carried out for four different combinations of the ellipsoid models $q_i = i, i^2$ and different isolation times $\gamma = 2, 3, 5, 20$. Interestingly, the prediction quality is remarkably good considering both, small search space dimensions $N = 40$,

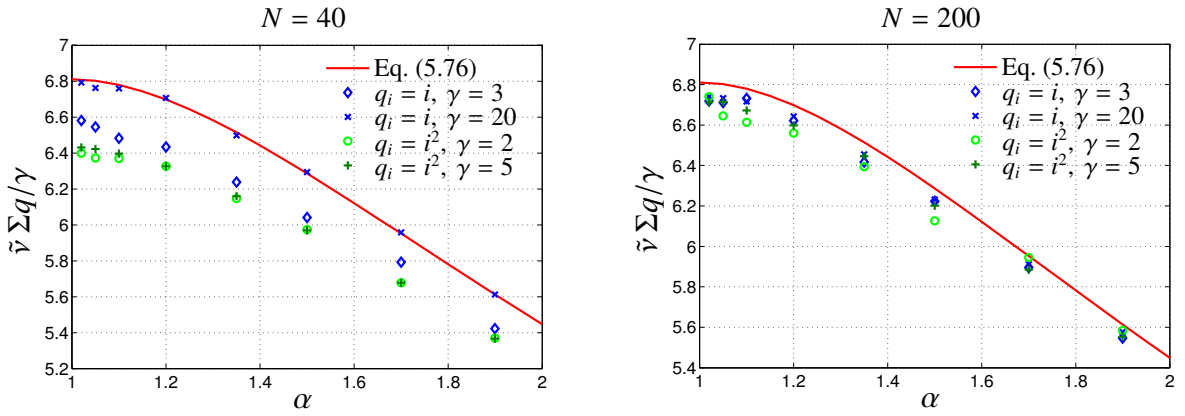

Figure 5.22.: The steady state mode eigenvalue $\tilde{\nu}$ multiplied by the normalization factor $\Sigma q/\gamma$ is plotted against the mutation strength control parameter α. A $[1, 2(3/3, 10)^{\gamma}]$-meta-ES is applied to the ellipsoid models $q_i = i$, and $q_i = i^2$. The experimentally obtained $\tilde{\nu}$ values are displayed as data points in search space dimension $N = 40$ and $N = 200$. Different values of the isolation length γ are illustrated to validate the estimate of the steady state mode eigenvalue (5.76).

and larger ones $N = 200$, respectively. Still, the deviations are reduced with growing dimensionality. For $N = 40$ the choice of $\gamma = 20$ almost matches the predicted eigenvalues. But this most certainly is a statistical fluke since the analysis was derived assuming rather small γ values. The choice of $\gamma = 20$ on the ellipsoid model $q_i = i$ in dimension $N = 40$ seems to be a marginal case. Because for larger isolation times the deviations increase rapidly insofar as the experimental values exceed the analytical predictions.

Having validated the steady state mode eigenvalue formula, it allows for the prediction of the $[1, 2(\mu/\mu_I, \lambda)^{\gamma}]$-meta-ES long-term behavior. Considering Eq. (5.66) and the corresponding convergence rate (5.76) yields the description of the respective steady state progress. Consequently, it is possible to derive a formula that estimates the expected running time of the $[1, 2(\mu/\mu_I, \lambda)^{\gamma}]$-meta-ES algorithm with isolation times $\gamma > 1$. This formula is calculated in the line presented for the $\gamma = 1$ case in Sec. 5.2.5. The steady state fitness dynamics are determined by use of the Eqs. (3.6) and (5.67). Accordingly, beginning at isolation period t_0 the objective function value realized by evaluation of the parental centroid vector after t additional isolation periods can be predicted by

$$F(\mathbf{y}^{(t_0+t)}) = \sum_{j=1}^{N} q_j^2 y_j^{(t_0+t)\,2} = \sum_{j=1}^{N} q_j^2 b_j \mathrm{e}^{-\tilde{\nu}(t_0+t)} = F(\mathbf{y}^{(t_0)})\mathrm{e}^{-\tilde{\nu}t}. \tag{5.77}$$

Hence, in the strategy's steady state the objective function value drops exponentially fast (with respect to the number of isolation periods) with time constant $\tau = 1/\tilde{\nu}$. This representation of the fitness dynamics provides an estimate for the expected number of isolation periods T needed to improve the objective function value by a factor $2^{-\beta}$. Considering the

relative change in the fitness value and Eq. (5.77) one obtains

$$2^{-\beta} = \frac{F(\mathbf{y}^{(t_0+T)})}{F(\mathbf{y}^{(t_0)})} = \mathrm{e}^{-\tilde{\nu}T}. \tag{5.78}$$

Taking the logarithm, and by applying (5.76), the expected running time T is computed as

$$T \simeq \frac{\beta \ln(2)}{4\mu c^2_{\mu/\mu,\lambda}} \frac{(1+\alpha^2)\Sigma q}{\alpha} \frac{1}{\breve{q}} \frac{1}{\gamma}. \tag{5.79}$$

Apparently, the expected number of isolation periods T is inversely proportional to the isolation length γ. For $\gamma = 1$ the formula specifies the expected running time of the $[1, 2(\mu/\mu_I, \lambda)^1]$-meta-ES derived in Sec. 5.2.5. That is, for sufficiently small γ the estimate in Eq. (5.79) generalizes the expected running time provided in Eq. (5.45). At this point it has to be noticed, that increasing the isolation time from γ to $\gamma + 1$ implies a rise by 2λ function evaluations within the inner ESs of the meta-ES algorithm. Conclusively, a rise in γ comes with a reduction of the expected number of isolation periods needed for the fitness improvement. However, the actual number of function evaluations performed during the process is not changed at all.

A verification of the approximation quality of the expected running time formula (5.79) is provided in Fig. 5.23. Therefore, the expected running time in terms of the number of isolation periods T of the $[1, 2(3/3_I, 10)^\gamma]$-meta-ES is plotted against the search space dimension N. Considering isolation periods of length $\gamma = 3$, and $\gamma = 5$ respectively, the running time of the meta-ES on the ellipsoid models $q_i = i$ and $q_i = i^2$. Using cumulation parameter $\alpha = 1.2$ the theoretical predictions for $\beta = 2$ are validated by comparison of real runs of Alg. 5.1. The experimental measurements are averaged over 100 independent ES runs. The standard deviation of the runs is depicted by the black error bars. In Fig. 5.23 a good agreement between theoretical and experimental results can be observed. Only in the range of rather small search space dimensions deviations of the experimental measurements from the theoretical predictions are noticeable. With growing search space dimension N the agreement of the curves and the data points improves.

5.4. Summary

This section considered the application of the dynamical systems approach to the analysis of mutation strength adaptation via meta-ES on the ellipsoid model. To this end, the evolution equations for the considered $[1, 2(\mu/\mu_I, \lambda)^1]$-meta-ES regarding isolation periods of length $\gamma = 1$ have been derived in a first step. The equations allow for the description of the strategy's evolutionary behavior and for the calculation of the normalized mutation strength evolution. For the normalized mutation strength dynamics on the ellipsoid model one can distinguish a transient and a "steady state" like phase. The latter is characterized by an oscillating behavior around the point of discontinuity σ_0. By identifying the point of discontinuity with the mean value dynamics of the normalized mutation strength one is able

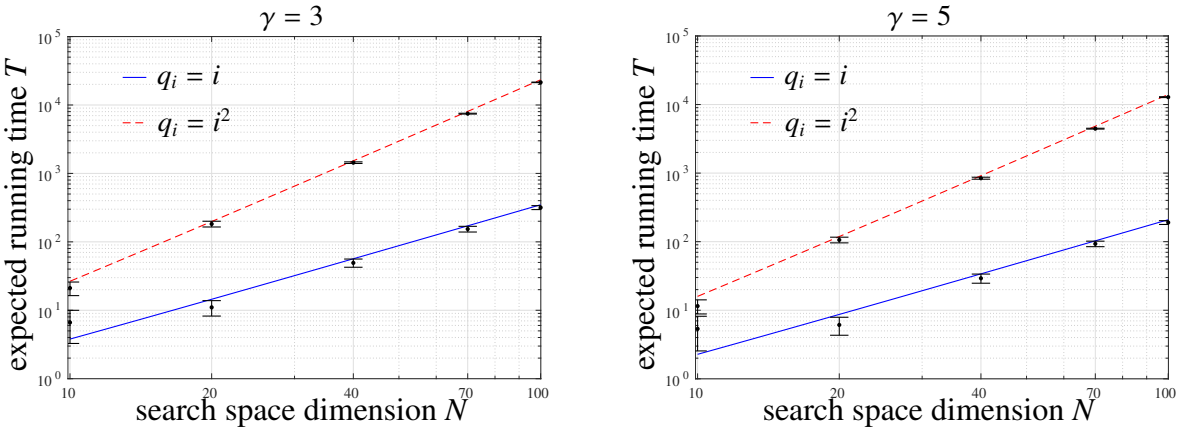

Figure 5.23.: The expected running time (5.79) of the meta-ES is plotted against the search space dimension from $N = 10$ to $N = 100$. The mutation strength control parameter $\alpha = 1.2$ is used within the $[1, 2(3/3, 10)^{\gamma}]$-meta-ES on the ellipsoid models $q_i = i$, and $q_i = i^2$. The experimentally obtained data are displayed by the error bar plots.

to describe the expected log-linear long term behavior of the meta-ES algorithm. Finally, an estimate concerning the expected running time of the meta-ES was presented.

Section 5.2 only considered the $\gamma = 1$ case. The analysis approach was extended to longer isolation periods $\gamma > 1$ in Sec. 5.3. Therefore, the progress within an isolation period of length γ is roughly modeled as the sum of γ progress steps. The modeling approach and its influence on the selection decision of the upper level ES were verified by use of one-generation experiments. In that situation one is able to provide evidence that larger γ values reduce the occurring ϵ_{Δ} fluctuations and thus slightly improve the detectability of the best inner ES (even for rather small α values). Furthermore, the evolution equations of the $1, 2(\mu/\mu_I, \lambda)^{\gamma}]$-meta-ES were approximated within a specified range of admissible isolation times γ. Following the analysis of the $\gamma = 1$ case, it was also possible to describe the normalized mutation strength (σ^*) dynamics in the meta-ES's steady state. Since the realization of σ^*_{ss} determines the long-term decline of Alg. 5.1, the convergence rate derivation was provided. Regarding the comparison to experimental algorithm runs, a good quality of the predictions for γ values between 1 and 10 were validated. The results allowed to compute the expected running time of $[1, 2(\mu/\mu_I, \lambda)^{\gamma}]$-meta-ES in terms of the required number of isolation periods. Considering the expected number of function evaluations needed for a specific fitness improvement, the analysis revealed independence of the choice of the isolation time γ. This is due to an increase of 2λ internal function evaluations per additional generation within a single isolation period.

Similar results of the running time were obtained for the $(\mu/\mu_I, \lambda)$-σSA-ES and for the $(\mu/\mu_I, \lambda)$-CSA-ES, cf. Chapters 3, and 4, respectively. However, depending on the choice of the specific strategy parameters, these strategies realize different normalized steady state mutation strengths σ^*_{ss}. The optimal normalized mutation strength on the ellipsoid model resides in the interval $[\mu c_{\mu/\mu,\lambda}, 2\mu c_{\mu/\mu,\lambda})$. The work of [Beyer and Melkozerov, 2014] showed that the σSA-ES performs sub-optimally on non-spherical ellipsoid models approaching σ^*_{ss}

in the vicinity of 1 when using standard parameter settings. As stated in Chapter 4, considering typical parameter choices mutation strength control by CSA yielded a normalized steady state mutation strength proportional to the number of parents, i.e., $\sigma^*_{ss} \propto \mu c_{\mu/\mu,\lambda}$. Using the standard choice of the control parameter $\alpha = 1.2$, the meta-ES also approached a normalized steady state mutation strength close to $\sigma^*_{ss} = \mu c_{\mu/\mu,\lambda}$. The $[1, 2(\mu/\mu_I, \lambda)^\gamma]$-meta-ES turned out to be more robust with respect to the choice of its control parameter α since it only has a minor influence on the overall performance.

Although it is unlikely in black-box optimization scenarios, given knowledge of the fitness landscape the performance of σSA-ES and CSA-ES can be improved by choosing appropriate strategy parameters. On the contrary, improvements of the meta-ES steady state performance caused by parameter tuning are unlikely. This is due to the limit cycle attractor σ^*_0 (5.17) that cannot be shifted towards a region of normalized mutation strength values which promise increased progress. That is, in expectation the meta-ES realizes a σ^*_{ss} similar to the CSA-ES (using standard strategy parameters). However, employing two inner ESs in each isolation period of the meta-ES requires twice the number of function evaluations to achieve about the same progress.

Notice, that the use of Eq. (5.45) is unsuitable for the sphere model. This is due to the derivation being based on the use of the linear approximation of the steady state mode eigenvalue (5.37) which is not applicable to the sphere model (see also Fig. 5.13). The analysis of the $[1, 2(\mu/\mu_I, \lambda)^\gamma]$-meta-ES on the sphere model was carried out in [Beyer et al., 2009] using a different approach. In contrast to the non-spherical ellipsoid model, the optimal normalized mutation strength on the sphere model is $\sigma^* = \mu c_{\mu/\mu,\lambda}$. On the sphere the meta-ES approaches a stable normalized mutation strength $\sigma^* > \mu c_{\mu/\mu,\lambda}$ considering sufficiently small parameters α. For larger α values σ^* fluctuates in limit cycles around the point of discontinuity σ^*_0 close to $\mu c_{\mu/\mu,\lambda}$. Hence, the meta-ES almost adapts the optimal σ on the sphere model provided that α is chosen appropriately. In this situation, a formula that allows for the prediction of the corresponding steady state progress was also provided.

Part II.

Evolution Strategies on the noisy ellipsoid model

6. The noisy ellipsoid model

6.1. Introduction to noisy optimization

In many real-world applications the problem complexity is increased by noise. The term *noise* summarizes the influences of various uncertainties occurring in the modeling of an optimization problem. It can stem from different sources such as randomized simulations, sensory disturbances, as well as unknown (or very complex) interactions which are modeled by stochastic components. Noise may impair the evaluation of the objective function or even the search space variables of the model. Either way, successive evaluations of the same input parameters result in different outcomes. The field of research addressing this type of problem is referred to as *noisy optimization*. Finding an optimal solution in the presence of noise is a great challenge for optimization strategies. Since their performance only relies on the observed fitness function value of a candidate solution direct optimization strategies provide promising concepts in this context. They exhibit less exposure to noise disturbance than classical deterministic methods which for example may fail due to corrupted gradient information.

Evolutionary Algorithms (EAs) proved to be successful for optimization in the presence of noise. Considering Evolution Strategies with regard to noisy optimization in particular, there already exist theoretical investigations on multiple test functions, e.g. [Arnold, 2002; Jin and Branke, 2005; Finck et al., 2011]. Explaining the working principles of ESs under noise influence, these analyses provide guidelines on the choice of specific strategy parameters. However, the performance of the ESs degrades under strong noise and can even prevent the EA from converging to the optimizer.

There exist different options to tackle the performance degradation of EAs that can be basically subdivided into three classes:

(a) reducing the noise observed by the EA by use of *resampling*, i.e. averaging over a number of κ objective function values,

(b) handling the noise by successively increasing the population size, or

(c) acting according to the concept "mutate large, but inherit small" proposed by Rechenberg [Rechenberg, 1994].

Notice, that only options (a) and (b) are taken into consideration in the following chapters.

Both methods, (a) and (b), implicate an increase of the required number n of fitness evaluations. In order to avoid an unnecessary excess of function evaluations, the question arises at which point to take the countermeasures (b) or (a), i.e. to increase the population size or to use the function value averaging. As far as option (a) is concerned, there is

a definite answer regarding the $(\mu/\mu_I, \lambda)$-Evolution Strategy (ES) on quadratic functions [Beyer et al., 2005; Beyer and Sendhoff, 2006]: It is better to increase the population size than to perform resampling. Accordingly, population size control is the noise handling method of choice within the next chapters.

No matter whether one uses option (a) or (b), both cases require techniques to detect the presence of noise. This can be easily done by resampling a candidate solution ($\kappa = 2$) because noise is reflected in changes of a candidate solution's measured fitness of two consecutive evaluations (for fixed $\boldsymbol{x}$). However, small noise strengths are usually well tolerated by the ES. That is, the ES can still approach the optimizer. In such cases, there is no need to handle this noise. Another approach introduced in the UH-CMA-ES [Hansen et al., 2009] considers the rank changes within the offspring individuals after resampling the population with $\kappa = 2$. If there are no or only a few rank changes, one can assume that the noise does not severely disturb the selection process. This approach is interesting but seems still to be too pessimistic, i.e., even if there is a lot of rank changes, there may be still progress towards the optimizer due to the genetic repair effect taking place by the intermediate recombination operator. In [Beyer and Sendhoff, 2006] a population size control rule was proposed which is based on the residual error. The dynamics of the $(\mu/\mu_I, \lambda)$-ES in a noisy environment with constant noise strength σ_ϵ will usually approach a steady state in a certain distance to the optimizer. At that point, fluctuations of the parental fitness values around their mean value can be observed. The population size is then increased if the fitness dynamics on average does not exhibit further progress.

This part of the thesis considers the ability of specific evolution strategies to deal with fitness noise disturbances by appropriately controlling their population size. Taking into account two different noise models, the underlying noisy optimization problem is introduced in this section: the noisy ellipsoid model. Furthermore, previously developed performance measures and theoretical results are recapped and generalized if possible. As promising studies on hierarchical ES on noisy environments already exist [Arnold and MacLeod, 2008], this part of the thesis aims at investigating the usability of a meta-ES which simultaneously controls its population size and its mutation strength. Representing the simplest ellipsoid model, the sphere model ($q_i = 1, \forall i = 1, \ldots, N$) is considered as a first step in Chap. 7. The dynamical behavior of a $[1, 4(\mu/\mu_I, \lambda)]$-meta-ES is analyzed and conclusions are drawn which motivate the design of the population control $(\mu/\mu_I, \lambda)$-CMSA-ES in the subsequent chapter. That ES variant successfully identifies noise related progress stagnations within the evolutionary process on the basis of a linear regression analysis of the observed fitness. This way it is able to adequately adapt a beneficial population size on the more general noisy ellipsoid model.

6.2. The noisy optimization problem

The way of modeling the noise is not immediately obvious. Noise models may vary by the sort of noise (additive or multiplicative), the applied noise distribution (Gaussian, Cauchy, etc.), and the working point of the noise (objective function or decision parameters). This work considers both, constant as well as distance proportional Gaussian distributed noise

which acts on the objective function. For gaining an insight into decision parameter noise it is referred to [Beyer and Sendhoff, 2006].

The noisy optimization problem considered is the so-called noisy ellipsoid model. The respective noisy fitness environment is modeled in the following way

$$\tilde{F}(\mathbf{y}) = F(\mathbf{y}) + \delta, \tag{6.1}$$

where $F(\mathbf{y}) \coloneqq \sum_{i=1}^{N} q_i y_i^2$ denotes the deterministic (ideal) objective function referred to as ellipsoid model (3.6), and the random variate δ describes the noise term. Further, $\tilde{F}(\mathbf{y})$ is denoted as the observed fitness of a candidate solution $\mathbf{y}$ on which the selection decision of the algorithm is based. That is, the corresponding candidate solutions' objective function evaluations are subject to noise perturbations. Thus the selection process may be biased by the noisy fitness values.

Within the thesis, two different types of fitness noise are considered: The first case concerns a noise term δ that does not scale with the objective function value

$$\delta \sim \sigma_\epsilon \mathcal{N}(0, 1), \tag{6.2}$$

i.e. a normally distributed noise term with mean zero and standard deviation $\sigma_\epsilon = const.$ is added to the original fitness of each offspring. Characteristic for the noise model of constant variance (6.2) is a monotonously increasing noise-to-signal ratio inversely proportional to the distance to the optimizer. It represents an additive noise model where the noise becomes more pronounced as the ES approaches the optimizer.

On the other hand, the noise term may depend on the current location in the search domain. One option to model this noise type is to distribute δ according to

$$\delta \sim \frac{2\sigma_\epsilon^* R_q^2(\mathbf{y})}{\Sigma q} \mathcal{N}(0, 1). \tag{6.3}$$

In this case, the standard deviation is $\sigma_\epsilon = 2\sigma_\epsilon^* R_q^2(\mathbf{y})/\Sigma q$, requiring $\sigma_\epsilon^* = const.$, and thus proportional to a candidate's squared distance from the optimizer. Conclusively, the noise model is also referred to as distance proportional noise.

In the case of the sphere model (3.7) ($q_i = 1,\ \forall i$), the term $R_q^2(\mathbf{y}^{(g)})$ already represents the fitness $F(\boldsymbol{y}^{(g)})$ of a candidate solution. Accordingly, the noise model (6.3) is also denoted fitness proportional noise model in that situation. It preserves a constant noise-to-signal ratio on the sphere model.

The standard deviation of the noise term σ_ϵ is referred to as the noise strength. Both noise models exclude correlations between successive evaluations of $\tilde{F}(\boldsymbol{x})$. Negative objective function values can be observed depending on the choice of σ_ϵ and the current location within the search domain. In Sec. 6.4 the differences of the noise models and important theoretical results are recapped.

6.3. Performance measures under noise

Alike the way the ES performance is measured on the ellipsoid model in part one of this thesis, the quadratic progress rate can also be derived for the noisy case. Using existing

results from [Melkozerov and Beyer, 2015] and [Arnold and Beyer, 2001] allows to draw conclusions on the strategy's dynamical behavior on the ellipsoid model. Another approach to measure the performance is characterizing the expected descent of an ES by the number of function evaluations needed. This way, theoretically grounded runtime bounds can be derived under additional assumptions. These approaches which successfully quantify the expected performance of evolution strategies on the noisy ellipsoid model are briefly introduced in the following sections.

6.3.1. The noisy quadratic progress rate

The progress rate provides the expected change in the search space of the optimization problem with respect to the distance change of the parental centroids of two consecutive generations to the optimizer. The derivation steps for the noisy quadratic progress rate formula are analogous to the noise-free case but taking into account the observed noisy fitness evaluations. The resulting formula for the quadratic progress rate (3.18) of the $(\mu/\mu_I, \lambda)$-ES along the ith axis of the noisy ellipsoid model has been derived in [Melkozerov and Beyer, 2015]. In the asymptotic limit ($N \to \infty$) it reads

$$\varphi_i^{II}(\sigma^{(g)}, \mathbf{y}^{(g)}) \simeq \frac{2\sigma^{(g)} c_{\mu/\mu,\lambda} q_i y_i^{(g)^2}}{\sqrt{(1+\varkappa^2) R_q^2(\mathbf{y}^{(g)})}} - \frac{\sigma^{(g)^2}}{\mu}. \tag{6.4}$$

Here, the term $\varkappa$ denotes the noise-to-signal ratio which is defined as

$$\varkappa^2 = \frac{\sigma_\epsilon^2}{4\sigma^2 R_q^2(\mathbf{y})}. \tag{6.5}$$

Alike the noise-free case (3.24), the derivation of Eq. (6.4) assumes the exclusion of ellipsoid models with dominating coefficients q_i.

Since in the general case the noise strength σ_ϵ may depend on the parameter vector $\mathbf{y}$ of an individual, it is normalized to obtain a formula which is invariant to the search space location. The normalization on the ellipsoid model [Melkozerov and Beyer, 2015] reads

$$\sigma_\epsilon^* = \frac{\sigma_\epsilon \Sigma q}{2R_q^2(\mathbf{y})}. \tag{6.6}$$

For $q_i = 1,\ \forall i = 1, \ldots, N$ this representation includes the noise strength normalization on the sphere model $\sigma_\epsilon^* := \frac{1}{2}\sigma_\epsilon N R^{-2}$, cf. [Arnold and Beyer, 2001], where $R := \|\mathbf{y}\|$ is the individual's euclidean distance to the optimizer.

Together with the mutation strength normalization (3.14), Eq. (6.6) allows for the derivation of a normalized version of the noisy component-wise quadratic progress rate

$$\varphi_i^{II*}(\sigma^{*(g)}) \simeq \frac{2\sigma^{*(g)} c_{\mu/\mu,\lambda} q_i y_i^{(g)^2}}{\sqrt{(1+\varkappa^2)}} - \frac{\sigma^{*(g)^2}}{\mu \Sigma q} R_q^2(\mathbf{y}). \tag{6.7}$$

Both representations (6.4), and (6.7) indicate the negative influence of a large noise-to-signal ratio $\varkappa$ on the progress of the evolution strategy. Considering, $\varkappa = 0$ the noisy quadratic progress rate formula yields the corresponding noise-free equations, Eqs. (3.23) and (3.24), used in Sec. 3.2. The accuracy of (6.7) is validated in [Melkozerov and Beyer, 2015] by one-generation experiments. In Sec. 6.4, Eq. (6.7) is used to predict the long-term behavior of $(\mu/\mu_I, \lambda)$-ES on the noisy ellipsoid model.

As already presented in [Beyer and Melkozerov, 2014] for the noise-free ellipsoid model, the noisy component-wise quadratic progress rate φ_i^{II} recovers the progress rate for the sphere model $\varphi_{sp}(R^{(g)}) = \mathrm{E}[R^{(g)} - R^{(g+1)}|R^{(g)}]$. The respective sphere model formula is obtained by application of the relation

$$\varphi_{sp}(R^{(g)}) \simeq \frac{\sum_{i=1}^{N} q_i \varphi_i^{II}(\sigma^{(g)}, \mathbf{y}^{(g)})}{R_q(\mathbf{y}^{(g)})}, \tag{6.8}$$

and consideration of $q_i = 1,\ \forall i = 1; \ldots, N$ as

$$\varphi_{sp}(R^{(g)}) \simeq \frac{c_{\mu/\mu,\lambda}\sigma^{(g)}}{\sqrt{1+\varkappa^2}} - \frac{N(\sigma^{(g)})^2}{\mu R^{(g)}}. \tag{6.9}$$

Notice, that $R^{(g)}$ in this formulation simply denotes the Euclidean distance of the objective parameter vector $\mathbf{y}$ to the optimizer of the sphere model. The precise mathematical derivation of φ_{sp} is provided in [Arnold and Beyer, 2001; Arnold, 2002]. Equation (6.9) will provide the basis of the theoretical investigation in the next chapter. There, the dynamics of a specific meta-ES will be analyzed on the fitness environment defined by the noisy sphere function.

6.3.2. Simple Regret

Another approach to evaluate the performance of an EA is considering the so-called Simple Regret. Instead of being a distance measure in the search space of the noisy optimization problem, it represents a progress measure in terms of the expected objective function improvement. The Simple Regret usually measures the algorithm's performance by the amount of objective function evaluations n needed to reach a certain expected fitness compared to the non-noisy objective function value at the optimizer. In the case of minimization of the noisy function $\tilde{F}(\boldsymbol{y}), \boldsymbol{y} \in \mathbb{R}^N$, the Simple Regret $\mathrm{SR}(n)$ is defined as

$$\mathrm{SR}(n) := \mathrm{E}[\tilde{F}(\boldsymbol{y}_n)] - F(\hat{\boldsymbol{y}}). \tag{6.10}$$

In this context, $\boldsymbol{y}_n$ is the object vector recommended by the strategy after n function evaluations, e.g. the parental centroid in the context of a $(\mu/\mu_I, \lambda)$-ES. With regard to the model of additive noise of constant variance, Eqs. (6.1) and (6.2), the expected noisy fitness value after n function evaluations is equal to the respective noise-free fitness value, i.e. $\mathrm{E}[\tilde{F}(\boldsymbol{y}_n)] = F(\boldsymbol{y}_n)$, and the Simple Regret directly becomes

$$\mathrm{SR}(n) := F(\boldsymbol{y}_n) - F(\hat{\boldsymbol{y}}). \tag{6.11}$$

One is interested in the relation of the Simple Regret and the number of function evaluations. Considering a log-log representation of the respective quantities, the convergence rate of the considered algorithms can be identified with the slope a of the log-log graph of the Simple regret dynamics plotted against the respective number of function evaluations

$$\limsup_{n\to\infty} \frac{\log \mathrm{SR}(n)}{\log n} = -a. \tag{6.12}$$

Considering a positive noise-to-signal ratio $\varkappa > 0$ in the location of the optimizer $\hat{\boldsymbol{y}}$, the respective slope in Eq. (6.12) is negative, i.e. $-a < 0$. In the case of fitness-proportional noise with $\tilde{F}(\hat{\boldsymbol{y}})$ it is possible to obtain a linear convergence order.

The performance measure has been used for the derivation of a theoretical running time result considering "Simple ES" in the context of additive noise. The term "Simple ES" refers to general Evolution Strategies which adapt the mutation strength in such a way that it scales with the distance to the optimizer. Examples that represent "Simple ES" according to this definition [Astete-Morales et al., 2015] are the $(\mu/\mu_I, \lambda)$-CSA-ES in Alg. 4.1 or the CMA-ES [Hansen, 2006b].

In this context, an important theoretical result is provided in the work of Astete-Morales, Cauwet and Teytaud [Astete-Morales et al., 2015]. Their theorem proves that "Simple ES" can only reach a slope $a > -\frac{1}{2}$ on quadratic objective functions that are subject to additive noise (6.2). Even the application of resampling or population upgrading for mitigation of the noise influence does not enhance the performance. The theorem is supported with experiments regarding particular Evolution Strategies designed for the treatment of fitness noise. Accordingly, "Simple ES" cannot reach the theoretical lower performance bound of $a = -1$ of all comparison-based direct search algorithms [Shamir, 2013]. The result is going to be relevant considering the empirically measured performance of a newly designed ES variant that is presented in Chapter 8 of this thesis. That strategy reaches a performance below the $a > -\frac{1}{2}$ "Simple-ES" bound.

6.4. Noise models

Focusing on the mentioned noise models, corresponding theoretical findings are summed up in this section. With regard to fitness noise of constant variance a generalization of sphere model results to the noisy ellipsoid model is presented. For both noise models the theoretical investigations imply that a rise of the population size is able to improve the Evolution Strategy's progress towards the optimizer on the noisy ellipsoid model. However, the rational point in the optimization process at which the population size should be increased still has to be determined. That problem will be addressed within the next chapters.

6.4.1. Fitness noise of constant variance

Regarding the additive noise model (6.2) the noise strength σ_ϵ is independent of the current location in the search domain. In this situation Evolution Strategies exhibit a common behavior: while the noise influence is neglectable in great distance from the optimizer it

gets more pronounced as the strategy approaches the optimizer. The ES exhibits some kind of steady state behavior as it fluctuates in the vicinity of the optimizer. On average this steady state resides in a certain residual distance from the optimal solution. The reason for this stagnation is that the selection of offspring is dominated by the noise term. As a result, the ES basically performs a random walk in this limit state. The expected residual steady state distance on the noisy sphere function was derived in [Arnold, 2002; Arnold and Beyer, 2001]. Its formulation for sufficiently small mutation strength values reads

$$R_{ss} \simeq \sqrt{\frac{N\sigma_\epsilon}{4\mu c_{\mu/\mu,\lambda}}}. \tag{6.13}$$

The residual distance formula (6.13) can be extended to non-spherical ellipsoid models. The steady state distance R_q^{ss} on the noisy ellipsoid model is determined by making use of the noisy quadratic progress rate (6.4). At this point, it has to be kept in mind that using the noisy asymptotical quadratic progress rate (6.4), analogously to the noise-free case, excludes ellipsoid models with dominant coefficients $q_j \gg q_i, \forall i \neq j$. Requiring that the further progress is zero in expectation after the ES has reached its noisy residual steady state distance R_q^{ss}, and making use of Eq. (6.4) one obtains the condition

$$\frac{\sigma}{2\mu c_{\mu/\mu,\lambda}} = \frac{q_i y_i^2}{R_q(\mathbf{y})\sqrt{(1+\varkappa^2)}}. \tag{6.14}$$

Inserting the noise-to-signal definition (6.5), multiplication of both sides by q_i, and summation over all i yields

$$\frac{\Sigma q}{2\mu c_{\mu/\mu,\lambda}} = \frac{2R_q^2(\mathbf{y})}{\sqrt{4\sigma^2 R_q^2(\mathbf{y}) + \sigma_\epsilon^2}} = \frac{R_q(\mathbf{y})}{\sqrt{4\sigma^2 + \frac{\sigma_\epsilon^2}{R_q^2(\mathbf{y})}}}. \tag{6.15}$$

Accordingly, by neglecting the term $4\sigma^2$ in the denominator of (6.15) the residual quantity R_q^{ss} can be derived in the limit of small mutation strengths

$$R_q^{ss} \simeq \sqrt{\frac{\sigma_\epsilon \Sigma q}{4\mu c_{\mu/\mu,\lambda}}}. \tag{6.16}$$

The presence of additive fitness noise of constant variance causes the Evolution Strategy to approach its residual steady state distance R_q^{ss} instead of converging towards the optimizer. Equation (6.16) provides a generalization of the sphere model result in Eq. (6.13). It indicates that increasing the population size is suitable to reduce the residual distance from the optimizer (given that the truncation ratio $\vartheta = \mu/\lambda$ is held constant).

Regarding additive fitness noise, the mutation strength dynamics of self-adaptive Evolution Strategies also approach a stationary state σ_{ss}. It can be derived from the asymptotic noisy self-adaptation response function that is also introduced in [Melkozerov and Beyer, 2015]

$$\psi(\sigma) \simeq \tau^2 \left(\frac{1}{2} + e_{\mu,\lambda}^{1,1} \frac{1}{1+\varkappa^2} - c_{\mu/\mu,\lambda} \frac{\sigma \Sigma q}{R_q(\mathbf{y})} \frac{1}{\sqrt{1+\varkappa^2}} \right). \tag{6.17}$$

In the stationary state the expected mutation strength change is zero, i.e. by virtue of (2.19) $\psi(\sigma_{ss}) = 0$ does hold. According to (6.17), this requires

$$0 \simeq \frac{1}{2} + e^{1,1}_{\mu,\lambda}\frac{1}{1+\varkappa^2} - c_{\mu/\mu,\lambda}\frac{\sigma_{ss}\Sigma q}{R_q(\mathbf{y})}\frac{1}{\sqrt{1+\varkappa^2}}. \tag{6.18}$$

Rearranging terms and considering the noise-to signal ratio (6.5) one obtains

$$0 \simeq \frac{1}{2} + e^{1,1}_{\mu,\lambda}\frac{1}{1+\varkappa^2} - \frac{2\sigma^2_{ss}c_{\mu/\mu,\lambda}\Sigma q}{\sigma_\epsilon}\frac{1}{\sqrt{1+\frac{1}{\varkappa^2}}}. \tag{6.19}$$

Assuming the noise-to-signal ratio $\varkappa^2 \to \infty$ and resolving Eq. (6.19) for σ_{ss} yields

$$\sigma_{ss} \simeq \sqrt{\frac{\sigma_\epsilon}{4c_{\mu/\mu,\lambda}\Sigma q}}. \tag{6.20}$$

The assumption $\varkappa \to \infty$ is justified, considering that the noise-to-signal ratio increases while the strategy approaches the optimizer.

Notice, that Eq. (6.20) only predicts the steady state mutation strength of self-adaptation ES that do not adapt the covariance matrix of the offspring distribution, since mutation strength and covariance matrix adaptation usually intertwine. An analysis of the covariance matrix adaptation that casts light on this interdependency is still missing.

6.4.2. Fitness noise of constant normalized variance

The second noise model applies noise of constant normalized variance. This noise model is also referred to as distance proportional noise, or fitness proportional noise in the case of the sphere model, respectively. By definition (6.3) the normalized noise strength

$$\sigma^*_\epsilon = \sigma_\epsilon\frac{\Sigma q}{2R_q(\mathbf{y})^2} = const., \tag{6.21}$$

is constant on the ellipsoid model. Accordingly, the noise strength σ_ϵ is proportional to the squared distance from the optimizer, i.e. one has

$$R_q(\mathbf{y})^2 \to 0 \quad \Rightarrow \quad \sigma_\epsilon \to 0. \tag{6.22}$$

Hence, considering this noise model the optimizer is supposed to be noise-free. According to the definition of the normalized noise strength σ^*_ϵ in Eq. (6.6) σ_ϵ increases quadratically with the distance from the optimizer. Distant candidate solutions are subject to huge noise perturbations which can lead the strategy to diverge from the optimizer. Notice, that the normalization in (6.21) relies on the distance of the parental centroid $\langle\mathbf{y}\rangle$ instead of being based on the currently evaluated offspring individual. Being asymptotically exact, this is a common simplification that aims at a mathematically more amenable approach. It is admissible, as the individual noise strengths equal the parental one in the asymptotical limit of $N \to \infty$, cf. [Finck, 2011].

According to the asymptotical normalized progress rate formula on the noisy ellipsoid model (6.7), positive progress in direction of the optimizer is directly related to the evolution condition

$$\sigma^{*2} + \sigma_\epsilon^{*2} < 4\mu^2 c_{\mu/\mu,\lambda}^2. \tag{6.23}$$

The term σ^* refers to the normalized mutation strength on the ellipsoid model as specified in Eq. (3.14). It is derived by requiring the component-wise quadratic progress to be positive in expectation ($\varphi_i^{II} > 0$). The condition follows by multiplication with q_i, summation over all components, and by solving the resulting inequality for σ^{*2}.

Equation (6.23) states that given upper values of the normalized normalized noise and mutation strengths there is a parental population size μ (μ/λ = const.) above which the ES converges to the optimizer. Regarding the limit of small normalized mutation strength σ^* condition (6.23) becomes

$$\mu > \frac{\sigma_\epsilon^*}{2c_{\mu/\mu,\lambda}}. \tag{6.24}$$

From Eq. (6.24) it can be deduced that, in the context of distance proportional noise, a positive progress of the Evolution Strategy in expectation is also connected to the population size. The condition states that sufficiently enlarging the population size results in the realization of positive progress and thus convergence to the noise-free optimizer.

7. Meta-ES analysis on the noisy sphere model

In this section, the focus is on the analysis of the usability of a specific meta-ES which simultaneously adapts the population size and the mutation strength. To this end, the meta-ES algorithm, Alg. 5.1, considered in the context of the noise-free ellipsoid model is extended by adding the ability to adapt the population size appropriately. Regarding the noisy sphere model ($q_i = 1, \forall i$) with additive fitness noise of constant variance (6.2), the ability of the specific meta-ES to deal with the noisy optimization problem is studied. By carrying out the theoretical analysis of the evolution behavior, a more thorough understanding of the interactions between the different dynamics is gained.

According to Chapter 6, the fitness environment of the N-dimensional sphere model under the influence of additive fitness noise with constant noise strength σ_ϵ is defined as

$$\tilde{F}(\mathbf{y}) = \sum_{j=1}^{N} y_j^2 + \sigma_\epsilon \mathcal{N}(0,1). \tag{7.1}$$

The fitness noise affects the selection mechanism of the meta-ES algorithm. That is, the measured fitness $\tilde{F}(\mathbf{y})$ of a candidate solution $\mathbf{y}$ will not longer comply with the ideal fitness $F(\mathbf{y})$. This may lead to the selection of inferior solutions based on their observed fitness while superior solutions may be eliminated.

Considering constant fitness noise throughout the search space, it is not possible to determine the exact location of the optimizer with an ES on the spherical fitness environment, see [Arnold, 2002]. After a number of generations, the distance to the optimizer will fluctuate around a nonzero mean which increases with increasing noise strength. This residual distance can be decreased by increasing the population size of the ES. Particularly, the focus of the analysis is on the control of the mutation strength σ as well as on the accurate adaptation of a beneficial parental population size μ. It is demonstrated by use of the idealized mean value dynamics (6.9), that the meta-ES variant increases the population size up to a predefined maximal value. This maximal value is introduced to prevent the perpetual rise of the population size. Subsequently, maintaining the maximal population size the strategy gradually reduces the mutation strength. As a consequence, the residual distance finally approached by the meta-ES variant is determined by the maximal population size, cf. Eq. (6.13).

The analysis within this chapter is divided into the following steps: the first step addresses the derivation of a formula that provides the expected progress over isolation periods of multiple generations. Afterwards, asymptotical analyses of the population size dynamics and the mutation strength dynamics are provided independently. This is followed by the

calculation of a description of the asymptotical normalized mutation strength growth. Apart from fluctuations, the predicted behavior is verified by comparison to real meta-ES runs. Finally, the nature of these fluctuations is under investigation and possible ways to mitigate the fluctuation influence are discussed.

7.1. The $[1, 4(\mu/\mu_I, \lambda)^\gamma]$-meta-ES

Before the theoretical analysis is performed, the $[1, 4(\mu/\mu_I, \lambda)^\gamma]$-meta-ES algorithm under consideration is introduced. Using a deterministic adaptation rule the outer ES controls the population sizes μ, and λ, as well as the mutation strength σ. This way it is expected to be able to deal with the noisy fitness environment (7.1).

The upper level strategy is presented in Alg. 7.1. In line 2 the parameter d is defined as the product of the initial isolation length γ and the initial population size μ_p. The parameter d is used as an upper bound for the strategy parameters γ and μ_p. It is kept constant to prevent the algorithm from permanently increasing the number of function evaluations employed within a single isolation period. The algorithm is running four competing inner $[(\mu/\mu_I, \lambda)^\gamma]$-ESs which start at the same initial search space location $\mathbf{y_p}$ (parental $\mathbf{y}$) but differ in the choice of the population size and the mutation strength. Two offspring mutation strength parameters $\tilde{\sigma}_1$ and $\tilde{\sigma}_2$ are generated in line 5 and 6, increasing and decreasing the parental mutation strength σ_p by the factor $\alpha > 1$. From line 7 up to line 9 the new population size parameters are created. At first two parameters $\tilde{\mu}_1$ and $\tilde{\mu}_2$ are computed by increasing/decreasing the parental μ_p by a factor β. If μ_p has already reached its lower bound, i.e. $\mu_p = 1$, or its upper bound d, μ_p is only modified in one direction. That is, it is increased or decreased, respectively, and kept constant for the other parameter. Dividing the new parental population sizes $\tilde{\mu}_j$ by the fixed truncation ratio ϑ leads to the corresponding offspring population size parameters $\tilde{\lambda}_1$ and $\tilde{\lambda}_2$. The isolation length parameters $\tilde{\gamma}_1$ and $\tilde{\gamma}_2$ are defined depending on $\tilde{\mu}_1$ and $\tilde{\mu}_2$ in line 10, always complying with the condition

$$d = \gamma\mu \quad \Leftrightarrow \quad d/\vartheta = \lambda\gamma. \tag{7.2}$$

Notice, in order to always obtain integer values for μ, λ, and γ, the initial μ_p, γ_p and β, $1/\vartheta$ are chosen as powers of two.

Identifying $\lambda\gamma$ with the number of function evaluations during a single inner ES run, the way of controlling γ in (7.2) keeps the number of function evaluations over all the observed isolation periods equal. Each combination of the two different population sizes $(\tilde{\mu}_j, \tilde{\lambda}_j)$ with corresponding isolation length $\tilde{\gamma}_j$ and the two mutation strength parameters $\tilde{\sigma}_j$ (j=1, 2) serves as strategy parameter set and is held constant within the inner ES. After having evolved over their associated isolation length, each inner ES returns the centroid of its final parental population $\mathbf{y_k}$ and its corresponding fitness value $F_k = F(\mathbf{y_k})$, $k = 1, \ldots, 4$. Finally the selection in the $[1, 4]$-meta-ES is performed in lines 15 to 17 using the standard notation "$m; \lambda'$" indicating the mth best population out of λ' populations with respect to the fitness value generated by the respective inner $(\mu/\mu, \lambda)$-ES. That is, the strategy parameters of the best inner population are used as parental parameters in the outer ES. The algorithm terminates after having met the specified termination criterion.

Algorithm 7.1 Pseudo code of the $[1, 4(\mu/\mu_I, \lambda)^{\gamma}]$-meta-ES. The Code of the inner ES is presented in Fig. 3.1.

Initialize $\left(\sigma_p, \mathbf{y_p}, \mu_p, \vartheta, \gamma\right)$;
$d \leftarrow \gamma\mu_p$
$t \leftarrow 0$;
repeat
  $\tilde{\sigma}_1 \leftarrow \sigma_p\alpha$;
  $\tilde{\sigma}_2 \leftarrow \sigma_p/\alpha$;
  $\tilde{\mu}_1 \leftarrow \min(\mu_p \cdot \beta, d)$;
  $\tilde{\mu}_2 \leftarrow \max(\mu_p/\beta, 1)$;
  $\tilde{\lambda}_1 \leftarrow \tilde{\mu}_1/\vartheta$;
  $\tilde{\lambda}_2 \leftarrow \tilde{\mu}_2/\vartheta$;
  $\tilde{\gamma}_1 \leftarrow d/\tilde{\mu}_1$;
  $\tilde{\gamma}_2 \leftarrow d/\tilde{\mu}_2$;
  $[\tilde{\mathbf{y}}_\mathbf{1}, \tilde{F}_1, \sigma_1, \mu_1] \leftarrow \mathrm{ES}(\tilde{\mu}_1, \tilde{\lambda}_1, \tilde{\gamma}_1, \tilde{\sigma}_1, \mathbf{y_p})$;
  $[\tilde{\mathbf{y}}_\mathbf{2}, \tilde{F}_2, \sigma_2, \mu_2] \leftarrow \mathrm{ES}(\tilde{\mu}_2, \tilde{\lambda}_2, \tilde{\gamma}_2, \tilde{\sigma}_1, \mathbf{y_p})$;
  $[\tilde{\mathbf{y}}_\mathbf{3}, \tilde{F}_3, \sigma_3, \mu_3] \leftarrow \mathrm{ES}(\tilde{\mu}_1, \tilde{\lambda}_1, \tilde{\gamma}_1, \tilde{\sigma}_2, \mathbf{y_p})$;
  $[\tilde{\mathbf{y}}_\mathbf{4}, \tilde{F}_4, \sigma_4, \mu_4] \leftarrow \mathrm{ES}(\tilde{\mu}_2, \tilde{\lambda}_2, \tilde{\gamma}_2, \tilde{\sigma}_2, \mathbf{y_p})$;
  $\sigma_p \leftarrow \sigma_{1;4}$;
  $\mu_p \leftarrow \mu_{1;4}$;
  $\mathbf{y_p} \leftarrow \mathbf{y_{1;4}}$;
  $t \leftarrow t + 1$;
until Termination Condition

The corresponding inner ES, see Alg. 3.1, generates a population of $\lambda = \mu/\vartheta$ offspring by adding σ mutation strength scaled vectors of independent, standard normally distributed components to the centroid $\mathbf{y}$ of the parental generation. The μ best candidates in terms of their fitness values are chosen out of these λ offspring and used to build the new parental centroid $\mathbf{y}$. Proceeding this way over γ generations, the tuple $[\mathbf{y}, F(\mathbf{y}), \sigma, \mu]$ is returned by the inner ES. The next section addresses the description of the inner ES dynamics when operating over multiple generations with fixed strategy parameters on the noisy sphere model.

7.2. Theoretical analysis of the inner strategy

This section studies the inner $(\mu/\mu, \lambda)$-ES dynamics evolving with fixed strategy parameter over γ generations. Assuming that the observed fitness is disturbed by additive noise the derivation of a prediction of the expected distance $R^{(g+\gamma)}$ from the optimizer at the end of a single isolation period of γ generations is of interest. The starting point of the theoretical analysis is the noisy asymptotic progress rate (6.9) of the sphere model. Taking into account the progress rate definition

$$\varphi^{(g)} = \mathrm{E}[R^{(g)} - R^{(g+1)}|R^{(g)}], \tag{7.3}$$

together with Eq. (6.9) yields the difference equation of the expected change in the distance to the optimizer between two consecutive generations

$$R^{(g)} - R^{(g+1)} = \frac{2c_{\mu/\mu,\lambda}R^{(g)}{\sigma^{(g)}}^2}{\sqrt{4(R^{(g)})^2{\sigma^{(g)}}^2 + {\sigma_\epsilon}^2}} - \frac{N{\sigma^{(g)}}^2}{2\mu R^{(g)}}. \tag{7.4}$$

Notice, this representation is obtained by insertion of the noise-to-signal ratio from Eq. (6.5).

On the basis of (7.4), the expected steady state distance $\tilde{R}_{ss}(\sigma, \sigma_\epsilon)$ can be computed. It predicts the residual distance to the optimizer which is reached by the inner ES if it runs for a sufficiently long number of generations given a fixed mutation strength σ and constant population sizes μ and λ. Solving the equation $0 = \varphi(\sigma, \sigma_\epsilon, \tilde{R}_{ss})$ for $\tilde{R}_{ss}$ results in

$$\begin{aligned}
\tilde{R}_{ss}(\sigma, \sigma_\epsilon) &= \sqrt{\frac{N^2\sigma^2 + \sqrt{4\mu^2 c^2_{\mu/\mu,\lambda}N^2\sigma_\epsilon^2 + N^4\sigma^4}}{8\mu^2 c^2_{\mu/\mu,\lambda}}} \\
\tilde{R}_{ss}(\sigma, \sigma_\epsilon) &= \hat{R}_{ss}(\sigma)\sqrt{\frac{1}{2}\left(1 + \sqrt{1 + \frac{\tilde{\varkappa}^2}{\hat{R}_{ss}\sigma^2}}\right)}
\end{aligned} \tag{7.5}$$

with noise-to-signal ratio $\tilde{\varkappa} = \sigma_\epsilon/\sigma$ and the noise-free steady state distance of the inner ES on the sphere model ($q_i = 1,\ \forall i$), see (3.28),

$$\hat{R}_{ss}(\sigma) = \frac{N\sigma}{2\mu c_{\mu/\mu,\lambda}}. \tag{7.6}$$

Considering small mutation strength sizes, i.e. $\sigma \to 0$, Eq. (7.5) is becoming

$$R_{ss} = \sqrt{\frac{N\sigma_\epsilon}{4\mu c_{\mu/\mu,\lambda}}} \tag{7.7}$$

which is already known as a good approximation of the expected steady state distance $\tilde{R}_{ss}$ in the vicinity of small mutation strengths, cf. Eq. (6.13).

Finding a closed analytical solution of the nonlinear difference equation (7.4) for $R^{(g+1)}$ is not possible. Hence, one is interested in a good approximation. The approximation of (7.4) is performed by derivation of a linear expression describing the dynamics towards the residual steady state distance $\tilde{R}_{ss}$. Therefore, by interpreting the right-hand side of (7.4)

$$\hat{\varphi}(R^{(g)}) = \frac{2c_{\mu/\mu,\lambda}R^{(g)}{\sigma^{(g)}}^2}{\sqrt{4(R^{(g)})^2{\sigma^{(g)}}^2 + {\sigma_\epsilon}^2}} - \frac{N{\sigma^{(g)}}^2}{2\mu R^{(g)}} \tag{7.8}$$

as a function of the distance from the optimizer $R^{(g)}$, it can be expanded into a Taylor series around $\tilde{R}_{ss}$. Because $\tilde{R}_{ss}$ represents the root of the progress rate, the constant term of the

Taylor expansion is zero. Omitting higher order terms of the Taylor expansion, Eq. (7.8) approximated by the linear expression

$$\hat{\varphi}(R^{(g)}) \simeq \left(\frac{8c_{\mu/\mu,\lambda}\tilde{R}_{ss}^2\sigma^4}{\sqrt{(\sigma_\epsilon^2 + 4\tilde{R}_{ss}^2\sigma^2)^3}} - \frac{2c_{\mu/\mu,\lambda}\sigma^2}{\sqrt{\sigma_\epsilon^2 + 4\tilde{R}_{ss}^2\sigma^2}} - \frac{N\sigma^2}{2\tilde{R}_{ss}^2\mu} \right)(R^{(g)} - \tilde{R}_{ss}) \tag{7.9}$$

Reduction of (7.9) to common denominators simplifies the expression

$$\hat{\varphi}(R^{(g)}) \simeq \left(\frac{N\sigma^2}{2\tilde{R}_{ss}^2\mu} + \frac{2c_{\mu/\mu,\lambda}\sigma^2\sigma_\epsilon^2}{(\sigma_\epsilon^2 + 4\tilde{R}_{ss}^2\sigma^2)^{\frac{3}{2}}} \right)(R^{(g)} - \tilde{R}_{ss}) \tag{7.10}$$

Substituting the right-hand side of Eq. (7.4) with the final result of Eq. (7.10) yields

$$R^{(g)} - R^{(g+1)} \simeq \left(\frac{N\sigma^2}{2\tilde{R}_{ss}^2\mu} + \frac{2c_{\mu/\mu,\lambda}\sigma^2\sigma_\epsilon^2}{(\sigma_\epsilon^2 + 4\tilde{R}_{ss}^2\sigma^2)^{\frac{3}{2}}} \right)(R^{(g)} - \tilde{R}_{ss}) \tag{7.11}$$

as a linear approximation of the difference equation (7.4). For reasons of clarity and comprehensibility the following abbreviations are introduced

$$a := \frac{N\sigma^2}{2\tilde{R}_{ss}^2\mu} \quad \text{and} \quad b := \frac{2c_{\mu/\mu,\lambda}\sigma^2\sigma_\epsilon^2}{(\sigma_\epsilon^2 + 4\tilde{R}_{ss}^2\sigma^2)^{\frac{3}{2}}}. \tag{7.12}$$

Hence, Eq. (7.11) becomes

$$R^{(g+1)} \simeq \left(R^{(g)} - \tilde{R}_{ss}\right)(1 - (a+b)) + \tilde{R}_{ss}. \tag{7.13}$$

Computing the distance $R^{(g+2)}$ after two consecutive generations

$$R^{(g+2)} \simeq \left(R^{(g+1)} - \tilde{R}_{ss}\right)(1 - (a+b)) + \tilde{R}_{ss} \quad \simeq \left(R^{(g)} - \tilde{R}_{ss}\right)(1 - (a+b))^2 + \tilde{R}_{ss} \tag{7.14}$$

and continuing this way yields the following equation for the expected distance $R^{(g+\gamma)}$ after one isolation period of γ generations

$$R^{(g+\gamma)} \simeq \left(R^{(g)} - \tilde{R}_{ss}\right)(1 - (a+b))^\gamma + \tilde{R}_{ss}. \tag{7.15}$$

At this point, the assumption that the sum $a + b$ is sufficiently small allows to apply the approximation

$$(1-x)^k \approx 1 - kx \quad \forall x \text{ with } |x| \ll 1. \tag{7.16}$$

The assumption $a + b \approx 0$ is valid considering sufficiently small mutation sizes σ, see also (7.12) for $\sigma \to 0$. Using (7.16) one obtains an even simpler approximation for the distance to the optimizer after a single inner ES isolation period

$$R^{(g+\gamma)} \simeq R^{(g)}(1 - (a+b)\gamma) + \tilde{R}_{ss}(a+b)\gamma. \tag{7.17}$$

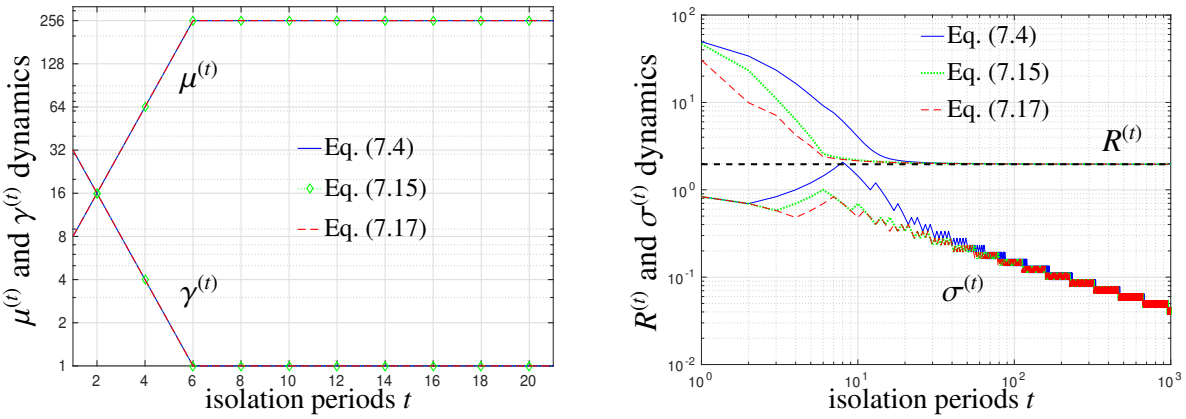

Figure 7.1.: Illustration of the iteratively computed meta-ES dynamics resulting from Eq. (7.4) and from its approximations in Eq. (7.15) and Eq. (7.17), respectively.

In order to confirm the good compliance between the original meta-ES dynamics resulting from Eq. (7.4) and their approximations, see Eq. (7.15) and Eq. (7.17), the iteratively generated dynamics are compared to each other.

The iteration proceeds the following way: Four pairs of strategy parameters are computed from the initial parameters. These are $(\beta\mu, \alpha\sigma)$, $(\beta\mu, \sigma/\alpha)$, $(\mu/\beta, \alpha\sigma)$, and $(\mu/\beta, \sigma/\alpha)$. For each combination of strategy parameters, the theoretical equations are iterated over a single isolation period. The length of the isolation period depends on the chosen population size, i.e. it is $\gamma = d/(\beta\mu)$ or $\gamma = (d\beta)/\mu$ respectively. The best (lowest function value) of the four independent runs by means of the generated fitness value is selected. Its strategy parameters, as well as its generated distance R, are used as initial parameters for the next iteration step. All results are computed from the same initial values. Figures 7.1 displays the $[1, 4(\mu/\mu_I, \lambda)^\gamma]$-meta-ES dynamics. Taking account of the asymptotic limit $N \to \infty$, the search space dimensionality of $N = 1000$ is chosen. The initial mutation strength is $\sigma_p = 1$ and the constant noise strength is set to $\sigma_\epsilon = 5$. The initial population sizes are $\mu_p = 4$ and $\lambda_p = 16$, respectively. This is due to the truncation ratio being $\vartheta = 1/4$. $\gamma_p = 64$ represents the initial isolation length. The adjustment parameters are $\alpha = 1.2$ and $\beta = 2$.

The left-hand side graphs in Fig. 7.1 presents the μ-dynamics, and the γ-dynamics, respectively. The strategy increases the population size μ up to its initially defined maximal value $d = 256$. Consequently by construction the corresponding γ-dynamics show the converse behavior. That is, the isolation length of the inner ES is reduced to 1 by the selection mechanism of the outer ES. The μ-dynamics as well as the γ-dynamics of the approximations, (7.15) and (7.17), perfectly match while they differ slightly from the dynamics of Eq. (7.4) which is represented by the solid blue line. But these differences can only be observed during the first few isolation periods. All three dynamics overlap after each has finally reached its maximal population size, and minimal isolation length respectively, and remain in this state until the algorithm terminates. The R-dynamics as well as the σ-dynamics are illustrated by the curves on the right-hand side of Fig. 7.1. Again the iteratively computed results of equations (7.4), (7.15), and (7.17) are compared.

In both cases, a similar pattern of the original dynamics and their approximations can be

observed. After a couple of isolation periods, the dynamics almost match. The meta-ES decreases the mutation strength. During the decline, the σ-dynamics show an oscillating behavior. Note that this oscillation phases grow with decreasing σ. While the oscillations slow down the decrease of the mutation strength, the meta-ES gradually reduces σ. A more detailed investigation of these oscillation behavior is provided in Sec. 7.4. Taking a look at the distance R to the optimizer one observes the dynamics approaching the residual steady state distance $\tilde{R}_{ss}$. In fact, since the σ-dynamics converge to zero the R-dynamics approach the approximated steady state distance $R_{ss} \approx 1.961$, see Eq. (7.7). The good agreement between the dynamics resulting from Eq. (7.4) and the dynamics iterating its approximations justifies the use of the approximations in the further theoretical investigation of the meta-ES.

7.3. The population size dynamics

Having looked at the meta-ES dynamics resulting from Alg. 7.1, this section focuses on the μ-dynamics of the meta-ES. Since all iterations in the previous section show the strategy's behavior to increase the parental population size μ to its maximum, one is interested in a theoretical explanation. Note, that $d := \mu\gamma$ is defined as the upper bound of the parameter μ, or γ, respectively. In the first step, the noise free fitness environment ($\sigma_\epsilon = 0$) is assumed throughout the analysis in Sec. 7.3.1. In this scenario the results from Sec. 7.2 allow for a rather simple examination of the strategy's population adaptation behavior. Afterwards, in Sec. 7.3.2 fitness noise is included into the considerations.

7.3.1. Noise-free fitness environment

The approximation (7.17) shows a good agreement with the results obtained by γ-fold application of Eq. (7.4). Making use of Eq. (7.17) simplifies the analysis considerably. Hence, it is used as the starting point of the following investigations. Assuming $\sigma_\epsilon^* = 0$, Eq. (7.17) transforms into

$$R^{(g+\gamma)} \simeq R^{(g)}(1 - a\gamma) + \tilde{R}_{ss} a\gamma. \tag{7.18}$$

Application of Eq. (7.6), and insertion of $a = \dfrac{2\mu c_{\mu/\mu,\lambda}^2}{N}$ from Eq. (7.12) together with $\gamma\mu = d$ (line 2 of Alg. 7.1) yields

$$R^{(g+\gamma)} \simeq R^{(g)}\left(1 - \frac{2c_{\mu/\mu,\lambda}^2}{N} d\right) + c_{\mu/\mu,\lambda}\sigma\gamma. \tag{7.19}$$

The first addend does no longer depend on either the population size parameter μ[1] or on the mutation strength parameter. This simplifies the following calculations significantly.

After each isolation period the outer ES computes two new parental population sizes μ by increasing and decreasing the parental population size of the best inner strategy by the parameter $\beta > 1$. In the same manner the algorithm builds two new mutation strengths σ by

[1] Assuming a sufficiently large population size such that $c_{\mu/\mu,\lambda}$ depends only on the truncation ratio ϑ.

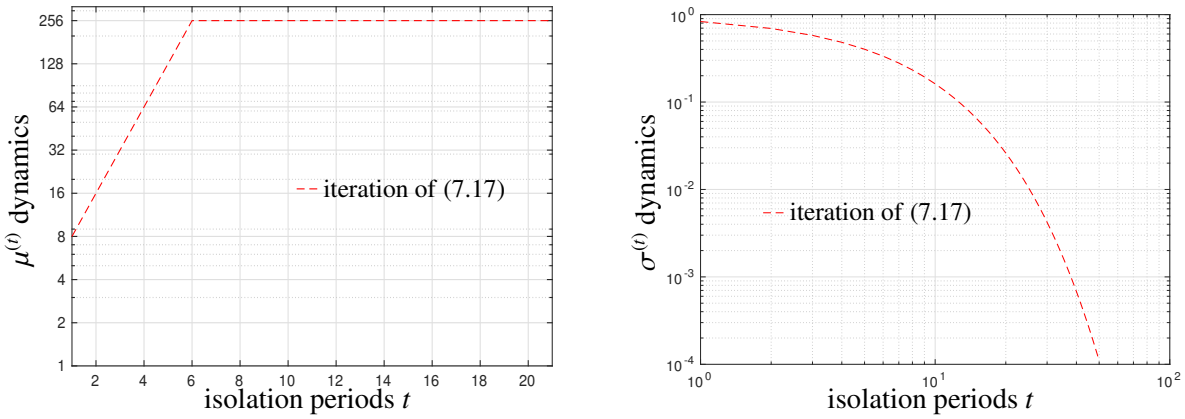

Figure 7.2.: On the left hand side the μ-dynamic resulting from the iteration of Eq. (7.17) is shown. The noise strength is $\sigma_\epsilon = 0$. The right hand side presents the respective σ dynamics. The initial population size is $\mu = 4$ and the initial isolation length is $\gamma = 64$, i.e. their upper bound is set to $d = 256$.

varying the mutation strength of the best inner strategy by the parameter α. Thus, the four new strategy parameters which will establish the next four inner ESs are obtained. They read

$$\mu_+ \coloneqq \tilde{\mu}_1 = \mu\beta \quad \text{and} \quad \mu_- \coloneqq \tilde{\mu}_2 = \mu/\beta, \tag{7.20}$$

as well as

$$\sigma_+ \coloneqq \tilde{\sigma}_1 = \sigma\alpha \quad \text{and} \quad \sigma_- \coloneqq \tilde{\sigma}_2 = \sigma/\alpha. \tag{7.21}$$

Notice, that $\mu_\pm$, and $\sigma_\pm$ correspond to $\tilde{\mu}_1$ and $\tilde{\mu}_2$, and $\tilde{\sigma}_1$ and $\tilde{\sigma}_2$ respectively, which have been mentioned in Sec. 7.1. During the next sections the analysis utilizes the following simplification related to the progress coefficients

$$c_{\mu/\mu,\lambda} \approx c_{\mu_+/\mu_+,\lambda_+} \approx c_{\mu_-/\mu_-,\lambda_-}. \tag{7.22}$$

This assumption is valid because in the asymptotic limit case the progress coefficient $c_{\mu/\mu,\lambda}$ only depends on the truncation ratio $\vartheta = \mu/\lambda$, see also [Beyer, 2001].

In the following, $R_{+-}^{(g+\gamma)}$ is identified with the expected distance realized by the inner ES that operates with μ_+ and σ_- over a single isolation period. The expected distances of the three other inner strategies $R_{++}^{(g+\gamma)}$, $R_{-+}^{(g+\gamma)}$, and $R_{--}^{(g+\gamma)}$ are defined analogously. Making use of Eq. (7.19) the ranking of the expected distance R to the optimizer is derived in Appendix C.1 as

$$R_{+-}^{(g+\gamma)} < R_{++}^{(g+\gamma)} < R_{--}^{(g+\gamma)} < R_{-+}^{(g+\gamma)}. \tag{7.23}$$

It can be observed that the meta-ES in expectation favors the inner ESs with higher population size μ and reduced mutation strength σ. Thus the meta-ES is expected to permanently increase the parental population size μ after each isolation period of γ generations until finally the upper bound d is reached. Consequently the strategy decreases the isolation length γ down to 1. Simultaneously, the meta-ES prefers the strategies which operate with the

decreased mutation strength σ_-. Thus $R_{+-}^{(g+\gamma)}$ dominates the other three expected distances. Accordingly, in the absence of fitness noise the μ- and σ-dynamics can be characterized by

$$\begin{aligned} \mu^{(g+\gamma)} &= \mu^{(g)}\beta \quad \text{and} \\ \sigma^{(g+\gamma)} &= \sigma^{(g)}/\alpha \end{aligned} \tag{7.24}$$

until the upper bound d of the population size parameter is reached. After that, the population size μ remains in its maximum while the mutation strength σ is decreased further on.

An illustration of the μ and σ dynamics in the noise-free fitness case is given in Fig. 7.2. The dynamics are generated by iteration of Eq. (7.17). Except for the noise strength ($\sigma_\epsilon = 0$) all initial parameters agree with their choices in Sec. 7.2. That is, $N = 1000$, $\mu_p = 4$, $\vartheta = 1/4$, $\lambda_p = 16$, $\beta = 2$, $\gamma_p = 64$, $\sigma_p = 1$ and $\alpha = 1.2$ are used. According to the predictions, see (7.24), the population size μ is increased until it reaches its maximal value d. Furthermore the meta-ES steadily decreases the mutation strength σ over the observed isolation periods.

7.3.2. Addressing fitness noise

The next step includes fitness noise into the considerations. It is already known that the choice of a higher population size allows for a lower residual distance [Arnold, 2002]. That is why, in the presence of fitness noise with constant noise strength σ_ϵ, the meta-ES algorithm is supposed to increases the population size μ to its maximum d just like in the noise-free case. Operating at maximal population size, the isolation inside the algorithm only proceeds over one generation, i.e. $\gamma = 1$. Considering isolation periods of length $\gamma = 1$ allows to analyze the μ dynamics. Moreover, assuming sufficiently small σ values, the change in the mutation strength between two consecutive isolation periods becomes neglectable. Using Eq. (7.4), as well as the sphere model specific normalizations (2.22) and (6.6), one obtains

$$R^{(g+1)} = R^{(g)} - \varphi^* \frac{R^{(g)}}{N}. \tag{7.25}$$

By considering (7.20) and ignoring the σ adaptation at this point, the terms $R_+^{(g+1)}$ and $R_-^{(g+1)}$ are introduced as the expected distances which are realized by the inner ES that operates with μ_+ and μ_-, respectively. Hence, the two expected distances at the end of the isolation period are calculated as

$$\begin{aligned} R_+^{(g+1)} &= R^{(g)} - \left(\frac{c_{\mu/\mu,\lambda}\sigma^{*2}}{\sqrt{\sigma_\epsilon^{*2} + \sigma^{*2}}} - \frac{\sigma^{*2}}{2\beta\mu} \right) \frac{R^{(g)}}{N}, \\ R_-^{(g+1)} &= R^{(g)} - \left(\frac{c_{\mu/\mu,\lambda}\sigma^{*2}}{\sqrt{\sigma_\epsilon^{*2} + \sigma^{*2}}} - \frac{\beta\sigma^{*2}}{2\mu} \right) \frac{R^{(g)}}{N}. \end{aligned} \tag{7.26}$$

Again the sign of their difference determines which strategy parameters are chosen in the outer ES. Thus, taking a look at

$$R_+^{(g+1)} - R_-^{(g+1)} = \left(\frac{\sigma^{*2}}{2\beta\mu} - \frac{\beta\sigma^{*2}}{2\mu}\right)\frac{R^{(g)}}{N} = \left(\frac{1}{\beta} - \beta\right)\frac{\sigma^{*2}}{2\mu}\frac{R^{(g)}}{N}. \tag{7.27}$$

governs the population size adaptation. Because of the condition $\beta > 1$ this difference is always negative

$$R_+^{(g+1)} - R_-^{(g+1)} < 0. \tag{7.28}$$

That is, once the meta-ES has reached its minimal isolation length $\gamma = 1$, the algorithm permanently increases the population size μ up to its maximum $\mu = d$ and maintains this state for the remaining isolation periods. This behavior has also been observed in Sec. 7.2, see Fig. 7.1.

7.4. The mutation strength dynamics

Due to the results of the iterated dynamics in Sec. 7.2 and the theoretical observations in Sec. 7.3, the $[1, 4(\mu, \lambda)^\gamma]$-meta-ES is regarded to continuously increase the parental population μ to its maximal value $d = \mu\gamma$. As a consequence, the isolation length γ reduces to 1 respectively. In this section it is assumed that the strategy has already reached its maximal population size and remains in this state according to Sec. 7.3.2. Therefore, the σ-dynamics can be analyzed regarding an $[1, 4(\mu, \lambda)^1]$-meta-ES with $\beta = 1$. That is, neither the population size μ nor the isolation length $\gamma = 1$ is changed by the outer ES anymore. Conclusively, it can be considered to be a $[1, 2(\mu/\mu_I, \lambda)^1]$-meta-ES with fixed μ. In the first step, Sec. 7.4.1 aims at a qualitative description of the σ dynamics. This allows for an interpretation of the mutation strength dynamics observed in Fig. 7.1. Afterwards in Sec. 7.4.2 the dynamics of the normalized mutation strength are considered. Using the normalized quantities the respective dynamics become independent of the search space location and a description of the σ^* dynamics' asymptotic growth can be provided.

7.4.1. Deriving the mutation strength dynamics

Focusing on the outer ES, it generates two new σ-values from the parental mutation strength $\sigma^{(t)}$ (t being the generation counter of the upper level ES)

$$\tilde{\sigma}_1 := \alpha\sigma^{(t)} \quad \text{and} \quad \tilde{\sigma}_2 := \sigma^{(t)}/\alpha. \tag{7.29}$$

Remembering Eq. (7.4), and writing σ instead of $\sigma^{(t)}$, this results in two expected distances $R^{(t+1)}$ at the end of isolation period $t + 1$

$$\begin{aligned} R_1^{(t+1)} &= R^{(t)} - \frac{\alpha\sigma c_{\mu/\mu,\lambda}}{\sqrt{1 + \frac{{\sigma_\epsilon}^2}{4{R^{(t)}}^2\alpha^2\sigma^2}}} + \frac{\alpha^2\sigma^2 N}{2\mu R^{(t)}}, \\ R_2^{(t+1)} &= R^{(t)} - \frac{\sigma c_{\mu/\mu,\lambda}}{\alpha\sqrt{1 + \frac{\alpha^2{\sigma_\epsilon}^2}{4{R^{(t)}}^2\sigma^2}}} + \frac{\sigma^2 N}{2\alpha^2\mu R^{(t)}}. \end{aligned} \tag{7.30}$$

Note, that $R_1^{(t+1)}$ and $R_2^{(t+1)}$ refer to the inner ES which operates with $\tilde{\sigma}_1$ and $\tilde{\sigma}_2$, respectively. The algorithm chooses the parameters of the strategy which generates the smaller distance to the optimizer. That is, the sign of the difference $R_1^{(t+1)} - R_2^{(t+1)}$ determines whether the meta-ES increases or decreases the mutation strength σ

$$\begin{aligned} R_+^{(t+1)} - R_-^{(t+1)} < 0 \quad &\Rightarrow \quad \sigma^{(t+1)} = \sigma^{(t)}\alpha \\ R_+^{(t+1)} - R_-^{(t+1)} > 0 \quad &\Rightarrow \quad \sigma^{(t+1)} = \sigma^{(t)}/\alpha. \end{aligned} \tag{7.31}$$

As demonstrated in App. C.2 this difference can be characterized by the discriminator function Δ, cf. Eq. (C.12),

$$\Delta := \frac{(\alpha^4 - 1)\sigma^*}{2\mu\alpha^2} - \frac{c_{\mu/\mu,\lambda}\sigma^*}{\alpha^2}\left(\frac{\alpha^4}{\sqrt{\alpha^2\sigma^{*2} + \sigma_\epsilon^{*2}}} - \frac{1}{\sqrt{\frac{\sigma^{*2}}{\alpha^2} + \sigma_\epsilon^{*2}}}\right). \tag{7.32}$$

Accordingly, the σ-dynamic depends only on the sign of Δ, i.e.,

$$\begin{aligned} \Delta < 0 \quad &\Rightarrow \quad \sigma^{(t+1)} = \sigma^{(t)}\alpha, \\ \Delta > 0 \quad &\Rightarrow \quad \sigma^{(t+1)} = \sigma^{(t)}/\alpha. \end{aligned} \tag{7.33}$$

Note that Δ depends on the normalized mutation strength σ^* as well as the normalized noise strength σ_ϵ^*. The discriminator function $\Delta(\sigma^*, \sigma_\epsilon^*)$ allows to determine the mutation strength evolution equation

$$\sigma^{(t+1)} = \sigma^{(t)}\alpha^{-\mathrm{sign}(\Delta(\sigma^{*(t)}, \sigma_\epsilon^{*(t)}))}. \tag{7.34}$$

The sign of Δ is plotted depending on σ^* and σ_ϵ^* in Fig. 7.3. The values of σ^* and σ_ϵ^* are varied within their range of positive progress from zero to $2\mu c_{\mu/\mu,\lambda}$, see Eq. (6.23). Negative values of $\Delta(\sigma^*, \sigma_\epsilon^*)$ are represented by the yellow region, and positive ones by the red region respectively. For example, if the strategy operates with a combination of σ^* and σ_ϵ^* values from the yellow region ($\Delta < 0$) it will increase the mutation strength after the isolation period. One is interested in the critical value $\sigma_0^* > 0$ around which the sign of $\Delta(\sigma^*, \sigma_\epsilon^*)$ changes. According to the combination of σ^* and σ_ϵ^* in Fig. 7.3 this critical value can be found on the black line between the two colored regions. Computing σ_0^* from Eq. (7.32) leads to

$$\sigma_0^* \simeq \sigma_\epsilon^* \sqrt{\sqrt{\left(\frac{\alpha^4 + 1}{\alpha^2}\right)^2 + 4\left(\frac{2\mu c_{\mu/\mu,\lambda}}{\sigma_\epsilon^*} - 1\right)} - \left(\frac{\alpha^4 + 1}{\alpha^2}\right)}. \tag{7.35}$$

The complete derivation of σ_0^* is performed in Appendix C.2. Dividing Eq. (7.35) by σ_ϵ^*, one obtains

$$\frac{\sigma_0^*}{\sigma_\epsilon^*} \simeq \sqrt{\sqrt{\left(\frac{\alpha^4 + 1}{\alpha^2}\right)^2 + 4\left(\frac{2\mu c_{\mu/\mu,\lambda}}{\sigma_\epsilon^*} - 1\right)} - \left(\frac{\alpha^4 + 1}{\alpha^2}\right)}. \tag{7.36}$$

Note that for $\sigma_\epsilon = const.$, it holds

$$\sigma_\epsilon^* = \frac{\sigma_\epsilon N}{2R^2} \overset{R \to R_{ss}}{\longrightarrow} 2\mu c_{\mu/\mu,\lambda}. \tag{7.37}$$

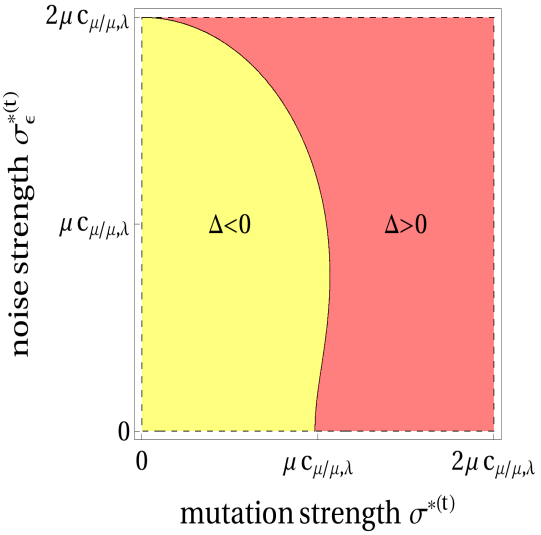

Figure 7.3.: On the sign of Δ depending on σ^* and σ^*_ϵ. For the illustration the strategy parameters are set to $\mu = 256$, $\vartheta = 1/4$, and $\alpha = 1.2$. The yellow area illustrates the region of negative discriminator function values that result in a mutation strength increase according to Eq. (7.33). Whereas the red area ($\Delta > 0$) displays the event of mutation strength reductions.

Taking (7.37) into account, one sees that in (7.36) the critical value σ^*_0 in relation to the normalized noise strength σ^*_ϵ is decreasing to zero in the asymptotic limit. Figure 7.4 displays this behavior. A continuous increase of σ^*_ϵ to its maximal value $2\mu c_{\mu/\mu,\lambda}$ drives $\sigma^*_0/\sigma^*_\epsilon$ and σ^*_0 to zero.

Considering σ^*_0, it allows to continue with the qualitative analysis of the σ-dynamics. Equation (7.33) becomes

$$\begin{aligned} \sigma^* < \sigma^*_0 \quad &\Rightarrow \quad \sigma^{(t+1)} = \sigma^{(t)}\alpha, \\ \sigma^* > \sigma^*_0 \quad &\Rightarrow \quad \sigma^{(t+1)} = \sigma^{(t)}/\alpha. \end{aligned} \tag{7.38}$$

According to these equations, the meta-ES adapts σ so that the normalized mutation strength σ^* reaches a certain vicinity to its point of discontinuity σ^*_0. In this region the σ dynamics enter a limit cycle. This corresponds to the oscillatory behavior of the σ dynamics which was already observed in Fig. 7.2. The limit cycle will only be left if the point of discontinuity σ^*_0 changes. Notice that σ^*_0 still depends on the normalized noise strength σ^*_ϵ. As long as the meta-ES reduces the distance R to the optimizer, σ^*_ϵ approaches its saturation value $2\mu c_{\mu/\mu,\lambda}$. Since the critical value σ^*_0 decreases by tendency, the strategy is able to leave the current σ limit cycle and decrease the mutation strength until it enters the next limit cycle. This behavior explains the σ dynamics in Sec. 7.2 where a rather slow mutation strength decrease in stepwise limit cycles is observed.

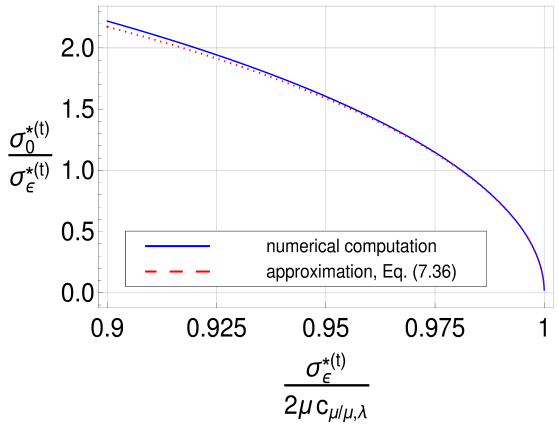

Figure 7.4.: The dashed red line shows the results of the approximation $\sigma_0^*/\sigma_\epsilon^*$, see Eq. (7.36). It is compared to the numerically computed root of Eq. (7.32) which is plotted with regard to σ_ϵ^* and represented by the solid blue line. The graph presents the results for $\sigma_\epsilon^*/2\mu c_{\mu/\mu,\lambda} \in [0.9, 1]$. One observes a good compliance between the numerical results and the approximation for σ_ϵ^* values in the vicinity of $2\mu c_{\mu/\mu,\lambda}$.

7.4.2. The normalized mutation strength dynamics

In order to analyze the steady state behavior of Alg. 7.1 on the noisy sphere model, the evolution of the normalized mutation strength σ^* has to be examined. For this purpose, the normalizations according to the sphere model are reconsidered, cf. Eq. (2.22). Applying those normalizations to Eq. (7.34) and taking into account the difference equation

$$R^{(t+1)} = R^{(t)}\left(1 - \frac{1}{N}\varphi^*(\sigma^{*(t)}\alpha^{-\mathrm{sign}(\Delta(\sigma^{*(t)},\sigma_\epsilon^{*(t)}))}, \sigma_\epsilon^{*(t)})\right), \tag{7.39}$$

cf. Eq. (7.4), finally yields the evolution equation of the normalized mutation strength dynamics

$$\sigma^{*(t+1)} = \sigma^{*(t)} \frac{\alpha^{-\mathrm{sign}(\Delta(\sigma^{*(t)},\sigma_\epsilon^{*(t)}))}}{1 - \frac{1}{N}\varphi^*(\sigma^{*(t)}\alpha^{-\mathrm{sign}(\Delta(\sigma^{*(t)},\sigma_\epsilon^{*(t)}))}, \sigma_\epsilon^{*(t)})}. \tag{7.40}$$

The goal of this paragraph is the computation of the expected normalized mutation strength σ^* around which the ES oscillates in its steady state.

At this point, it should be noticed that the σ^*-dynamic directly interacts with the σ_ϵ^*-dynamic. The latter determines the critical value σ_0^* and thereby the strategy's behavior to increase or decrease the (normalized) mutation strength. That is, one has to solve an iterative mapping depending on $\sigma^{*(t)}$ and $\sigma_\epsilon^{*(t)}$

$$\sigma^{*(t+1)} = f_\sigma(\sigma^{*(t)}, \sigma_\epsilon^{*(t)}; \alpha, \mu, N). \tag{7.41}$$

Regarding the normalizations (6.6) as well as (2.22), and by making use of the difference

equation (7.4), an iterative mapping of the σ_ϵ^*-dynamics is derived

$$\sigma_\epsilon^{*(t+1)} = \frac{\sigma_\epsilon^{*(t)}}{\left(1 - \frac{1}{N}\varphi^*(\sigma^{*(t)}\alpha^{-\text{sign}(\Delta(\sigma^{*(t)},\sigma_\epsilon^{*(t)}))}, \sigma_\epsilon^{*(t)})\right)^2}. \tag{7.42}$$

For the calculation of the asymptotic dynamics some asymptotically exact simplifications have to be applied. The comprehensive derivation is presented in Appendix C.3. As a first step, a simplification of the σ_ϵ^* dynamics is calculated in the limit of a small normalized mutation strength relative to the normalized noise strength, i.e. $\sigma^*/\sigma_\epsilon^* \to 0$,

$$\sigma_\epsilon^{*(t+1)} \simeq \sigma_\epsilon^* + \frac{\sigma^{*2}\alpha^{-2\text{sign}(\Delta(\sigma^*,\sigma_\epsilon^*))}}{\mu N}\left(2\mu c_{\mu/\mu,\lambda} - \sigma_\epsilon^*\right). \tag{7.43}$$

The second step provides an approximation for the discriminator function $\Delta(\sigma^*, \sigma_\epsilon^*)$ in Eq. (7.32).

According to Eq. (C.36), the sign of Δ and, by implication, the decision inside the meta-ES to increase or decrease the mutation strength σ, or σ^* respectively, is only depending on the approximated discriminator function

$$\tilde{\Delta}(\sigma^*, \sigma_\epsilon^*) = \frac{\alpha^4 + 1}{2\alpha^2}\sigma^{*2} - \sigma_\epsilon^*\left(2\mu c_{\mu/\mu,\lambda} - \sigma_\epsilon^*\right). \tag{7.44}$$

In Fig. 7.5 $\Delta(\sigma^*, \sigma_\epsilon^*)$, see Eq. (7.32), and its approximation $\tilde{\Delta}(\sigma^*, \sigma_\epsilon^*)$ are compared. The gray region ($\tilde{\Delta} > 0, \Delta < 0$) represents the trade-off between the exact Δ and its approximation (7.44).

Especially in the asymptotically interesting region of small σ^* values and $\sigma_\epsilon^* \approx 2\mu c_{\mu/\mu,\lambda}$, the approximation shows a good agreement with Δ. The results of the iterative computations of the original dynamics (7.40) and (7.42) lead to the conclusion that the σ^*-dynamics mainly depend on the α term. That is, the term $(1 - \varphi^*/N)$ in (7.40) can be neglected and by combination with Eq. (7.44) this yields the following approximation of the σ^*-dynamics

$$\sigma^{*(t+1)} = \sigma^{*(t)}\alpha^{-\text{sign}(\tilde{\Delta}(\sigma^{*(t)},\sigma_\epsilon^{*(t)}))}. \tag{7.45}$$

A conclusive asymptotic approximation of the σ_ϵ^*-dynamics is found by inserting Eq. (7.44) into Eq. (7.43)

$$\sigma_\epsilon^{*(t+1)} \simeq \sigma_\epsilon^{*(t)} + \frac{\left(\sigma^{*(t)}\alpha^{-\text{sign}(\tilde{\Delta}(\sigma^{*(t)},\sigma_\epsilon^{*(t)}))}\right)^2}{\mu N}\left(2\mu c_{\mu/\mu,\lambda} - \sigma_\epsilon^{*(t)}\right). \tag{7.46}$$

Note, if σ^* is in the vicinity of σ_0^*, i.e. $\tilde{\Delta} \approx 0$, the analysis of the meta-ES predicts an oscillatory behavior in the σ^* values. Such a behavior is observed in Fig. 7.6(a). The actual σ^* dynamics have a globally decreasing tendency superimposed by local oscillations.

In Fig. 7.6 the approximations (7.45) and (7.46) are validated by comparing them with the original σ^* and σ_ϵ^* dynamics from Eq. (7.40) and Eq. (7.42), respectively. The normalized noise strength is depicted in relation to its saturation value $2\mu c_{\mu/\mu,\lambda}$. Both dynamics are

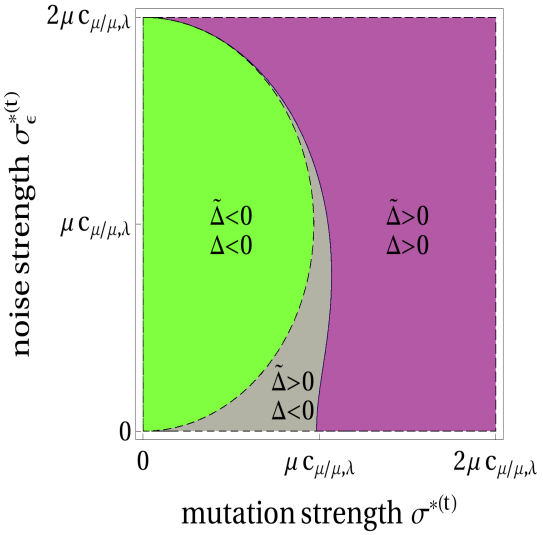

Figure 7.5.: Illustration of the trade-off (gray area) between Δ, Eq. (7.32) and its approximation $\tilde{\Delta}$, Eq. (7.44).

iterated over one million isolation periods of $\gamma = 1$ generation using a population size of $\mu = 10$ and a truncation ratio $\vartheta = 1/4$. The search space dimension is $N = 100$ and the adjustment parameter is set to $\alpha = 1.05$. The iterations start with $\sigma_\epsilon^{*(0)} = 2\mu c_{\mu/\mu,\lambda} - 0.1$ and $\sigma^{*(0)} = \sqrt{(2\mu c_{\mu/\mu,\lambda})^2 - \sigma_\epsilon^{*(0)^2}}$ to ensure the compliance with condition (6.23).

Having a look at the magnified region in Fig. 7.6(a), the oscillating behavior of the normalized mutation strength dynamics can be noticed. The decline of the normalized mutation strength dynamics is governed by σ_0^* which on its part depends on the σ_ϵ^* dynamics. From the continuous decrease of the difference $2\mu c_{\mu/\mu,\lambda} - \sigma_\epsilon^*$ in Fig. 7.6(b) it can be deduced that $\sigma_\epsilon^* \to 2\mu c_{\mu/\mu,\lambda}$. Accordingly, the critical value σ_0^* slowly decreases, see Eq. (7.35). This way the σ^* dynamics are able to leave their limit cycles from time to time which leads to the observable stepwise descent. Note, that the oscillation phases grow with the reduction of the normalized mutation strength σ^*.

After having evolved over a sufficiently large number of isolation periods, it can be observed that in both cases the slopes of the approximations and the original dynamics match. Therefore, one can use the approximation in order to compute the rate at which the mutation strength dynamics descent. To this end, the quantity $\delta^{(t)}$ is introduced

$$\delta^{(t)} = 2\mu c_{\mu/\mu,\lambda} - \sigma_\epsilon^{*(t)}, \tag{7.47}$$

It measures the deviation of the normalized noise strength σ_ϵ^* from its saturation value $2\mu c_{\mu/\mu,\lambda}$. Inserting (7.47) into (7.46), one obtains

$$\delta^{(t+1)} = \left(1 - \frac{\sigma^{*(t)^2}}{\mu N} \alpha^{-2\mathrm{sign}(\tilde{\Delta}(\sigma^{*(t)}, \sigma_\epsilon^{*(t)}))}\right) \delta^{(t)}. \tag{7.48}$$

As one can see in Fig. 7.6(a), there are periods in the σ^* evolution where the σ^* values exhibits oscillatory behavior. This is reflected in the oscillatory change in the sign of $\tilde{\Delta}$.

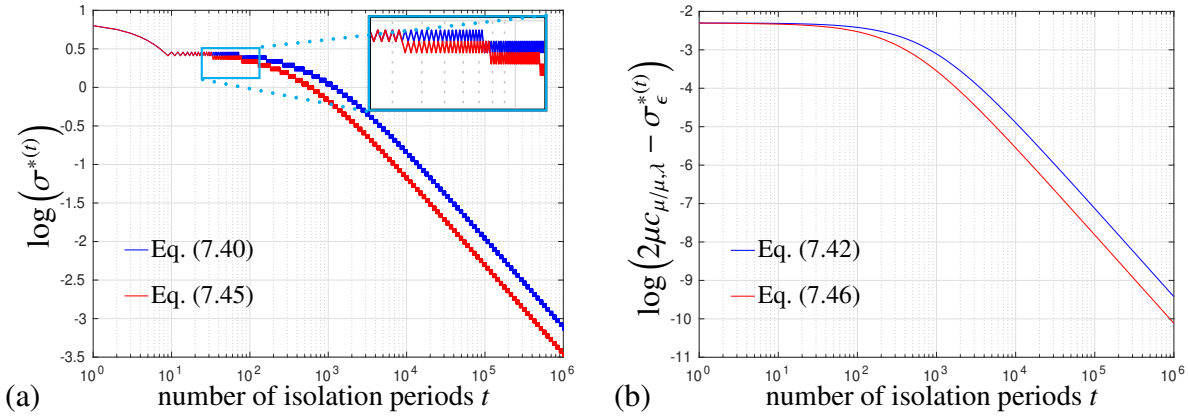

Figure 7.6.: (a): Comparison of the iterated σ^*-dynamic from Eq. (7.40) represented by the blue line and its asymptotic approximation from Eq. (7.45) depicted as the red dashed line. The step-wise oscillatory descent is observable in the magnified box. (b): Comparison of the corresponding σ^*_ϵ dynamics resulting from Eq. (7.42) and (7.46), respectively.

Since σ^*_0 corresponds to $\tilde{\Delta} = 0$, one has to mathematically treat the behavior at $\tilde{\Delta} = 0$, i.e. $\text{sign}(\tilde{\Delta}) = \text{sign}(0) = 0$. This immediately leads to the recurrence equation

$$\delta^{(t+1)} = \left(1 - \frac{\sigma^{*(t)2}}{\mu N}\right)\delta^{(t)} = \left(1 - \frac{\sigma^{*(t)2}}{\mu N}\right)^{t+1} \delta^{(0)}. \tag{7.49}$$

Equation (7.49) allows for the simplification of Eq. (7.44) in order to make a prediction about the asymptotic behavior of the σ^*-dynamics. In a first step Eq. (7.47) is inserted into (7.44) yielding

$$\tilde{\Delta}(\sigma^*, \delta^{(t)}) = \frac{\alpha^4 + 1}{2\alpha^2}\sigma^{*2} - 2\mu c_{\mu/\mu,\lambda}\delta^{(t)} + \delta^{(t)^2}. \tag{7.50}$$

Applying (7.49) then yields

$$\tilde{\Delta}(\sigma^*, \delta^{(t)}) = \frac{\alpha^4 + 1}{2\alpha^2}\sigma^{*2} - 2\mu c_{\mu/\mu,\lambda}\left(1 - \frac{\sigma^{*2}}{\mu N}\right)^t \delta^{(0)} + \left(1 - \frac{\sigma^{*2}}{\mu N}\right)^{2t} \delta^{(0)^2}. \tag{7.51}$$

Making use of the approximation

$$\left(1 - \frac{\sigma^{*2}}{\mu N}\right)^t \simeq \left(1 - t\frac{\sigma^{*2}}{\mu N}\right) \tag{7.52}$$

which is admissible for $\sigma^{*2}/\mu N \ll 1$, the $\tilde{\Delta}(\sigma^*, \delta^{(0)})$ term is asymptotically ($N \to \infty$) approximated by

$$\tilde{\Delta}(\sigma^*, \delta^{(t)}) = \frac{\alpha^4 + 1}{2\alpha^2}\sigma^{*2} - 2\mu c_{\mu/\mu,\lambda}\left(1 - t\frac{\sigma^{*2}}{\mu N}\right)\delta^{(0)} + \left(1 - 2t\frac{\sigma^{*2}}{\mu N}\right)\delta^{(0)^2}. \tag{7.53}$$

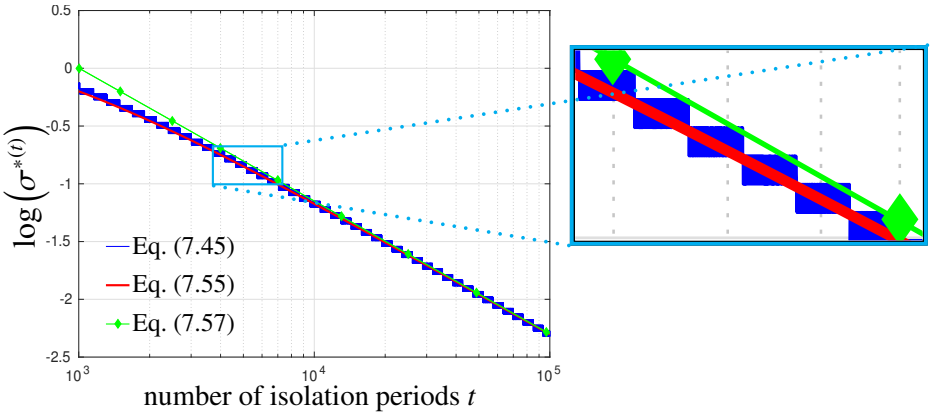

Figure 7.7.: Comparison of the results from Fig. 7.6(a) with the prediction of Eqs. (7.55) and (7.57). The dynamics of (7.55) are depicted by the solid red line which overlaps with the oscillating blue curve representing the dynamics of Eq. (7.45). Due to logarithmic scaling, the oscillation behavior of Eq. (7.45) is reflected by the solid blue rectangles. Their gradual steady state reduction is governed by the rate at which the point of discontinuity approaches zero, cf. (7.57). The green line with diamond markers represents the result of Eq. (7.57).

Further transformations of Eq. (7.53)

$$\tilde{\Delta}(\sigma^*, \delta^{(t)}) = \left[\frac{\alpha^4+1}{2\alpha^2} + \left(\frac{2\delta^{(0)}(\mu c_{\mu/\mu,\lambda} - \delta^{(0)})}{\mu N}\right) t\right] \sigma^{*2} - 2\mu c_{\mu/\mu,\lambda}\delta^{(0)} + \delta^{(0)^2}, \tag{7.54}$$

allow for the approximation of its point of discontinuity σ_0^*. It agrees with the root of $\tilde{\Delta} \stackrel{!}{=} 0$ which is obtained as

$$\sigma_0^* \simeq \sqrt{\frac{(2\mu c_{\mu/\mu,\lambda} - \delta^{(0)})\delta^{(0)}}{\frac{\alpha^4+1}{2\alpha^2} + \left(\frac{2\delta^{(0)}(\mu c_{\mu/\mu,\lambda} - \delta^{(0)})}{\mu N}\right) t}}. \tag{7.55}$$

Conclusively, in the asymptotic limit the point of discontinuity σ_0^* is approximated by Eq. (7.55). The mutation strength dynamics oscillate around σ_0^*. Thus, a description of the asymptotic σ^*-dynamics is found that only depends on the initial deviation $\delta^{(0)}$ of σ_ϵ^* from $2\mu c_{\mu/\mu,\lambda}$ (cf. Eq. (7.47)) and on the number of isolation periods t.

At this point, it is assumed that the fraction

$$\frac{(\alpha^4+1)}{2\alpha^2}\frac{1}{t} \stackrel{t\to\infty}{\longrightarrow} 0 \tag{7.56}$$

approaches zero for $t \to \infty$. This way an even simpler expression describing the asymptotic growth rate is obtained

$$\sigma_0^* \simeq \frac{\tau}{\sqrt{t}}. \tag{7.57}$$

Here, the term τ substitutes the following expression in (7.56)

$$\tau := \sqrt{\frac{\mu N(2\mu c_{\mu/\mu,\lambda} - \delta^{(0)})}{2\mu c_{\mu/\mu,\lambda} - 2\delta^{(0)}}}. \tag{7.58}$$

After a sufficiently large number of isolation periods, the descent of σ_0^* is described by Eq. (7.57). It decreases obeying a square root law proportional to τ. Since the σ^* dynamics oscillate around σ_0^* they consequently decrease with the same rate. That is, having evolved over a large number of isolation periods, the normalized mutation strength dynamics of the meta-ES approach zero. In order to illustrate the compliance of this results, they are displayed in Fig. 7.7.

The solid green line in Fig. 7.7 depicts the approximation of σ_0^* from Eq. (7.55). Equation (7.57) is represented by the dashed blue line. One observes that the growth characteristics overlap in the asymptotic limit. It can be seen that the dashed red line, which asymptotically approximates the σ^*-dynamics, see Eq. (7.45), oscillates perfectly around the point of discontinuity σ_0^*.

At this point one can draw the following conclusion concerning the asymptotic growth rate of the σ-dynamics. First note that the distance to the optimizer R is nearly constant in the vicinity of the steady state distance R_{ss}. Considering $R \to R_{ss}$ and (6.13) one obtains

$$\sigma^* = \frac{N}{R}\sigma \simeq \sqrt{\frac{4\mu c_{\mu/\mu,\lambda} N}{\sigma_\epsilon}}\sigma. \tag{7.59}$$

Thus in the asymptotic limit the σ-dynamics exhibits a similar behavior as the σ^*-dynamics: The mutation strength oscillates around a critical value σ_0 which asymptotically decreases with t according to

$$\sigma_0 \simeq \frac{\tilde{\tau}}{\sqrt{t}}. \tag{7.60}$$

Similar to σ_0^*, it decreases according to a square root law, however, with a different time constant

$$\tilde{\tau} = \sqrt{\frac{\sigma_\epsilon(2\mu c_{\mu/\mu,\lambda} - \delta^{(0)})}{8c_{\mu/\mu,\lambda}\left(\mu c_{\mu/\mu,\lambda} - \delta^{(0)}\right)}}. \tag{7.61}$$

7.5. Simulations

Having derived a theoretical description of the meta-ES long-term behavior on the noisy sphere model, this section focuses on a comparison of the analytical investigations with experimental runs of the $[1, 4(\mu/\mu_I, \lambda)^\gamma]$-meta-ES algorithm, cf. Alg. 7.1. This way the compliance of the theoretical predictions with real meta-ES behavior can be checked.

Figure 7.8 illustrates the comparison for a relatively small choice of the mutation strength control parameter α in search space dimension $N = 1000$. The algorithm is initialized with parental population size $\mu_p = 2$ and truncation ratio $\vartheta = 1/4$ yielding $\lambda_p = 8$. The

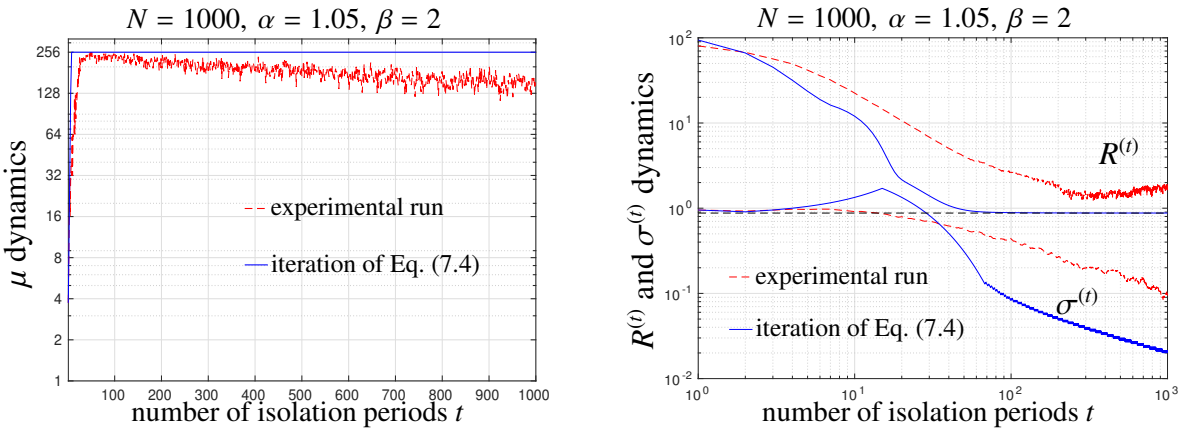

Figure 7.8.: The meta-ES dynamics resulting from Eq. (7.4) are compared to experimental runs of Alg. 7.1. All experiments as well as the iteration of Eq. (7.4) are initialized at $\sigma^p = 1$, $\mu_p = 2$, $\gamma_p = 128$, and $(\mathbf{y_p})_i = 10\ \forall i = 1, \ldots, N$. The dashed red line displays the average over 20 independent experimental runs.

adjustment parameter of the population size is $\beta = 2$. The initial isolation time is set to $\gamma_p = 128$ which leads to an upper bound of $d = 256$ for the μ and γ dynamics. The mutation strength is initialized at $\sigma_p = 1$ with adjustment parameter $\alpha = 1.05$. As the starting point of the algorithm the initial object parameter vector $(\mathbf{y_p})_i = 10,\ i = 1, \ldots, N$ is chosen. This allows for a better observation of the point at which the influence of the constant fitness noise gains importance. The constant noise strength is set to $\sigma_\epsilon = 1$. After evolving over 1000 isolation periods the algorithm terminates. The theoretical results are obtained by the iteration of Eq. (7.4) on the basis of the same initial values. In the figures, the results of the iteration are displayed by the solid blue lines. Notice, that due to the modeling approach of the dynamical system, the iterative dynamics rely on the knowledge of the ideal fitness values in the selection process of the best inner ES. Whereas the selection in the experiments is based on the observed noisy fitness of the centroids returned by the inner strategies. This leads to deviations between iteratively generated and experimental results. A reduction of the deviations is attained by use of multiple experiments. Averaged over 20 independent runs of the algorithm the experimental results are presented as dashed red lines in Fig. 7.8.

During the first 10 isolation periods, the iterative and the experimental dynamics nearly match. Then the effects of the fitness noise can be observed. Regarding the population size dynamics, the left-hand side of Fig. 7.8 illustrates a good agreement provided that the strategy is able to increase the population size μ. After having reached the maximal value $d = 256$, the corresponding isolation time is $\gamma = 1$. In this state, the μ-dynamics can either remain in its maximum or decrease again. Unlike the theoretical predictions suggest, the experimental μ-dynamics leaves the state of maximal population size. Despite the population size fluctuates under the influence of noise, one can measure the meta-ES algorithm's tendency to favor greater population sizes. The iteratively computed R-dynamics approaches its expected residual steady state distance R_{ss}. This steady state distance is displayed by the dashed black line in the right-hand side graph in Fig. 7.8. The decline of the experimentally obtained R dynamics decelerates. This results from the reduction of the isolation time γ

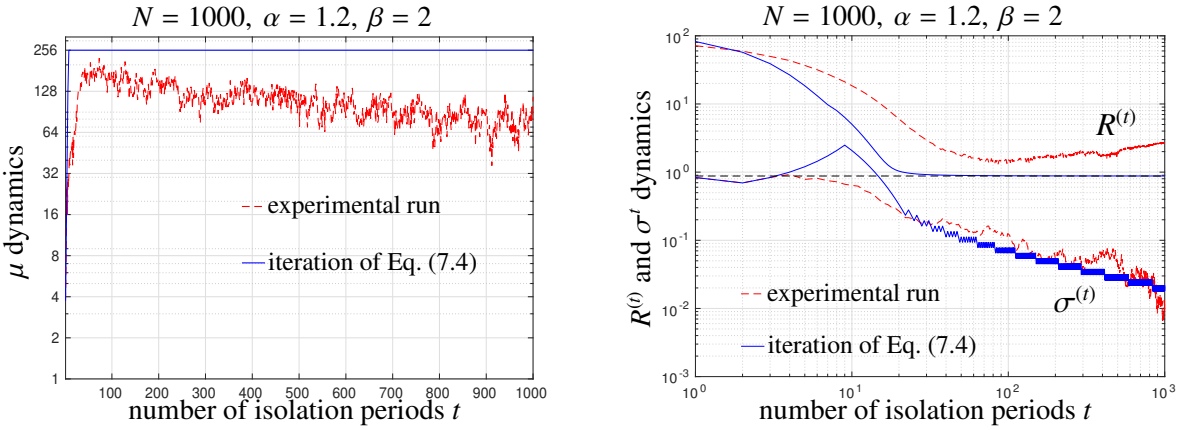

Figure 7.9.: The iterative dynamics resulting from Eq. (7.4) are compared to the experimental runs of Alg. 7.1. The mutation strength adjustment parameter is set to $\alpha = 1.2$. The initialization is similar to that used in Fig. 7.8. The experimental dynamics are averaged over 20 independent meta-ES runs.

being induced by increasing the population size.

In the case of small isolation times, and considering the influence of the fitness noise, allows for an explanation of the fluctuations. The smaller the fitness value the more it is affected by the noise. As the strategy approaches its residual steady state distance $\tilde{R}_{ss}$ the noise disturbs the selection process. That is, the algorithm may select an inner strategy which decreases the population size because it has the best observed noisy fitness. This leads the meta-ES to leave its maximal population size $\mu = 256$ and directly influences the steady state distance $\tilde{R}_{ss}$. Decreasing μ values cause $\tilde{R}_{ss}$ to rise and consequently the R-dynamics increase, cf. the right-hand side of Fig. 7.8. Since the population size is adjusted by the factor $\beta = 2$ these changes of the steady state distance can be relatively large.

Figure 7.9 displays basically the same dynamics as Fig.7.8, but differs in the choice of the parameter α. Using $\alpha = 1.2$ seems to control the σ values more adequately. Note that, within the investigations considered in Chapter 5, small choices of the mutation strength control parameter α resulted in great fluctuations. The interpretation that the choice of $\alpha = 1.05$ is too small to yield a sufficient discriminability of the four inner ESs is misleading in the context of the sphere model. While small α values appeared inappropriate during the investigation of the noise-free ellipsoid model, the analysis in [Beyer et al., 2009] revealed that small realizations of the parameter α on the sphere model, in fact, enable the meta-ES to approach a stable stationary state. Thus the fluctuation behavior observed in Fig. 7.8, and Fig. 7.9 respectively, is supposed to be a result of the noise influence on the selection process of the upper level ES in Alg. 7.1.

At the point where the population size reaches its maximum, the empirically generated results reveal significant deviations from the theoretical predictions. However, both dynamics show the same tendency to decrease the mutation strength σ. Increasing the α factor, e.g. $\alpha = 1.2$, ensures a faster adaptation of the σ values and thus getting closer to the theoretical σ curve, the general deviation tendency does not change. The seemingly improved σ adaptation comes along with greater deviations appearing in the population size dynamics

and the corresponding dynamics of the residual distance.

The rather large deviations observed are due to the noisy fitness information which has not been included in the modeling of the selection process of the outer ES. The theoretical analysis neglects the influence of fitness noise on the selection process of the outer ES. The dynamics resulting from the iteration of the theoretical equations rely on the knowledge of the expected ideal fitness values returned by the inner ESs. Whereas the selection in the experiments is based on the observed noisy fitness of the final parental centroids. This leads to significant deviations between theoretical and experimental dynamics. In order to confirm this explanation, experiments have been conducted discussed in the following sections.

7.5.1. A discussion of the fluctuations

Since the modeling approach leading to the iterative dynamics assumes a noise-free selection, the idea is to simulate the noisy selection process. Thus the real meta-ES run should be emulated by adding noise to the fitness values of the theoretical predictions. In each isolation period, a simulated noise term is added to the four iteratively generated fitness values resulting from the inner ESs. Selection within the iteration is then performed by choosing the best of these four "noisy" fitness values. The inner ES corresponding to the best of the observed fitness values provides its strategy parameters to the next iteration step. The noise term is modeled by a normally distributed random number with mean 0. Its variance is varying with the isolation period. For each isolation period, this variance is determined by measuring the empirical variance of the four function values in the according isolation period of the real meta-ES run. The empirical variances are averaged over 20 independent simulations. Also, the iterative dynamics incorporating noise are averaged over 20 independent runs. Note, that the experimental dynamics are generated as explained in the beginning of this section. The initialization is maintained as well. The iteration of Eq. (7.4) equipped with noise in the selection process of the outer ES is referred to as noisy iteration. The corresponding dynamics are illustrated by the solid blue lines in Fig. 7.10. The experimental dynamics are again represented by dashed red lines. Regarding the distance to the optimizer in this situation both dynamics fail to approach the minimal residual steady state distance R_{ss} corresponding to the maximal parental population size $\mu = d$.

The deviations are a result of fluctuations in the μ dynamics illustrated on the left-hand side of Fig. 7.10. The noisy iteration, as well as the experimental dynamics, show larger deviations from the maximal parental population size $\mu = d$ with increasing number of isolation periods t. This behavior results from the influence of fitness noise on the selection of the best observed inner ES. Also on the right-hand side of Fig. 7.10 an improved agreement of the dynamics is observable. In each case, the iterative and the experimental dynamics behave similarly. Thus the behavior of the experimental dynamics can be reconstructed better by considering noise disturbances in the selection process of the theoretical model. This indicates that the deviations are - at least partially - a result of the disregard of selection noise in the theoretical modeling. However, integrating selection noise into the theoretical analysis does not seem appropriate. Since the strategy is working suboptimally on the noisy problem, a more desirable point of interest is tuning the meta-ES algorithmically to an improved long-term behavior. The next subsection presents an attempt in this direction.

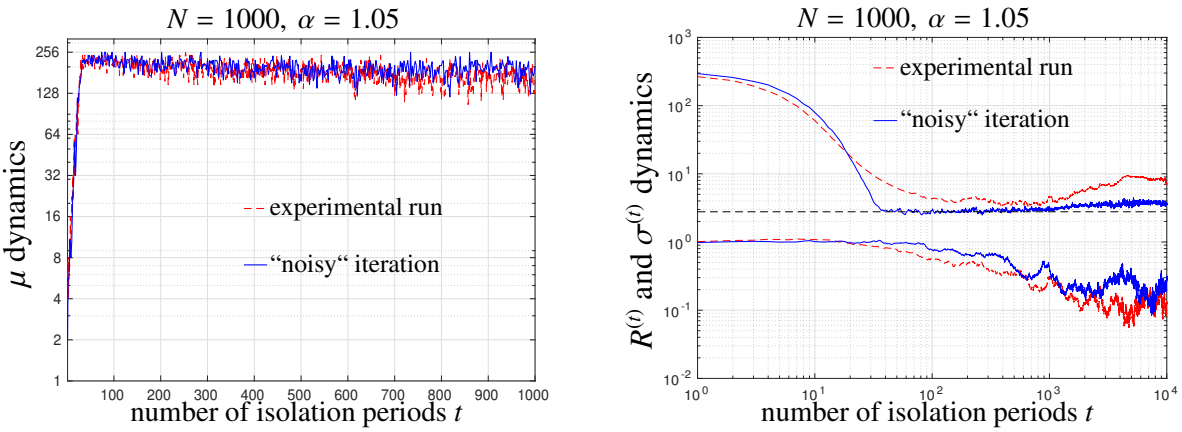

Figure 7.10.: Comparison of the iterative dynamics of Eq. (7.4) with simulated selection noise with the experimental runs of Alg. 7.1. The mutation strength adjustment parameter is set to $\alpha = 1.05$. The initialization is similar to that used in Fig. 7.8. The experimental dynamics are averaged over 20 independent meta-ES runs.

7.5.2. On enhancing the selection decision

Considering the performance degeneration caused by the noise influence on the selection process within the upper level ES, the focus of this section is on algorithmically adjusting the meta-ES selection decision. Trying to average out the noise influence on the selection in the real meta-ES algorithm, the experimental dynamics are supposed to exhibit an improved agreement with the theoretical predictions.

In a first attempt, the selection mechanism in the upper level ES is changed from picking the inner strategy with the best fitness to selecting the inner ES which offers the best average fitness within its finally generated parental population. Since the fitness evaluation of the final centroid at the end of the inner ES is subject to the fitness noise, it has a great influence on the observed quality of the inner strategies. This additional function evaluation of the final parental centroid found by the inner strategies can be avoided by returning the average of the μ best noisy function values $\langle \tilde{F} \rangle_\mu$ of the final population. Each inner ES returns an average fitness of its final parental population

$$\langle F \rangle_\mu \leftarrow \frac{1}{\mu} \sum_{m=1}^{\mu} F_{m;\lambda}. \tag{7.62}$$

Thus the inner ES which averagely generated the best population is selected and its strategy parameters are passed to the next generation. However, despite being promising this modification turns out unable to improve the long-term behavior of the meta-ES algorithm. In fact, one observe a slight increase of the deviations in the μ dynamics. In the first isolation periods, the experimental dynamics approach the steady state distance to the optimizer. But with growing influence of the fitness noise also the modified meta-ES acts like the originally proposed meta-ES. That is, it finally approaches a residual distance within the range of possible population sizes instead of reaching the lowest possible distance to the optimizer. The

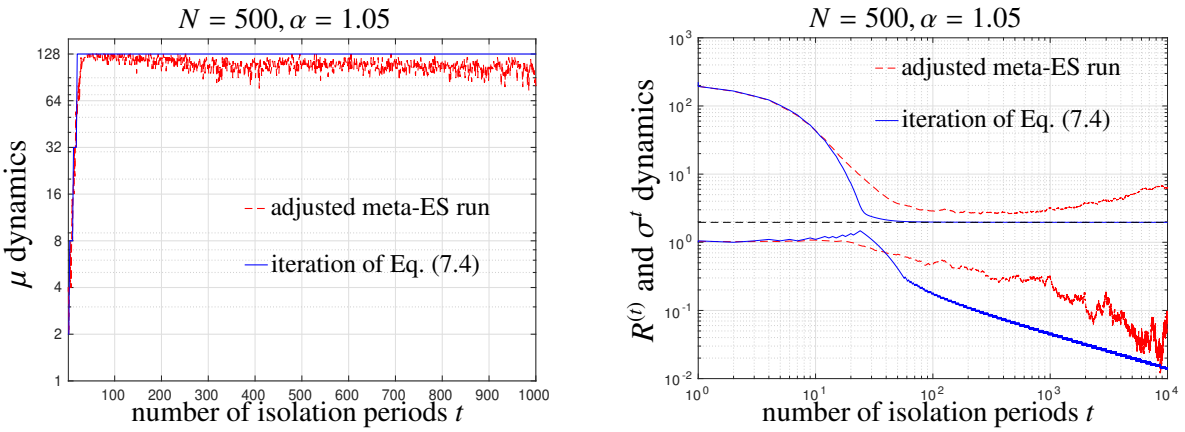

Figure 7.11.: The iterative dynamics of Eq. (7.4) are compared to the experimental results. The experimental dynamics are obtained from runs of Alg. 7.1 that base the selection decision of the upper level ES on the resampled fitness (7.63). The mutation strength adjustment parameter is set to $\alpha = 1.05$. The initialization is similar to that used in Fig. 7.8. The experimental dynamics are averaged over 20 independent meta-ES runs.

illustration of this unsuccessful method is omitted here.

Another approach to improve the selection ability of the meta-ES variant is making use of resampling in the evaluation process of candidate solutions. Resampling is supposed to lower the influence of the fitness noise on the fitness values. Hence, the influence of the noise on the selection decision will be mitigated. Therefore, the parental centroids of the four inner ES are repeatedly (k times) evaluated at the end of an isolation period. The selection is then based on the mean fitness value returned after the resampling process

$$\bar{F} \leftarrow \frac{1}{k} \sum_{i=1}^{k} \bar{F}_i. \tag{7.63}$$

During the experiments, $k = 10$ samples of the final parental centroids fitness have been generated. The selection of the best inner ES is based on the mean value of these k fitness samples. The related experimental dynamics are displayed compared to the iteratively generated dynamics of Eq. (7.4) in Fig. 7.11. It can be observed that resampling only the fitness values of the four centroids in the outer ES slightly improves the compliance of the dynamics. However, in the long-run the deviations occur again. But the fluctuations in the μ dynamics appear smaller and accordingly the distance to the theoretically predicted steady-state distance slightly reduces. The agreement of the dynamics might be further improved by increasing the number of reevaluations, or by making use of resampling at every single function evaluation within the algorithm. This way of proceeding would provide a much higher effort in terms of function evaluations as the original $[1, 4(\mu/\mu_I, \lambda)^\gamma]$-meta-ES (Alg. 7.1) is already requiring $4\lambda\gamma$ function evaluations per isolation period.

7.6. Summary

This chapter investigated the ability of a $[1, 4(\mu/\mu_I, \lambda)^\gamma]$-meta-ES to simultaneously control the population size μ and the mutation strength σ on the noisy sphere model. In particular, under the influence of fitness noise with constant variance. A theoretical analysis of the strategy's adaptation behavior has been presented. Considering asymptotically exact approximations the general behavior of the population size and the mutation strength dynamics has been calculated. While the population size (μ) dynamics increase exponentially fast up to the predefined μ-bound, the σ dynamics exhibit a one over square root law when approaching the steady state. Accordingly, the approach to the steady state is rather slow.

The derivations presented assumed an error-free selection process in the meta strategy. In that point, the analysis deviates from the real meta-ES. This deviation is the main reason for the deviations observed when comparing the theoretical results with real meta-ES experiments. One might consider incorporating the noisy selection process of the outer ES in the analysis. This way the theoretical model would gain accuracy in reproducing the experimental dynamics. However, this is not considered to be a reasonable direction of research since it would only describe the behavior of a suboptimally performing ES variant.

The results rather indicate that the considered meta-ES variant is not well suited for this noisy optimization problem. This leads to the question how to change the meta-ES algorithmically such that it exhibits a better long-term behavior. That is, the selection process of the outer ES must be improved. The adjustments presented are either unsuccessful or they are gaining leverage only connected to a very high effort in terms of function evaluations. For that reason, it is arguable to search for other ES variants methods that offer a higher potential to successfully deal with noise disturbances than the proposed meta ES variant. A promising step in that direction is presented in the next chapter of this thesis.

8. The population control CMSA-ES on the noisy ellipsoid model

8.1. Introduction

Addressing the problem of fitness noise on the ellipsoid model, see Sec. 6.2, this chapter introduces an ES that is able to deal with the disturbances related to the mentioned noise models. As the σ self-adaptation exhibits a favorable bias on the mutation strength adaptation in noisy environments, [Hansen, 2006a], the covariance matrix self-adaptation ES is considered to provide the basis of the newly proposed algorithm.

The strategy employs a detection mechanism that is able to identify noise disturbances. The noise detection is based on a linear regression analysis of the noisy fitness dynamics observed during the evolution of the CMSA-ES population. Estimating the slope of the linear regression line, the direction of the trend can be determined by computation of a confidence interval on the slope estimator. This way, the algorithm is able to infer whether the trend of the fitness dynamics exhibits decreasing tendencies or not. The strategy allows for the detection of noise influences on the Evolution Strategy's progress. Thus the resulting algorithm is able to take remedial actions by increasing the population size in the case that progress stagnations or divergence behavior are caused by noise influences. Conversely, the algorithm is designed to reduce the population size again, once the noise influences, i.e. stagnations or divergence behavior, have been overcome by a predefined amount of time.

Acting this way, the population control CMSA-ES (pcCMSA-ES), adapts a beneficial population size during the evolutionary process. In contrast to the $[1, 4(\mu/\mu_I, \lambda)^\gamma]$-meta-ES, the population control does not only rely on a single measurement, but on the observed trend of a whole fitness sequence. Hence, the adaptation decision is less exposed to the noise perturbations. Accordingly, the pcCMSA-ES reveals a great performance improvement. However, a theoretical analysis of the respective approach is substantially more difficult. Therefore, as a proof of concept, the approach is validated by empirical investigations.

The applicability of the proposed algorithm is demonstrated on the noisy ellipsoid model considering the two contrasting noise variants motivated in Sec. 6. Providing the basis of the newly designed algorithm the considered $(\mu/\mu_I, \lambda)$-CMSA-ES together with illustrations of its general behavior in noisy fitness environments are briefly recapped in Sec. 8.2. The noise detection by linear regression analysis is presented and applied to the CMSA-ES in Sec. 8.3, and Sec. 8.4, respectively. Finally, simulations on the ellipsoid model are provided in Sec. 8.5. The observed behavior of the CMSA variant agrees with existing theoretical predictions, see [Arnold, 2002; Beyer and Sendhoff, 2006; Beyer et al., 2005]. The chapter concludes with a discussion of the simulation results that yield a remarkable observation in

the context of additive fitness noise. That is, investigating the Simple Regret performance dynamics 6.3.2, the pcCMSA-ES reaches a slope of -1 approximately for a sufficiently large number of function evaluations n. This is in contrast to a Theorem in Astete-Morales et al. [2015] already mentioned before in Sec. 6.3.2.

8.2. The CMSA-ES

The method for noise handling developed in this chapter is integrated into the CMSA-ES. Hence, the standard CMSA-ES is reviewed in this section to accentuate the necessary adjustments presented in the following sections. The corresponding pseudo code of the $(\mu/\mu_I, \lambda)$-CMSA-ES is displayed in Alg. 8.1.

In each iteration the $(\mu/\mu_I, \lambda)$-CMSA-ES generates λ offspring candidate solutions with individual mutation strength σ_l sampled from a log-normal distribution (line 4). The mutation strength can be interpreted as an individual scaling factor. Within the algorithm it is controlled by the learning parameter τ_σ. The standard choice of this learning parameter is $\tau_\sigma = 1/\sqrt{2N}$. Additionally, a random vector $\boldsymbol{s}_l - b - ax_i$ is sampled from a normal distribution with the covariance matrix $\boldsymbol{C}$. This covariance matrix is adapted during the algorithm in order to take into account the distribution of previously generated successful candidate solutions. The mutation vector $\boldsymbol{z}_l$ of each offspring is determined by the product $\sigma_l \boldsymbol{s}_l$. Finally, the new offspring is created by adding the mutation vector to the parental centroid of the prior generation and its fitness evaluated. The features of the best μ of of λ offspring are passed to the subsequent generation, i.e. the mutation strength centroid $\langle\sigma\rangle$ and the parameter vector centroid $\langle\boldsymbol{y}\rangle$, respectively. The covariance matrix is updated according to the rule in line 14 at the end of each generation generation. This procedure is repeated until a termination criterion is met.

Algorithm 8.1 The pseudo code of the standard $(\mu/\mu_I, \lambda)$-CMSA-ES.

1: Initialization: $g \leftarrow 0$; $\langle\sigma\rangle \leftarrow \sigma^{(init)}$; $\langle\boldsymbol{y}\rangle \leftarrow \boldsymbol{y}^{(init)}$; $C \leftarrow \boldsymbol{I}$;
2: **repeat**
3: **for** $l \leftarrow 1$ to λ **do**
4: $\sigma_l \leftarrow \langle\sigma\rangle \mathrm{e}^{\tau_\sigma \mathcal{N}(0,1)}$
5: $\boldsymbol{s}_l \leftarrow \sqrt{C}\mathcal{N}(\boldsymbol{0}, \boldsymbol{I})$
6: $\boldsymbol{z}_l \leftarrow \sigma_l \boldsymbol{s}_l$
7: $\boldsymbol{y}_l \leftarrow \langle\boldsymbol{y}\rangle + \boldsymbol{z}_l$
8: $f_l \leftarrow f(\boldsymbol{y}_l)$
9: **end for**
10: $g \leftarrow g + 1$
11: $\langle\boldsymbol{z}\rangle \leftarrow \frac{1}{\mu}\sum_{m=1}^{\mu} \boldsymbol{z}_{m;\lambda}$
12: $\langle\sigma\rangle \leftarrow \frac{1}{\mu}\sum_{m=1}^{\mu} \sigma_{m;\lambda}$
13: $\langle\boldsymbol{y}\rangle \leftarrow \langle\boldsymbol{y}\rangle + \langle\boldsymbol{z}\rangle$
14: $C \leftarrow \left(1 - \frac{1}{\tau_c}\right) C + \frac{1}{\tau_c}\langle\boldsymbol{s}\boldsymbol{s}^\top\rangle$
15: **until** termination condition

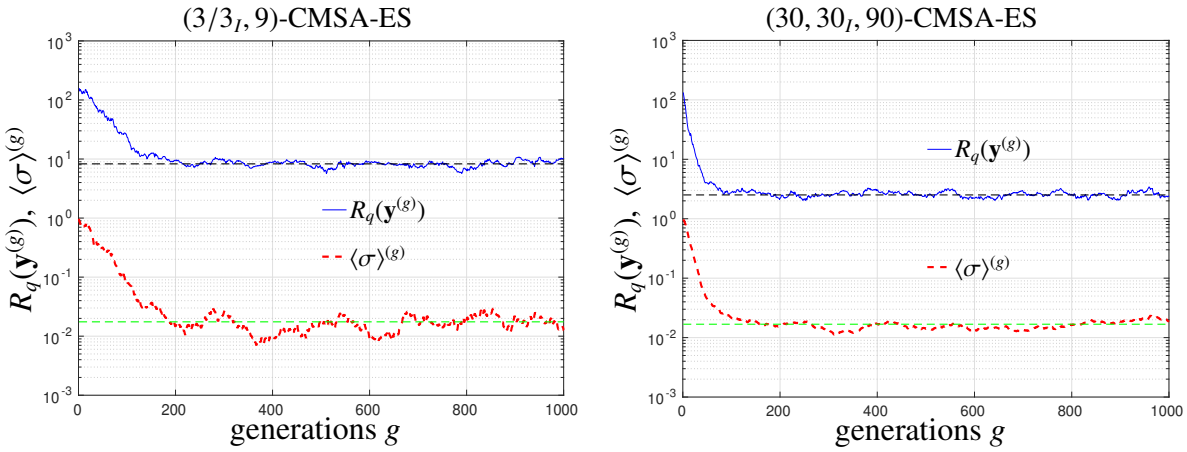

Figure 8.1.: The illustration of the CMSA-ES dynamics on the noisy ellipsoid model with noise of constant variance $\sigma_\epsilon = 1$. The black and green dashed lines display the theoretically expected steady state quantities of the respective dynamics, cf. 6.4.1. The exemplary runs are initialized using $\sigma^{(init)} = 1$, $\boldsymbol{y}^{(init)} = \mathbf{1} \in \mathbb{R}^N$, as well as the standard recommendation of $\tau_\sigma = 1/\sqrt{2N}$.

An intuition of the CMSA-ES dynamics on the noisy ellipsoid model is provided in Fig. 8.1 and Fig. 8.2. Fig. 8.1 illustrates the typical behavior of Alg. 8.1 under the influence of fitness noise of constant variance (6.2). The impact of distance proportional fitness noise (6.3) on the CMSA-ES dynamics is demonstrated in Fig. 8.2. To that point, a $(\mu/\mu_I, \lambda)$-CMSA-ES is applied to the noisy ellipsoid model $q_i = i$, $i = 1, \ldots, N$ in search space dimension $N = 40$, cf. Eq. (6.1).

In Fig. 8.1 the mutation strength dynamics as well as the residual distance dynamics are displayed considering noise of constant variance $\sigma_\epsilon = 1$. Taking a look at the dynamics of the parental centroid's weighted distance to the optimizer

$$R_q(\mathbf{y}^{(g)}) = \sqrt{\sum_{j=1}^{N} q_j^2 y_j^{(g)^2}}$$

it can be seen that the $(3/3_I, 9)$-CMSA-ES approaches its theoretically derived residual steady sate distance R_{ss}, cf. Eq. (6.16), that is displayed by the dashed black horizontal line. Increasing the population sizes to $\mu = 30$ and $\lambda = 90$ results in a distinct reduction of this residual steady state distance. This observation substantiates both the correctness of the steady state formula (6.16) as well as the assertion that an increase of the population sizes is able to improve the ultimately realized distance to the optimizer. At the same time, the mutation strength dynamics approach their steady state σ_{ss} which has been computed in Eq. (6.20) under the assumption of a disabled covariance matrix adaptation. That is, in order to illustrate the compliance of the theoretical prediction in Eq. (6.20) with experimental runs, the covariance matrix update in Alg. 8.1 has been turned off for the creation of the exemplary illustration of the CMSA-ES behavior in Fig. 8.1 and Fig. 8.2. Notice that, enabling the covariance matrix update would not substantially modify the qualitative behavior of the strategy in this scenario. Additionally, in the cases of rather large population

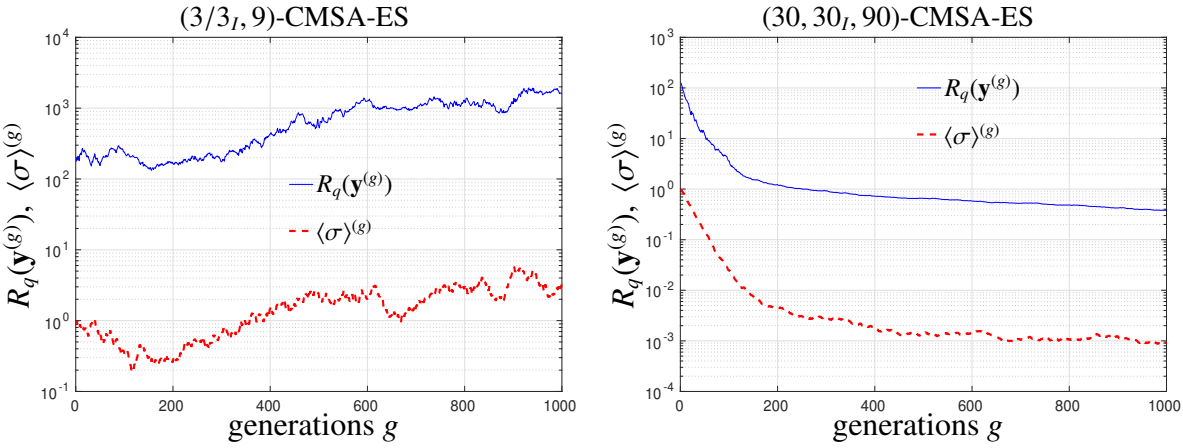

Figure 8.2.: The illustration of the CMSA-ES dynamics on the noise ellipsoid model with noise of constant normalized variance $\sigma_\epsilon^* = 5$. The exemplary runs of Alg. 8.1 are initialized using $\sigma^{(init)} = 1$, $\boldsymbol{y}^{(init)} = \mathbf{1} \in \mathbb{R}^N$, as well as the standard recommendation of $\tau_\sigma = 1/\sqrt{2N}$.

sizes, strong noise influence on the covariance matrix adaptation might cause the mutation strength dynamics to diverge.

Further on, Fig. 8.2 focuses on the distance proportional noise case with $\sigma_\epsilon^* = 5$. Again the $R_q(\mathbf{y}^{(g)})$ and the $\langle\sigma\rangle^{(g)}$ dynamics of the $(\mu/\mu_I, \lambda)$-CMSA-ES with two different population size settings are presented. It can be observed that the $(3/3_I, 9)$-CMSA-ES on the left-hand side is not able to achieve an improvement towards the optimizer. Instead, due to the strong noise influence at the starting distance from the optimizer it exhibits a certain divergence behavior. That is, the parental population size is too small to sufficiently satisfy condition (6.23), i.e. $\mu \gg \sigma_\epsilon^*/(2c_{\mu/\mu,\lambda})$. Making use of larger populations on the right-hand side of Fig. 8.2 the strategy successfully overcomes the initial strong noise region. As the noise becomes less pronounced when shortening the distance $R_q(\mathbf{y}^{(g)})$ the $(30/30_I, 90)$-CMSA-ES is able to gradually approach the optimizer. Hence, the benefits of a population size enlargement are also observable for the noise model of constant normalized noise variance.

For both noise models the theoretical investigations imply that a rise of the population size is able to improve the Evolution Strategy's progress towards the optimizer. However, to prevent an excess of function evaluations, the rational point in the optimization process at which the population size should be increased still has to be determined. This problem is addressed within the next section.

8.3. Stagnation detection by use of linear regression analysis

Stagnation or divergence behavior is accompanied by a non-negative trend within the observed fitness value dynamics of the ES (minimization considered). For trend analysis a regression model of the parental centroid fitness sequence of length L is used. If the slope

of this model is *significantly* negative, the ES converges. In the opposite case, the population size must be increased. The decision will be based on statistical hypothesis testing.

Considering a not too long series of observed parental centroid fitness values, the observed time series can be approximated piecewise by a linear regression model. That is, a straight line is fitted through a set of L data points $\{(x_i, y_i),\ i = 1, \ldots, L\}$ in such a manner that the sum of squared residuals of the model

$$y_i = ax_i + b + \epsilon_i \tag{8.1}$$

is minimal. Here ϵ_i models the random fluctuations. Determining the optimal a and b is a standard task yielding [Kenney, 2013]

$$\hat{a} = \frac{\sum_{i=1}^{L}(x_i - \bar{x})(y_i - \bar{y})}{\sum_{i=1}^{L}(x_i - \bar{x})^2} \qquad \text{and} \qquad \hat{b} = \bar{y} - \hat{a}\bar{x}, \tag{8.2}$$

where $\bar{x}$ and $\bar{y}$ represent the sample means of the observations. Due to the ϵ_i random fluctuations the *estimate* $\hat{a}$ itself is a random variate. Therefore, the real (but unknown) a value can only be estimated by use of a confidence interval. Assuming L sufficiently large, the central limit theorem guarantees that the estimator $\hat{a}$ of a is asymptotically normally distributed with mean a. Thus, the sum of squared residuals $\sum_{i=1}^{L}(y_i - b - ax_i)^2$ is distributed proportionally to χ^2_{L-2} with $L - 2$ degrees of freedom and is independent of $\hat{a}$, cf. [Kenney, 2013]. This allows to construct a test statistic

$$T_{L-2} = \frac{\hat{a} - a}{s_{\hat{a}}} \qquad \text{with} \qquad s_{\hat{a}} = \sqrt{\frac{\sum_{i=1}^{L}(y_i - \hat{b} - \hat{a}x_i)^2}{(L-2)\sum_{i=1}^{L}(x_i - \bar{x})^2}}, \tag{8.3}$$

where T_{L-2} is a t-distributed random variate with $L - 2$ degrees of freedom [Kenney, 2013].

Since $\hat{a}$ is a random variate, an observed $\hat{a} < 0$ does not guarantee convergence. Therefore, a hypothesis test will be used to put the decision on a statistical basis. Let $\mathrm{H}_0 : a \geq 0$ be the hypothesis that the ES increases the population size (because of non-convergence). We will only reject H_0 if there is significant evidence for the alternative $\mathrm{H}_1 : a < 0$. (In the latter case, the population size will not be increased.) That is, a left tailed test is to be performed with a significance level α (probability of wrongly rejecting H_0), i.e. $\Pr[\hat{a} < c|\mathrm{H}_0] = \alpha$, where c is the threshold (to be determined) below which the correct H_0 is rejected with error probability α. Resolving the left equation in (8.3) for $\hat{a}$ yields $\hat{a} = a + s_{\hat{a}}T_{L-2}$ and therefore $\Pr[a + s_{\hat{a}}T_{L-2} < c|\mathrm{H}_0] = \alpha$. This is equivalent to $\Pr[T_{L-2} < (c - a)/s_{\hat{a}}|\mathrm{H}_0] = \alpha$. Noting that $\Pr[T_{L-2} < (c - a)/s_{\hat{a}}] = F_{T_{L-2}}((c - a)/s_{\hat{a}})$ is the cdf of T_{L-2}, one can apply the quantile function yielding $(c - a)/s_{\hat{a}} = t_{\alpha;L-2}$, where $t_{\alpha;L-2}$ is the α quantile of the t-distribution with $L - 2$ degrees of freedom. Solving for c one obtains $c = a + s_{\hat{a}}t_{\alpha;L-2}$. Thus, $c \geq s_{\hat{a}}t_{\alpha;L-2}$ and as threshold ($a = 0$) one gets $c = s_{\hat{a}}t_{\alpha;L-2}$. That is, if

$$\hat{a} < s_{\hat{a}}t_{\alpha;L-2} \tag{8.4}$$

H_0 is rejected indicating a significant negative trend (i.e., convergence towards the optimizer, no population size increase needed).

8.4. The population control CMSA-ES algorithm

Combining the convergence hypothesis test of Sec. 8.3 with the basic $(\mu/\mu_I, \lambda)$-CMSA-ES introduced in [Beyer and Sendhoff, 2008] an ES with adaptive population size control, the *population control* (pc)CMSA-ES is presented in Alg. 8.2. Until the algorithm has generated a list $\mathcal{F}$ of L parental centroid function values an ordinary CMSA-ES run with truncation ratio ϑ is performed over L generations: In each generation the $(\mu/\mu_I, \lambda)$-CMSA-ES generates λ offspring with individual mutation strengths σ_l, see lines 4 to 10. The mutation strength σ_l can be interpreted as an individual scaling factor that is self-adaptively evolved using the learning parameter $\tau_\sigma = \frac{1}{\sqrt{2N}}$ (N – search space dimension). The mutation vector $\boldsymbol{z}_l$ of each offspring depends on the covariance matrix $\boldsymbol{C}$ which corresponds to the distribution of previously generated successful candidate solutions. The update rule can be found in line 30 where $\tau_c = 1 + \frac{N(N+1)}{2\mu}$ is used. After creation of the offspring, the objective function (fitness) values are calculated. Having completed the offspring population, the algorithm selects those μ of the λ offspring with the best (noisy) fitness values $\tilde{F}_{m;\lambda}$, $m = 1, \ldots, \mu$. Notice, $m;\lambda$ denotes the mth best out of λ individuals. Accordingly, the notation $\langle . \rangle$ refers to the construction of the centroid of the respective values corresponding to the μ best offspring solutions. For example, the centroid of the mutation strengths is $\langle \sigma \rangle = \frac{1}{\mu} \sum_{m=1}^{\mu} \sigma_{m;\lambda}$. Subsequently, the pcCMSA-ES examines the list $\mathcal{F}$ using the linear regression approach. The hypothesis test (8.4) is implemented within the program `detection`($\mathcal{F}_{int}, \alpha$), line 19. Analyzing the fitness interval $\mathcal{F}_{int}$, it returns the decision variable $td = 1$ if (8.4) is fulfilled, else $td = 0$. The parameter α refers to the significance level of the hypothesis test. As long as a negative trend is detected the algorithm acts like the original CMSA-ES. Indication of a non-negative trend ($td = 0$) leads to an increase of the population size μ by multiplication with the factor $c_\mu > 1$, line 21, keeping the truncation ratio $\vartheta = \mu/\lambda$ constant by line 4. In order to prevent the next hypothesis test from being biased by old fitness values, the detection procedure is interrupted for L generations (line 26). Additionally, the covariance matrix adaptation in line 30 is turned off, once the algorithm has encountered significant noise impact. For this purpose, the parameter $adjC$ is set to zero in line 22. Stalling the covariance matrix update is necessary to avoid a random matrix adaptation process resulting in a rise of the condition number of $\boldsymbol{C}$ without gaining any useful information from the noisy environment.

In the case the hypothesis test returned $td = 1$, i.e. (8.4) is fulfilled, there is a significant convergence trend. In such a situation one can try to minimize the efforts and reduce the population size in line 24. Such a reduction can make sense in the distance dependent noise case (6.2) where there is a minimal population size above which the ES converges without further population size increase. That is, the pcCMSA-ES increases first the population size aggressively and after reaching convergence, the population size is slowly decreased to its nearly optimal value. Hence, the reduction factor b_μ should be related to that of c_μ, e.g. $b_\mu = \sqrt[k]{c_\mu}$ ($k = 2$, or 3), or can be chosen independently, but should fulfill $b_\mu < c_\mu$.

Regarding fitness environments where the ES has to deal temporarily with noisy regions, it might be beneficial to turn the covariance matrix adaptation on again once the ES has left the noisy region. That is if a significant negative trend is present again the parameter $adjC$ should be reset to one in order to gain additional information about advantageous search

Algorithm 8.2 The pcCMSA Evolution Strategy. The linear regression analysis method for progress stagnation identification is implemented within the subroutine `detection`($\boldsymbol{F}_{int}, \alpha$).

Initialization: $g \leftarrow 0$; $wait \leftarrow 0$; $\langle\sigma\rangle \leftarrow \sigma^{(init)}$; $\langle\boldsymbol{y}\rangle \leftarrow \boldsymbol{y}^{(init)}$;
  $\mu \leftarrow \mu^{(init)}$; $\mu_{\min} \leftarrow \mu^{(init)}$; $\boldsymbol{C} \leftarrow \boldsymbol{I}$; $adjC \leftarrow 1$; $\mathcal{F} = \{\}$
repeat
  $\lambda \leftarrow \lfloor \mu/\vartheta \rfloor$
  for $l \leftarrow 1$ to λ **do**
    $\sigma_l \leftarrow \langle\sigma\rangle \mathrm{e}^{\tau_\sigma \mathcal{N}(0,1)}$
    $\boldsymbol{s}_l \leftarrow \sqrt{\boldsymbol{C}}\mathcal{N}(\boldsymbol{0}, \boldsymbol{I})$
    $\boldsymbol{z}_l \leftarrow \sigma_l \boldsymbol{s}_l$
    $\boldsymbol{y}_l \leftarrow \langle\boldsymbol{y}\rangle + \boldsymbol{z}_l$
    $\tilde{F}_l \leftarrow \tilde{F}(\boldsymbol{y}_l)$
  end for
  $g \leftarrow g + 1$
  $\langle\boldsymbol{z}\rangle \leftarrow \frac{1}{\mu}\sum_{m=1}^{\mu} \boldsymbol{z}_{m;\lambda}$
  $\langle\sigma\rangle \leftarrow \frac{1}{\mu}\sum_{m=1}^{\mu} \sigma_{m;\lambda}$
  $\langle\boldsymbol{y}\rangle \leftarrow \langle\boldsymbol{y}\rangle + \langle\boldsymbol{z}\rangle$
  add $\tilde{F}(\langle\boldsymbol{y}\rangle)$ **to** $\mathcal{F}$
  if $g > L \wedge wait = 0$ **then**
    $\mathcal{F}_{int} \leftarrow \mathcal{F}(g - L : g)$
    $td \leftarrow$ `detection`$(\mathcal{F}_{int}, \alpha)$
    if $td = 0$ **then**
      $\mu \leftarrow \mu c_\mu$
      $adjC \leftarrow 0$
    else
      $\mu \leftarrow \max\left(\mu_{\min}, \lfloor \mu/b_\mu \rfloor\right)$
    end if
    $wait \leftarrow L$
  else
    $wait \leftarrow wait - 1$
  end if
  $\boldsymbol{C} \leftarrow \left(1 - \frac{1}{\tau_c}\right)^{adjC} \boldsymbol{C} + \frac{adjC}{\tau_c}\langle \boldsymbol{s}\boldsymbol{s}^\top \rangle$
until termination condition
return $\langle\boldsymbol{y}\rangle$

directions. This can easily be obtained by inserting $adjC \leftarrow 1$ after line 24. However, as for the noisy fitness environments considered here, this adjustment is not able to provide significant improvements in terms of the ES's progress and therefore has not been implemented. Its influence on the performance in the context of disparate optimization problems remains to be investigated in future studies.

8.5. Experimental investigations

The behavior of the proposed pcCMSA-ES algorithm is investigated on the noisy ellipsoid model (6.1)

$$F(\boldsymbol{y}) = \sum_{i=1}^{N} q_i y_i^2 \tag{8.5}$$

with noise types (6.2) and (6.3). Especially, the cases $q_i = 1$ (sphere model) and $q_i = i, i^2$ are considered in this and the following section. In the simulations resulting in Fig. 8.3 the pcCMSA-ES is initialized with standard parameter settings in search space dimension $N = 40$. The initial mutation strength is set to $\sigma^{(init)} = 1$ and the optimization starts at search space parameter vector $\boldsymbol{y}^{(init)} = \mathbf{1}$.

The initial population sizes are set to $\mu = 3$ and $\lambda = 9$. Accordingly, the truncation ratio $\vartheta = \frac{\mu}{\lambda} = \frac{1}{3}$ is kept constant during all pcCMSA-ES runs. As a first choice, the distance proportional factors that control the rise and decline of the population sizes are $c_\mu = 2$, and $b_\mu = \sqrt{c_\mu}$, respectively. Further, the length L of the $\tilde{F}$-data collection phases has to chosen long enough to ensure a sufficient F improvement as well as reliable hypothesis test result. As demonstrated in [Beyer and Melkozerov, 2014], the effort to get an expected relative F improvement is proportional to the quotient of the trace of the Hessian of F and its minimal eigenvalue. Hence, for the sphere the effort is proportional to N and for the $q_i = i^2$ ellipsoid proportional to $\Sigma q := \sum_{i=1}^{N} q_i$. In the experiments $L = \Sigma q$ is used. The significance level of the hypothesis test in line 19 of Alg. 8.2 is $\alpha = 0.05$.

Taking a look at Fig. 8.3, the solid blue lines represent the $R_q(\mathbf{y}^{(g)})$ dynamics while the $\langle\sigma\rangle^{(g)}$ dynamics are illustrated using dashed red lines. The left-hand graph displays the dynamics resulting from fitness noise of constant noise variance $\sigma_\epsilon = 1$. In the right-hand graph, the distance proportional noise of constant normalized noise variance $\sigma_\epsilon^* = 5$ is depicted.

For the additive noise model ($\sigma_\epsilon = 1$), a decline of the residual distance to the optimizer comes with the (successive) increase of the population size. This population size dynamic is implicitly provided by the solid black step function that illustrates the theoretical residual steady state distance (6.16) overlaying the $R_q(\mathbf{y}^{(g)})$ dynamics. This distance is reached by the CMSA-ES after a sufficiently long generation period (keeping μ and λ constant). Since the pcCMSA-ES changes the population size successively, the theoretical estimate (6.16) can be used to check whether the population size dynamics of the pcCMSA-ES works satisfactorily. That is, after the pcCMSA-ES has approached the residual distance corresponding to its current population size the algorithm is able to detect the respective stagnation and consequently increases the population size. Acting this way, the pcCMSA is able to approach a lower residual steady state distance during the subsequent generations. Interestingly, the decline of the residual distance is not followed by the strategy's mutation strength dynamics.

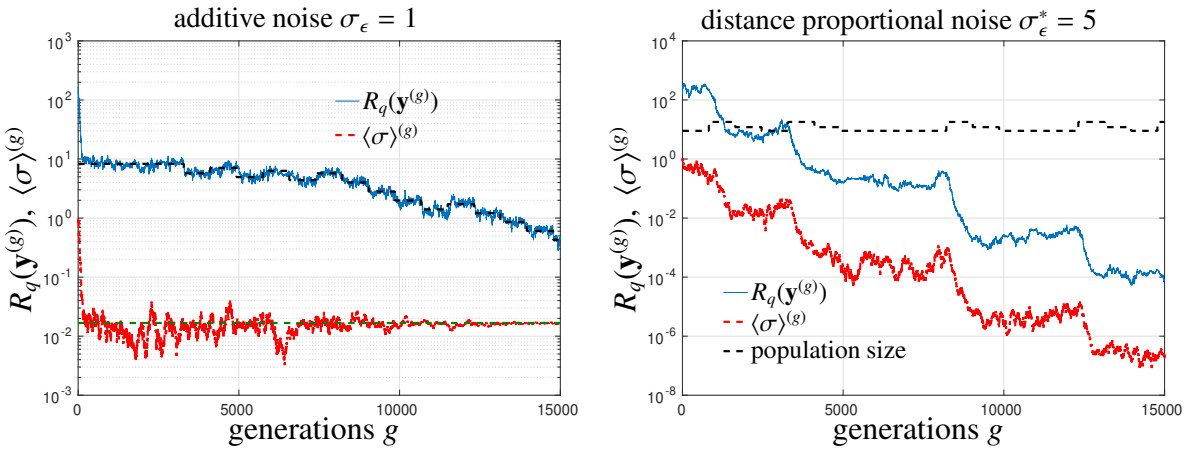

Figure 8.3.: The dynamics of the (μ, μ_I, λ)-pcCMSA-ES subject to additive fitness noise of strength $\sigma_\epsilon = 1$ and distance proportional noise of normalized noise strength $\sigma_\epsilon^* = 5$ is illustrated on the noisy ellipsoid model with coefficients $q_i = i$.

The $\langle\sigma\rangle$ dynamics rather approaches a steady state behavior. Notice that for reasons of compliance with the illustrations of the standard CMSA-ES in Fig. 8.1, the covariance matrix update of Alg. 8.2 has been turned off during the simulation. Accordingly, even though the pcCMSA-ES successively approaches the optimizer the predicted mutation strength steady state $\langle\sigma\rangle_{ss}$ in Eq. (6.20) is also reached on the left-hand side of Fig. 8.3. This behavior is more closely examined in the following section.

Having a look at the distance proportional noise case ($\sigma_\epsilon^* = 5$) on the right-hand side of Fig. 8.3, both dynamics decrease almost in parallel with the number of generations. The corresponding offspring population size dynamics ($\lambda = \mu/\vartheta$) of the pcCMSA-ES run is displayed by the dashed black step function. After the first $L = \Sigma q$ function evaluations the strategy identifies no significant progress towards the optimizer. Hence, the population sizes are increased (keeping $\vartheta = 1/3$ constant). In accordance with the evolution condition (6.23) for the distance proportional noise model, the result is a distinct decline of the residual distance. Approaching the optimizer, the mutation strength adaptation reduces the $\langle\sigma\rangle$ values. As the observed fitness sequence suggests a significantly negative slope the population size is gradually reduced after the following test decisions until the initial population size is reached again and the noise influence begins to predominate again. Conclusively, the proceeding is repeated. This results in the population size fluctuations and the successive decline of the $R_q(\mathbf{y}^{(g)})$ and $\langle\sigma\rangle^{(g)}$ dynamics being observable in Fig. 8.3.

Taken as a whole, the illustrations in Fig. 8.3 demonstrate the ability of the pcCMSA-ES algorithm to identify noise related stagnations in the observed fitness sequence and to adequately control the population sizes. This way, convergence in direction of the optimizer on the noisy ellipsoid model (6.1) is ensured. In the next section, these observations are confirmed by considering the ellipsoid models $q_i = 1, i^2$ and the remarkable implication of the pcCMSA-ES convergence behavior on theoretical runtime results is discussed.

8.6. Inspecting the simple regret dynamics

The dynamical behavior observed in Fig. 8.3 is substantiated by the dynamics illustrated in Fig. 8.4 and 8.5. There, the sphere model $q_i = 1$ as well as the ellipsoid model $q_i = i^2$ are considered. Figure 8.4 shows the pcCMSA-ES dynamics for the (6.2) case of constant $\sigma_\epsilon = 1$ noise. By contrast, Fig. 8.5 displays the distance proportional noise (6.3) case. Apart from providing an extra proof of concept for the ability of the pcCMSA-ES to deal with perturbations caused by both noise models, the figures are aiming at the inspection of the Simple Regret dynamics, cf. Eq. (6.10). In order to be able to take the corresponding theoretically assertion by [Astete-Morales et al., 2015], see 6.3.2, correctly into account all dynamics are plotted against the number of function evaluations. Particularly under noise of constant variance, the pcCMSA exhibits a remarkable convergence behavior.

In the simulations the pcCMSA-ES is initialized with standard parameter settings and $\sigma^{(init)} = 1$ at $\boldsymbol{y}^{(init)} = \mathbf{1}$ in search space dimension $N = 30$. The initial population sizes are set to $\mu = 3$ and $\lambda = 9$ resulting in a truncation ratio $\vartheta = \frac{\mu}{\lambda} = \frac{1}{3}$ during the runs. The population size factors are $c_\mu = 2$ and $b_\mu = \sqrt{c_\mu}$. The significance level of the hypothesis test in line 19 of Alg. 8.2 is $\alpha = 0.05$. The length L of the $\tilde{F}$-data collection phases is chosen as $L = 5N$ and $L = \Sigma q$ in the experiments.

Considering the sphere model as well as the ellipsoid model $q_i = i^2$ with search space dimensionality $N = 30$, in Fig. 8.4 four dynamics are plotted against the number of function evaluations n: the noise-free fitness of the parental centroid $\mathrm{SR}(n) = f(\langle \boldsymbol{y} \rangle)$ (blue), the corresponding weighted residual distance $R_q(n) = R_q(\langle \boldsymbol{y} \rangle)$ (red), and the mutation strength $\langle \sigma \rangle$ (green). The solid black step function predicts the residual steady state distance according to Eq. (6.16). In both cases, it is steadily reduced with each μ elevation.

Considering the simple regret curves (blue) in Fig. 8.4, after a transient phase one observes that the ES on average continuously approaches the optimizer at a linear order in the log-log-plot. That means that $\mathrm{SR}(n) \propto n^a$ with $a < 0$. The parallel decreasing dashed (magenta) lines $h(n) \propto n^{-1}$ indicate that the pcCMSA-ES actually realizes an $a \approx -1$. Fitting linear curves (solid magenta) to those $\mathrm{SR}(n)$ graphs, using the technique described by Eqs. (8.1)–(8.3), one can calculate the confidence intervals for a given confidence level, e.g. 95%, which is displayed in Fig. 8.4. The observation of $a \approx -1$ is remarkable since it apparently seems to violate the theorem by [Astete-Morales et al., 2015] that states that "Simple ES" can only reach a slope $a > -\frac{1}{2}$. The authors even supported their theorem with experiments regarding a tailored (1 + 1)-ES with resampling that came close to $-\frac{1}{2}$ and the UH-CMA-ES [Hansen et al., 2009] that produced only a-values in the range of -0.1 to -0.3. Having a closer look at the assumptions made to prove the theorem, one finds the reason in the definition of "Simple ES". It contains a common assumption regarding the operation of ES – the scale invariance of the mutations. Roughly speaking, the expected value of the mutation strength should scale with the distance to the optimizer. That is, as the strategy approaches the optimizer, the mutation strength should be shrinking. Looking at the (green) $\langle \sigma \rangle$ dynamics in Fig. 8.4 one sees that this assumption does not hold for the pcCMSA-ES. Remarkably, $\langle \sigma \rangle$ reaches a constant steady state value. Since theorems cannot be wrong, unlike the (1 + 1)-ES and the UH-CMA-ES, the pcCMSA-ES does not match the definition of a "Simple ES". While the pcCMSA-ES approaches a fixed mutation strength, on average it

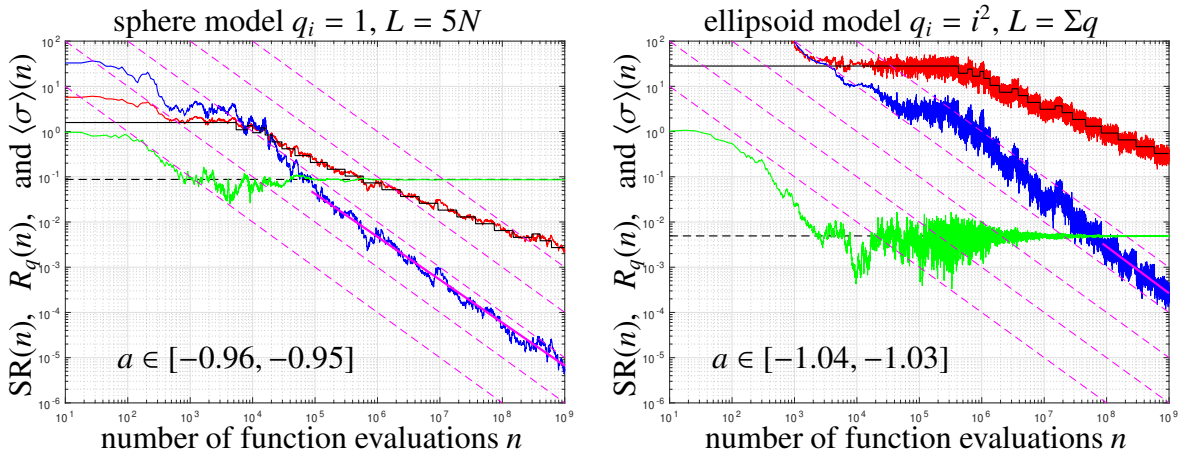

Figure 8.4.: The dynamical behavior of the pcCMSA-ES subject to additive fitness noise of strength $\sigma_\epsilon = 1$.

approaches the optimizer continuously as can be seen in Fig. 8.4 where the dynamics of the weighted residual distance R_q, Eq. (3.25) to the optimizer is displayed (red curves). Alike the situation in Fig. 8.3, the R_q dynamics closely follows the prediction of (6.16) which is displayed as (black) staircase curves.

As a second example, the case of distance dependent noise is considered in Fig. 8.5. The noise variance vanishes when approaching the optimizer. Considering the sphere model as well as the ellipsoid model $q_i = i^2$ with search space dimensionality $N = 30$, again four dynamics are plotted against the number of function evaluations n: the simple regret of the parental centroid $\langle \boldsymbol{y} \rangle$ (blue), the corresponding residual distance $R_q(\langle \boldsymbol{y} \rangle)$ (red), and the mutation strength $\langle \sigma \rangle$ (green). The solid black staircase presents the offspring population size $\lambda = \lfloor \mu/\vartheta \rfloor$. It illustrates the population size adaptation behavior of the pcCMSA-ES.

According to the progress rate theory for the noisy ellipsoid [Melkozerov and Beyer, 2015], the population size needed to ensure convergence can be estimated by considering the evolution condition in Eq. (6.23)

$$4\mu^2 c^2_{\mu/\mu,\lambda} > \sigma^{*2} + \sigma^{*2}_\epsilon. \tag{8.6}$$

Here, the normalized quantities are defined as $\sigma^* := \sigma\Sigma q/R_q$ and $\sigma^*_\epsilon := \sigma_\epsilon \Sigma q/(2R_q^2)$, cf. (3.14) and (6.6). According to Eq. (8.6), the population sizes are increased up to a value where the strategy is able to establish continuous progress towards the optimizer. Afterwards, the population size fluctuates around that specific value.

Figure 8.5 shows the dynamics of the pcCMSA-ES on sphere and ellipsoid ($q_i = i^2$) model with normalized noise strengths $\sigma^*_\epsilon = 10$ and $\sigma^*_\epsilon = 4$, respectively. Taking a look at the solid blue lines representing the simple regret (being the noise-free fitness dynamics $f(\langle \boldsymbol{y} \rangle)$), one observes initially an increase of the parental simple regret. That is, the pcCMSA-ES departs from the optimizer. This is due to the choice of the initial population size of $\mu = 3$, $\lambda = 9$ being too small. However, after the first L generations, the first hypothesis test indicates divergence and the population size μ is increased by a factor $c_\mu = 2$. This increase is repeated two or three times as can be seen considering the (black) staircase curves displaying λ in Fig. 8.5.

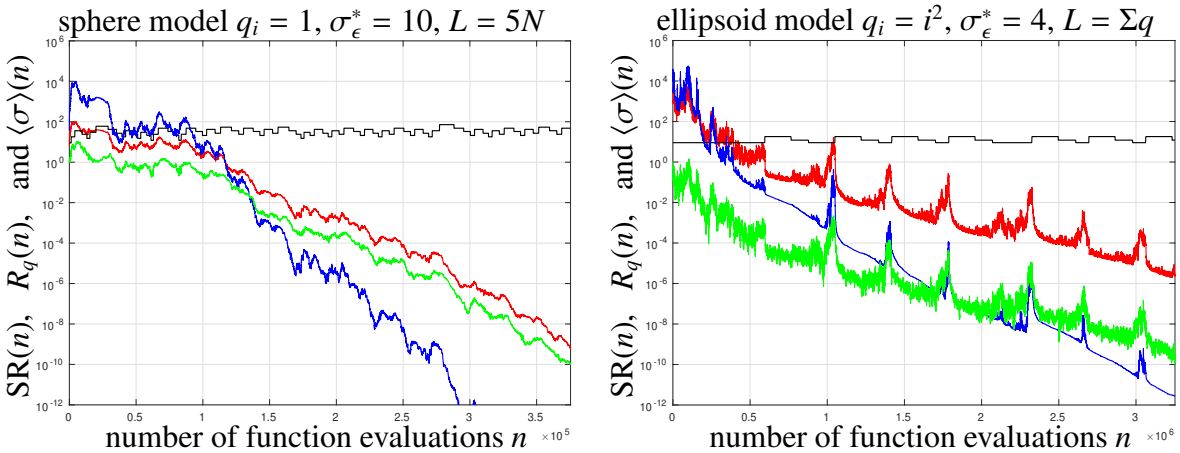

Figure 8.5.: The dynamical behavior of the pcCMSA-ES subject to distance dependent noise of normalized noise strength σ^*_ϵ.

Reaching a population size that guarantees a decline of the SR-curves, see (8.6), the hypothesis test in line 19 of Alg. 8.2 returns 1 (indicating convergence). Accordingly, the population size is reduced again. This behavior is also reflected by the dynamics of the residual distance to the optimizer $R_q(\langle \boldsymbol{y} \rangle)$ (red). This attests that the pcCMSA-ES is able to adapt an appropriate population size needed to comply with Eq. (8.6) rather than simply increasing it arbitrarily. In contrast to the previous case of additive noise, the mutation strength dynamics in Fig. 8.5 indicate a successive reduction of the noise strength σ. This is due to the decreasing influence of the distance dependent noise as the ES approaches the optimizer. In such cases the behavior of a "Simple ES" is desirable. The pcCMSA-ES behaves as such and demonstrates its ability to exhibit a linear convergence order similar to the non-noisy case. However, it has to be pointed out that the current population size reduction rule can result in interrupted convergence behavior in cases of very strong distance dependent noise. This can be inferred from the peaks in the right graph of Fig. 8.5. An attempt to address this disruption would be shortening both the test interval length L as well as the waiting time *wait* of the algorithm after each population size reduction and enlarging them again after a population size escalation, respectively. Also switching off the population size reduction might be a reasonable approach. Eventually, the population size control configuration under severe distance proportional noise should be examined more closely in future investigations.

8.7. Summary

This chapter presented an ES for the treatment of noisy optimization problems that is based on the CMSA-ES. Within its concept a mechanism for identification of noise-related stagnations or divergence behavior is integrated. Consequently, having identified noise related behavior the algorithm increases the size of the parental as well as the offspring population. This way it improves the likelihood to approach closer residual distances to the optimizer. Significant noise disturbances become noticeable by the absence of a clearly negative trend

(minimization considered) within the noisy fitness dynamics. The slope of the trend can be deduced from the corresponding linear regression line. The estimated trend is used in a hypothesis test to decide whether there is convergence to the optimizer. If no further significant noise influences are discovered in subsequent tests the population size is gradually reduced to avoid unnecessary function evaluations. This way the algorithm is capable of adapting the appropriate population size. Accordingly, the adjusted CMSA-ES is denoted population control covariance matrix self-adaptation Evolution Strategy – pcCMSA-ES.

As a proof of concept, the pcCMSA-ES was tested on the noisy ellipsoid model considering two noise models, which obey different characteristics. The additive fitness noise case with constant noise strength σ_ϵ requires a permanent increase of the population size. On the other hand, the distance dependent noise case (which is equivalent to fitness proportionate noise in the case of the sphere model) requires only a limited population size increase. A well-crafted EA should be able to handle both cases (and of course, non-noisy optimization problems as well). The empirical investigation of the strong noise case $\sigma_\epsilon = \text{const.}$ revealed a remarkable behavior of the pcCMSA-ES. The dynamics by which this ES approaches the optimizer seems to be already the fastest one can expect from a direct search algorithm on quadratic functions. The simple regret obeys an n^a dynamics with $a \approx -1$. This is remarkable since "Simple ES" should only allow for an $a \geq -1/2$ no matter how the noise is handled. The reason for this behavior is that unlike "Simple ES" the pcCMSA-ES does not scale the mutation strength σ in proportion to the distance to the optimizer in case of strong noise. This is different to other ESs such as (1 + 1) or UH-CMA. However, if there is no strong noise, pcCMSA-ES behaves like a "Simple ES".

The pcCMSA-ES requires the fixing of additional exogenous strategy parameters. Particularly, the length L of the interval of observed fitness values that are considered in a single test decision has to be examined more closely. L should be large enough to ensure a sufficient evolution (convergence) of the fitness values. From the progress rate theory, it is known that the number of generations needed for a certain fitness improvement scale with the quotient of the trace of the Hessian of F and its smallest eigenvalue. Therefore, L should be chosen proportional to N (search space dimensionality) in the sphere model case and to $\frac{N}{6}(N + 1)(2N + 1)$ in the case of the ellipsoid model $q_i = i^2$. However, in the black-box scenario, the Hessian is not known. However, as long as the initial noise influence is small, the pcCMSA-ES transforms the optimization problem gradually into a local sphere model. In such cases, the $L \propto N$ choice should suffice. If, however, the noise is already strong in the initial phase, there is no definitive choice and the user has to make a guess regarding the trace vs. minimum eigenvalue ratio. Choosing L too large has a negative influence on the efficiency of the ES. It affects the lead time of the algorithm needed to establish an initial interval of fitness observations $\mathcal{F}_{int}$ as well as the waiting time *wait*. The parameter *wait* governs the length of the waiting period after a single population adjustment. After a transient phase of *wait* generations the algorithm starts again with the analysis of the fitness dynamics. It is not evident whether the parameter *wait* should depend on the length L of the fitness interval. The waiting time is essential to prevent wrong test decisions based on fitness dynamics resulting from different population specifications.

9. Outlook

Conclusively, a comprehensive view on forthcoming research connected to the results obtained in the thesis is provided.

The first thesis part addressed the completion of the analyses corresponding to the three most commonly used mutation strength adaptation mechanisms in the context of Evolution Strategies. This task is accomplished with the analysis of the CSA in Chapter 4, and the meta-ES (variant) in Chapter 5, respectively. Although, one could think of the examination of other meta-ES variants. For example, employing additional hierarchical levels for the simultaneous tuning of multiple strategy parameters, like μ or even α. However, this would, of course, result in a rise of the analysis complexity as well as the evaluation costs of the strategy.

The analysis presented concerned the non-noisy fitness case. As a next step, one should investigate noisy fitness functions as well as dynamically changing fitness functions. Furthermore, the analysis approach should also be able to tackle the dynamics of the CMA-ES: The first step has already been completed, the modeling of the cumulative step size adaptation. Thinking of the end-to-end analysis of current state-of-the-art Evolution Strategies, like CMA-ES and CMSA-ES, on the ellipsoid model, the covariance matrix adaptation still remains to be analyzed. Additionally, the theoretical investigations of the mutation strength control still lack analyses of more general test function classes. Also taking into account constrained optimization problems still provides room for elaborate examinations.

Facing with the second part of the thesis, there remains work for future research activities, too. Regarding the noisy ellipsoid model, there is still need for investigations considering other noise models and diverse ES variants for the noise treatment.

For the proposed hierarchical ES in Chapter 7, one may think of various measures how to improve the selection process. Besides considering the resampling of fitness values, one could think of minimal isolation times $\gamma > 1$ to obtain more reliable fitness values (moving average). Making use of racing algorithms also could improve the selection of the inner ES configuration that is best suited to proceed in the noisy environment. However, the ideas to improve the meta-ES variant always come along with increased effort in terms of function evaluations.

Having a look at the pcCMSA-ES, it requires the configuration of the additional exogenous strategy parameters. That is, the length L of the observed fitness sequence $\mathcal{F}_{int}$ that is considered in a single test decision has to be examined more closely. It determines the lead time of the algorithm needed to establish an initial interval of fitness observations $\mathcal{F}_{int}$ as well as the waiting time *wait*. The parameter *wait* governs the length of the waiting period after a single population adjustment. It is necessary to prevent wrong test decisions based on fitness dynamics resulting from diverse population sizes. Still, the question remains whether it is adequate to connect the parameter *wait* to the length L of the fitness

sequence. There are also open questions regarding a profound choice of the population size change parameters c_μ and b_μ and the significance level $\alpha = 0.05$ used. All these questions should be also tackled by extended empirical investigations considering different test functions and noise scenarios. Considering other noise distributions (like Cauchy distributed noise), the pcCMSA-ES will require the use of nonparametric hypothesis tests. To this point, the Mann-Kendall hypothesis test [Mann, 1945] appears to represent an appropriate application. Regarding theory, the analysis of certain aspects of the pcCMSA-ES seems to be possible using and extending the results presented in [Melkozerov and Beyer, 2015]. For example, the derivation of the remarkable, empirically observed, $\mathrm{SR}(n) \propto n^{-1}$ law is clearly another task for future research.

Appendix

Appendix A.

Deriving the CSA dynamics

A.1. The expected value of $||\langle \mathbf{z} \rangle^{(g)}||^2$

This paragraph addresses the calculation of the expected value of $||\langle \mathbf{z} \rangle^{(g)}||^2$. The expected value of the squared Euclidean norm of $\langle \mathbf{z} \rangle^{(g)}$ can be expressed by the sum of the expected values of its squared components $\langle \mathbf{z} \rangle_i^{(g)}$, i.e.

$$\mathrm{E}\left[||\langle \mathbf{z} \rangle^{(g)}||^2\right] = \mathrm{E}\left[\sum_{i=1}^{N} \left(\langle z \rangle_i^{(g)}\right)^2\right] = \sum_{i=1}^{N} \mathrm{E}\left[\left(\langle z \rangle_i^{(g)}\right)^2\right]. \tag{A.1}$$

Each component $\langle \mathbf{z} \rangle_i^{(g)}$ consists of the mean values of the respective components obtained from the μ out of λ most advantageous mutation vectors that found the current parental population. Making again use of the linearity of the expected value operator, the expected value of the squared single components of the mutation vector centroid reads

$$\mathrm{E}\left[\left(\langle z \rangle_i^{(g)}\right)^2\right] = \mathrm{E}\left[\left(\frac{1}{\mu}\sum_{m=1}^{\mu} (\mathbf{z}_{m;\lambda})_i\right)^2\right] = \frac{2}{\mu^2} \underbrace{\mathrm{E}\left[\sum_{l=2}^{\mu}\sum_{m=1}^{l-1} (\mathbf{z}_{l;\lambda})_i (\mathbf{z}_{m;\lambda})_i\right]}_{=\mathrm{E}_1} + \frac{1}{\mu^2} \underbrace{\mathrm{E}\left[\sum_{m=1}^{\mu} (\mathbf{z}_{m;\lambda})_i^2\right]}_{=\mathrm{E}_2} \tag{A.2}$$

The sums of product moments E_1 and E_2 within this equation have been derived in the appendix of [Beyer and Melkozerov, 2014]. Obtained in the asymptotic limit $N \to \infty$ they read

$$\mathrm{E}_1 = \mu(\mu - 1) \frac{e_{\mu,\lambda}^{2,0} q_i^2 y_i^{(g)2}}{\sum_{j=1}^{N} q_j^2 \left(y_j^{(g)2} + \frac{\sigma^{(g)2}}{2}\right)}, \tag{A.3}$$

and

$$\mathrm{E}_2 = \mu \left[1 + \frac{e_{\mu,\lambda}^{1,1} q_i^2 y_i^{(g)2}}{\sum_{j=1}^{N} q_j^2 \left(y_j^{(g)2} + \frac{\sigma^{(g)2}}{2}\right)}\right]. \tag{A.4}$$

Notice that the definition of the general progress coefficients $e_{\mu,\lambda}^{a,b}$ is mentioned in (3.17).

Inserting (A.3), and (A.4), into Eq. (A.2) one obtains

$$\mathrm{E}\left[\left(\langle z \rangle_i^{(g)}\right)^2\right] = \frac{\mu - 1}{\mu} \frac{e_{\mu,\lambda}^{2,0} q_i^2 y_i^{(g)2}}{\sum_{j=1}^{N} q_j^2 \left(y_j^{(g)2} + \frac{\sigma^{(g)2}}{2}\right)} + \frac{1}{\mu}\left[1 + \frac{e_{\mu,\lambda}^{1,1} q_i^2 y_i^{(g)2}}{\sum_{j=1}^{N} q_j^2 \left(y_j^{(g)2} + \frac{\sigma^{(g)2}}{2}\right)}\right], \tag{A.5}$$

and combining the fractions yields

$$\mathrm{E}\left[\left(\langle z\rangle_i^{(g)}\right)^2\right] = \frac{1}{\mu}\left[1 + \frac{q_i^2 y_i^{(g)2}}{R_q^2(\mathbf{y}^{(g)})}\frac{(\mu-1)e_{\mu,\lambda}^{2,0} + e_{\mu,\lambda}^{1,1}}{1 + \frac{\sum_{j=1}^N q_j^2}{R_q^2(\mathbf{y}^{(g)})}\frac{\sigma^{(g)2}}{2}}\right]. \tag{A.6}$$

The aggregation of all N components of the mutation vector centroid yields

$$\mathrm{E}\left[\|\langle\mathbf{z}\rangle^{(g)}\|^2\right] = \frac{1}{\mu}\left(N + \frac{(\mu-1)e_{\mu,\lambda}^{2,0} + e_{\mu,\lambda}^{1,1}}{1 + \frac{\sum_{j=1}^N a_j^2}{R_q^2(\mathbf{y}^{(g)})}\frac{\sigma^{(g)2}}{2}}\right). \tag{A.7}$$

Both expressions, (A.6) and consequently (A.7), can be simplified considerably if the conditions in (3.22) holds. Conclusively, the term $q_i^2 y_i^{(g)2}\left((\mu-1)e_{\mu,\lambda}^{2,0} + e_{\mu,\lambda}^{1,1}\right)$ in Eq. (A.6) can be neglected and the equation reads

$$\mathrm{E}\left[\left(\langle z\rangle_i^{(g)}\right)^2\right] = \frac{1}{\mu}. \tag{A.8}$$

After summing up all components Eq. (A.7) becomes

$$\mathrm{E}\left[\|\langle\mathbf{z}\rangle^{(g)}\|^2\right] = \frac{N}{\mu}. \tag{A.9}$$

This facilitation is asymptotically correct for $N \to \infty$ and will additionally be justified by comparisons of the two different iteratively generated dynamics (using Eq. (A.7) or Eq. (A.9), respectively) with the dynamics of real $(\mu/\mu_I, \lambda)$-CSA-ES runs in Sec. 4.2.

A.2. The expected change of the scalar product

This paragraph is concerned with the calculation of the expected value of the scalar product $\mathbf{s}^{(g)\top}\langle\mathbf{z}\rangle^{(g)}$ of the search path $\mathbf{s}$ and the mutation vector centroid $\langle\boldsymbol{z}\rangle$. Coming up with a closed-form solution turns out to be very difficult. Nonetheless, the change of the expected scalar product value between two consecutive generations can be formulated as a recurrence equation.

In order to establish the difference equation the expected values of $\mathrm{E}[\langle z\rangle_i^{(g)}]$ and $\mathrm{E}[\langle z\rangle_i^{(g+1)}]$ need to be calculated in the first place. Using of the renormalized version of the first-order progress rate (3.13) one obtains

$$\frac{\sigma^{(g)} c_{\mu/\mu,\lambda} q_i y_i^{(g)}}{R_q(\mathbf{y}^{(g)})} = \mathrm{E}\left[y_i^{(g)} - y_i^{(g+1)}\right] = \mathrm{E}\left[y_i^{(g)} - \left(y_i^{(g)} + \sigma^{(g)}\langle z\rangle_i^{(g)}\right)\right] = -\sigma^{(g)}\mathrm{E}\left[\langle z\rangle_i^{(g)}\right], \tag{A.10}$$

or, respectively,

$$\mathrm{E}\left[\langle z\rangle_i^{(g)}\right] = \frac{-c_{\mu/\mu,\lambda} q_i y_i^{(g)}}{R_q(\mathbf{y}^{(g)})}. \tag{A.11}$$

Adding a term $\epsilon_{\langle z\rangle_i^{(g)}}$ that describes the stochastic fluctuations to the expected value $\mathrm{E}\left[\langle z\rangle_i^{(g)}\right]$, the ith component of the mutation vector of the parental centroid $\langle z\rangle_i^{(g)}$ in generation g can be modeled as

$$\langle z\rangle_i^{(g)} = \mathrm{E}\left[\langle z\rangle_i^{(g)}\right] + \epsilon_{\langle z\rangle_i^{(g)}}. \tag{A.12}$$

According to (A.11), the expected value of the ith component in generation $g+1$ is

$$\mathrm{E}\left[\langle z\rangle_i^{(g+1)}\right] = \frac{-c_{\mu/\mu,\lambda} q_i y_i^{(g+1)}}{R_q(\boldsymbol{y}^{(g+1)})} = \frac{-c_{\mu/\mu,\lambda} q_i y_i^{(g+1)}}{\sqrt{\sum_{j=1}^N q_j^2 y_j^{(g+1)^2}}}. \tag{A.13}$$

For the further analysis it is desirable to represent the right-hand side of Eq. (A.13) by means of the ES state in the previous generation g. This is achieved by taking into account line 10 of the CSA-ES in Alg. 4.1 and the definition of the quadratic progress rate in Eq. (3.24)

$$\mathrm{E}\left[\langle z\rangle_i^{(g+1)}\right] = \frac{-c_{\mu/\mu,\lambda} q_i \left(y_i^{(g)} + \sigma^{(g)}\langle z\rangle_i^{(g)}\right)}{\sqrt{\sum_{j=1}^N q_j^2 \left(y_j^{(g)2} - \varphi_j^{II}\right)}} = \frac{-c_{\mu/\mu,\lambda} q_i \left(y_i^{(g)} + \sigma^{(g)}\langle z\rangle_i^{(g)}\right)}{R_q(\mathbf{y}^{(g)}) \sqrt{1 - \frac{\sum_{j=1}^N q_j^2 \varphi_j^{II}}{R_q^2(\mathbf{y}^{(g)})}}}. \tag{A.14}$$

Provided that the quotient

$$\delta\left(\sigma^{(g)}, \mathbf{y}^{(g)}\right) := \frac{\sum_{j=1}^N q_j^2 \varphi_j^{II}}{R_q^2(\mathbf{y}^{(g)})} \tag{A.15}$$

is sufficiently small, Taylor expansion of Eq. (A.14) up to the linear term yields

$$\mathrm{E}\left[\langle z\rangle_i^{(g+1)}\right] \simeq \frac{-c_{\mu/\mu,\lambda} q_i \left(y_i^{(g)} + \sigma^{(g)}\langle z\rangle_i^{(g)}\right)}{R_q(\mathbf{y}^{(g)})} \left(1 + \frac{1}{2}\delta\left(\sigma^{(g)}, \mathbf{y}^{(g)}\right)\right). \tag{A.16}$$

Figure A.1 provides a verification of the assumption $\left|\delta\left(\sigma^{(g)}, \mathbf{y}^{(g)}\right)\right| \ll 1$ by plotting the experimentally generated mean values of the quotient δ against the search space dimensionality N. Analogously to (A.12) the ith component of the mutation vector of the parental centroid $\langle z\rangle_i^{(g+1)}$ in generation $g+1$ can be described by the sum of its expected value and a term $\epsilon_{\langle z\rangle_i^{(g+1)}}$ denoting the stochastic fluctuations

$$\begin{aligned}\langle z\rangle_i^{(g+1)} &= \mathrm{E}\left[\langle z\rangle_i^{(g+1)}\right] + \epsilon_{\langle z\rangle_i^{(g+1)}} \\ &\simeq \frac{-c_{\mu/\mu,\lambda} q_i \left(y_i^{(g)} + \sigma^{(g)}\langle z\rangle_i^{(g)}\right)}{R_q(\mathbf{y}^{(g)})} \left(1 + \frac{1}{2}\delta\left(\sigma^{(g)}, \mathbf{y}^{(g)}\right)\right) + \epsilon_{\langle z\rangle_i^{(g+1)}}.\end{aligned} \tag{A.17}$$

Equations (A.11) and (A.17) can now be used to derive the difference equation for the scalar product. According to Alg. 4.1, line 11, the search path components are updated by

$$s_i^{(g+1)} = (1-c)s_i^{(g)} + \sqrt{\mu c(2-c)}\langle z\rangle_i^{(g)}. \tag{A.18}$$

By multiplication with $\langle z\rangle_i^{(g+1)}$ Eq. (A.18) becomes

$$s_i^{(g+1)}\langle z\rangle_i^{(g+1)} = (1-c)s_i^{(g)}\langle z\rangle_i^{(g+1)} + \sqrt{\mu c(2-c)}\langle z\rangle_i^{(g)}\langle z\rangle_i^{(g+1)}, \tag{A.19}$$

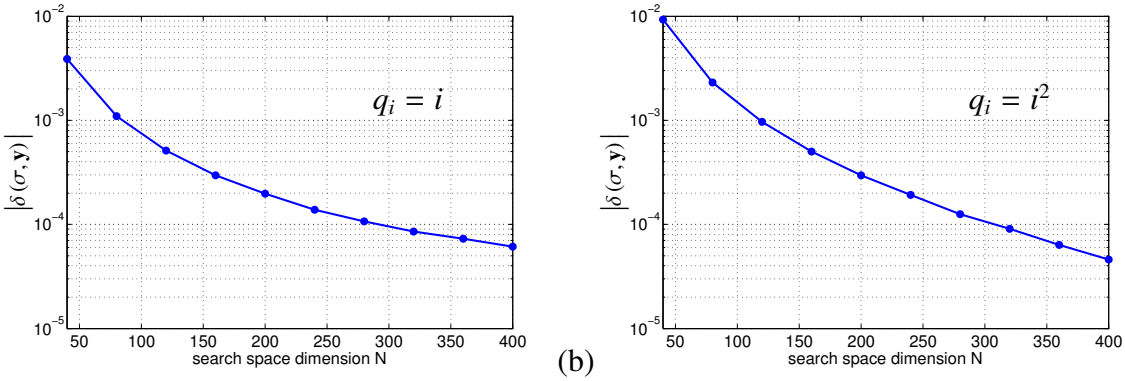

(a) (b)

Figure A.1.: Mean values of $\delta\left(\sigma^{(g)}, \mathbf{y}^{(g)}\right)$ plotted against the search space dimension N. Each data point is obtained by averaging over 10^5 generations and 100 independent runs of a $(3/3_I, 10)$-CSA-ES.

and by insertion of (A.17) the ith addend of the scalar product $\mathbf{s}^\top \langle \mathbf{z} \rangle^{(g+1)}$ in generation $g+1$ reads

$$\begin{aligned} & s_i^{(g+1)} \langle z \rangle_i^{(g+1)} \\ & \simeq (1-c) s_i^{(g)} \left(\frac{-c_{\mu/\mu,\lambda} q_i \left(y_i^{(g)} + \sigma^{(g)} \langle z \rangle_i^{(g)} \right)}{R_q(\mathbf{y}^{(g)})} \left(1 + \frac{1}{2} \delta\left(\sigma^{(g)}, \mathbf{y}^{(g)} \right) \right) + \epsilon_{\langle z \rangle_i^{(g+1)}} \right) \\ & \quad + \sqrt{\mu c (2-c)} \langle z \rangle_i^{(g)} \left(\frac{-c_{\mu/\mu,\lambda} q_i \left(y_i^{(g)} + \sigma^{(g)} \langle z \rangle_i^{(g)} \right)}{R_q(\mathbf{y}^{(g)})} \left(1 + \frac{1}{2} \delta\left(\sigma^{(g)}, \mathbf{y}^{(g)} \right) \right) + \epsilon_{\langle z \rangle_i^{(g+1)}} \right). \end{aligned} \tag{A.20}$$

Considering the asymptotic limit case, the δ terms in (A.20) can be neglected. Thus solving the brackets and combining the fluctuation terms yields

$$\begin{aligned} s_i^{(g+1)} \langle z \rangle_i^{(g+1)} \simeq & (1-c) s_i^{(g)} \frac{-c_{\mu/\mu,\lambda} q_i y_i^{(g)}}{R_q(\mathbf{y}^{(g)})} + (1-c) s_i^{(g)} \frac{-c_{\mu/\mu,\lambda} q_i \sigma^{(g)} \langle z \rangle_i^{(g)}}{R_q(\mathbf{y}^{(g)})} \\ & + \sqrt{\mu c (2-c)} \langle z \rangle_i^{(g)} \frac{-c_{\mu/\mu,\lambda} q_i y_i^{(g)}}{R_q(\mathbf{y}^{(g)})} + \sqrt{\mu c (2-c)} \langle z \rangle_i^{(g)} \frac{-c_{\mu/\mu,\lambda} q_i \sigma^{(g)} \langle z \rangle_i^{(g)}}{R_q(\mathbf{y}^{(g)})} \\ & + \left((1-c) s_i^{(g)} + \sqrt{\mu c (2-c)} \langle z \rangle_i^{(g)} \right) \epsilon_{\langle z \rangle_i^{(g+1)}}. \end{aligned} \tag{A.21}$$

Rearranging the terms and making use of Eqs. (A.11) and (A.12) yields

$$\begin{aligned} s_i^{(g+1)} \langle z \rangle_i^{(g+1)} \simeq & (1-c) \left(1 - \frac{c_{\mu/\mu,\lambda} q_i \sigma^{(g)}}{R_q(\mathbf{y}^{(g)})} \right) s_i^{(g)} \langle z \rangle_i^{(g)} \\ & + \sqrt{\mu c (2-c)} \left(\langle z \rangle_i^{(g)} \frac{-c_{\mu/\mu,\lambda} q_i y_i^{(g)}}{R_q(\mathbf{y}^{(g)})} + \frac{-c_{\mu/\mu,\lambda} q_i \sigma^{(g)}}{R_q(\mathbf{y}^{(g)})} \left(\langle z \rangle_i^{(g)} \right)^2 \right) \\ & + \left((1-c) s_i^{(g)} + \sqrt{\mu c (2-c)} \langle z \rangle_i^{(g)} \right) \epsilon_{\langle z \rangle_i^{(g+1)}} - (1-c) s_i^{(g)} \epsilon_{\langle z \rangle_i^{(g)}}. \end{aligned} \tag{A.22}$$

The terms $\langle z\rangle_i^{(g)}$ are pairwise stochastically independent variates (with respect to the generation counter), consequently all terms containing perturbations $\epsilon_{\langle z\rangle_i^{(g+1)}}$ and $\epsilon_{\langle z\rangle_i^{(g)}}$ in (A.22) have the expected value zero. That is, calculating expected values of Eq. (A.22) one gets

$$\begin{aligned}
&\mathrm{E}\left[s_i^{(g+1)}\langle z\rangle_i^{(g+1)}\right] \\
&\simeq (1-c)\left(1-\frac{c_{\mu/\mu,\lambda}q_i\sigma^{(g)}}{R_q(\mathbf{y}^{(g)})}\right)\mathrm{E}\left[s_i^{(g)}\langle z\rangle_i^{(g)}\right] \\
&\quad+\sqrt{\mu c(2-c)}\left(\mathrm{E}\left[\langle z\rangle_i^{(g)}\right]\frac{-c_{\mu/\mu,\lambda}q_i y_i^{(g)}}{R_q(\mathbf{y}^{(g)})}+\frac{-c_{\mu/\mu,\lambda}q_i\sigma^{(g)}}{R_q(\mathbf{y}^{(g)})}\mathrm{E}\left[\left(\langle z\rangle_i^{(g)}\right)^2\right]\right).
\end{aligned} \tag{A.23}$$

In order to justify the approximation of (A.22) by expected value expressions, the iterative dynamics resulting from Eq. (A.23) are compared with experimental runs of the ES in Sec. 4.2. Taking into account Eq. (A.11) again, one obtains

$$\begin{aligned}
\mathrm{E}\left[s_i^{(g+1)}\langle z\rangle_i^{(g+1)}\right] &\simeq (1-c)\left(1-\frac{c_{\mu/\mu,\lambda}q_i\sigma^{(g)}}{R_q(\mathbf{y}^{(g)})}\right)\mathrm{E}\left[s_i^{(g)}\langle z\rangle_i^{(g)}\right] \\
&\quad+\sqrt{\mu c(2-c)}\left(\frac{c_{\mu/\mu,\lambda}^2 q_i^2 y_i^{(g)2}}{R_q^2(\mathbf{y}^{(g)})}-\frac{c_{\mu/\mu,\lambda}q_i\sigma^{(g)}}{R_q(\mathbf{y}^{(g)})}\mathrm{E}\left[\left(\langle z\rangle_i^{(g)}\right)^2\right]\right).
\end{aligned} \tag{A.24}$$

Addition of the N components yields the expected value of the scalar product

$$\begin{aligned}
\mathrm{E}\left[\mathbf{s}^{(g+1)^\top}\langle\mathbf{z}\rangle^{(g+1)}\right] &\simeq (1-c)\mathrm{E}\left[\mathbf{s}^{(g)^\top}\langle\mathbf{z}\rangle^{(g)}\right]-(1-c)\frac{c_{\mu/\mu,\lambda}\sigma^{(g)}}{R_q(\mathbf{y}^{(g)})}\sum_{i=1}^{N}q_i\mathrm{E}\left[s_i^{(g)}\langle z\rangle_i^{(g)}\right] \\
&\quad+c_{\mu/\mu,\lambda}^2\sqrt{\mu c(2-c)}\left(1-\frac{\sigma^{(g)}}{c_{\mu/\mu,\lambda}R_q(\mathbf{y}^{(g)})}\sum_{i=1}^{N}q_i\mathrm{E}\left[\left(\langle z\rangle_i^{(g)}\right)^2\right]\right).
\end{aligned} \tag{A.25}$$

Considering the simplification (A.8), Eq. (A.25) transforms into

$$\begin{aligned}
\mathrm{E}\left[\mathbf{s}^{(g+1)^\top}\langle\mathbf{z}\rangle^{(g+1)}\right] &\simeq (1-c)\mathrm{E}\left[\mathbf{s}^{(g)^\top}\langle\mathbf{z}\rangle^{(g)}\right]-(1-c)\frac{c_{\mu/\mu,\lambda}\sigma^{(g)}}{R_q(\mathbf{y}^{(g)})}\sum_{i=1}^{N}q_i\mathrm{E}\left[s_i^{(g)}\langle z\rangle_i^{(g)}\right] \\
&\quad+c_{\mu/\mu,\lambda}^2\sqrt{\mu c(2-c)}\left(1-\frac{\sigma^{(g)}\Sigma q}{c_{\mu/\mu,\lambda}R_q(\mathbf{y}^{(g)})}\frac{1}{\mu}\right).
\end{aligned} \tag{A.26}$$

At this point, the mutation strength normalization (3.14) can be applied to obtain a difference equation which is independent of the current search space location. Thus the expected transition of the scalar product can be expressed in terms of the normalized mutation strength $\sigma^{*(g)}$

$$\begin{aligned}
\mathrm{E}\left[\mathbf{s}^{(g+1)^\top}\langle\mathbf{z}\rangle^{(g+1)}\right] &\simeq (1-c)\mathrm{E}\left[\mathbf{s}^{(g)^\top}\langle\mathbf{z}\rangle^{(g)}\right]-(1-c)\frac{c_{\mu/\mu,\lambda}\sigma^{*(g)}}{\Sigma q}\sum_{i=1}^{N}q_i\mathrm{E}\left[s_i^{(g)}\langle z\rangle_i^{(g)}\right] \\
&\quad+c_{\mu/\mu,\lambda}^2\sqrt{\mu c(2-c)}\left(1-\frac{\sigma^{*(g)}}{\mu c_{\mu/\mu,\lambda}}\right).
\end{aligned} \tag{A.27}$$

A.3. The normalized mutation strength dynamics

Starting point for the derivation of the difference equation which describes the normalized mutation strength dynamics is the evolution equation of σ, i.e. Eq. (III.2) in Tab. 4.3. Proceeding to normalized quantities (3.14) leads to

$$\sigma^{*(g+1)} \frac{\sqrt{\sum_{j=1}^{N} q_j^2 y_j^{(g+1)^2}}}{\Sigma q} = \sigma^{*(g)} \frac{R_q(\mathbf{y}^{(g)})}{\Sigma q} \left(1 + \tilde{\psi}\left(\sigma^{*(g)}, \mathbf{y}^{(g)}\right)\right). \tag{A.28}$$

This equation can be rearranged to

$$\sigma^{*(g+1)} = \sigma^{*(g)} \frac{R_q(\mathbf{y}^{(g)})}{\sqrt{\sum_{j=1}^{N} q_j^2 y_j^{(g+1)^2}}} \left(1 + \tilde{\psi}\left(\sigma^{*(g)}, \mathbf{y}^{(g)}\right)\right). \tag{A.29}$$

Concentrating on the quotient of square roots yields

$$\frac{R_q(\mathbf{y}^{(g)})}{\sqrt{\sum_{j=1}^{N} q_j^2 y_j^{(g+1)^2}}} = \sqrt{\frac{R_q^2(\mathbf{y}^{(g)})}{R_q^2(\mathbf{y}^{(g)}) - \sum_{j=1}^{N} q_j^2 \varphi_j^{II(g)}}} = \sqrt{\frac{1}{1 - \sum_{j=1}^{N} q_j^2 \varphi_j^{II(g)} \Big/ R_q^2(\mathbf{y}^{(g)})}}. \tag{A.30}$$

Provided that the term $\sum_{j=1}^{N} q_j^2 \varphi_j^{II(g)} \Big/ R_q^2(\mathbf{y}^{(g)})$ is sufficiently small, see (A.15), Eq. (A.30) is approximated by Taylor expansion up to the linear term

$$\frac{R_q(\mathbf{y}^{(g)})}{\sqrt{\sum_{j=1}^{N} q_j^2 y_j^{(g+1)^2}}} \simeq 1 + \frac{1}{2} \frac{\sum_{j=1}^{N} q_j^2 \varphi_j^{II(g)}}{R_q^2(\mathbf{y}^{(g)})}. \tag{A.31}$$

Remembering the component-wise quadratic progress rate formula (3.24), the fraction on the right-hand side of (A.31) becomes

$$\frac{\sum_{i=1}^{N} q_i^2 \varphi_i^{II(g)}}{R_q^2(\mathbf{y}^{(g)})} = \frac{2\sigma^{*(g)} c_{\mu/\mu,\lambda}}{\Sigma q} \frac{\sum_{i=1}^{N} q_i^3 y_i^{(g)^2}}{R_q^2(\mathbf{y}^{(g)})} - \frac{\sigma^{*(g)^2}}{\mu} \frac{\sum_{i=1}^{N} q_i^2}{(\Sigma q)^2}, \tag{A.32}$$

and in conclusion one obtains

$$\frac{R_q(\mathbf{y}^{(g)})}{\sqrt{\sum_{j=1}^{N} q_j^2 y_j^{(g+1)^2}}} \simeq 1 + \frac{\sigma^{*(g)} c_{\mu/\mu,\lambda}}{\Sigma q} \frac{\sum_{i=1}^{N} q_i^3 y_i^{(g)^2}}{R_q^2(\mathbf{y}^{(g)})} - \frac{\sigma^{*(g)^2}}{2\mu} \frac{\sum_{i=1}^{N} q_i^2}{(\Sigma q)^2}. \tag{A.33}$$

Conclusively, inserting (A.33) into Eq. (A.29) the evolution equation of the normalized mutation strength σ^* asymptotically yields

$$\sigma^{*(g+1)} = \sigma^{*(g)} \left(1 + \frac{\sigma^{*(g)} c_{\mu/\mu,\lambda}}{\Sigma q} \frac{\sum_{i=1}^{N} q_i^3 y_i^{(g)^2}}{R_q^2(\mathbf{y}^{(g)})} - \frac{\sigma^{*(g)^2}}{2\mu} \frac{\sum_{i=1}^{N} q_i^2}{(\Sigma q)^2}\right) \left(1 + \tilde{\psi}\left(\sigma^{*(g)}, \mathbf{y}^{(g)}\right)\right), \tag{A.34}$$

with $\tilde{\psi}\left(\sigma^{*(g)}, \mathbf{y}^{(g)}\right)$ from Eq. (4.27).

Appendix B.

Deriving the meta-ES dynamics

B.1. The normalized mutation strength dynamics

The description of the normalized mutation strength σ^* is realized by derivation of the corresponding evolution equation. Recalling the mutation strength normalization in (3.14) yields

$$\sigma^{*(g+1)} = \sigma^{(g+1)} \frac{\Sigma q}{\sqrt{\sum_{j=1}^{N} q_j^2 \left(y_j^{(g+1)}\right)^2}}. \tag{B.1}$$

Considering the evolution equation of the mutation strength in (5.12) leads to

$$\sigma^{*(g+1)} = \sigma^{(g)} \alpha^{-\mathrm{sign}(\Delta(\sigma^{*(g)}))} \frac{\Sigma q}{\sqrt{\sum_{j=1}^{N} q_j^2 \left(y_j^{(g+1)}\right)^2}}, \tag{B.2}$$

and by making use of the progress rate definition (3.18), Eq. (B.2) becomes

$$\sigma^{*(g+1)} = \sigma^{(g)} \alpha^{-\mathrm{sign}(\Delta(\sigma^{*(g)}))} \frac{\Sigma q}{\sqrt{\sum_{j=1}^{N} q_j^2 y_j^{(g)2} - \sum_{j=1}^{N} q_j^2 \varphi_j^{II}(\sigma^{(g)} \alpha^{-\mathrm{sign}(\Delta(\sigma^{*(g)}))})}}. \tag{B.3}$$

By remembering abbreviation (3.25) and by rearranging the terms one obtains

$$\sigma^{*(g+1)} = \sigma^{(g)} \alpha^{-\mathrm{sign}(\Delta(\sigma^{*(g)}))} \frac{\Sigma q}{R_q(\mathbf{y}^{(g)})} \frac{1}{\sqrt{1 - \frac{\sum_{j=1}^{N} q_j^2 \varphi_j^{II}(\sigma^{(g)} \alpha^{-\mathrm{sign}(\Delta(\sigma^{*(g)}))})}{R_q^2(\mathbf{y}^{(g)})}}}. \tag{B.4}$$

Conclusively, after renormalization (3.14), the evolution equation of the normalized mutation strength reads

$$\sigma^{*(g+1)} = \frac{\sigma^{*(g)} \alpha^{-\mathrm{sign}(\Delta(\sigma^{*(g)}))}}{\sqrt{1 - \frac{\sum_{j=1}^{N} q_j^2 \varphi_j^{II}(\sigma^{(g)} \alpha^{-\mathrm{sign}(\Delta(\sigma^{*(g)}))})}{R_q^2(\mathbf{y}^{(g)})}}}. \tag{B.5}$$

This is an iterative mapping of the form $\sigma^{*(g+1)} = f_\sigma\left(\sigma^{*(g)}; \alpha\right)$. Such recurrence equations can exhibit qualitatively different dynamics like stable fixed points, limit cycles, and chaotic behaviors. Since the influence of the Ellipsoid model, as well as the influence of parameters like α and N, on Eq. (B.5) is not evident one is interested in further simplifications. That is, considering (3.24) and (3.25), after some straight forward operations the fraction within the square root of (B.5) becomes

$$\frac{\sum_{j=1}^{N} q_j^2 \varphi_j^{II}\left(\sigma^{(g)}\alpha^{-\mathrm{sign}(\Delta(\sigma^{*(g)}))}\right)}{R_q^2(\mathbf{y}^{(g)})} \tag{B.6}$$

$$= \frac{1}{R_q^2(\mathbf{y}^{(g)})} \sum_{j=1}^{N} q_j^2 \left(\frac{2\sigma^{(g)}\alpha^{-\mathrm{sign}(\Delta(\sigma^{*(g)}))} c_{\mu/\mu,\lambda} q_j y_j^{(g)2}}{R_q(\mathbf{y}^{(g)})} - \frac{\left(\sigma^{(g)}\alpha^{-\mathrm{sign}(\Delta(\sigma^{*(g)}))}\right)^2}{\mu} \right) \tag{B.7}$$

$$= \frac{1}{R_q^2(\mathbf{y}^{(g)})} \left(\sum_{j=1}^{N} q_j^2 \frac{2\sigma^{(g)}\alpha^{-\mathrm{sign}(\Delta(\sigma^{*(g)}))} c_{\mu/\mu,\lambda} q_j y_j^{(g)2}}{R_q(\mathbf{y}^{(g)})} - \sum_{j=1}^{N} q_j^2 \frac{\left(\sigma^{(g)}\alpha^{-\mathrm{sign}(\Delta(\sigma^{*(g)}))}\right)^2}{\mu} \right) \tag{B.8}$$

$$= \frac{2\sigma^{(g)}\alpha^{-\mathrm{sign}(\Delta(\sigma^{*(g)}))} c_{\mu/\mu,\lambda} \sum_{j=1}^{N} q_j^3 y_j^{(g)2}}{R_q^2(\mathbf{y}^{(g)}) R_q(\mathbf{y}^{(g)})} - \frac{\left(\sigma^{(g)}\alpha^{-\mathrm{sign}(\Delta(\sigma^{*(g)}))}\right)^2}{\mu R_q^2(\mathbf{y}^{(g)})} \sum_{j=1}^{N} q_j^2 \tag{B.9}$$

$$= \frac{2\sigma^{*(g)}\alpha^{-\mathrm{sign}(\Delta(\sigma^{*(g)}))} c_{\mu/\mu,\lambda} \sum_{j=1}^{N} q_j^3 y_j^{(g)2}}{\Sigma q R_q^2(\mathbf{y}^{(g)})} - \frac{\left(\sigma^{*(g)}\alpha^{-\mathrm{sign}(\Delta(\sigma^{*(g)}))}\right)^2}{\mu} \frac{\sum_{j=1}^{N} q_j^2}{(\Sigma q)^2} \tag{B.10}$$

$$= \frac{\sum_{j=1}^{N} q_j^2}{(\Sigma q)^2} \left(2c_{\mu/\mu,\lambda}\sigma^{*(g)}\alpha^{-\mathrm{sign}(\Delta(\sigma^{*(g)}))} \frac{\Sigma q \sum_{j=1}^{N} q_j^3 y_j^{(g)2}}{\sum_{j=1}^{N} q_j^2 \sum_{j=1}^{N} q_j^2 y_j^{(g)2}} - \frac{\left(\sigma^{*(g)}\alpha^{-\mathrm{sign}(\Delta(\sigma^{*(g)}))}\right)^2}{\mu} \right). \tag{B.11}$$

For reasons of clarity and comprehensibility the abbreviation

$$Q := \frac{\Sigma q \sum_{j=1}^{N} q_j^3 y_j^2}{\sum_{j=1}^{N} q_j^2 \sum_{j=1}^{N} q_j^2 y_j^2} \tag{B.12}$$

is introduced. The evolution equation of the normalized mutation strength σ^* can then be reformulated as

$$\sigma^{*(g+1)} = \frac{\sigma^{*(g)}\alpha^{-\mathrm{sign}(\Delta(\sigma^{*(g)}))}}{\sqrt{1 - \frac{\sum_{j=1}^{N} q_j^2}{(\Sigma q)^2} \left(2c_{\mu/\mu,\lambda} Q \sigma^{*(g)}\alpha^{-\mathrm{sign}(\Delta(\sigma^{*(g)}))} - \frac{\left(\sigma^{*(g)}\alpha^{-\mathrm{sign}(\Delta(\sigma^{*(g)}))}\right)^2}{\mu} \right)}}. \tag{B.13}$$

This also is an iterative mapping of the form $\sigma^{*(g+1)} = \tilde{f}_\sigma\left(\sigma^{*(g)}; \alpha\right)$ which is still difficult to analyze due to the Q-term. Hence, one is interested to replace the Q-term with an approximation that allows for a convenient analysis of the normalized mutation strength dynamics. Such an approximation can be derived based on a few assumptions. Consistently, the approximation result is validated by comparison to experimental measurements of the Q-term values.

Assuming that

(i) the meta-ES is already operating in its steady state,

(ii) the meta-ES exhibits y_i^2 dynamics similar to those observed in the CSA-ES case that allow to establish the eigenvalue problem presented in Sec. 4.3.2,

(iii) the steady state mutation strength σ^*_{ss} realized by the meta-ES resides in the range where the linear steady state mode eigenvalue approximation (4.44) is admissible,

it is possible to derive an approximation of the Q-term based on the CSA analysis results obtained in Sec. 4.3. The resulting formula also provides a sufficiently accurate approximation in the meta-ES case. Notice, that the correctness of assumptions (ii) and (iii) is clarified in Sec. 5.2.4 by derivation of the respective eigenvalue problem in the meta-ES context and the corresponding steady state dynamics.

Regarding the analysis in Sec. 4.3, and remembering the *Ansatz* (4.29), the Q-term already emerged within Eq. (4.48). Taking into account assumption (iii), the left-hand side of Eq. (4.48) can be replaced by the the linear ν value approximation (4.44). Proceeding like this, yields an equation

$$\sigma^*_{ss} c_{\mu/\mu,\lambda} \frac{\breve{q}}{\Sigma q} \simeq \frac{\sum_{i=1}^N q_i^2}{(\Sigma q)^2} \left(\sigma^*_{ss} c_{\mu/\mu,\lambda} Q - \frac{{\sigma^*_{ss}}^2}{2\mu} \right), \tag{B.14}$$

that can be solved for the Q-term. Straight forward rearrangements finally yield the approximation

$$Q \simeq \frac{\sigma^*_{ss}}{2\mu c_{\mu/\mu,\lambda}} + \Sigma q \frac{\breve{q}}{\sum_{i=1}^N q_i^2}. \tag{B.15}$$

Notice that $\breve{q} := \min\left\{ q_j \,|\, j = 1, \ldots, N \right\}$ denotes the smallest ellipsoid coefficient. Being derived in the limit of the strategy's steady state, Eq. (B.15) depends on the steady state mutation strength realization. However, without major loss of accuracy it can be interpreted as a function of the normalized mutation strength σ^*

$$Q(\sigma^{*(g)}) \simeq \frac{\sigma^{*(g)}}{2\mu c_{\mu/\mu,\lambda}} + \Sigma q \frac{\breve{q}}{\sum_{i=1}^N q_i^2}. \tag{B.16}$$

Keep in mind that Eq. (B.16) is obtained in the limit of sufficiently small normalized mutation strength that allow for the applicability of the convergence rate linearization (4.44). In the representation of Eq. (B.16) the Q-term allows for the analysis of the normalized mutation strength dynamics.

The use of approximation (B.16) is justified by comparison to the Q-term dynamics corresponding to Eq. (B.12). To this end, the Q values are calculated by use of the y_i^2 dynamics within real meta-ES runs on the ellipsoid model $q_i = i$ in search space dimensions $N = 40$ and $N = 200$. The corresponding normalized mutation strengths measurements are used for the computation of the approximated Q dynamics according to (B.16). Additionally, the same line of action is carried out considering the iteratively generated dynamics based

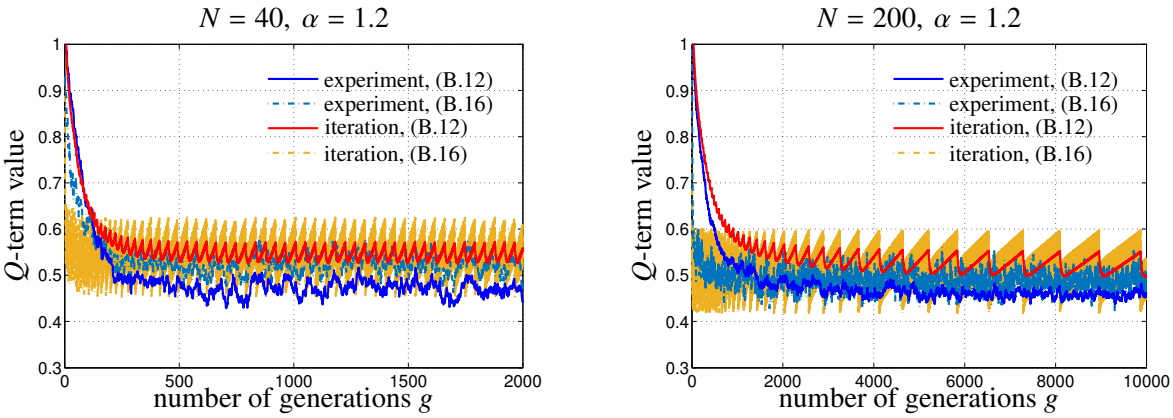

Figure B.1.: The Q-term dynamics of the $[1, 2(3/3_I, 10)^1]$-meta-ES on the Ellipsoid model ($q_i = i$). The strategy is initialized at $y_i^{(0)} = 1\ \forall i$ with $\sigma_0 = 1$ and control parameter $\alpha = 1.2$ is illustrated for $N = 40$ and $N = 200$.

on Eq. (5.12). The comparison is illustrated in Fig. B.1. The experimentally obtained Q-term (B.12) and the corresponding approximation (B.16) is displayed by use of solid blue lines, and the dashed light blue lines, respectively. The iterative Q dynamics and its approximation are represented by the solid red and the dashed orange line. As the meta-ES approaches its steady state, the agreement of (B.16) and (B.12) increases in both cases (experimental and iterative dynamics). Considering search space dimensionality $N = 200$, it can be observed that the curves move closer together. The illustrations in Fig. B.1 validate the applicability of approximation (B.16) in the strategy's steady state.

Consequently, replacing Q in (B.13) with $Q(\sigma^{*(g)}\alpha^{-\mathrm{sign}(\Delta(\sigma^{*(g)}))})$ and making use of approximation (B.16), one obtains a recurrence equation of the normalized mutation strength which is independent of the current distance from the optimizer

$$\sigma^{*(g+1)} \simeq \frac{\sigma^{*(g)}\alpha^{-\mathrm{sign}(\Delta(\sigma^{*(g)}))}}{\sqrt{1 - \dfrac{2c_{\mu/\mu,\lambda}\sigma^{*(g)}\alpha^{-\mathrm{sign}(\Delta(\sigma^{*(g)}))}\breve{q}}{\Sigma q}}}. \tag{B.17}$$

Making use of eq. (B.17) allows for the illustration of the normalized mutation strength dynamics in Sec. 5.2.3.

B.2. Deriving the oscillation interval

This paragraph is concerned with the analytical derivation of the interval boundaries of the normalized mutation strength σ^* observed in Fig. 5.8(a). The derivation is based on the recurrence equation of the normalized mutation strength dynamics (B.17) that was obtained by application of the approximation of the Q-term (B.16). Understanding the evolution equation (B.17) as an iterative mapping of the form $\sigma^{*(g+1)}) = \bar{f}_\sigma(\sigma^{*(g)}; \alpha)$, it allows for the derivation of the oscillation interval. Referring to the right-sided limit of the normalized

mutation strength oscillation interval as $\hat{\sigma}^*$, it represents the limit up to which σ^* can possibly be increased during the oscillation phase. The right-side of the isolation interval $\hat{\sigma}^*$ is approached for $\sigma^* \to \sigma_0^* - 0$, cf. Eqs. (5.17) and (5.18). Further, the left-sided interval boundary is denoted $\check{\sigma}^*$. It can be calculated analogously, see (5.18), by considering (B.17) in the limit of $\sigma^* \to \sigma_0^* + 0$. Consequently, the boundaries of the oscillation interval are defined as

$$\hat{\sigma}^* := \lim_{\sigma^* \to \sigma_0^* - 0} \bar{f}_\sigma(\sigma^*), \tag{B.18}$$

and

$$\check{\sigma}^* := \lim_{\sigma^* \to \sigma_0^* + 0} \bar{f}_\sigma(\sigma^*). \tag{B.19}$$

Taking into account the iterative mapping (B.17), and considering the point of discontinuity (5.17)

$$\sigma_0^* = \frac{2\mu c_{\mu/\mu,\lambda}\, \alpha}{\alpha^2 + 1} \tag{B.20}$$

the left-sided limit of the normalized mutation strength oscillation interval is obtained as

$$\hat{\sigma}^* := \lim_{\sigma^* \to \sigma_0^* - 0} \bar{f}_\sigma(\sigma^*) = \frac{\sigma_0^* \alpha}{\sqrt{1 - \dfrac{2c_{\mu/\mu,\lambda}\sigma_0^* \alpha \check{q}}{\Sigma q}}} = \frac{2\mu c_{\mu/\mu,\lambda}}{\alpha^2 + 1} \frac{\alpha^2}{\sqrt{1 - 4\mu c_{\mu/\mu,\lambda}^2 \dfrac{\alpha^2}{1+\alpha^2} \dfrac{\check{q}}{\Sigma q}}}. \tag{B.21}$$

In the same manner, the right-sided limit is calculated as

$$\check{\sigma}^* := \lim_{\sigma^* \to \sigma_0^* + 0} \bar{f}_\sigma(\sigma^*) = \frac{\sigma_0^*}{\alpha \sqrt{1 - \dfrac{2c_{\mu/\mu,\lambda}\sigma_0^* \check{q}}{\alpha \Sigma q}}} = \frac{2\mu c_{\mu/\mu,\lambda}}{\alpha^2 + 1} \frac{1}{\sqrt{1 - 4\mu c_{\mu/\mu,\lambda}^2 \dfrac{1}{1+\alpha^2} \dfrac{\check{q}}{\Sigma q}}}. \tag{B.22}$$

B.3. Approximating the progress over an isolation period of multiple generations

Considering an isolation time $\gamma = 2$, the inner strategies operate with fixed mutation strength σ over two generations. In the first place, the $y_i^{(g+2)^2}$ state at generation $g + 2$ is associated with the state $y_i^{(g)^2}$ at generation g. Making use of the progress rate definition (3.18), one obtains the component-wise difference equations for subsequent generations, i.e. in particular

$$y_i^{(g+1)^2} = y_i^{(g)^2} - \varphi_i^{II}(\sigma^{(g)}, \mathbf{y}^{(g)}), \tag{B.23}$$

and

$$y_i^{(g+2)^2} = y_i^{(g+1)^2} - \varphi_i^{II}(\sigma^{(g)}, \mathbf{y}^{(g+1)}), \tag{B.24}$$

respectively. Accordingly, inserting (B.23) into (B.24) yields

$$y_i^{(g+2)^2} = y_i^{(g)^2} - \varphi_i^{II}(\sigma^{(g)}, \mathbf{y}^{(g)}) - \varphi_i^{II}(\sigma^{(g)}, \mathbf{y}^{(g+1)}). \tag{B.25}$$

By use of the component-wise quadratic progress rate formula (3.24) one obtains

$$y_i^{(g+2)^2} = y_i^{(g)^2} - \frac{2\sigma^{(g)} c_{\mu/\mu,\lambda} q_i y_i^{(g)^2}}{\sqrt{\sum_{j=1}^N q_j^2 y_j^{(g)^2}}} + \frac{\sigma^{(g)^2}}{\mu} - \frac{2\sigma^{(g)} c_{\mu/\mu,\lambda} q_i y_i^{(g+1)^2}}{\sqrt{\sum_{j=1}^N q_j^2 y_j^{(g+1)^2}}} + \frac{\sigma^{(g)^2}}{\mu}. \tag{B.26}$$

Taking into account the fourth addend of (B.26), by making use of (B.23), (3.24) and the abbreviation (3.25) it can be expressed as

$$\frac{2\sigma^{(g)} c_{\mu/\mu,\lambda} q_i y_i^{(g+1)^2}}{R_q(\mathbf{y}^{(g+1)})} = \frac{2\sigma^{(g)} c_{\mu/\mu,\lambda} q_i y_i^{(g)^2}}{R_q(\mathbf{y}^{(g+1)})} - \frac{4\sigma^{(g)^2} c_{\mu/\mu,\lambda}^2 q_i^2 y_i^{(g)^2}}{R_q(\mathbf{y}^{(g+1)}) R_q(\mathbf{y}^{(g)})} + \frac{2 c_{\mu/\mu,\lambda} q_i \sigma^{(g)^3}}{\mu R_q(\mathbf{y}^{(g+1)})}. \tag{B.27}$$

Provided that the mutation strength $\sigma^{(g)}$ is small the addend containing $\sigma^{(g)^3}$ only has a small contribution on the right-hand side of Eq. (B.27). Regarding the longterm behavior of the σ and y_i^2 dynamics the respective term in fact approaches zero since the numerator decreases at a faster rate as the denominator. Conclusively, it can be neglected and by rearranging the remaining terms in (B.27) one obtains

$$\frac{2\sigma^{(g)} c_{\mu/\mu,\lambda} q_i y_i^{(g+1)^2}}{R_q(\mathbf{y}^{(g+1)})} = \frac{2\sigma^{(g)} c_{\mu/\mu,\lambda} q_i y_i^{(g)^2}}{R_q(\mathbf{y}^{(g+1)})} \left(1 - \frac{2\sigma^{(g)} c_{\mu/\mu,\lambda} q_i}{R_q(\mathbf{y}^{(g)})}\right). \tag{B.28}$$

Moreover, assuming that there exists no dominant ellipsoid coefficient q_i, i.e., that the condition

$$q_i \ll \sum_{j=1}^N q_j, \quad \forall j = 1, \ldots, N, \tag{B.29}$$

is satisfied, the fraction $2\sigma^{(g)} c_{\mu/\mu,\lambda} q_i / R_q(\mathbf{y}^{(g)})$ on the right-hand side of Eq. (B.28) can be neglected in the asymptotic limit $N \to \infty$. Accordingly, the reformulation of the square root in the denominator of (B.28) in terms of the y_i^2 state in generation g yields

$$\frac{2\sigma^{(g)} c_{\mu/\mu,\lambda} q_i y_i^{(g+1)^2}}{R_q(\mathbf{y}^{(g+1)})} \simeq \frac{2\sigma^{(g)} c_{\mu/\mu,\lambda} q_i y_i^{(g)^2}}{R_q(\mathbf{y}^{(g)}) \sqrt{1 - \dfrac{\sum_{i=1}^N q_j^2 \varphi_j^{II}(\sigma^{(g)})}{R_q^2(\mathbf{y}^{(g)})}}}. \tag{B.30}$$

Due to the previous investigations in App. A.2, see Eq. (A.15), the fraction term under the square root is sufficiently small and has only a negligible impact on the right-hand side of Eq. (B.30). As a result, the fourth addend in Eq. (B.26) can be approximated by

$$\frac{2\sigma^{(g)} c_{\mu/\mu,\lambda} q_i y_i^{(g+1)^2}}{R_q(\mathbf{y}^{(g+1)})} \simeq \frac{2\sigma^{(g)} c_{\mu/\mu,\lambda} q_i y_i^{(g)^2}}{R_q(\mathbf{y}^{(g)})}. \tag{B.31}$$

Further, the reinsertion of (B.31) into Eq. (B.25) results in a convenient approximation of the progress after two consecutive generations within the inner ES

$$y_i^{(g+2)^2} \simeq y_i^{(g)^2} - \frac{2\sigma^{(g)} c_{\mu/\mu,\lambda} q_i y_i^{(g)^2}}{R_q(\mathbf{y}^{(g)})} + \frac{\sigma^{(g)^2}}{\mu} - \frac{2\sigma^{(g)} c_{\mu/\mu,\lambda} q_i y_i^{(g)^2}}{R_q(\mathbf{y}^{(g)})} + \frac{\sigma^{(g)^2}}{\mu}. \tag{B.32}$$

Reconsidering the component-wise quadratic progress rate formula (3.24), Eq. (B.32) can be condensed to

$$y_i^{(g+2)^2} \simeq y_i^{(g)^2} - 2\varphi_i^{II}(\sigma^{(g)}, \mathbf{y}^{(g)}). \tag{B.33}$$

That is, the progress of the component-wise distance to the optimizer after two generations can be approximated by applying the one-generation progress rate to the initial state twice. Making use of this formulation of the progress over an isolation period of two consecutive generations ($\gamma = 2$), it can be transferred to an approximation of the $\gamma > 2$ case in Sec. 5.3.2.

Appendix C.

Meta-ES on the noisy sphere model

C.1. Comparing the noise-free population dynamics

Considering the four new strategy parameters established within the $[1, 4(\mu/\mu_I, \lambda)^\gamma]$-meta-ES in Alg. 7.1 the focus of this section is on the noise-free population size dynamics. For reasons of comprehensibility, below the strategy parameter are denoted as

$$\mu_+ \coloneqq \tilde{\mu}_1 = \mu\beta \quad \text{and} \quad \mu_- \coloneqq \tilde{\mu}_2 = \mu/\beta, \tag{C.1}$$

as well as

$$\sigma_+ \coloneqq \tilde{\sigma}_1 = \sigma\alpha \quad \text{and} \quad \sigma_- \coloneqq \tilde{\sigma}_2 = \sigma/\alpha. \tag{C.2}$$

Identifying $R_{+-}^{(g+\gamma)}$ with the expected distance realized by the inner ES that operates with $\mu_+ = \mu\beta$ and $\sigma_- = \sigma/\alpha$ over a single isolation period a comparison of the inner ESs' outcomes is practicable. The expected distances of the three other inner strategies $R_{++}^{(g+\gamma)}$, $R_{-+}^{(g+\gamma)}$, and $R_{--}^{(g+\gamma)}$ are defined analogously. Consequently, using the progress formula (7.19) yields

$$\begin{aligned}
R_{++}^{(g+\gamma)} &= R^{(g)}\left(1 - \frac{2c_{\mu/\mu,\lambda}^2}{N}d\right) + c_{\mu/\mu,\lambda}\sigma\alpha\frac{\gamma}{\beta}, \\
R_{+-}^{(g+\gamma)} &= R^{(g)}\left(1 - \frac{2c_{\mu/\mu,\lambda}^2}{N}d\right) + c_{\mu/\mu,\lambda}\frac{\sigma}{\alpha}\frac{\gamma}{\beta}, \\
R_{-+}^{(g+\gamma)} &= R^{(g)}\left(1 - \frac{2c_{\mu/\mu,\lambda}^2}{N}d\right) + c_{\mu/\mu,\lambda}\sigma\alpha\gamma\beta, \\
R_{--}^{(g+\gamma)} &= R^{(g)}\left(1 - \frac{2c_{\mu/\mu,\lambda}^2}{N}d\right) + c_{\mu/\mu,\lambda}\frac{\sigma}{\alpha}\gamma\beta.
\end{aligned} \tag{C.3}$$

The algorithm chooses the strategy parameter of the inner ES which generates the smallest distance R to the optimizer. That is, by comparing two expected distances the sign of their difference indicates which strategy is preferred by the meta-ES. Thus in order to compare all four inner strategies against each other six different cases have to be considered. At first the four cases which differ in the population parameter μ are examined. Remembering the

condition $1 < \alpha < \beta$ one obtains

$$\begin{aligned}
R_{++}^{(g+\gamma)} - R_{-+}^{(g+\gamma)} &= c_{\mu/\mu,\lambda}\sigma\gamma\frac{(\alpha - \alpha\beta^2)}{\beta} &< 0,\\
R_{++}^{(g+\gamma)} - R_{--}^{(g+\gamma)} &= c_{\mu/\mu,\lambda}\sigma\gamma\frac{(\alpha^2 - \beta^2)}{\alpha\beta} &< 0,\\
R_{+-}^{(g+\gamma)} - R_{-+}^{(g+\gamma)} &= c_{\mu/\mu,\lambda}\sigma\gamma\left(\frac{1}{\alpha\beta} - \alpha\beta\right) &< 0,\\
R_{+-}^{(g+\gamma)} - R_{--}^{(g+\gamma)} &= c_{\mu/\mu,\lambda}\sigma\gamma\frac{(\alpha - \alpha\beta^2)}{\alpha^2\beta} &< 0.
\end{aligned} \tag{C.4}$$

It can be observed that the meta-ES favors the inner ESs with the higher population size μ. Thus the meta-ES is expected to permanently increase the parental population size μ after each isolation period of γ generations until finally the upper bound d is reached. Consequently the strategy decreases the isolation length γ down to 1. Next, the focus is on the two remaining cases

$$\begin{aligned}
R_{++}^{(g+\gamma)} - R_{+-}^{(g+\gamma)} &= c_{\mu/\mu,\lambda}\sigma\gamma\frac{(\alpha^2\beta - \beta)}{\alpha\beta^2} &> 0,\\
R_{-+}^{(g+\gamma)} - R_{--}^{(g+\gamma)} &= c_{\mu/\mu,\lambda}\sigma\gamma\frac{(\alpha^2\beta - \beta)}{\alpha} &> 0.
\end{aligned} \tag{C.5}$$

It is observable that the meta-ES prefers the strategies which operate with the decreased mutation strength σ_-. Thus $R_{+-}^{(g+\gamma)}$ dominates the other three expected distances. That is, the meta-ES is to be expected to choose the inner strategy which increases the population size μ and simultaneously decreases the mutation strength σ. Consequently, the ranking of the expected distances to the optimizer which is realized by the four inner ESs reads

$$R_{+-}^{(g+\gamma)} < R_{++}^{(g+\gamma)} < R_{--}^{(g+\gamma)} < R_{-+}^{(g+\gamma)}. \tag{C.6}$$

C.2. Derivation of the mutation strength dynamics

For the characterization of the expected σ transition realized by the $[1, 4(\mu/\mu_I, \lambda)]$-meta-ES on the noisy sphere model only the mutation strength control step is considered in the following. Before each isolation period the outer ES generates two new σ-values from the parental mutation strength $\sigma^{(t)}$. Here, t refers to the generation number of the upper level ES, i.e. to the number of isolation periods.

$$\begin{aligned}
\sigma_1 &:= \alpha\sigma^{(t)}\\
\sigma_2 &:= \sigma^{(t)}/\alpha.
\end{aligned} \tag{C.7}$$

Remembering the progress rate (7.4), and writing σ instead of $\sigma^{(t)}$, this results in two expected distances $R^{(t+1)}$ at the end of isolation period $t+1$

$$\begin{aligned} R_1^{(t+1)} &= R^{(t)} - \frac{\alpha\sigma c_{\mu/\mu,\lambda}}{\sqrt{1+\frac{{\sigma_\epsilon}^2}{4{R^{(t)}}^2\alpha^2\sigma^2}}} + \frac{\alpha^2\sigma^2 N}{2\mu R^{(t)}}, \\ R_2^{(t+1)} &= R^{(t)} - \frac{\sigma c_{\mu/\mu,\lambda}}{\alpha\sqrt{1+\frac{\alpha^2{\sigma_\epsilon}^2}{4{R^{(t)}}^2\sigma^2}}} + \frac{\sigma^2 N}{2\alpha^2\mu R^{(t)}}. \end{aligned} \tag{C.8}$$

Note that in contrast to Sec. 7.3, $R_1^{(t+1)}$ and $R_2^{(t+1)}$ now refer to the inner ES which operates with σ_1 and σ_2, respectively. The algorithm chooses the strategy parameters of the strategy which generates the smaller distance to the optimizer. That is, the sign of the difference $R_1^{(t+1)} - R_2^{(t+1)}$ determines whether the meta-ES increases or decreases the mutation strength σ

$$\begin{aligned} R_1^{(t+1)} - R_2^{(t+1)} < 0 \quad &\Rightarrow \quad \sigma^{(t+1)} = \sigma^{(t)}\alpha \\ R_1^{(t+1)} - R_2^{(t+1)} > 0 \quad &\Rightarrow \quad \sigma^{(t+1)} = \sigma^{(t)}/\alpha. \end{aligned} \tag{C.9}$$

Making use of (C.8), the expected difference can be expressed by

$$\begin{aligned} R_1^{(t+1)} - R_2^{(t+1)} &= \frac{\alpha^2\sigma^2 N}{2\mu R^{(t)}} - \frac{\alpha\sigma c_{\mu/\mu,\lambda}}{\sqrt{1+\frac{{\sigma_\epsilon}^2}{4{R^{(t)}}^2\alpha^2\sigma^2}}} - \frac{\sigma^2 N}{2\alpha^2\mu R^{(t)}} + \frac{\sigma c_{\mu/\mu,\lambda}}{\alpha\sqrt{1+\frac{\alpha^2{\sigma_\epsilon}^2}{4{R^{(t)}}^2\sigma^2}}} \\ &= \frac{\sigma^2 N}{2\mu R^{(t)}}\left(\alpha^2 - \frac{1}{\alpha^2}\right) - \left(\frac{\alpha\sigma c_{\mu/\mu,\lambda}}{\sqrt{1+\frac{{\sigma_\epsilon}^2}{4{R^{(t)}}^2\alpha^2\sigma^2}}} - \frac{\sigma c_{\mu/\mu,\lambda}}{\alpha\sqrt{1+\frac{\alpha^2{\sigma_\epsilon}^2}{4{R^{(t)}}^2\sigma^2}}}\right). \end{aligned} \tag{C.10}$$

Now considering normalized quantities, it transforms into

$$\begin{aligned} R_1^{(t+1)} - R_2^{(t+1)} &= \sigma\left[\frac{\sigma^*}{2\mu}\left(\alpha^2 - \frac{1}{\alpha^2}\right) - c_{\mu/\mu,\lambda}\left(\frac{\alpha}{\sqrt{1+\frac{\sigma_\epsilon^{*2}}{\alpha^2\sigma^{*2}}}} - \frac{1}{\alpha\sqrt{1+\frac{\alpha^2\sigma_\epsilon^{*2}}{\sigma^{*2}}}}\right)\right] \\ &= \sigma\left[\frac{(\alpha^4-1)\sigma^*}{2\mu\alpha^2} - \frac{c_{\mu/\mu,\lambda}\sigma^*}{\alpha^2}\left(\frac{\alpha^4}{\sqrt{\alpha^2\sigma^{*2}+\sigma_\epsilon^{*2}}} - \frac{1}{\sqrt{\frac{\sigma^{*2}}{\alpha^2}+\sigma_\epsilon^{*2}}}\right)\right]. \end{aligned} \tag{C.11}$$

The term in the square brackets of Eq. (C.11) defines a discriminator function Δ

$$\Delta(\sigma^*, \sigma_\epsilon^*) := \frac{(\alpha^4-1)\sigma^*}{2\mu\alpha^2} - \frac{c_{\mu/\mu,\lambda}\sigma^*}{\alpha^2}\left(\frac{\alpha^4}{\sqrt{\alpha^2\sigma^{*2}+\sigma_\epsilon^{*2}}} - \frac{1}{\sqrt{\frac{\sigma^{*2}}{\alpha^2}+\sigma_\epsilon^{*2}}}\right) \tag{C.12}$$

Note that, this discriminator function Δ depends on the normalized mutation strength σ^* as well as the normalized noise strength σ_ϵ^*. Its sign determines the σ-dynamic

$$\begin{aligned} \Delta < 0 \quad &\Rightarrow \quad \sigma^{(t+1)} = \sigma^{(t)}\alpha, \\ \Delta > 0 \quad &\Rightarrow \quad \sigma^{(t+1)} = \sigma^{(t)}/\alpha. \end{aligned} \tag{C.13}$$

Thus, using $\Delta(\sigma^*, \sigma_\epsilon^*)$ the evolution equation of the mutation strength becomes

$$\sigma^{(t+1)} = \sigma^{(t)} \alpha^{-\operatorname{sign}(\Delta(\sigma^{*(t)}, \sigma_\epsilon^{*(t)}))}. \tag{C.14}$$

At this point, the critical value $\sigma_0^* > 0$ around which the sign of $\Delta(\sigma^*, \sigma_\epsilon^*)$ changes is of special interest. It can be calculated by resolving Eq. (C.12) for its root. That is, σ_0^* satisfies the condition

$$\frac{(\alpha^4 - 1)}{2\mu c_{\mu/\mu,\lambda}} \overset{!}{=} \frac{\alpha^4}{\sigma_\epsilon^* \sqrt{1 + \frac{\alpha^2 \sigma^{*2}}{\sigma_\epsilon^{*2}}}} - \frac{1}{\sigma_\epsilon^* \sqrt{1 + \frac{\sigma^{*2}}{\alpha^2 \sigma_\epsilon^{*2}}}}. \tag{C.15}$$

Finding an analytical expression for σ_0^* of (C.15) is very demanding. Therefore, the following approximation is applied in order to make the analysis tractable

$$\sqrt{1 + \frac{\sigma^{*2}}{\sigma_\epsilon^{*2}}} \simeq 1 + \frac{\sigma^{*2}}{2\sigma_\epsilon^{*2}}. \tag{C.16}$$

Assuming $\sigma^{*2}/\sigma_\epsilon^{*2} < 1$, it follows by Taylor expansion of the square root. This simplification is admissible provided that the meta-ES has reached a certain vicinity to its steady state R_{ss}, cf. Eq. (7.7). Accordingly, Eq. (C.15) reads

$$\frac{(\alpha^4 - 1)\sigma_\epsilon^*}{2\mu c_{\mu/\mu,\lambda}} \simeq \frac{\alpha^4}{1 + \frac{\alpha^2 \sigma^{*2}}{2\sigma_\epsilon^{*2}}} - \frac{1}{1 + \frac{\sigma^{*2}}{2\alpha^2 \sigma_\epsilon^{*2}}}. \tag{C.17}$$

Converting the fractions to a common denominator, one gets

$$\frac{(\alpha^4 - 1)\sigma_\epsilon^*}{2\mu c_{\mu/\mu,\lambda}} \simeq \frac{(\alpha^4 - 1)}{1 + \frac{\sigma^{*2}}{2\alpha^2 \sigma_\epsilon^{*2}} + \frac{\alpha^2 \sigma^{*2}}{2\sigma_\epsilon^{*2}} + \frac{\sigma^{*4}}{4\sigma_\epsilon^{*4}}}, \tag{C.18}$$

and rearranging the terms leads to

$$\frac{2\mu c_{\mu/\mu,\lambda}}{\sigma_\epsilon^*} \simeq 1 + \frac{\sigma^{*2}}{2\alpha^2 \sigma_\epsilon^{*2}} + \frac{\alpha^2 \sigma^{*2}}{2\sigma_\epsilon^{*2}} + \frac{\sigma^{*4}}{4\sigma_\epsilon^{*4}}. \tag{C.19}$$

The application minor rearrangements yields a biquadratic equation in σ^*

$$\sigma^{*4} + 2\frac{\alpha^4 + 1}{\alpha^2} \sigma_\epsilon^{*2} \sigma^{*2} + 4\sigma_\epsilon^{*4} \left(1 - \frac{2\mu c_{\mu/\mu,\lambda}}{\sigma_\epsilon^*}\right) \simeq 0. \tag{C.20}$$

Solving this equation for $\sigma^{*2} > 0$ yields

$$\sigma_0^{*2} \simeq -\frac{\alpha^4 + 1}{\alpha^2} \sigma_\epsilon^{*2} + \sqrt{\sigma_\epsilon^{*4} \left[\left(\frac{\alpha^4 + 1}{\alpha^2} \right)^2 + 4 \left(\frac{2\mu c_{\mu/\mu,\lambda}}{\sigma_\epsilon^*} - 1 \right) \right]}. \tag{C.21}$$

Taking the square root finally results in the desired σ_0^* formula

$$\sigma_0^* \simeq \sigma_\epsilon^* \sqrt{\sqrt{\left(\frac{\alpha^4+1}{\alpha^2}\right)^2 + 4\left(\frac{2\mu c_{\mu/\mu,\lambda}}{\sigma_\epsilon^*} - 1\right)} - \left(\frac{\alpha^4+1}{\alpha^2}\right)}. \tag{C.22}$$

In this representation the critical mutation strength σ_0^* depends on the population sizes, the normalized noise strength σ_ϵ^* as well as on the control parameter α.

C.3. Approximation of the discriminator function

Aiming at the computation of the discriminator function that governs the normalized mutation strength dynamics, the focus is on the iterative mapping of the normalized noise strength dynamics from Eq. (7.42)

$$\sigma_\epsilon^{*(t+1)} = \frac{\sigma_\epsilon^{*(t)}}{\left(1 - \frac{1}{N}\varphi^*(\sigma^{*(t)}\alpha^{-\mathrm{sign}(\Delta(\sigma^{*(t)},\sigma_\epsilon^{*(t)}))}, \sigma_\epsilon^{*(t)})\right)^2}. \tag{C.23}$$

To obtain a more manageable expression a simplification of the normalized progress rate is desirable. Beginning with the progress rate of the inner $(\mu/\mu_I, \lambda)$-ES on the noisy sphere model (6.9), the application of (2.22), and (6.6) yields the normalized progress rate formula

$$\varphi^*(\sigma^*, \sigma_\epsilon^*) = \frac{c_{\mu/\mu,\lambda}\sigma^{*2}}{\sqrt{\sigma_\epsilon^{*2} + \sigma^{*2}}} - \frac{\sigma^{*2}}{2\mu}. \tag{C.24}$$

Equation (C.24) can be asymptotically ($\sigma^*/\sigma_\epsilon^* \to 0$) expressed by

$$\varphi^*(\sigma^*, \sigma_\epsilon^*) = \frac{c_{\mu/\mu,\lambda}\sigma^{*2}}{\sigma_\epsilon^*\sqrt{1 + \frac{\sigma^{*2}}{\sigma_\epsilon^{*2}}}} - \frac{\sigma^{*2}}{2\mu} \simeq \sigma^{*2}\left(\frac{c_{\mu/\mu,\lambda}}{\sigma_\epsilon^*} - \frac{1}{2\mu}\right). \tag{C.25}$$

Converting the fractions to a common denominator and referring to the approximation of the progress rate as $\tilde{\varphi}^*(\sigma^*, \sigma_\epsilon^*)$ leads to

$$\tilde{\varphi}^*(\sigma^*, \sigma_\epsilon^*) := \frac{\sigma^{*2}}{2\mu\sigma_\epsilon^*}\left(2\mu c_{\mu/\mu,\lambda} - \sigma_\epsilon^*\right). \tag{C.26}$$

Consequently, ignoring the quadratic φ^{*2} term and replacing φ^* with $\tilde{\varphi}^*$ (C.26), one obtains a simpler description of the σ_ϵ^* dynamics (C.23)

$$\sigma_\epsilon^{*(t+1)} \simeq \frac{\sigma_\epsilon^*}{\left(1 - \frac{2}{N}\tilde{\varphi}^*(\sigma^*\alpha^{-\mathrm{sign}(\Delta(\sigma^*,\sigma_\epsilon^*))}, \sigma_\epsilon^*)\right)}. \tag{C.27}$$

Further, considering small progress in the asymptotic limit allows to apply the following simplification

$$\frac{1}{1-x} \simeq 1 + x \quad \forall\, x \text{ with } |x| \ll 1. \tag{C.28}$$

It is obtained by first order Taylor expansion and transforms (C.27) into

$$\sigma_\epsilon^{*(t+1)} \simeq \sigma_\epsilon^{*(t)} \left(1 + \frac{2}{N}\tilde{\varphi}^*(\sigma^{*(t)}\alpha^{-\text{sign}(\Delta(\sigma^{*(t)},\sigma_\epsilon^{*(t)}))}, \sigma_\epsilon^{*(t)})\right). \tag{C.29}$$

Inserting $\tilde{\varphi}^*$, Eq. (C.26), one finally obtains the recurrence equation

$$\sigma_\epsilon^{*(t+1)} \simeq \sigma_\epsilon^* + \frac{\sigma^{*2}\alpha^{-2\text{sign}(\Delta(\sigma^*,\sigma_\epsilon^*))}}{\mu N}\left(2\mu c_{\mu/\mu,\lambda} - \sigma_\epsilon^*\right). \tag{C.30}$$

In the next step an approximation for the discriminator function $\Delta(\sigma^*, \sigma_\epsilon^*)$, cf. Eq. (7.32), is derived. Assuming $\sigma^*/\sigma_\epsilon^* \to 0$, the square roots in (7.32) can be simplified according to the rule

$$\sqrt{1+x} \simeq 1 + \frac{x}{2} \quad \forall\, x \text{ with } |x| \ll 1, \tag{C.31}$$

which is also based on first order Taylor expansion of the square root. Consequently, one finds the following asymptotical approximation

$$\Delta(\sigma^*, \sigma_\epsilon^*) \simeq \frac{\sigma^*}{2\mu}\frac{\alpha^4 - 1}{\alpha^2} - \frac{\sigma^* c_{\mu/\mu,\lambda}}{\alpha^2\sigma_\epsilon^*}\left(\frac{\alpha^4}{\left(1 + \frac{\alpha^2\sigma^{*2}}{2\sigma_\epsilon^{*2}}\right)} - \frac{1}{\left(1 + \frac{\sigma^{*2}}{2\alpha^2\sigma_\epsilon^{*2}}\right)}\right). \tag{C.32}$$

Equation (C.32) can further be transformed into

$$\begin{aligned}\Delta(\sigma^*, \sigma_\epsilon^*) \simeq& \frac{\sigma^*}{\alpha^2}\left[\frac{(\alpha^4-1)}{2\mu} - \frac{c_{\mu/\mu,\lambda}}{\sigma_\epsilon^*}\left(\frac{(\alpha^4-1)}{1 + \frac{\alpha^4+1}{\alpha^2}\frac{\sigma^{*2}}{2\sigma_\epsilon^{*2}} + \frac{\sigma^{*4}}{4\sigma_\epsilon^{*4}}}\right)\right] \\ =& \frac{\sigma^*(\alpha^4-1)}{\alpha^2}\left(\frac{1}{2\mu} - \frac{4c_{\mu/\mu,\lambda}\sigma_\epsilon^{*3}}{4\sigma_\epsilon^{*4} + \sigma^{*4} + 2\frac{\alpha^4+1}{\alpha^2}\sigma_\epsilon^{*2}\sigma^{*2}}\right).\end{aligned} \tag{C.33}$$

Considering small mutation strengths, i.e. $\sigma \to 0$, the term σ^{*4} in the denominator of the subtrahend can be neglected. Thus, one obtains

$$\Delta(\sigma^*, \sigma_\epsilon^*) \simeq \frac{\sigma^*(\alpha^4-1)}{\alpha^2}\left(\frac{1}{2\mu} - \frac{c_{\mu/\mu,\lambda}\sigma_\epsilon^*}{\sigma_\epsilon^{*2} + \frac{\alpha^4+1}{2\alpha^2}\sigma^{*2}}\right). \tag{C.34}$$

The reduction to a common denominator finally yields

$$\Delta(\sigma^*, \sigma_\epsilon^*) \simeq \frac{\sigma^*(\alpha^4-1)}{2\mu\alpha^2\left(\sigma_\epsilon^{*2} + \frac{\alpha^4+1}{2\alpha^2}\sigma^{*2}\right)}\left(\sigma_\epsilon^{*2} + \frac{\alpha^4+1}{2\alpha^2}\sigma^{*2} - 2\mu c_{\mu/\mu,\lambda}\sigma_\epsilon^*\right). \tag{C.35}$$

In this representation, the sign of Δ and, by implication, the decision inside the meta-ES to increase or decrease the mutation strength σ or σ^*, respectively, by the factor α is now only depending on the bracketed terms in the numerator. That is, the bracketed expressions define a new discriminator function $\tilde{\Delta}(\sigma^*, \sigma_\epsilon^*)$ which after small rearrangements reads

$$\tilde{\Delta}(\sigma^*, \sigma_\epsilon^*) = \frac{\alpha^4+1}{2\alpha^2}\sigma^{*2} - \sigma_\epsilon^*\left(2\mu c_{\mu/\mu,\lambda} - \sigma_\epsilon^*\right). \tag{C.36}$$

The use of Eq. (C.36) allows for the description of the behavior of the point of discontinuity σ_0^*. Finally, this provides the characterization of the normalized steady state mutation strength dynamics in Sec. 7.4.2.

Bibliography

Arnold, D. V. (2002). *Noisy optimization with evolution strategies*. Kluwer Academic Publishers.

Arnold, D. V. (2007). On the use of evolution strategies for optimising certain positive definite quadratic forms. In Lipson, H., editor, *GECCO*, pages 634–641. ACM.

Arnold, D. V. and Beyer, H.-G. (2001). Local Performance of the $(\mu/\mu_I, \lambda)$-ES in a Noisy Environment. In W., M. and W., S., editors, *Foundations of Genetic Algorithms VI*, pages 127–141. Morgan Kaufmann.

Arnold, D. V. and Beyer, H.-G. (2004). Performance analysis of evolutionary optimization with cumulative step length adaptation. *IEEE Transactions on Automatic Control*, 49(4):617–622.

Arnold, D. V. and Beyer, H.-G. (2010). On the Behaviour of Evolution Strategies Optimising Cigar Functions. *Evol. Comput.*, 18(4):661–682.

Arnold, D. V. and MacLeod, A. (2008). Step Length Adaptation on Ridge Functions. *Evolutionary Computation*, 16(2):151–184.

Astete-Morales, S., Cauwet, M.-L., and Teytaud, O. (2015). Evolution Strategies with Additive Noise: A Convergence Rate Lower Bound. In *Proceedings of the 2015 ACM Conference on Foundations of Genetic Algorithms XIII*, FOGA '15, pages 76–84, New York, NY, USA. ACM.

Audet, C. (2014). *A Survey on Direct Search Methods for Blackbox Optimization and Their Applications*, pages 31–56. Springer New York, New York, NY.

Beyer, H.-G. (1995). Towards a Theory of Evolution Strategies: Self-Adaptation. *Evolutionary Computation*, 3(3):311–347.

Beyer, H.-G. (2001). *The Theory of Evolution Strategies*. Natural Computing Series. Springer.

Beyer, H.-G. and Arnold, D. V. (2003). Qualms Regarding the Optimality of Cumulative Path Length Control in CSA/CMA-evolution Strategies. *Evol. Comput.*, 11(1):19–28.

Beyer, H.-G., Arnold, D. V., and Meyer-Nieberg, S. (2005). A New Approach for Predicting the Final Outcome of Evolution Strategy Optimization Under Noise. *Genetic Programming and Evolvable Machines*, 6(1):7–24.

Beyer, H.-G., Dobler, M., Hämmerle, C., and Masser, P. (2009). On strategy parameter control by Meta-ES. In *Genetic and Evolutionary Computation Conference, GECCO 2009, Proceedings, Montreal, Québec, Canada, July 8-12*, pages 499–506.

Beyer, H.-G. and Finck, S. (2008). On the performance of evolution strategies on noisy PDQFs: Progress rate analysis. In *Evolutionary Computation, 2008. CEC 2008. (IEEE World Congress on Computational Intelligence). IEEE Congress on*, pages 495–502.

Beyer, H.-G. and Hellwig, M. (2012). Mutation strength control by Meta-ES on the sharp ridge. In *Genetic and Evolutionary Computation Conference, GECCO '12, Philadelphia, PA, USA, July 7-11*, pages 305–312.

Beyer, H.-G. and Melkozerov, A. (2014). The Dynamics of Self-Adaptive Multi-Recombinant Evolution Strategies on the General Ellipsoid Model. *IEEE Transactions on Evolutionary Computation*, 18(5):764–778.

Beyer, H.-G. and Schwefel, H.-P. (2002). Evolution strategies - A comprehensive introduction. *Natural Computing*, 1(1):3–52.

Beyer, H.-G. and Sendhoff, B. (2006). Evolution Strategies for Robust Optimization. In *Evolutionary Computation, 2006. CEC 2006. IEEE Congress on*, pages 1346–1353.

Beyer, H.-G. and Sendhoff, B. (2008). Covariance Matrix Adaptation Revisited – The CMSA Evolution Strategy –. In Rudolph, G., Jansen, T., Beume, N., Lucas, S., and Poloni, C., editors, *Parallel Problem Solving from Nature – PPSN X*, volume 5199 of *Lecture Notes in Computer Science*, pages 123–132. Springer Berlin Heidelberg.

Finck, S. (2011). *Analysis of Evolution Strategies on a Subset of Quadratic Functions and Methods for Comparing Optimization Strategies.* PhD thesis, Institut für Angewandte und Experimentelle Mechanik, Universität Stuttgart, Deutschland.

Finck, S. and Beyer, H.-G. (2012). Performance Analysis of the Simultaneous Perturbation Stochastic Approximation Algorithm on the Noisy Sphere Model. *Theor. Comput. Sci.*, 419:50–72.

Finck, S., Beyer, H.-G., and Melkozerov, A. (2011). Noisy optimization: a theoretical strategy comparison of ES, EGS, SPSA & IF on the noisy sphere. In Krasnogor, N. and Lanzi, P. L., editors, *GECCO*, pages 813–820. ACM.

Fogel, L., Owens, A., and Walsh, M. (1966). *Artificial Intelligence Through Simulated Evolution*. John Wiley & Sons.

Hansen, N. (1998). *Verallgemeinerte individuelle Schrittweitenregelung in der Evolutionsstrategie. Eine Untersuchung zur entstochastisierten,koordinatensystemunabhängigen Adaptation der Mutationsverteilung*. Mensch und Buch Verlag, Berlin. ISBN 3-933346-29-0.

Hansen, N. (2006a). An analysis of mutative σ-self-adaptation on linear fitness functions. *Evolutionary Computation*, 14(3):255–275.

Hansen, N. (2006b). The CMA evolution strategy: a comparing review. In Lozano, J., Larranaga, P., Inza, I., and Bengoetxea, E., editors, *Towards a new evolutionary computation. Advances on estimation of distribution algorithms*, pages 75–102. Springer.

Hansen, N., Arnold, D. V., and Auger, A. (2015). *Evolution Strategies*, pages 871–898. Springer Berlin Heidelberg, Berlin, Heidelberg.

Hansen, N., Niederberger, A. S. P., Guzzella, L., and Koumoutsakos, P. (2009). A Method for Handling Uncertainty in Evolutionary Optimization With an Application to Feedback Control of Combustion. *IEEE Trans. Evolutionary Computation*, 13(1):180–197.

Hansen, N. and Ostermeier, A. (1996). Adapting arbitrary normal mutation distributions in evolution strategies: the covariance matrix adaptation. In *Evolutionary Computation, 1996., Proceedings of IEEE International Conference on*, pages 312–317.

Hansen, N. and Ostermeier, A. (2001). Completely Derandomized Self-Adaptation in Evolution Strategies. *Evolutionary Computation*, 9(2):159–195.

Herdy, M. (1992). Reproductive Isolation as Strategy Parameter in Hierarichally Organized Evolution Strategies. In Männer, R. and Manderick, B., editors, *PPSN*, pages 209–. Elsevier.

Herdy, M. (1993). The Number of Offspring As Strategy Parameter in Hierarchically Organized Evolution Strategies. *SIGBIO Newsl.*, 13(2):2–9.

Holland, J. (1975). *Adaptation in natural and artificial systems: an introductory analysis with applications to biology, control, and artificial intelligence*. University of Michigan Press.

Jägersküpper, J. (2006). How the (1+1) ES Using Isotropic Mutations Minimizes Positive Definite Quadratic Forms. *Theor. Comput. Sci.*, 361(1):38–56.

Jin, Y. and Branke, J. (2005). Evolutionary optimization in uncertain environments-a survey. *IEEE Trans. Evolutionary Computation*, 9(3):303–317.

Kenney, J. (2013). *Mathematics of Statistics*. Number 1-2. Literary Licensing, LLC.

Khare, A. and Rangnekar, S. (2013). A review of particle swarm optimization and its applications in solar photovoltaic system. *Applied Soft Computing*, 13(5):2997 – 3006.

Kolda, T. G., Lewis, R. M., and Torczon, V. (2003). Optimization by direct search: New perspectives on some classical and modern methods. *SIAM Review*, 45(3):385–482.

Mann, H. B. (1945). Nonparametric Tests Against Trend. *Econometrica*, 13(3):pp. 245–259.

Melkozerov, A. and Beyer, H.-G. (2010). On the analysis of self-adaptive evolution strategies on elliptic model: first results. In Pelikan, M. and Branke, J., editors, *GECCO*, pages 369–376. ACM.

Melkozerov, A. and Beyer, H.-G. (2015). Towards an Analysis of Self-Adaptive Evolution Strategies on the Noisy Ellipsoid Model: Progress Rate and Self-Adaptation Response. In *GECCO 2015, Madrid, Spain*, pages 297–304. ACM.

Meyer-Nieberg, S. (2007). *Self-adaptation in evolution strategies.* PhD thesis, Dortmund University of Technology. http://d-nb.info/997728450.

Meyer-Nieberg, S. and Beyer, H.-G. (2005). On the analysis of self-adaptive recombination strategies: first results. In *Congress on Evolutionary Computation*, pages 2341–2348. IEEE.

Meyer-Nieberg, S. and Beyer, H.-G. (2008). Why noise may be good: additive noise on the sharp ridge. In Ryan, C. and Keijzer, M., editors, *GECCO*, pages 511–518. ACM.

Meyer-Nieberg, S. and Beyer, H.-G. (2012). The Dynamical Systems Approach - Progress Measures and Convergence Properties. In Rozenberg, G., Bäck, T., and Kok, J. N., editors, *Handbook of Natural Computing*, pages 741–814. Springer.

Mohan, B. C. and Baskaran, R. (2012). A survey: Ant colony optimization based recent research and implementation on several engineering domain. *Expert Systems with Applications*, 39(4):4618 – 4627.

Nelder, J. A. and Mead, R. (1965). A simplex method for function minimization. *The Computer Journal*, 7(4):308–313.

Oliver, M. A. and Webster, R. (1990). Kriging: a method of interpolation for geographical information systems. *International Journal of Geographical Information Systems*, 4(3):313–332.

Ostermeier, A., Gawelczyk, A., and Hansen, N. (1994). Step-Size Adaption Based on Non-Local Use of Selection Information. In *Parallel Problem Solving from Nature - PPSN III, Jerusalem, Israel, October 9-14*, pages 189–198.

Powell, M. J. D. (2006). *The NEWUOA software for unconstrained optimization without derivatives*, pages 255–297. Springer US, Boston, MA.

Rechenberg, I. (1973). *Evolutionsstrategie: Optimierung technischer Systeme nach Prinzipien der biologischen Evolution*. Problemata, 15. Frommann-Holzboog.

Rechenberg, I. (1978). Evolutionsstrategien. 8:83–114.

Rechenberg, I. (1994). *Evolutionsstrategie 94*, volume 1 of *Werkstatt Bionik und Evolutionstechnik*. Frommann-Holzboog, Stuttgart.

Schwefel, H.-P. (1975). *Evolutionsstrategie und numerische Optimierung*. Technische Universität Berlin.

Schwefel, H.-P. (1977). *Numerische Optimierung von Computer-Modellen mittels der Evolutionsstrategie*. Interdisciplinary systems research; 26. Birkhäuser, Basel.

Shamir, O. (2013). On the Complexity of Bandit and Derivative-Free Stochastic Convex Optimization. In *COLT - The 26th Annual Conference on Learning Theory, NJ, USA*, pages 3–24.

Torczon, V. (1997). On the convergence of pattern search algorithms. *SIAM Journal on Optimization*, 7(1):1–25.